Universidad Autónoma de Madrid

Programa de Doctorado en Biociencias Moleculares

BIOTECHNOLOGICAL PLATFORMS FOR ARYL-ALCOHOL OXIDASES BY DIRECTED EVOLUTION

JAVIER VIÑA GONZÁLEZ

TESIS DOCTORAL

Madrid, 2019

Departamento de Biología Molecular
Facultad de Ciencias
Universidad Autónoma de Madrid

BIOTECHNOLOGICAL PLATFORMS FOR ARYL-ALCOHOL OXIDASES BY DIRECTED EVOLUTION

INSTITUTO DE CATÁLISIS Y PETROLEOQUÍMICA

CONSEJO SUPERIOR DE INVESTIGACIONES CIENTÍFICAS

Institute of Catalysis and Petrochemistry (ICP)
Spanish Council for Scientific Research (CSIC)

Javier Viña González
Licenciado en Bioquímica

Director: Dr. Miguel Alcalde Galeote

Tutora: Dr. Elena Bogónez Peláez

TESIS DOCTORAL

Madrid, 2018

A mis padres

In memory of E. Wesley Graham

AGRADECIMIENTOS

En primer lugar debo agradecer la financiación que me ha permitido seguir mis estudios doctorales. Los proyectos europeos “Optimized oxidoreductases for medium and large scale industrial biotransformations (INDOX FP7-KBBE-2013-7-613549)” y “New enzymatic oxidation/oxyfunctionalization technologies for added value bio-based products. (ENZOX2 H2020-BBI-PPP-2015-2-720297)”. Los proyectos nacionales “Evolución dirigida de oxidoreductasas ligninolíticas modernas y ancestrales para el diseño de una levadura de podredumbre blanca (DEWRY BIO2013-43407-R)”, “Evolución dirigida y computacional de ligninasas (LIGNOLUTION BIO2016-79106-R)“ y “Química sintética mediante enzimas quiméricas de fusión diseñadas por evolución dirigida y computacional (EVOCHIMERA Y2018/BIO-4738)”. También agradecerle apoyo de la red Europea COST (http://www.cost.eu/) para la asistencia a congresos, simposios y a la escuela de verano. He sido muy afortunado.

Al Profesor Ángel T. Martínez del Centro de Investigaciones Biológicas (CIB), coordinador de los proyectos europeos que enmarcaron esta Tesis. Gracias por la experiencia. Siguiendo en el CIB: Muchas gracias a la Dra. Marta Pérez-Boada y al Dr. Javier Ruiz-Dueñas por todos los momentos inolvidables en los viajes. Gracias a la Dr. Patricia Ferreira y la Dra. Ana Serrano por la inestimable ayuda a entender mi sistema de trabajo. También querría agradecer la Dra. Susana Camarero y a Isabel P y Felipe, pues os sentimos como parte de nuestro grupo.

Gracias a mi director el Dr. Miguel Alcalde por darme esta oportunidad. Tras varios años de gran entendimiento solo queda en mi gratitud por todo el apoyo profesional y personal. Te agradezco que me hayas traído hasta aquí. Te agradezco que veas en mí lo que puedo llegar a ser.

Gracias a mi tutora la Dra. Elena Bogónez. Siempre dispuesta a ayudar, a facilitar y a solucionar problemas.

Al Dr. Francisco Plou, por el gran recuerdo como profesor en el Máster, por estar siempre a nuestro lado para darnos apoyo en química y de cualquier otro tipo, por tratarme como a uno de sus estudiantes y dejarme cacharrear y aprender en su laboratorio. Al Profesor Antonio Ballesteros, un pedacito de tu legado en biocatálisis sigue adelante en cada uno de nosotros. Muchas gracias por el apoyo, es un orgullo pertenecer a vuestra familia científica.

Dar las gracias se queda corto para la gente del Instituto de Catálisis: A Eva y a Diana, por estar siempre dispuestas a guiarnos. A David por enseñarme con gran paciencia y generosidad,

por tu apoyo constante y directo. A Patch, muchas gracias por respaldarme siempre y estar pendiente de mi, me haces sentir como en casa. A Javi gracias por subirme el ánimo en tantos momentos y por todos los divertidos recuerdos. A Isa, me enseñaste lo que es un abrazo en un laboratorio, siempre un amor. A Ivan, thanks for sharing your great philosophy and being like a rock to us. A Bernardo, ¿qué te voy a decir? un brother in lab para mí y más. A Pati, gracias por tantas cosas… por ser mi compañera de batallas y fantasías, ha sido, es y será un honor. A mis colaboradores directos. Mi primera Padawan Katarina, una máquina en el laboratorio y una amiga a la que tengo mucho cariño. Al Dr. Jiawey Yang, thank you for showing me that other ways are possible. A Diego, trabajador entusiasta, gracias por todo tu esfuerzo. Bajando de Piso. A Lopa gracias por iluminar tantos días grises con tu simpatía. A Noa gracias por tu ayuda en el HPLC, siempre nos quedará gudetama. A Lucía gracias por ser siempre tan atenta y cariñosa. A Fadia, sabes más que una enciclopedia, gracias por tus pláticas y tu contagiosa onda de las buenas. A Joselu por los buenos momentos y charlas en las comidas y a David por ser el más majete del segundo piso. A toda la gente que ha pasado y nos ha bendecido con su presencia: Mar, Valeria, Adela, Leire, Sofía, Berndjan, Elvin, Joaquín, Vianney, Mehdi, Carla, Gordana, Juan, Morgane y más… También en el ICP: al grupo del Dr. Manuel Ferrer. Moni, Rafa, Cosco, Sandra, David… por estar ahí siempre cuando necesitamos que alguien esté ahí. Muchas Gracias a los chicos de Biocatálisis: a Lara, a Chiara, a Alejandro, a Janaina, a María, a Cristina y tantos otros.

Gracias al Dr. Francisco Valero y al Dr. José Luis Montesinos de la Universidad Autónoma de Barcelona (UAB) por acogerme en su laboratorio, abrirme al mundo de los fermentadores y enseñarme la fantástica Ciudad Condal. Thanks to Professor Anton Glieder from the Graz University of Technology (TUGraz) for letting me grow as a scientist during my stay there dealing with everything *Pichia.* Thank you for all the resources, your confidence and your kindness. Also thanks to Kay, Anna and Christian for the constant help.

Desde pequeño he querido trabajar en el laboratorio. Gracias a María, a las Cármenes y a Cris por tantos años de apoyo, de buenos y malos momentos, por no dejarme caer y poder conseguir mis objetivos. A mis amigos de la carrera y el Máster, a Belén, a Sara, a Juan, a María, a Arancha, gracias por todo el apoyo entre cafés... Gracias especiales a Saúl por sus sabios consejos y ejemplo. También gracias a mis amigos y compañeros en Madrid que me han apoyado tanto solamente sabiendo que ‘hago mutantes’…

Los mayores agradecimientos son para la familia. Gracias por estar siempre esperando. Por pasar la vida en la cocina. Por correr cuando lo necesito. Por las charlas nocturnas. Por preocuparse. Por darme felicidad. Por traerme esperanza.

Thank you Wess. Forever.

SUMMARY

The aryl-alcohol oxidase (AAO) is a fungal flavoenzyme that supplies H_2O_2 to the ligninolytic consortium during natural wood decay. Being active on a wide array of aromatic alcohols, this GMC oxidase presents a highly enantioselective mechanism of great interest in organic synthesis processes. The most powerful strategy for the AAO to meet industrial standards is the engineering of its properties by directed evolution. In the present Doctoral Thesis, an evolutionary platform for the AAO from *Pleurotus eryngii* was developed in order to: (i) obtain functional expression in yeasts, (ii) design a secondary benzyl-alcohol oxidase, and (iii) explore the enzymatic conversion of furfural derivatives.

To achieve functional expression in *Saccharomyces cerevisiae*, the AAO gene was fused to different signal peptides including chimeric versions of the mating-α factor and the killer K1 toxin preprosequences. The platform for *in vitro* evolution was completed with a dual high-throughput screening assay to detect H_2O_2 that included a method based on the Fenton reaction. To enhance secretion, several libraries were created combining classical evolution (*i.e.* mutagenic PCR and DNA shuffling) with structure-guided evolution by MORPHING. The final secretion variant FX9, carried four mutations in the signal peptide and two substitutions in the mature protein including the consensus/ancestral H91N. The FX9 improved secretion up to 4.5 mg/L and presented high stability and kinetic values similar to the native enzyme. FX9 was cloned and expressed in *Pichia pastoris* maintaining expression levels and main biochemical properties. When the production was scaled-up in 5L fermenter, AAO production was increased to 25.5 mg/L.

FX9 was further evolved to selectively oxidize secondary benzyl alcohols. The residual activity on chiral molecules was unlocked with the modulation fo the catalytic pocket by combinatorial saturation mutagenesis. After four generations, that included a site-directed recombination step to polish mutations, LanDo variant harboured five new substitutions increasing the catalytic efficiency with 1-(*p*-methoxyphenyl)-ethanol in 3 orders of magnitude with a 99% ee.

Exploring the transformation of 5-hydroxymethylfurfural (HMF) into furan-2,5-dicarboxylic acid (FDCA), FX9 acquired mutation F501W that improved catalytic efficiency on HMF 3-fold and showed for the first time the performance of three consecutive oxidations for the AAO.

RESUMEN

La aril-alcohol oxidasa (AAO) es una flavoenzima fúngica que suple H_2O_2 al consorcio ligninolítico durante la degradación natural de la madera. Siendo activa con una amplia variedad de alcoholes aromáticos, esta oxidasa GMC presenta un mecanismo altamente enantioselectivo de gran interés en procesos de síntesis orgánica. La estrategia más potente para adaptar a la AAO a estándares industriales es la ingeniería de sus propiedades mediante técnicas de evolución dirigida. En la presente Tesis Doctoral, una plataforma evolutiva para la AAO de *Pleurotus eryngii* fue desarrollada con el objetivo de: (i) obtener expresión funcional en levaduras, (ii) diseñar una aril-alcohol oxidasa activa con alcoholes secundarios, y (iii) explorar la conversión enzimática de derivados del furfural.

Para obtener expresión funcional en *Saccharomyces cerevisiae*, el gen de la AAO se fusionó a diferentes péptidos señales incluyendo versiones quiméricas de las secuencias prepro del factor-α y la toxina killer K1. La plataforma para la evolución *in vitro* se completó con un ensayo dual de *screening* para la detección de H_2O_2 incluyendo un método basado en la reacción de Fenton. Para mejorar la secreción, se crearon varias librerías combinando evolución clásica (PCR mutagénica y DNA shuffling) con evolución focalizada con el método MORPHING. La variante final FX9, con alta estabilidad y constantes cinéticas similares a la enzima nativa, presentó cuatro mutaciones en el péptido señal y dos substituciones en la proteína madura incluyendo la consenso/ancestral H91N. FX9 se expresó en *S. cerevisiae* con valores de 4.5 mg/L y fue posteriormente clonada y expresada en *Pichia pastoris* a escala de fermentador de 5 L alcanzando niveles de secreción 25.5 mg/L y manteniendo sus propiedades bioquímicas generales.

La variante FX9 fue sometida a posteriores ciclos de evolución, incluyendo el remodelado del bolsillo catalítico por mutagénesis saturada combinatorial, para la oxidación de alcoholes bencílicos secundarios. Las cinco mutaciones introducidas en la variante LanDo aumentaron la eficiencia catalítica con 1-(*p*-methoxyphenyl)-ethanol en 3 órdenes de magnitud con un 99 % ee.

Explorando la transformación del 5-hydroxymethylfurfural (HMF) en furan-2,5-dicarboxylic acid (FDCA), FX9 adquirió la mutación F501W que mejoró 3 veces la eficiencia catalítica con HMF y demostró por primera vez la catálisis de 3 oxidaciones consecutivas para la AAO.

CONTENTS

1 INTRODUCTION 1

1.1 Aryl-alcohol oxidase 3

1.1.1 Natural context and general aspects 3

1.1.2 The AAO from *P. eryngii* as part of the GMC superfamily 5

1.1.3 Mechanistic and structural aspects of the AAO catalysis 8

1.2 Biotechnological and industrial applications of AAO 10

1.2.1 Deracemization of benzyl secondary alcohols 11

1.2.2 Furfural derivatives cascade reactions 12

1.3 Directed evolution 12

1.3.1 *Saccharomyces cerevisiae* as a tool-box for DNA diversity 15

2 OBJECTIVES 19

3 Focused directed evolution of aryl-alcohol oxidase in yeast by using chimeric signal peptides 23

3.1 INTRODUCTION 25

3.2 MATERIALS AND METHODS 27

3.3 RESULTS AND DISCUSSION 35

3.4 CONCLUSIONS AND OUTLOOK 46

3.5 SUPPLEMENTARY MATERIAL 47

4 Directed evolution method in *Saccharomyces cerevisiae*: Mutant library creation and screening 49

4.1 INTRODUCTION 52

4.2 PROTOCOL 53

4.3 REPRESENTATIVE RESULTS 59

4.4 DISCUSSION 61

5 Functional expression of aryl-alcohol oxidase in *Saccharomyces cerevisiae* and *Pichia pastoris* by directed evolution. 63

5.1 INTRODUCTION 66

5.2 MATERIAL AND METHODS 67

5.3 RESULTS AND DISCUSSION 73

5.4 CONCLUSIONS 79

6 Structure-Guided Evolution of Aryl Alcohol Oxidase from *Pleurotus eryngii* for the Selective Oxidation of Secondary Benzyl Alcohol 81

6.1 INTRODUCTION 84

6.2 MATERIALS AND METHODS 85

6.3 RESULTS AND DISCUSSION 91

6.4 CONCLUSIONS 104

6.5 SUPPLEMENTARY MATERIAL 105

7 Sequential oxidations of 5-hydroxymethyl furfural to furan-2,5-dicarboxylic acid by an evolved aryl-alcohol oxidase 111

7.1 INTRODUCTION 114

7.2 RESULTS AND DISCUSSION 117

7.3 CONCLUSIONS 122

7.4 MATERIAL AND METHODS 122

7.5 SUPPLEMENTARY MATERIAL 126

8 GLOBAL DISCUSSION 127

8.1 Directed evolution platform for AAO 129

8.1.1 Functional expression in *Saccharomyces cerevisiae* 130

8.1.2 Chimeric fusion genes for yeast expression 130

8.1.3 Dual high-throughput screening for AAO activity 131

8.1.4 Finding ancestral mutation H91N by directed evolution 132

8.2 Tandem-yeast expression system for AAO 133

8.2.1 Enhanced secretion by DNA shuffling and MORPHING at the signal peptide 133

8.2.2 Functional expression in *Pichia pastoris* 134

8.2.3 The glycosylation effect on the AAO 135

8.3 Secondary benzyl-alcohol oxidase by directed evolution 136

8.3.1 Atypical activity with secondary alcohols by saturation mutagenesis........ 136

8.3.2 Further mutational benefits by MORPHING 136

8.3.3 Site-directed *in vivo* recombination to polish mutational load.................. 137

8.3.4 Biochemical and computational analysis of LanDo variant........................ 137

8.4 Directed evolution to increase FFCA oxidation with AAO 139

8.4.1 Directed evolution of AAO for HMF and FFCA oxidation 140

8.4.2 Mutational analysis for the Bantha variant... 140

9 CONCLUSIONS 127

9.1 CONCLUSIONS 144

9.2 CONCLUSIONES.. 146

10 REFERENCES 149

11 ANNEX 164

11.1 Publications from the Doctoral Thesis.. 166

11.2 Other publications from the author 166

11.3 Copy of the publications from the doctoral thesis 168

ACRONYMS

AAO	Aryl-alcohol oxidase
ABTS	2,2'-azino-bis(3-ethylbenzothiazoline-6-sulphonic acid)
bp	Base pairs
CDH	Cellobiose dehydrogenase
DFF	2,5-Diformylfuran
dNTPs	Deoxyribonucleotides
DyP	Dye decolorizing peroxidase
$_{Ec}$AAO	Wild-type AAO expressed in *E. coli*
ee	Enantiomeric excess
epPCR	Error-prone PCR
FAD	Flavin adenine dinucleotide
FDCA	Furan-2,5-dicarboxylic acid
FFCA	5-Formyl-2-furancarboxylic acid
GLX	Glyoxal oxidase
GMC	Clucose-Methanol-Choline
GOX	Glucose oxidase
HMF	5-hydrodymethylfurfural
HMFO	5-hydrodymethylfurfural oxidase
HRPLs	High redox potential laccases
HTS	High throughput screening
IVOE	*in vivo* Overlap Extension
k_{cat}	Catalytic constant
k_{cat}/K_m	Catalytic efficiency
K_m	Michaelis-Menten constant
LiP	Lignin peroxidase
MnP	Manganese peroxidase
MORPHING	Mutagenic Organized Recombination Process by Homologous *IN vivo* Grouping
MOX	Methanol oxidase
MtL	*Myceliopthora thermophila* laccase
OD_{600}	Optical density at 600 nm
P_{AOX1}	Alcohol oxidase I promoter

PDB	Protein data bank
PELE	Protein Energy Landscape Exploration
P2O	Pyranose oxidase
QR	Quinone reductase
SEM	Selective expression medium
T_{50}	kinetic-thermostability
T_a	Thermoactivity
UPO	Unspecific peroxygenase
VP	Versatile peroxidase
wtAAO	Wild-type AAO expressed in *E. coli*

CHAPTER I:

INTRODUCTION

1.1 Aryl-alcohol oxidase

1.1.1 Natural context and general aspects

The aryl-alcohol oxidase (AAO, EC 1.1.3.7) is a fungal extracellular flavoenzyme that plays the role of H_2O_2 supplier to peroxidases and peroxygenases during natural lignin degradation. Representing around 10-25% of lignocellulose, the most abundant biological feedstock in nature, lignin is a recalcitrant three-dimensional aromatic biopolymer that only a few organisms, mainly belonging to white-rot fungi, are able to degrade (Isikgor and Becer 2015; Zhou et al. 2011). Indeed, the coordinated fungal attack on lignin by white-rot basidiomycetes is mediated by an enzymatic consortium formed by high-redox potential peroxidases (lignin peroxidases -LiP-, manganese peroxidases -MnP-, versatile peroxidases –VP-, dye decolorizing peroxidases -DyP-), unspecific peroxygenases -UPO-, laccases and enzymes that supply H_2O_2 (Martinez et al. 2005; Martinez et al. 2009), **Figure 1.1**. Accordingly, the set of H_2O_2 supplying enzymes is comprising different oxidases including: i) glyoxal oxidase (GLX), a copper radical enzyme that works in synergy with LiP and MnP (Kersten and Cullen 2007); pyranose oxidase (P2O), a FAD-dependent enzyme with an activity that can be also related to the reduction of the quinones produced during the lignin combustion (Leitner et al. 2001); and the AAO which coordinates its oxidative activity with the action of intracellular dehydrogenases creating an aromatic alcohol/aldehyde redox cycle to generate a constant supply of H_2O_2 to the ligninolytic peroxidases and peroxygenases (Hernandez-Ortega et al. 2012a). AAO activity was first detected in *Trametes versicolor* cultures (Farmer et al. 1960) and since then it has been found in several other species including *Fussarium* species (Iwahara et al. 1980; Regalado et al. 1999), *Pleurotus* species (Bourbonnais and Paice 1988; Guillen et al. 1992; Sannia et al. 1991; Varela et al. 2000; Galperin et al. 2016), *Bjerkandera adusta* (Romero et al. 2009), *Botrytis cinerea* (Goetghebeur et al. 1993), *Geotrichum candidum dec 1* (Kim et al. 2001), *Phanerochaete chrysosporium* (Asada et al. 1995) and *Ustilago maydis* (Couturier et al. 2016)). Initially located on the hyphal surface, the monomeric extracellular AAO presents activity on lignin-derived molecules as well as aromatic fungal metabolites. Additionally, the released H_2O_2 generates highly reactive hydroxyl radicals via the Fenton reaction ($Fe^{2+} + H_2O_2 \rightarrow OH^{\bullet} + OH^{-} + Fe^{3+}$). These oxygen species can act as diffusible electron carriers that help to depolymerize the lignin structures (Hernandez-Ortega et al. 2012a).

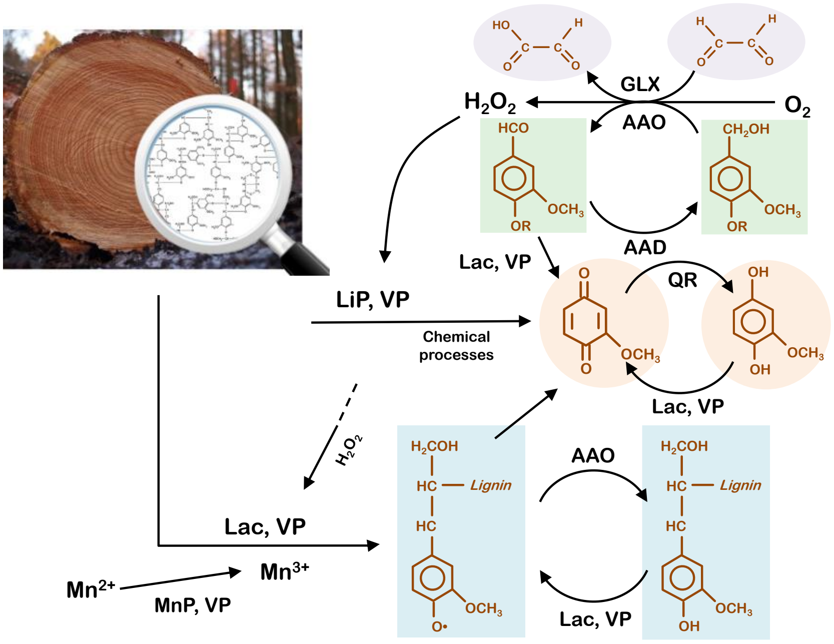

Figure 1.1. Scheme of the ligninolytic consortium of enzymes. AAO: aryl-alcohol oxidase, Lac: laccases, LiP: lignin peroxidases, MnP: manganese peroxidases, VP: versatile peroxidases, GLX: glyoxal oxidase, AAD: aryl-alcohol deshidrogenase, QR: quinone reductases. *The exact physiological role of DyP and UPO within the ligninolytic secretome is still pending on further studies.

From the pool of identified AAOs, the oxidase from *Pleurotus eryngii* is the most extensively characterized, being these studies the framework and departure point for this Doctoral Thesis. The first identification of AAO activity in *P. eryngii* cultures is dated in 1988 (Guillén et al. 1990), but it was during the early nineties when the enzyme was purified and characterized as a monomeric flavoprotein of 72.6 kDa with a glycosylation contribution of around 15% (Guillén et al. 1992). In the time following, the obtainment and cloning of the AAO gene (Varela et al. 1999) opened the door to the heterologous expression of the enzyme in *Emericella nidulans* (Varela et al. 2001) as well as in *Escherichia coli* after *in vitro* refolding (Ruiz-Dueñas et al. 2006). Considering its substrate scope, the AAO is capable of oxidizing primary benzyl alcohols with different chemical arrangements. The enzyme presents the highest activity with electron donor substituents on the aromatic ring, such as with *p*-methoxybenzyl alcohol (anysil alcohol), the natural substrate of the enzyme and a metabolite present in fungal cultures. Additionally, the AAO can oxidize unsubstituted benzyl alcohol and, with similar reaction rates, halogenated benzyl alcohols. Not only the enzyme shows efficiency with aromatic alcohols, but the AAO is also highly active with aliphatic polyunsaturated alcohols like 2,4-hexadien-1-ol (Ferreira et al. 2005). Recently the substrate palette of alcohols has been expanded with the conversion of the single unsaturated *trans*-2-hexen-1-nol for the preparation of Green note *trans*-2-hexenal (van Schie et al. 2018). Already hinted by the presence of excessive stoichiometric molecules of H_2O_2 upon alcohol oxidation, the AAO also catalyzes the oxidation of aromatic aldehydes into the correspondent acids. The preference of *p*-nitrobenzaldehyde, with electron withdrawing substituent on the aromatic ring, suggests an analogous reaction mechanism as in the oxidation of alcohols via *gem*-diol species (Ferreira et al. 2010), **Table 1.1**.

1.1.2 The AAO from *P. eryngii* as part of the GMC superfamily

From a taxonomic point of view, the AAO belongs to the GMC (glucose-methanol-choline) superfamily of oxidoreductases. Among the members of this group of flavoenzymes we can also find glucose oxidase (GOX), methanol oxidase (MOX), choline oxidase, cholesterol oxidase, cellobiose dehydrogenase (CDH), pyranose oxidase and 5-Hydroxymethylfurfural oxidase (HMFO) (Wongnate and Chaiyen 2013; Dijkman et al. 2015). In recent years, the mimivirus has been described as the fourth largest virus ever discovered. Interestingly, the R135 protein from the *Acanthamoeba polyphaga mimivirus*, one of the major components of the outer layer of the virus, is classified as a putative GMC-type oxidoreductase with one of the closest sequence identity (18%) with the AAO from *P. eryngii* (Klose et al. 2015). Showing differential catalytic activities, GMC oxidoreductases show a related architecture based on several consensus sequences. The most characteristic structural trait is the conserved ADP-binding ßαß motif contained in the N-terminus, this super-secondary structure is related to the binding of nucleotides and it is indeed present in the AAO within its FAD-binding domain (Fernández et al. 2009; Cavener 1992). A recent evolutionary study of 10 polyporales genomes with the identification of 95 GMCs has defined the presence of two main groups: AAOs (42 sequences) and MOXs (39 sequences) followed by small groups of CDHs, P2Os, and GOXs. As proof of the main role in lignin degradation, AAO sequences were six-fold more present in white-rot species compared with the cellulose degrading brown-rot fungi (Ferreira et al. 2015a).

Table 11. Catalytic efficiencies of the AAO from *P. eryngii* for representative substrates.

		k_{cat}/K_m (s^{-1} mM^{-1})
Benzyl alcohol	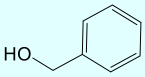	47 ± 9
p-Fluorobenzyl alcohol	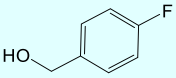	59 ± 6
m-Fluorobenzyl alcohol	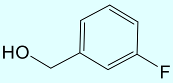	13 ± 1
p-Chlorobenzyl alcohol	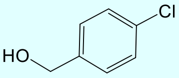	398 ± 32
m-Chlorobenzyl alcohol	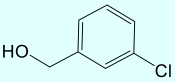	203 ± 4
p-Methoxybenzyl alcohol	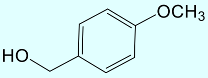	5230 ± 620
m-Methoxybenzyl alcohol	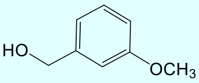	65 ± 24
Veratryl alcohol	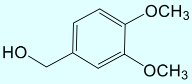	210 ± 5
Isovanillyl alcohol	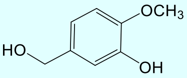	152 ± 5
3-Chloro-*p*-methoxybenzyl alcohol	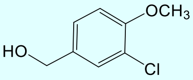	4090 ± 200
2,4-Hexadien-1-ol	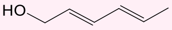	1270 ± 60
Cinnamyl alcohol	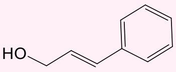	78 ± 11
m-Chlorobenzaldehyde	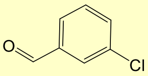	0.64 ± 0.05
3-Chloro-*p*-methoxybenzaldehyde	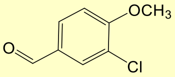	0.085 ± 0.006
m-Fluorobenzaldehyde	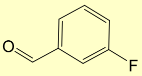	0.40 ± 0.02
p-Nitrobenzaldehyde	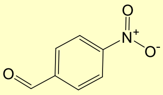	0.31 ± 0.006

*Data adapted from Carro et al. 2016.

The crystallographic structure of the AAO from *P. eryngii* was resolved with a resolution of 2.4 Å after *E. coli* expression and *in vitro* refolding in 2009 (PDB entry: 3FIM), **Figure 1.2**. In a polypeptide of 566 residues, its structure is arranged in two main domains: the FAD binding domain and the substrate binding domain. The most interesting topological feature on the protein is the buried active site where the access of the solvent is strictly limited by an aromatic constriction. Hydrophobic channels to access the active site are related to gas substrates like molecular oxygen. Other oxidases with access-challenged active cavities are cholesterol oxidase and vanillyl-alcohol oxidase while the formation of multimeric complexes is the strategy of P2O and GOX as a limitation of the substrate entrance. As observed on the crystal, the catalytic cavity contains a non-covalently bound FAD molecule and the catalytic His502 and His546 while the hydrophobic bottleneck connecting this active site with the solvent is formed by Tyr92, Phe367 and Phe501 (Fernández et al. 2009), **Figure 1.3**. Site-directed experiments at positions Tyr92, Phe501, His502 and His546 have highlighted the importance of those residues for the catalytic activity of the AAO (Ferreira et al. 2006).

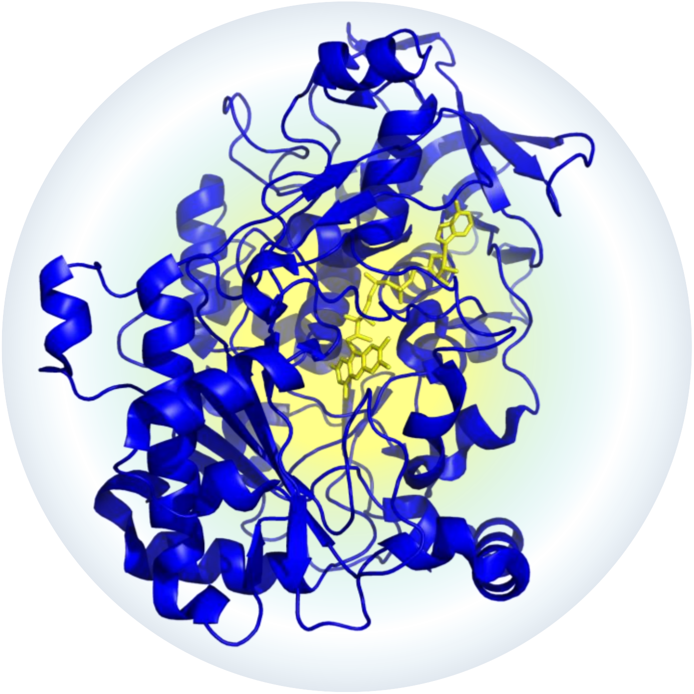

Figure 1.2. AAO crystal structure. Based on the PDB structure 3FIM. The FAD cofactor is depicted in yellow.

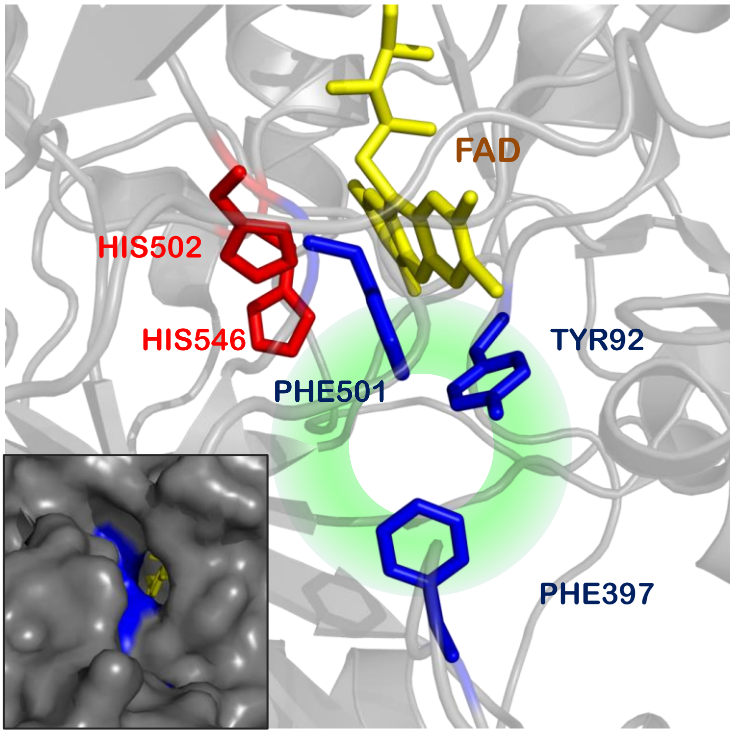

Figure 1.3. Active site of the AAO. Mapping of the residues forming the aromatic constriction highlighted in blue, the catalytic His residues (in red) and the FAD in yellow. The inset shows the access channel to the active site (on surface mode).

1.1.3 Mechanistic and structural aspects of the AAO catalysis

The insights of the mechanism of action of the AAO have been thoroughly studied during the last years by experimental and computational approaches (Ferreira et al. 2009; Hernandez-Ortega et al. 2011a; Hernandez-Ortega et al. 2012c). Accordingly, the catalytic cycle of the AAO involves dehydrogenative oxidation including two half-reactions, **Figure 1.4**:

(i) the reductive half-reaction where the donor alcohol is two-electron oxidized by the FAD, receiving the cofactor one of the α-Hs from the alcohol through a highly enantioselective hydride transfer, yielding the aldehyde product and the reduced flavin.

(ii) the oxidative half-reaction in which molecular oxygen is two-electron reduced by the FAD producing H_2O_2 and releasing the reoxidized cofactor.

The alcohol oxidation is the rate limiting step with a hydride transfer to the cofactor and a proton transfer to the catalytic base. This half-reaction takes place via a concerted non-synchronous bond breaking mechanism.

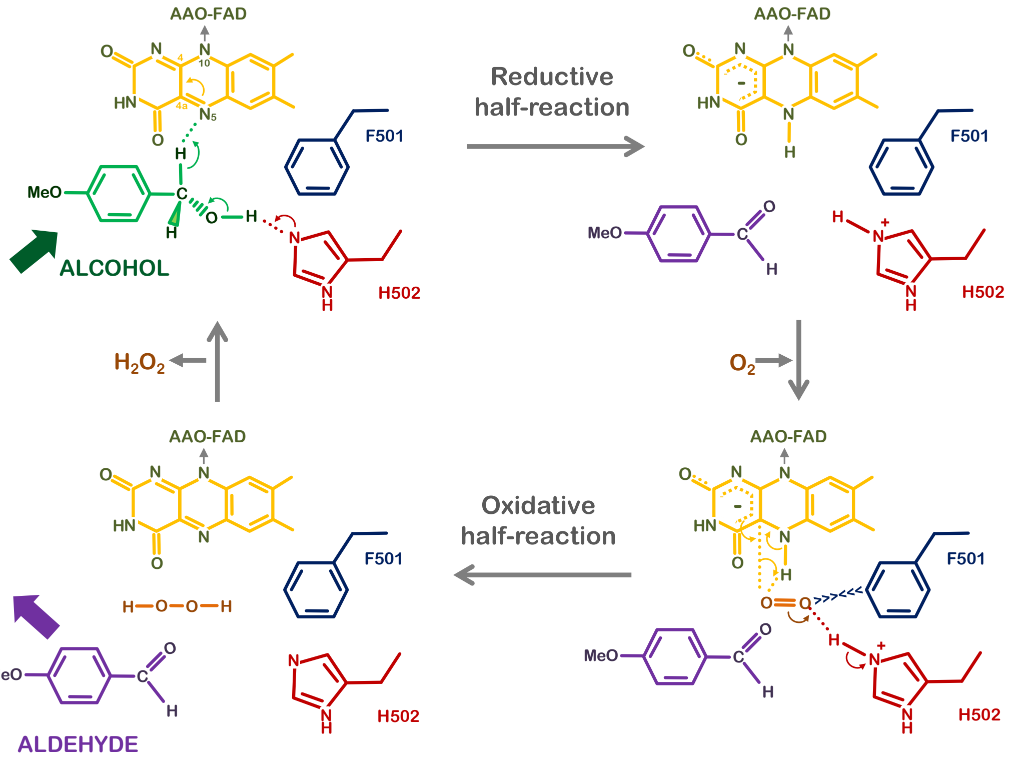

Figure 1.4. AAO catalytic cycle. Details of the half-reactions catalyzing the oxidation of alcohols into aldehydes. Adapted from Hernandez-Ortega et al. 2012a.

Ligand diffusion studies with aromatic and aliphatic primary alcohols situated the substrate entrance to the enzyme next to Pro402 at around 17 Å from the cofactor ring. Further on the diffusion, oscillations on loop Gln395-Thr406 were observed together with the substrate transit (Hernandez-Ortega et al. 2011a). This loop is a characteristic feature in the GMC enzymes, presenting insertions and deletions, whose presence can be related to a mechanism of substrate diffusion control on monomeric proteins. The Phe397 of the aromatic constriction oscillates with the substrate acting as a gate on the channel pathway, and therefore it has different implications on the catalytic activity. Accordingly, the presence of Phe397 on the hydrophobic funnel to the active site benefits the correct positioning of the substrate and the subsequent reactivity. Another important implication is that the regulation of the product release is facilitated by the movements of the phenylalanine side chain (Carro et al. 2018). Further substrate migration towards the active site readjusts the side chains of Leu315, Ile391 and Tyr92. Not fully conserved into the GMC superfamily, the Tyr92 of the aromatic constriction stabilizes the alcohol/aldehyde benzylic rings at the active site via π-π stacking interactions that regulate the mechanistic traffic of the aldehyde products and the molecular O_2 (Ferreira et al. 2015b). The third residue part of the aromatic constriction, the Phe501, plays an important role in the oxidative half-reaction of the mechanism.

Diffusion simulations with O_2 pointed out the importance of the presence of the side chain of Phe501 for the correct positioning of the substrate in relation to the flavin C4a and the His502 Nϵ (Hernandez-Ortega et al. 2011b). The core of the active cavity of the AAO presents two histidine residues, His502 and His546, with their side chains oriented to the upper part of the FAD cofactor. As another consensual structural feature, conserved His-His and His-Asn residue pairs are located at catalytic distances to the FAD throughout the active sites of the GMC superfamily members. With studies that shown a dramatic decrease of the catalytic efficiency with the removal of the His502, compared with a modest effect when His546 is mutated, together with molecular dynamic predictions of unprotonated Nϵ for His502, this residue is pointed to play the role of catalytic base receiving a proton transfer concerted to the hydride transfer to the FAD. The role of His546 consists of the H-binding of the alcohol facilitating a proper substrate positioning (Hernandez-Ortega et al. 2012b).

1.2 Biotechnological and industrial applications of AAO

The AAO activity on a broad range of alcohols and aldehydes together with the production of H_2O_2 from atmospheric O_2, have awakened biotechnological interests for several potential industrial applications. Mimicking its natural role within the ligninolytic consortium, the AAO could be part of a self-sufficient synthetic secretome in a proper industrial host as yeast (referred to as "white-rot yeast") (Gonzalez-Perez and Alcalde 2014; Martinez et al. 2017). An engineered microbe including the most interesting fungal enzymes could fulfil a number of destinations in biorefineries like the production of biofuels and added value chemicals. It is also worth noting that the gradual release of H_2O_2 can fit self-sufficient systems with peroxidases/peroxygenases for efficient cascade reactions. Such systems could be explored with the co-expression of the enzymes or with the creation of chimeric fusion proteins (Gonzalez-Perez and Alcalde 2014; Alcalde 2015). Another collaborative example is the use of laccase combined with AAO for pulp bleaching in the paper industry (Sigoillot et al. 2005). Not to be underestimated is the potential use of AAO as biocatalyst in organic synthesis. One characteristic case is the production of flavors and fragrances like aromatic aldehydes such as benzaldehyde (bitter almond aroma), cinnamaldehyde (cinnamon flavor and aroma) or anisaldehyde (anisic aroma) (Lapadatescu et al. 2000). Among the most exciting application areas for AAO biotransformations are the resolution of chiral mixtures of alcohols and the catalysis of furfural-derivate cascade reactions. Indeed they are an important part of the core in the present Doctoral Thesis, and therefore they are further explained below.

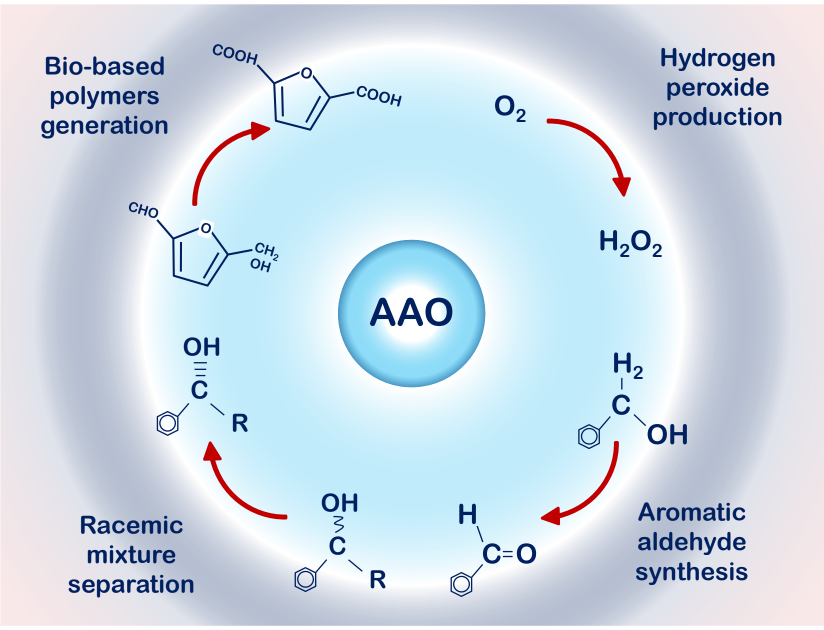
Bio-based polymers generation
Hydrogen peroxide production
COOH
COOH
O
CHO
CH2 OH
O_2
H_2O_2
AAO
OH
C
R
H_2
C
OH
OH
C
R
H
C=O
Racemic mixture separation
Aromatic aldehyde synthesis

Figure 1.5. Scheme of the biotechnological applications of the AAO.

1.2.1 Deracemization of benzyl secondary alcohols

Chiral chemistry presents a continuous challenge in drug development processes. Indeed, enantiopure building blocks are heavily demanded to grant medical drugs particular biological activities (Caldwell 2001; Sekhon 2013; Chhabra et al. 2013). Along those lines, the AAO makes a promising candidate for the enantioselective oxidation of chiral benzyl alcohols. As mentioned in section 1.1.3., the mechanism for alcohol oxidation by the AAO consists of a hydride abstraction from the Cα position of the alcohol simultaneous to a proton transfer to the catalytic base of the enzyme. The stereoselectivity of the hydride transfer has been extensively studied by Hernandez-Ortega et. Al (2012c). The relative positions at the active site of the *p*-methoxybenzyl alcohol, the FAD cofactor and the catalytic His502 were estimated by ligand diffusion computational simulations. Accordingly, PELE software situated the pro-R α-hydrogen at 2.4 Å from the flavin N5 and the hydroxy hydrogen at 2.5 Å from the His502 Nϵ. These favorable positions are in agreement with the experimental data obtained with the use of deuterated *p*-methoxybenzyl alcohols and the calculation of kinetic isotope effects (KIE). Primary KIE values of around 6 were estimated for the R enantiomer, that is, a stereoselective hydride abstraction happens from the pro-R position. Unfortunately, the activity with the secondary 1-(*p*-methoxyphenyl)ethanol appeared residual with orders of magnitude lower apparent efficiency compared with primary alcohols. On the grounds that a wider space in the restricted active site would avoid steric hindrances and better accommodate a bulkier secondary substrate, the variant F501A was created to remove the side chain of the aromatic residue. As a result, the activity with primary alcohols was reduced improving the relative activity with the secondary substrate (Hernandez-Ortega et al. 2012c). Hence, this variant is an interesting departure point to increase the total activity with chiral substrates by protein engineering.

1.2.2 Furfural derivatives cascade reactions

Greener renewable technologies could be developed with an efficient production of added value molecules and platform chemicals from biomass feedstocks. The 5-hydroxymethylfurfural (HMF) is one of the bio-derived chemicals with bigger biotechnological potential that can be easily obtained from biomass as a sugar dehydration product (Van Putten et al. 2013). Three consecutive oxidations transform HMF into furan-2,5-dicarboxylic acid (FDCA), a promising building block that can be used in polymer industry. FDCA can be enzymatically prepared from HMF through the sequential two e^- oxidation of two furanic intermediates, 2,5-diformylfuran (DFF) and 5-formyl-2-furancarboxylic acid (FFCA). This biocatalytic conversion has been mainly studied for two oxidases from the GMC superfamily, the AAO from *Pleurotus eryngii* and the bacterial 5-hydroxymethylfurfural oxidase (HMFO; 1.1.3.47) from *Methylovorus sp*. The HMFO presents a catalytic profile similar to the AAO. Apart from furfural derivatives, this flavoenzyme is mainly active on primary aromatic alcohols and conjugated aliphatic systems like 2,4-hexadien-1-ol. Also similarly, the HFMO is not able to oxidize secondary alcohols and it is active on hydrated aldehydes. Taking into account these common characteristics it is interesting that the sequence similarity between both oxidases is remarkably low (<30%) while their natural roles clearly also diverge considering the HMFO is an intracellular enzyme (Dijkman and Fraaije 2014). The AAO is considered inactive towards FFCA while the HMFO is the first oxidase described performing the three consecutive oxidations from HMF to FDCA, although long incubation times are needed because of the low activity with FFCA (Dijkman et al. 2014). Thus, directed evolution methodologies could be applied to the AAO to help overcoming the constriction of the FFCA into FDCA oxidation.

1.3 Directed evolution

To convert native enzymes into industrial catalysts, protein engineering approaches can be applied to sculpt their properties in defined applications. The best present-day methodology to dominate such challenge is without doubt directed evolution, from the pioneering work of Prof. Frances H. Arnold, recently awarded the Nobel Prize in Chemistry 2018 for this invention and its implication in a more sustainable chemistry, **Figure. 1.6** . Giving a conceptual twist to the well-known evolution algorithm from Charles Darwin (i.e. "*the survival of the fittest*"), the directed evolution cycle is connected by three essential steps: i) generation of DNA diversity by random mutagenesis and/or recombination; ii) functional expression of the library in a proper heterologous host organism; and iii) screening of the expressed variants considering the characteristics of interest. This process is repeated until the desired enzyme trait arises, **Figure 1.7** (Bloom and Arnold 2009; Turner 2009; Bornscheuer et al. 2012; Molina-Espeja et al. 2016).

During the last 15 years, strong efforts have been made to evolve the different oxidoreductases from the ligninolytic consortium, addressing needs that range from bioremediation to green synthetic chemistry. In these enterprises, reliable heterologous functional expression platforms, ad-hoc library creation methods, and specific screening assays and computational protocols have been applied to fully exploit the true power of evolution (Alcalde 2015). Some of these examples are listed below:

(i) The directed evolution of the medium-redox potential laccase from *Myceliophthora thermophila* (MtL) enhanced secretion levels in *S. cerevisiae* from scratch up to 18 mg/L, (Bulter et al. 2003). Afterward, the secreted variant was adapted to be active in organic co-solvents (Zumárraga et al. 2007), alkaline pH (Torres-Salas et al. 2013) and then evolved to synthesize heteropolymeric dyes (Vicente et al. 2016). Two high-redox potential laccases (HRPLs) from *Pycnoporus cinnabarinus* (PcL) and the PM1 basidiomycete (PM1L) were also evolved for functional expression in yeast achieving secretion numbers of 2 and 8 mg/L respectively (Camarero et al. 2012; Mate et al. 2010). The PM1L was subsequently evolved to be active in human plasma and blood (Mate et al. 2013b) and more recently to increase its redox potential (Mateljak et al. 2019), as well as to create a family of thermostable chimeras (Mateljak et al., 2019).

(ii) The versatile peroxidase from *Pleurotus eryngii* was functionally expressed in *S. cerevisiae* by directed evolution reaching secretion levels of 21 mg/L. Afterward, the stabilities of the enzyme towards temperature (Garcia-Ruiz et al. 2012) and H_2O_2 (Gonzalez-Perez et al. 2014b) were enhanced and, more recently, its pH profile was shifted to basic conditions (Gonzalez-Perez et al. 2016).

(iii) In like manner, the unspecific peroxygenase from *Agrocybe aegerita* was secreted in yeasts thanks to directed evolution (8 mg/L in *S. cerevisiae* and over 200 mg/L in *Pichia pastoris*) (Molina-Espeja et al. 2014; Molina-Espeja et al. 2015) and it has since been evolved for the production of 1-naphtol from naphthalene (Molina-Espeja et al. 2016), for the synthesis of human-drug metabolites (HDMs) (Gomez de Santos et al. 2018; Gomez de Santos et al. 2019) as well as submitted to neutral drift and focused evolution for activity and stability (Mate et al. 2017; Martin -Diaz et al., 2018).

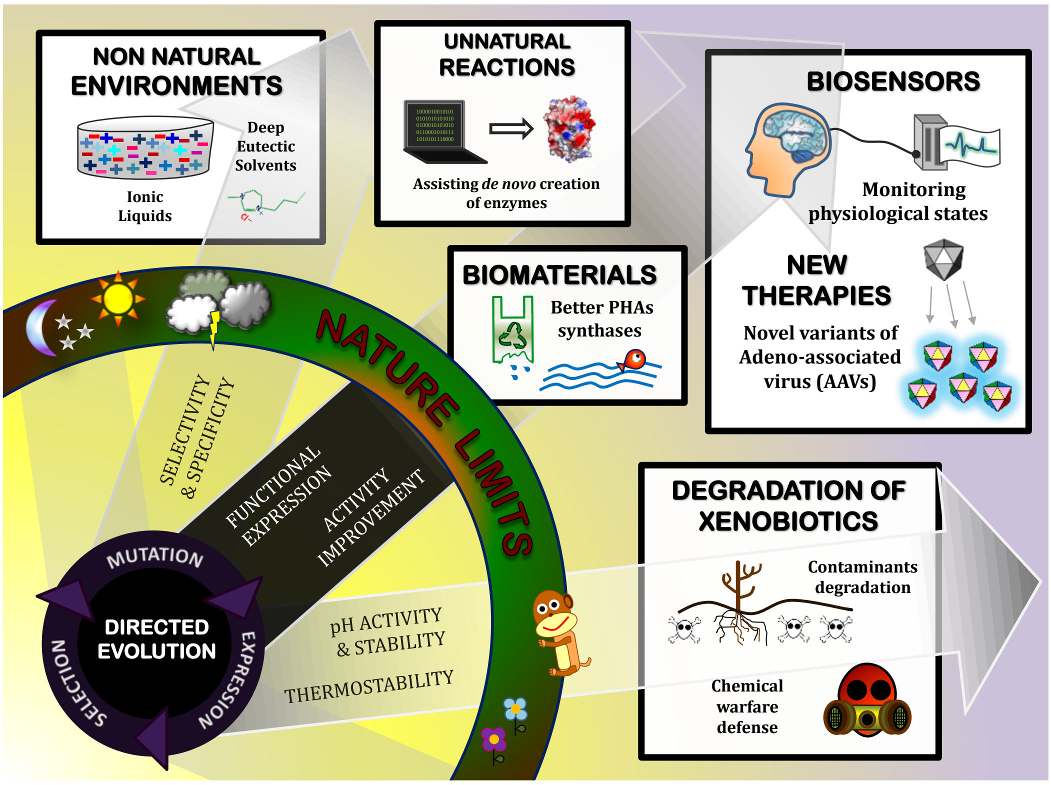
NON NATURAL ENVIRONMENTS
Deep Eutectic Solvents
Ionic Liquids
UNNATURAL REACTIONS
Assisting de novo creation of enzymes
BIOSENSORS
Monitoring physiological states
NEW THERAPIES
Novel variants of Adeno-associated virus (AAVs)
BIOMATERIALS
Better PHAs synthases
DEGRADATION OF XENOBIOTICS
Contaminants degradation
Chemical warfare defense
NATURE LIMITS
SELECTIVITY & SPECIFICITY
FUNCTIONAL EXPRESSION
ACTIVITY IMPROVEMENT
pH ACTIVITY & STABILITY
THERMOSTABILITY
MUTATION
EXPRESSION
SELECTION
DIRECTED EVOLUTION

Figure 1.6. Directed evolution beyond the nature limits. Pushing the boundaries of the biotechnological rainbow, directed evolution has borrowed enzymes from their role as biological elements to be developed into active and stable catalysts in unnatural environments. Mimicking Darwin's algorithm of natural selection, the artificial evolution process is giving rise to customized enzymes with uses within pharma, chemical, environmental and energy sectors.

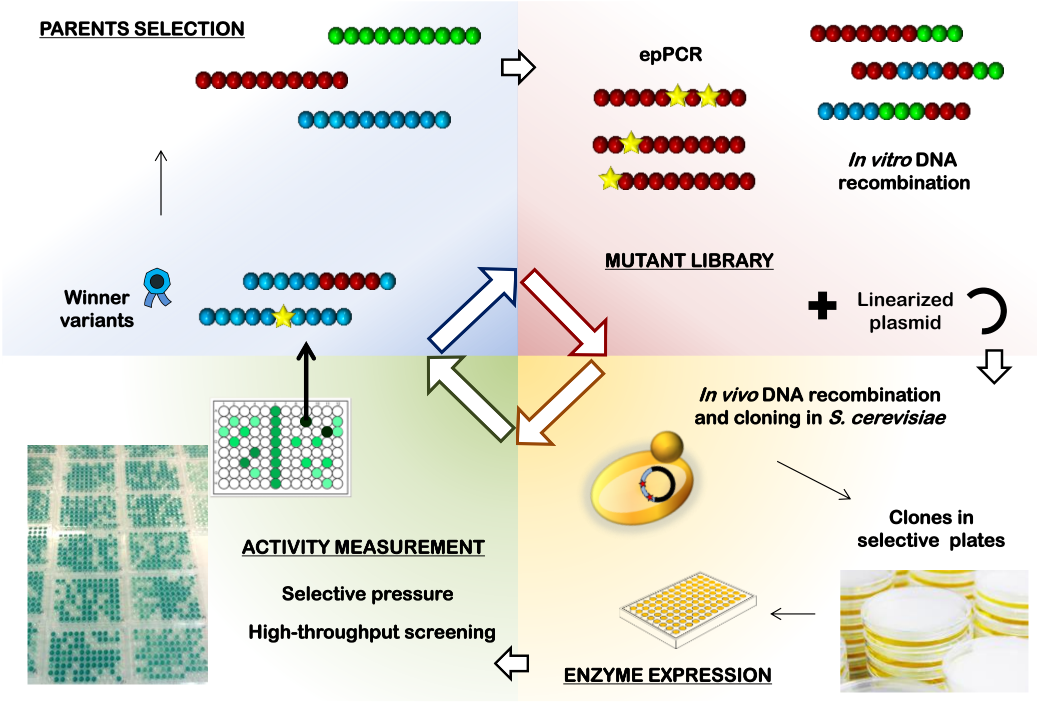
PARENTS SELECTION
epPCR
In vitro DNA recombination
MUTANT LIBRARY
Linearized plasmid
Winner variants
In vivo DNA recombination and cloning in S. cerevisiae
Clones in selective plates
ACTIVITY MEASUREMENT
Selective pressure
High-throughput screening
ENZYME EXPRESSION

Figure 1.7. Representation of a standard directed evolution cycle. the three main steps in a laboratory evolution round are: the generation of molecular diversity; the functional expression of the mutant library in a proper host and the screening of improved variants, 'winners'.

1.3.1 *Saccharomyces cerevisiae* as a tool-box for DNA diversity

Without doubt, one of the most important advantages of *S. cerevisiae* for directed evolution is its high frequency of homologous DNA recombination, a useful molecular tool-box for the development of library creation methods. The Rad51 recombinase (ortholog of the bacterial recA) and other ancillary factors organize the recombination machinery of *S. cerevisiae* allowing DNA fragments with 40 homologous nucleotides to be assembled with 60% efficiency (Mate et al. 2017; Gonzalez-Perez et al. 2012; Van Komen et al. 2006). This feature not only facilitates the *in vivo* cloning of libraries into linearized expression vectors in a single transformation step but also opens the door to boost genetic diversity. Thus, a continuously growing family of DNA recombination methods based on the *in vivo* gap repair mechanism in yeast is available in the laboratory to aid the evolution of ligninases and many other enzymes.

Based on the engineering of specific overlapping homologous areas, the IVOE (In Vivo Overlap Extension) protocol has been developed as a fast and reliable way to achieve site directed mutagenesis (introducing deletion and insertion mutations), to construct site-saturation combinatorial libraries, and to perform gene assembly, while the proof-reading apparatus of *S. cerevisiae* precludes the insertion of unwanted mutations (Alcalde 2010). Due to its simplicity and versatility, IVOE has become indispensable for our ligninase directed evolution campaigns, **Figure**

1.8.A. (Alcalde 2015; Mate et al. 2017). Likewise, the *in vivo* shuffling of beneficial mutations is systematically applied to the evolution of laccases, VPs and UPOs. As long as DNA sequence identities are above 50% and mutations are situated at a distance of at least 20 residues from each other, *in vivo* shuffling can be used to search for beneficial combinatorial effects among the offspring of variants (Kevin R et al. 1997), **Figure 1.8.B**.

With the aim of creating smarter libraries that place less of a demand on screening, MORPHING (Mutagenic Organized Recombination Process by Homologous IN vivo Grouping) has proved to be a useful mutagenesis/recombination technique in the evolution of ligninases (Gonzalez-Perez and Alcalde 2014a). Through MORPHING, random mutations and recombination events can be introduced in specific segments while protecting the remaining protein structure from mutagenesis, **Figure 1.8.C**. Mutant segments as short as 30 amino acids are subjected to mutagenic PCR, whereas the remaining regions are amplified with high-fidelity polymerases. The resulting DNA fragments are flanked with homologous overhangs and they are spliced *in vivo* along with the linearized plasmid in a one-pot transformation step. While MORPHING has been successfully used to evolve signal peptides (Gonzalez-Perez and Alcalde 2014a; Molina-Espeja et al. 2014), it has also been applied in the focused evolution of many relevant biochemical properties of ligninases. One of the first examples of MORPHING was the improvement of the VP tolarance in the presence of H_2O_2 (Gonzalez-Perez et al. 2014b). Independent segments were selected to introduce mutations using loads from 1 to 5 mutation per segment in order to identify important structural determinants for the oxidative stabilization of VP. One of the last cases of MORPHING involved adapting UPO for the selective synthesis of HDMs. After molecular docking simulations with the beta blocker propranolol, a protein segment that contains important recognition motifs was subjected to MORPHING. As a result, a single substitution (F191S) at the entrance of the heme access channel was seen to produce a dramatic enhancement of two orders of magnitude in the catalytic efficiency for propranolol, with 99% regioselectivity during the synthesis of the HDM 5-OH propranolol (Gomez de Santos et al. 2018). Most of these protocols along with new methods based on yeast physiology (see site-directed recombination *in vivo*, **Chapter VI**) have been applied in the current Doctoral Thesis to engineer a set of efficient AAO variants.

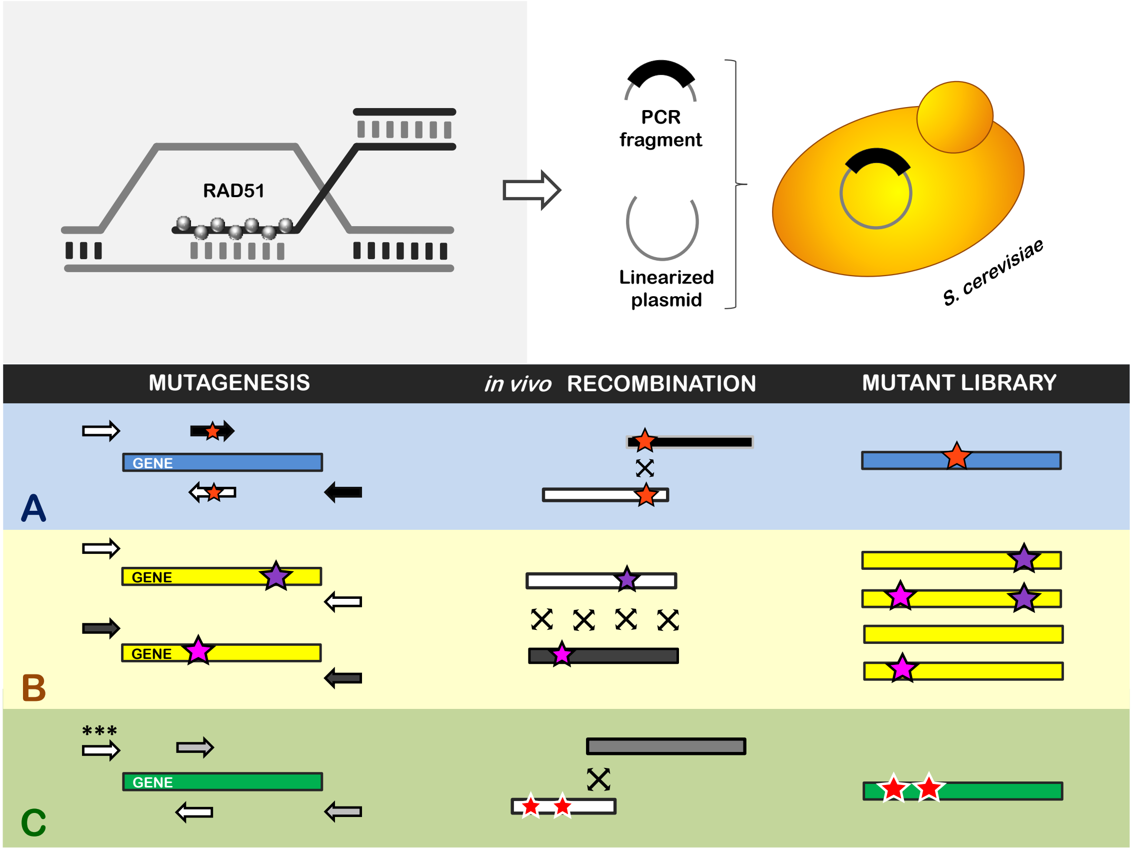
RAD51
PCR fragment
Linearized plasmid
S. cerevisiae
MUTAGENESIS
in vivo RECOMBINATION
MUTANT LIBRARY
GENE
A
GENE
GENE
B
***
GENE
C

Figure 1.8 Library creation methodologies on *S. cerevisiae*: Based in the homologous DNA recombination machinery: (A) IVOE; (B) DNA Shuffling; (C) MORPHING.

CHAPTER II:

OBJECTIVES

The main objectives of this Doctoral Thesis are the development of a platform for the directed evolution of AAO to unlock the synthetic abilities of this enzyme, which we have targeted them in the resolution of racemic mixtures of secondary alcohols as well as in the synthesis of DFCA from HMF. These goals are comprising the following tasks:

- To achieve functional expression (secretion) in *Saccharomyces cerevisiae*, a proper host organism for directed evolution experiments.
- To develop sensitive and robust high-throughtput screening assays whereby screening AAO mutant libraries.
- To generate `*smart*´ mutant libraries aided by the high frecuency of homologous DNA recombination of *S. cerevisiae*.
- To set up a tandem-yeast expression system for the design (in *S. cerevisae*) and overproduction (in *Pichia pastoris*) of AAO variants.
- To unlock the activity of the AAO for secondary benzyl-alcohols by directed evolution.
- To complete the three sequential oxidation from HMF to FDCA by AAO.

CHAPTER III:

Focused directed evolution of aryl-alcohol oxidase in yeast by using chimeric signal peptides

This Chapter represents the departure point of this Doctoral Thesis, in which we established the bases for the directed evolution of AAO, including a reliable heterologous expression system together with sensitive “blind” HTS assay for designing biochemical properties.

CHAPTER III

Focused directed evolution of aryl-alcohol oxidase in yeast by using chimeric signal peptides

Javier Viña-González, David González-Pérez, Patricia Ferreira, Ángel T. Martínez
and Miguel Alcalde

Applied and Environmental Microbiology 81: 6451-6462.

http://doi.org/10.1128/AEM.01966-15

Aryl-alcohol oxidase (AAO) is an extracellular flavoprotein that supplies ligninolytic peroxidases with H_2O_2 during natural wood decay. With a broad substrate specificity and highly stereoselective reaction mechanism, AAO is an attractive candidate for studies into organic synthesis and synthetic biology, yet the lack of suitable heterologous expression systems has precluded its engineering by directed evolution. In this study, the native signal sequence of AAO from *Pleurotus eryngii* was replaced by those of the mating α-factor and the K1 Killer toxin, as well as different chimeras of both prepro-leaders in order to drive secretion in *Saccharomyces cerevisiae*. The secretion of these AAO constructs increased in the order preproα-AAO>preαproK-AAO>preKproα-AAO>preproK-AAO. The chimeric preαproK-AAO was subjected to focused-directed evolution with the aid of a dual screening assay based on the Fenton reaction. Random mutagenesis and DNA recombination was concentrated on two protein segments (Met[α1]-Val109, Phe392-Gln566) and an array of improved variants was identified, among which the FX7 mutant (harboring the H91N mutation) showed a dramatic 96-fold improvement in total activity with secretion levels of 2 mg/L. Analysis of the N-terminal sequence of the FX7 variant confirmed the correct processing of the preαproK hybrid peptide by the KEX2 protease. FX7 showed higher stability in terms of pH and temperature whereas the pH activity profiles and the kinetic parameters were maintained. The Asn91 lies in the flavin attachment loop motif, and it is a highly conserved residue in all members of the GMC superfamily, except *P. eryngii* and *P. pulmonarious* AAO. The *in vitro* involution of the enzyme by restoring the consensus ancestor Asn91 promoted AAO expression and stability.

3.1 INTRODUCTION

Aryl-alcohol oxidase (AAO, EC 1.1.3.7) is a flavoenzyme of the GMC (glucose-methanol-choline) oxidoreductase superfamily, the members of which share an N-terminal FAD-binding domain containing the canonical ADP-binding motif. Secreted by several white-rot fungi, this monomeric flavoprotein plays an essential role in natural lignin degradation (Hernandez-Ortega et al. 2012a). Accordingly, AAO oxidizes lignin-derived compounds and aromatic fungal metabolites, releasing H_2O_2 that is required by ligninolytic peroxidases to attack the plant cell-wall (Ruiz-Dueñas and Martínez 2009). Moreover, the H_2O_2 produced by AAO is an efficient vehicle to generate highly reactive hydroxyl radicals through the Fenton reaction ($Fe^{2+} + H_2O_2 \rightarrow OH^{\bullet} + OH^{-} + Fe^{3+}$), such that $OH^{\bullet}$ can act as a diffusible electron carrier to depolymerize plant polymers. AAO oxidizes a variety of aromatic benzyl (and some aliphatic polyunsaturated) alcohols to the corresponding aldehydes. In addition, AAO participates in the oxidation of aromatic aldehydes to the corresponding acids and also has activity of furfural derivatives (Ferreira et al. 2010).

The past few years have witnessed an intense effort to discern the basis and mechanism of action underlying AAO catalysis (Ferreira et al. 2010; Ferreira et al. 2006; Ferreira et al. 2009; Hernandez-Ortega et al. 2011a; Hernandez-Ortega et al. 2011b; Hernandez-Ortega et al. 2012a; Hernandez-Ortega et al. 2012b; Ferreira et al. 2015b). The AAO catalytic cycle involves dehydrogenative oxidation mediated by two half-reactions: i) the reductive half-reaction in which the donor alcohol is two-electron oxidized by the FAD co-factor, the latter receiving one of the alcohol's α-Hs through a hydride transfer process that yields the aldehyde product and the reduced flavin; and ii) the oxidative half-reaction, in which O_2 is two-electron reduced by the FAD, releasing H_2O_2 and the reoxidized flavin (Ferreira et al. 2009).

Directed molecular evolution is by far the best strategy currently available to design enzymes to industrial standards (Bloom and Arnold 2009; Turner 2009; Jäckel and Hilvert 2010; Bornscheuer et al. 2012). However, AAO has not been subjected to directed evolution, probably due to the lack of appropriate functional expression systems. Indeed, AAO has only been heterologous expressed in *Aspergillus nidulans* (Varela et al. 2001), an unsuitable host for directed evolution experiments (Pourmir and Johannes 2012), and in *Escherichia coli* after the in vitro refolding of inclusion bodies, an approach non-compatible with directed evolution campaigns (Ruiz-Dueñas et al. 2006).

In the current study, the native signal peptide of AAO was replaced by two different signal sequences to drive its functional expression in *Saccharomyces cerevisiae*: i) the signal prepro-leader of the mating α-factor of *S. cerevisiae*, which has been used widely to evolve different ligninases (Mate et al. 2010; Camarero et al. 2012; Garcia-Ruiz et al. 2012; Molina-Espeja et al. 2014; Alcalde 2015; Garcia-Ruiz et al. 2014); and ii) the signal prepro(δ)-leader and the γ-spacer-segment of the K1 killer toxin, which have been seen to be useful in boosting β-lactamase secretion in yeast (Cartwright et al. 1992; Zhu et al. 1993). For the first time, chimeric versions of these leaders were designed by combining the different pre- and pro-regions, and these constructs were subjected to conventional and focused-directed evolution using a very sensitive dual high-throughput screening assay based on the Fenton reaction. The best mutant identified dramatically improved the total activity and stability being readily secreted by yeast. Indeed, this active, highly stable and soluble AAO variant is a promising point of departure for new engineering goals.

3.2 MATERIALS AND METHODS

All chemical were reagent-grade purity. Ferrous ammonium sulfate, xylenol orange, sorbitol, benzyl alcohol, p-methoxybenzyl alcohol, veratryl (3,4-dimethoxybenzyl) alcohol, 2,4-hexadien-1-ol, ABTS (2,2'-azino-bis(3-ethylbenzothiazoline-6-sulphonic acid)), Horseradish peroxidase (HRP), *Taq* polymerase and the Yeast Transformation Kit were purchased from Sigma (Madrid, Spain). Zymoprep Yeast Plasmid Miniprep, Yeast Plasmid Miniprep Kit I and Zymoclean Gel DNA Recovery Kit were from Zymo Research (Orange, CA). Restriction enzymes *BamHI* and *XhoI* were from New England Biolabs (Hertfordshire, UK). I-Proof high fidelity DNA polymerase was from Biorad (USA). The episomal shuttle vector pJRoC30 was from the California Institute of Technology (CALTECH, USA) and plasmids pRE1219 and pJRoC30-δγN2C1 were kindly donated by Dr. Susana Camarero (CIB-CSIC Madrid). E. coli XL2-Blue competent cells were from Stratagene (La Jolla, CA, US) whereas the protease deficient *S. cerevisiae* strain BJ5465 (MATa *ura3-52 trp1 leu2Δ1 his3Δ200 pep4::HIS3 prb1Δ1.6R can1 GAL*) was from LGC Promochem (Barcelona, Spain).

Culture media

Minimal medium SC contained 100 mL 6.7% (w:v) sterile yeast nitrogen base, 100 mL 19.2 g/L sterile yeast synthetic drop-out medium supplement without uracil, 100 mL sterile 20% raffinose (w:v), 700 mL sddH2O and 1 mL 25 g/L chloramphenicol. YP medium contained 10 g yeast extract, 20 g peptone and ddH_2O to 650 mL whereas YPD medium also contained 20% glucose (w:v). AAO expression medium contained 144 mL YP 1.55x, 13.4 ml 1M KH_2PO_4 pH 6.0 buffer, 22.2 mL 20% galactose (w:v), 0.222 ml 25 g/L chloramphenicol and ddH_2O to 200 mL. Luria Broth (LB) medium contained 10 g sodium chloride, 5 g yeast extract, 10 g peptone, 1 mL 100 mg/mL ampicillin and ddH_2O to 1 L.

Fusion genes and signal chimeric leaders

AAO mature protein was fused to both the α-factor prepro-leader (preproα-AAO, construct i) and to the prepro(δ)-γ regions of the preprotoxine K1 killer (preproK-AAO, construct ii)). In addition, two chimeric signal peptides were constructed and attached to the AAO: the α-factor pre-leader fused to the γ segment of the K1 Killer toxin, (preαproK-AAO, construct iii); and the prepro(δ)-signal sequence of the K1 Killer toxin fused to the α-factor pro-leader, (preKproα-

AAO, construct iv). The design of overlapping areas of ~40 bp between adjacent fragments allowed the in vivo fusion of the different genetic elements using the *S. cerevisiae* homologous recombination machinery.

AAO was amplified from pflag1AAO vector (Ruiz-Dueñas et al. 2006) using oligo sense AAO/N-ter (5'-GCCGATTTTGACTACGTTGTCGTCG-3') and oligo antisense AAO/C-ter/pJRo-overhang (5'-CATAACTAATTACATGATGCGGCCCTCTAGATGCATGCTCGAGCGGCCGCCTACTGATCAGCCTTGATAAGATCGGCT-3'; the overhang for pJRoC30 is underlined). The α-factor prepro-leader (89 residues including the STE13 cleavage site EAEA) was obtained from pJRoC30-αVP (Garcia-Ruiz et al. 2014) using oligo sense RMLN (5'- CCTCTATACTTTAACGTCAAGG-3') and oligo antisense αC-ter/AAO-overhang (5'-CCGCGTTCCCCGCCCCGACGACAACGTAGTCAAAATCGGCAGCTTCAGCCTCTCTTTTCTC-3'; the overhang for AAO is underlined). Preα fragment, to create preαproK AAO, was amplified from pJRoC30-αVP with oligo sense RMLN and oligo antisense preαC-ter/proK-overhang (5'-AGTCGTTAGCTGGGAGTATACTAATACCATGTTCATTTAAGTTGACTGGAGCAGCTAATG-3'; the overhang for the proK is underlined), this fragment was designed to include the 19 residues of the α-preleader plus the first 4 residues –APVN- of the α-proleader. Proα fragment (66 residues and STE13 cleavage site), to create preKproα-AAO was obtained from pJRoC30-αVP with oligo sense proα/N-ter (5'- GCTCCAGTCAACACTACAAC-3') and oligo antisense αC-ter/AAO-overhang. Prepro(δ)-leader from the K1 killer toxin, used as preK leader, (47 residues long including the C-terminal EAP acid environment) with different overhangs (for subsequent assembly in yeast to give rise to different chimeras), was obtained from two independent PCR reactions from plasmid pRE1219 which contains the prepro(δ) region (1-44 residues) and the α-toxin subunit (45-149 residues): i) to be fused in preproK-AAO with oligo sense preKN-ter/pJRo-overhang (5'-TATACTTTAACGTCAAGGAGAAAAAACTATAGGATCATAGGATCCATGACGAAGCCAACCCAAGTATTA-3'; the overhang for pJRoC30 is underlined) and oligo antisense preKC-ter/proK-overhang (5'-AGTCGTTAGCTGGGAGTATACTAATACCATGTTCATTTAACGGCGCTTCACGTTTTAGTAATGACACTGGT-3'; the overhang for proK is underlined) and ii) with preKN-ter/pJRo-overhang as oligo sense and preKC-ter/proα-overhang (5'-TTTGTGCCGTTTCATCTTCTGTTGTAGTGTTGACTGGAGCCGGCGCTTCACGTTTTAGTAATGACACTGGT-3'; the overhang for proα is underlined) as antisense primer to be part of the preKproα-AAO. The truncated γ-spacer-segment from the K1 killer toxin (64 residues), proK segment in both preproK-AAO and preαproK-AAO, was obtained from pJRoC30-δγN2C1 with oligo sense proKN-ter (5'-TTAAATGAACATGGTATTAGTATACTCCCA-3') and antisense proKC-ter/AAO-overhang (5'-CCGCGTTCCCCGCCCCGACGACAACGTAGTCAAAATCGGCACGCTTGGCCACTGCTGGAAT-3'; the overhang for AAO is underlined) primers.

pJRoC30 was linearized with *BamHI* and *XhoI*. PCRs were performed in a final volume of 50 µL containing 250 nm each primer, 10 ng of template, dNTPs; 200 µM each, 50% dimethylsulfoxide (DMSO) (v:v) and 0.02 U/L iProof high fidelity polymerase. The amplification reactions were carried out in thermal cycler MycyclerTM (BIO-RAD, USA). PCR cycles followed were 98°C for 30 seconds (1 cycle); 98°C for 10 seconds, 50°C for 25 seconds and 72°C for 60 seconds (28 cycles); and 72°C for ten minutes (1 cycle). PCR fragments and linearized vector were loaded onto a preparative agarose gel (0.75%; w:v), and purified using Zymoclean gel DNA recovery kit. PCR products (400 ng each) were mixed with the linearized vector (100 ng; ratio PCR product: vector = 4:1) and transformed in yeast (Yeast transformation kit) promoting the recombination and cloning in vivo. Transformed cells were plated in SC (synthetic complete) drop-out plates and incubated for 3 days at 30°C; individual clones were fermented in 96-well plates and screened for AAO activity. For each positive construct, the plasmids were extracted and sequenced. Fusions were re-transformed into yeast and fermented in 100 mL flask monitoring cell growth and activity (with ABTS-HRP and FOX [Ferrous Oxidation by Xylenol orange] assays, see below) over the time.

Focused-directed AAO evolution

All the PCR products were cleaned, concentrated, loaded onto a low melting-point preparative agarose gel (0.75%, w:v) and purified using the Zymoclean Gel DNA Recovery kit before being cloned into pJRoC30. The plasmid was linearized with *BamHI* and *XhoI*. pJRoC30-preαproK-AAO variant was used as DNA template for focused random mutagenesis. The preαproK-AAO fusion was split into three different segments for MORPHING (Mutagenic Organized Recombination Process by Homologous IN vivo Grouping) (Gonzalez-Perez et al. 2014). Amplified by PCR, each fragment included homologous overlapping overhangs of ~50 bp so that the whole gene could be reassembled in vivo by transformation into *S. cerevisiae*. Mutagenic regions M-I and M-II (590 bp and 528 bp respectively excluding recombination areas) were submitted to *Taq*/$MnCl_2$ amplification and the remaining segment (844 bp) was amplified by high-fidelity PCR. To adjust the mutagenic loads small mutant libraries (around 500 clones each) were created with equal concentration of DNA template and different $MnCl_2$ concentrations (0.025, 0.05 and 0.01 mM combining both segments and with 0.05 mM in segment M-I and 0.025 mM in segment M-II). The percentage of inactive clones (with less than 10% of the parent activity) was calculated to estimate mutational loads. Four mutant libraries were created. Two mutagenic libraries (~1000 clones each) were prepared targeting segment M-I or segment M-II independently for random mutagenesis. The third library (~1000 clones, library M-I-II) was constructed assembling mutagenic segments (M-I and M-II) flanking a non-mutagenic amplification in the middle of the gene. Finally the whole preαproK-AAO fusion was submitted to *Taq*/$MnCl_2$ amplification (library M-IV) adjusting the mutational rate to 1-3 mutations per gene (~2000 clones). Concentrations of 0.05 and 0.01 mM $MnCl_2$ were used for MORPHING and full gene random mutagenesis, respectively.

Mutagenic PCR of targeted segments: Reaction mixtures were prepared in a final volume of 50 µL containing DNA template (0.92 ng/µL), 90 nM oligo sense (RMLN for segment M-I and AAOMBP 5'-AACTCTGCTCATTGGGAGACCATCT-3' for segment M-II), 90 nM Reverse primer (AAO92C 5'-CCCAGTTCCATCCTTCATCGCCA-3' for segment M-I and RMLC 5'-GGGAGGGCGTGAATGTAAGC-3' for segment M-II) , 0.3 mM dNTPs (0.075 mM each), 3% (v:v) (DMSO), 1.5 mM $MgCl_2$, increasing concentrations of MnCl2 (0.025, 0.05, 0.1 mM) and 0.05 U/µL Taq DNA polymerase. Mutagenic PCRs parameters were: 95°C for 2 min (1 cycle); 95°C for 45 s, 50°C for 45 s, 74°C for 45 s (28 cycles); and 74°C for 10 min (1 cycle).

High-fidelity PCR: Reaction mixtures were prepared in a final volume of 50 µL containing: DNA template (0.2 ng/µL), 250 nM oligo sense HFF (5'-TTCGATCGCTATGCGGCTGTC AC-3'), 250 nM oligo antisense HFR (5'-GGGTGGAACCATTGGTTGGAAAAG-3'). High-fidelity PCRs were performed using the following parameters: 98°C for 30 s (1 cycle); 98°C for 10 s, 55°C for 25 s, 72°C for 45 s (28 cycles); and 72°C for 10 min (1 cycle).

Whole gene reassembly: The whole gene was cloned and recombined in vivo by transformation into *S. cerevisiae*. PCR products were mixed in equimolar amounts (400 ng) and transformed with linearized plasmid (200 ng) into chemically competent cells. Transformed cells were plated on SC drop-out plates and incubated for 3 days at 30°C. Colonies containing the whole autonomously replicating vector were picked and screened for activity.

High-throughput screening (HTS) assay

Individual clones were picked and cultured in sterile 96-well plates containing 50 µL of minimal medium (SC). In each plate, column number 6 was inoculated with the parental type (internal standard) and well H1 with $URA3^-$ *S. cerevisiae* cells (negative control). Plates were sealed to prevent evaporation and incubated at 30°C, 225 rpm and 80% relative humidity in a humidity shaker (Minitron-INFORS, Biogen, Spain). After 48 hours, 160 µL of expression medium were added to each well and cultured for additional 48 hours. Finally, 20 µL of supernatants were screened for activity with FOX and HRP-ABTS assays using veratryl or *p*-methoxybenzyl alcohol as substrate as describe below. One unit of AAO activity is defined as the amount of enzyme that converts 1 µmol of alcohol to H_2O_2 per min under the reaction conditions.

Chemical (direct) FOX assay: Aliquots of 20 µL of yeast supernatants were transferred with liquid handler robotic station Freedom EVO (Tecan, Männedorf, Switzerland) and incubated with

20 µL substrate (2 mM *p*-methoxybenzyl alcohol or 10 mM veratryl alcohol in 100 mM phosphate buffer pH 6.0) during 30 min at room temperature, then 160 µL of FOX reagent were added with Multidrop™ Combi Reagent Dispenser (Thermo Scientific, Massachusetts, USA) to assess the AAO H_2O_2 production (final concentration of FOX mixture in the well: 100 µM xylenol orange, 250 µM $Fe(NH_4)_2(SO_4)_2$ and 25 mM H_2SO_4) (Gay et al. 1999). Plates were recorded in end-point mode at 560 nm using a spectrophotometer SPECTRAmax 384 PLUS (Molecular Devices, Sunnyvale, CA); it took ~20 min incubation to develop an intense and stable colorimetric response. The relative activities were calculated from the difference between the Abs values after incubation to that of the initial measurement normalized to the parental type for each plate. To enhance method sensitivity, several additives may be added to the reagent, such as organic co-solvents (DMSO, ethanol, methanol) or sorbitol (Rhee et al. 2010). In our case, the response was amplified by adding a final concentration of 100 mM sorbitol which acts as chain amplifier generating additional ferric ions to increase the response of the method (Bou et al. 2008). The assay was validated by determining the coefficient of variance, the linearity of the response and the detection limit. The detection limit was calculated by the Blank determination method on a 96-well plate with triplicate standards (0, 0.5, 1, 1.5, 2, 2.5, 3 y 4 µM H_2O_2) and several portions of supernatants from *S. cerevisiae* URA3$^-$ lacking plasmid (Shrivastava and Gupta 2011). FOX signal stability was tested with different H_2O_2 concentrations (0, 2, 4, 6, 8, 10, 15 and 18 µM) throughout 300 min at 24°C.

Enzymatic (indirect) HRP-ABTS assay: Aliquots of 20 µL of yeast supernatants were added to 180 µL of HRP-ABTS reagent (final concentrations of HRP-ABTS reagent in the well: 1mM *p*-methoxybenzyl alcohol or 5 mM veratryl alcohol, 2.5 mM ABTS, 1µg/mL HRP in 100 mM phosphate buffer pH 6.0) dispensed with Multidrop™ Combi Reagent Dispenser. The plates were incubated at room temperature and measured in end-point or kinetic mode at 418nm ($\varepsilon_{ABTS\bullet+}$ = 36000 M^{-1} cm^{-1}).

The dual HTS-assay incorporated two consecutive re-screenings to rule out the selection of false positives

i) First re-screening: Aliquots of 5 µL of the best clones of the screening were transferred to new sterile 96-well plates with 50 µL of minimal medium per well. Columns 1 and 12 plus rows A and H were not used to prevent the appearance of false positives. After 24 h of incubation at 30°C and 225 rpm, 5 µL were transferred to the adjacent wells and further incubated for 24 h. Finally, 160 µL of expression medium were added and plates were incubated for 48 h. Accordingly, every single mutant was grown in 4 independent wells. Parental type was subjected to the same procedure (lane D, wells 7-11). Plates were assessed using the same HTS protocol of the screening described above.

ii) Second re-screening: An aliquot from the best clones from the first re-screening was inoculated in 3 ml YPD medium and incubated at 30°C for 24 h at 225 rpm. The plasmids from these cultures were recovered with Zymoprep yeast plasmid miniprep kit I. As the product of the Zymoprep was impure and the DNA extracted was very low concentrated, the shuttle vectors were transformed into super-competent *E. coli* XL2-Blue cells and plated onto LB-ampicillin (LB-amp) plates. Single colonies were selected to inoculate 5 ml of LB-amp medium, and incubated overnight at 37°C and 225 rpm. The plasmids from the best mutants and the parental type were extracted (NucleoSpin plasmid kit) and transformed into *S. cerevisiae*. Five colonies for each mutant were picked and re-screened as described above.

AAO production and purification

Production of recombinant AAO variants in *S. cerevisiae*: A single colony from the *S. cerevisiae* clone containing the AAO fusion gene was picked from a SC drop-out plate, inoculated in SC medium (20 mL) and incubated for 48 h at 30ºC and 220 rpm (Minitron-INFORS, Biogen Spain). An aliquot of cells was removed and used to inoculate minimal medium (100 mL) in a 500 mL flask (OD_{600} = 0.25). The cells completed two growth phases (6–8 h; OD_{600} = 1) and then expression medium (900 mL) was inoculated with the pre-culture (100 mL) (OD_{600} of 0.1). After incubating for 72 h at 25ºC and 220 rpm (maximal AAO activity; OD_{600} = 25–30), the cells were recovered by centrifugation at 4500 rpm and 4ºC (Avanti J-E centrifuge, Beckman Coulter Inc. CA) and the supernatant was double-filtered (using both glass membrane filter and a nitrocellulose membrane of 0.45 µm pore size).

Purification of AAO mutant: AAO (FX7 variant) was purified by FPLC (ÄKTA purifier; GE Healthcare, UK). The crude extract was concentrated and dialyzed in 20 mM piperazine buffer (buffer P, pH 5.5) by tangential ultrafiltration (Pellicon; Millipore, USA) through a 10-kDa-pore-size membrane (Millipore, USA) by means of a peristaltic pump (Masterflex easy load; Cole-Parmer, USA). The sample was filtered and loaded onto a weak anion-exchange column (HiTrap Q FF; GE Healthcare) pre-equilibrated with buffer P and coupled to the ÄKTA purifier system. The proteins were eluted with a linear gradient of buffer P + 1M NaCl in two phases at a flow rate of 1 ml/min: from 0 to 50 % during 15 min and from 50 to 100% in 2 min. Fractions with AAO activity were pooled, dialyzed against buffer P, concentrated and loaded onto a high-resolution resin, strong-anion-exchange column (Biosuite MonoQ 10 cm; Waters, USA) pre-equilibrated in buffer P. The proteins were eluted with a linear gradient from 0 to 0.5 M of NaCl in two phases at a flow rate of 1 ml/min: from 0 to 50 % during 20 min and from 50 to 100% in 2 min. Fractions with AAO activity were pooled, dialyzed against buffer 20 mM phosphate buffer pH 6.0, concentrated and further purified with a Superose 12 HR 10/30 molecular exclusion column (Amersham Bioscience) pre-equilibrated with 150 mM NaCl in phosphate buffer pH 6.0 at a flow rate of 0.5 ml/min. The fractions with AAO activity were pooled, dialyzed against buffer 20 mM phosphate buffer pH 6.0, concentrated and stored a -20°C. Throughout the purification protocol the fractions were analyzed by SDS-polyacrylamide gel electrophoresis (PAGE) on 10% gels, in which the proteins were stained with Protoblue Safe (National Diagnostics, USA). All protein concentrations were calculated using Bio-Rad protein assay reagent (Bio-rad, USA) and BSA as standard for protein concentration.

Production and purification of native AAO from *E. coli*: the native AAO heterologous expressed in *E. coli* after *in vitro* refolding ($_{Ec}$AAO) was produced and purified as described elsewhere (Ruiz-Dueñas et al. 2006).

Biochemical characterization

MALDI–TOF-MS Analysis and pI Determination: The MALDI–TOF-MS experiments were performed on an Autoflex III MALDI-TOF-TOF instrument with a smartbeam laser (Bruker Daltonics). The spectra were acquired using a laser power just above the ionization threshold, and the samples were analysed in the positive-ion detection and delayed extraction linear mode. Typically, 1000 laser shots were summed into a single mass spectrum. External calibration was performed, using the BSA from Bruker, covering the range 15000–70000 Da. Purified FX7 (8 µg) was subjected to two-dimensional electrophoresis gel in order to determine the pI.

N-terminal analysis: Purified AAO was subjected to SDS/PAGE, and the protein band was blotted onto PVDF membranes. The PVDF membrane was stained with Coomassie Brilliant Blue R-250, after which the enzyme band was excised and processed for N-terminal amino acid sequencing on a precise sequencer at the Core facilities of Helmholtz Centre for Infection Research, Germany.

Determination of kinetic-thermostability (T_{50}): Appropriate dilutions of purified FX7 and $_{Ec}$AAO were prepared for the assay while the samples of parental preαproK-AAO were from crude supernatants. The gradient scale ranging from 30 to 80°C was established as follows: 30.0, 31.4, 34.8, 39.3, 45.3, 49.9, 53, 55, 56.8, 59.9, 64.3, 70.3, 75, 78.1 and 80°C. This gradient profile was achieved using a thermocycler (Mycycler, Bio-Rad, USA). After 10 min of incubation, FX7 and $_{Ec}$AAO samples were removed and chilled out on ice for 10 min and incubated further at room temperature for 5 min. Finally, samples of 20 µl were added to 180 µl volumes of 100 mM sodium phosphate pH 6.0 buffer containing 1mM *p*-methoxybenzyl alcohol and activity was measured as anisaldehyde production as absorption at 285 nm (ε_{285} = 16,950 M^{-1} cm^{-1}). In the case of parental preαproK-AAO supernatants, the samples were subjected to the ABTS-HRP assay described above for the screening. Thermostability values were calculated from the ratio between the residual activities incubated at different temperature points and the initial activity at room temperature. The T_{50} value was determined by the transition midpoint of the inactivation curve of the protein as a function of temperature, which in our case was defined as the temperature at which the enzyme lost 50% of its activity following an incubation of 10 minutes. All reactions were performed by triplicate.

Thermoactivity (T_a): Enzyme dilutions of purified FX7 (33 nM, final concentration) and $_{Ec}$AAO (18 nM, final concentration) were prepared in such a way that aliquots of 20 µL gave rise to a linear response in kinetic mode. The optimum temperature for activity was estimated in pre-warmed 96-well reading plates (Labnet VorTemp 56 Shaking Incubator, Labnet International, USA) with 100 mM sodium phosphate pH 6.0 containing *p*-methoxybenzyl alcohol 1 mM at the corresponding temperatures (25, 30, 40, 50, 60, 70, 80, 90 and 99°C incubated in an Eppendorf Thermomixer Comfort, Thermo Fisher Scientific, Massachusetts, USA). Reactions were performed by triplicate and *p*-methoxybenzyl alcohol oxidation was followed by aldehyde production at 285 nm.

Kinetic parameters: Kinetic constants for AAO were estimated in 100 mM sodium phosphate pH 6.0. The final enzyme concentrations used were: with *p*-methoxybenzyl alcohol, 33 and 18 nM for FX7 and $_{Ec}$AAO, respectively; with veratryl alcohol, 38 and 32 nM for FX7 and $_{Ec}$AAO, respectively; with benzyl alcohol, 62 and 47 nM for FX7 and $_{Ec}$AAO, respectively; and with 2,4 hexadien-1-ol, 15 and 4 nM for FX7 and $_{Ec}$AAO, respectively. Reactions were performed by triplicate and substrates oxidations were followed by measuring the absorption at 285 nm for *p*-methoxybenzyl alcohol, ε_{285} = 16,950 M^{-1} cm^{-1}; 310 nm for veratryl alcohol, ε_{310} = 9,300 M^{-1} cm^{-1}; 250 nm for benzyl alcohol, ε_{250} = 13,800 M^{-1} cm^{-1}; 280 nm for 2,4-hexadien-1-ol, ε_{280} = 30,140 M^{-1} cm^{-1}. Steady-state kinetics parameters were determined by fitting the initial reactions rates at different substrate concentrations to the Michaelis-Menten equation for one substrate, $v/e = k_{cat}.S/(K_m + S)$ where *e* represent the enzyme concentration, k_{cat} is the maximal turnover rate, S is the substrate concentration and K_m the Michaelis constant. Data were fit using SigmaPlot 10.0 (Systat. Software Inc. Richmond, CA, USA).

pH-activity and stability profiles: Appropriate dilutions of enzyme samples were prepared in such a way that aliquots of 20 µL gave rise to a linear response in kinetic mode. The optimum pH activity was determined using 100 mM citrate-phosphate-borate buffer at different pH values (2.0, 3.0, 4.0, 5.0, 6.0, 7.0, 8.0 and 9.0) containing the corresponding alcohol concentration (0.3, 5, 9, and 1.2 mM for *p*-methoxybenzyl alcohol, veratryl alcohol, benzyl alcohol, and 2,4-hexadien-1-ol, respectively). To measure pH stability, enzyme samples were incubated at different times over a range of pH values. The residual activity was deduced from the activity before and after incubation with 0.3 mM *p*-methoxybenzyl alcohol in 100 mM phosphate buffer pH 6.0.

Protein modeling: A structural model of the AAO from *P. eryngii* crystal structure at a resolution of 2.55 Ǻ (Protein Data Bank Europe [PDB] accession number 3FIM, (Fernández et al. 2009) was used as scaffold for the wild type AAO model and the FX7 mutant homology model, obtained by PyMol (Schrodinger LLC.; http://www.pymol.org).

DNA sequencing: All genes were verified by DNA sequencing (BigDye Terminator v3.1 Cycle Sequencing Kit). The primers used were common to the four constructions: primers sense, RMLN and AAOsec1F 5'-GTGGATCAACAGAAGATTTCGATCG-3' and primers antisense RMLC 5'-GCTTACATTCACGCCCTCCC-3', AAOsec2R 5'-GTGGTTAGCAATGAGCGCGG-3' and AAOsec3R 5'-GGAGTCGAGCCTCTGCCCCT-3'.

3.3 RESULTS AND DISCUSSION

Construction of chimeric signal prepro-leaders

In terms of yeast expression, the replacement of native signal peptides to foster foreign protein secretion has been used widely for years. Recently, the directed evolution of the α-factor prepro-leader permitted the functional expression of antibodies (Rakestraw et al. 2009) and different classes of ligninases (including high-redox potential laccases, versatile peroxidases and unspecific peroxygenases) (Mate et al. 2010; Camarero et al. 2012; Garcia-Ruiz et al. 2012; Molina-Espeja et al. 2014; Alcalde 2015). In this study, the prepro-leaders from the mating α-factor and the K1 killer toxin, along with their chimeric combinations, were tailored and attached to the native AAO for functional expression and directed evolution. The mating α-factor signal sequence is formed by 19 and 64 amino acids from the pre- and pro-leader, respectively (Zsebo et al. 1986; Shuster 1991; Romanos et al. 1992), **Figure 1A**. The pre-leader initiates endoplasmic reticulum translocation and it is finally removed by the action of a signal peptidase that cuts between residues 19 and 20. The pro-leader contains three Asn linked glycosylation sites, and it is thought to be involved in the folding and maturation of the protein before it is packed into vesicles for exocytosis. The pro-leader is processed in the Golgi compartment by the action of the KEX2, STE13 and KEX1 proteases, although the latter is not needed for heterologous protein secretion. The K1 killer prepro-toxin is preceded by a prepro-sequence of 44 residues -prepro(δ)- that undergoes similar processing as the α-factor prepro-leader, albeit without the requirement of STE13 and KEX1 activity (Cartwright et al. 1992; Zhu et al. 1993; Schmitt and Breinig 2006), **Figure 1B**. The prepro-toxin contains an internal γ-segment of 85 residues with three extra KEX2 recognition sites for processing in the Golgi. Bearing in mind the common features of these two prepro-leaders in terms of processing and secretion, the following four fusion constructs were attached to the mature AAO, **Figure 1C**: i) the preproα-AAO containing the full α-factor prepro-leader; ii) the preproK-AAO formed by the prepro(δ) of K1 toxin connected to a truncated version (64 residues) of the γ-segment known to be important for correct processing (the truncated segment stretched from position 169 to 233 and preserved the three N-glycosylation sites: N181, N203 and N216 (Cartwright et al. 1992); iii) the chimeric preαproK-AAO comprising the α-factor pre-leader fused to the truncated γ-segment; and iv) the chimeric preKproα-AAO formed by the prepro(δ) of the K1 toxin linked to the α-factor pro-leader. In addition, we modified the prepro(δ) containing constructs -fusions ii) and iv)- by site directed mutagenesis to modify the P43-R44 KEX2 recognition site to K43-R44, as this substitution was associated with a 50-fold enhancement in KEX2 catalytic efficiency (Brenner and Fuller 1992).

The fusion constructs were spliced in *S. cerevisiae*, and taking advantage of the high frequency of in vivo homologous DNA recombination of this yeast overlapping areas of ~50 bp guaranteed correct DNA assembly of the different genetic elements and the linearized plasmid without altering the ORF (Gonzalez-Perez et al. 2012). The activity of each AAO construct against veratryl alcohol was assayed in microtiter microscale fermentations (96-well plates) and the four fusions produced detectable AAO activity in the culture broth, which was consistent in the two colorimetric assays used (see below). The secretion driven by the corresponding constructs was preproα-AAO> preαproK-AAO> preKproα-AAO> preproK-AAO. We verified by DNA sequencing that the constructs did not incorporate mutations in the mature protein or in the prepro-sequences (apart from the aforementioned P43K substitution), and that all the elements were properly assembled *in vivo* as intended.

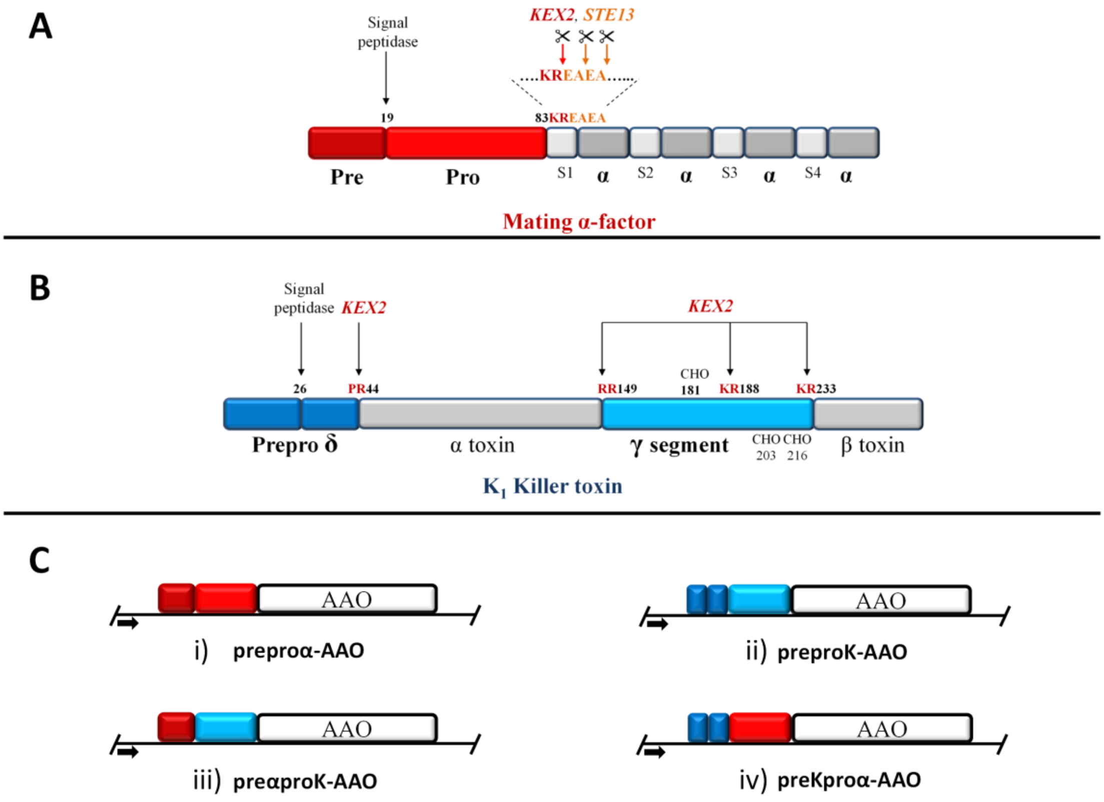
A
Signal peptidase
KEX2, STE13
....KREAEA......
19
83KREAEA
Pre
Pro
S1
α
S2
α
S3
α
S4
α
Mating α-factor
B
Signal peptidase
KEX2
KEX2
26
PR44
RR149
CHO 181
KR188
KR233
Prepro δ
α toxin
γ segment
CHO CHO 203 216
β toxin
K1 Killer toxin
C
AAO
i) preproα-AAO
ii) preproK-AAO
iii) preαproK-AAO
iv) preKproα-AAO

Figure 1. Prepro-leaders used and chimeric signal peptides engineered for functional AAO expression in *S. cerevisiae*. (A) Mating α-factor, (B) K1 killer prepro-toxin; (C) AAO fusions for functional expression. The different processing sites for the KEX2 and STE13 signal peptidases are indicated in each case. The yeast mating pheromone α prepro-polyprotein precursor contains a hydrophobic N-terminal pre-sequence (dark red) followed by an N-glycosylated pro-sequence (red). The K1 killer toxin is derived from a 316 residue prepro-toxin. The unprocessed precursor consist of a prepro(δ) sequence (dark blue) that contains a 26 residue signal peptide. The γ segment (light blue) separating the alpha- and beta- toxin subunits was also used to engineer the chimeras.

Fermentations were translated from the high-throughput format to larger volumes (10 mL) for each construct studied. Irrespective of the substrate (*p*-methoxybenzyl or veratryl alcohol), the hierarchy of activity of the fusion genes was maintained: preproα-AAO, (1.5 U/L), preαproK-AAO (0.5 U/L), preKproα-AAO (0.35 U/L) and preproK-AAO (0.06 U/L), **Figure 2**. We tried to enhance the membrane permeability of the yeast by adding ethanol to the expression medium, yet the activity detected was 5-fold lower, which was probably due to growth inhibition as a consequence of changes in yeast physiology and the redox balance of the medium (Cortassa et al. 1995).

Directed evolution of preαproK-AAO

Of the four AAO constructs, the preproα-AAO produced the highest secretion, although the risk of inefficient processing of the α-proleader by STE13 ruled out its use. Given that little STE13 is found in the Golgi apparatus, the secreted heterologous protein maintains an extra EAEA spacer dipeptide at the N-terminus, as previously demonstrated in the evolution of other oxidoreductases fused to preproα (laccases and peroxidases) (Mate et al. 2010; Garcia-Ruiz et al. 2012; Mate et al. 2013). This problem may be circumvented by: i) suppressing the cleavage site for STE13; ii) enhancing the expression of STE13; or iii) deleting the whole α-factor pro-leader. However, this may drive the intracellular accumulation and/or the secretion of partially processed forms, no matter the strategy used (Brake 1990). It is worth noting that the N-terminal of AAO interacts with the FAD molecule through a network of H-bonds, such that an extra-N-terminal sequence could modify these contacts jeopardizing catalysis (Shrivastava and Gupta 2011; Dym and Eisenberg 2001). As a correct processing is crucial to conserve the integrity and orientation of the attached FAD prosthetic group in the tertiary structure of AAO, the preαproK-AAO construct, in which the proK fragment is exclusively processed by the abundant KEX2, was chosen as the point of departure for engineering.

To enhance the activity and secretion of the preαproK-AAO in yeast several mutant libraries were constructed by conventional and guided-directed evolution. The latter was performed by MORPHING, a one-pot focused domain mutagenesis method supported by the in vivo gap repair mechanism of *S. cerevisiae* (Gonzalez-Perez et al. 2014). By MORPHING, we can direct random mutations and recombination events to short sequences, while keeping the remaining parts of the gene unaltered. Two protein segments of the preαproK-AAO (M-I: Met[α1]-Val109; M-II: Phe392-Gln566) were studied simultaneously through this approach, **Figure 3**. The M-I segment includes the preαproK (to evolve the chimeric leader for secretion) plus a region of the mature AAO (Ala1-Thr110 Val109) that contains the FAD-binding domain at its N-terminus along with several structural determinants in the nearby substrate access channel -Val54, Pro55, His91, Tyr92, Pro79, Val90- (Ferreira et al. 2006; Hernández-Ortega et al. 2011; Fernández et al. 2009). The M-II segment contains the catalytic pocket including the His546 involved in substrate positioning, the catalytic base His502, and the aromatic residues Phe397 and Phe501. These latter amino acids create a hydrophobic gate in conjunction with Tyr92 of the M-I segment, thereby blocking access to the active channel (Hernandez-Ortega et al. 2012a; Ferreira et al. 2006; Fernández et al. 2009).

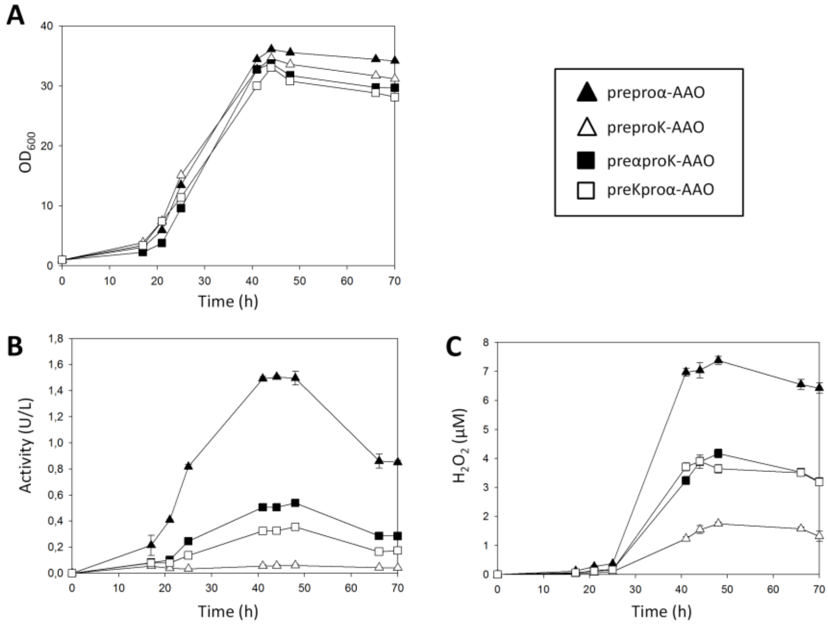

Figure 2. Expression of the AAO fusions in *S. cerevisiae*. (A) Shake flask fermentation -growth curves-, (B) AAO activity measured in the HRP-ABTS assay. (C) H_2O_2 production measured in the FOX assay. The preproα-AAO fusion achieved the highest yields in terms of cell growth and enzymatic activity (OD_{600} = 36; 1.5 U/L after 44 hours), followed by the preαproK-AAO, preKproα-AAO and preproK-AAO fusions. Clone activity and H_2O_2 production were evaluated in triplicate and each point includes the standard deviation.

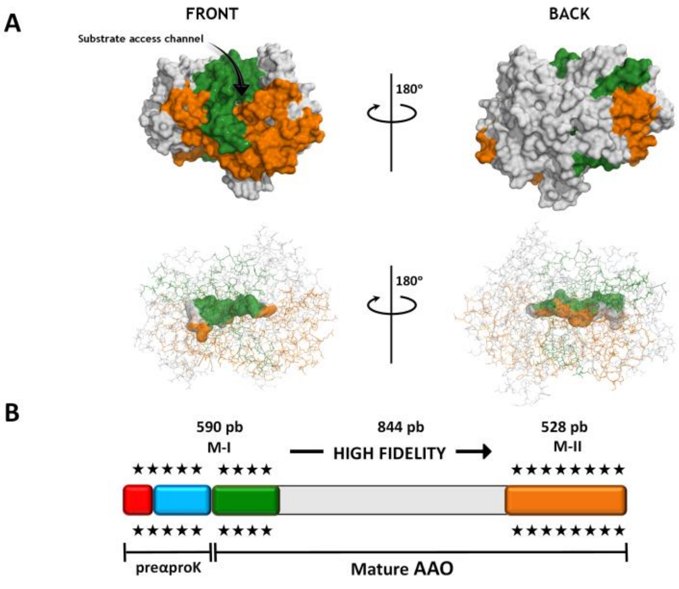
A
FRONT
BACK
Substrate access channel
180°
180°
B
590 pb
M-I
844 pb
HIGH FIDELITY
528 pb
M-II
preαproK
Mature AAO

Figure 3. AAO segments for focused directed evolution. The M-I (590 bp) and M-II (528 bp) segments are highlighted in green and orange, respectively. The segment from 591-1435 bp (in white) was amplified by high-fidelity polymerase to guarantee that no mutations are introduced in this area.

A total of three focused mutant libraries were constructed (single M-I and M-II, and M-I-II combined), as well as one conventional mutant library (targeting the full preαproK-AAO construction by random mutation and DNA recombination; M-IV). Mutational loads were adjusted to introduce 1 to 3 amino acid changes per protein, and the four libraries were explored with a highly sensitive dual high-throughput screening system to detect AAO activity irrespective of the substrate. This method coupled a standard HRP/ABTS indirect colorimetric assay to a direct chemical method (FOX) based on the Fenton reaction in order to detect little concentrations of H_2O_2. The latter is typically used to measure H_2O_2 in biological fluids, and more recently to determine L-amino acid oxidase and lipoxygenase activities (Gay et al. 1999; Rhee et al. 2010; Yu et al. 2013; Kumar et al. 2011) but to our best knowledge it has never been used to evolve H_2O_2 producing enzymes. The limit of sensitivity of the FOX assay was 2 µM H_2O_2 and it was further shifted to 0.4 µM H_2O_2 through the inclusion of sorbitol to propagate the response (see Materials and Methods for details). Two consecutive re-screenings were carried out to avoid the selection of false positives. After exploring ~5000 clones, we identified five mutants with a total activity improvement over the parental type ranging from 2- to 5-fold and significantly, the FX7 variant (H91N) from the combined M-I-II MORPHING displayed a dramatic 96-fold improvement in total activity with respect to the parental type, **Table 1**. The remaining mutations found in these variants (i.e. T[K150]A, S88T, L170M, I194V, D341N, R481S) are located at a distance of >20 residues from one another, making them suitable candidates for future DNA shuffling studies or to be evaluated by site-directed recombination.

Table 1. Selected mutants of the preαproK-AAO libraries.

Variant	Library	Mutation	Location	Secondary motif	Total activity improvement (in fold)*	T_{50} (°C)
FX7	M-I-II	$_{\text{CAC}}$H91N$_{\text{AAC}}$	FAD-binding domain	Loop	96	64.3
13H2	M-IV	$_{\text{ATA}}$I194V$_{\text{GTA}}$	Substrate-binding Domain	Loop	4.94	60.8
10G5	M-IV	$_{\text{TTG}}$L170M$_{\text{ATG}}$	Substrate-binding Domain	Alpha helix	4.91	60.5
7A11	M-II	$_{\text{GAT}}$D341N$_{\text{AAT}}$	Substrate-binding Domain	Alpha helix	4.59	59.3
4C7	M-II	$_{\text{AGA}}$R481S$_{\text{AGT}}$	Substrate-binding Domain	Loop	4.49	61.5
12G12	M-I	$_{\text{ACA}}$T[50K]A$_{\text{GCA}}$ $_{\text{AGC}}$S88T$_{\text{ACC}}$	Signal peptide; FAD-binding domain	Loop	1.94	61.8
preαproK-AAO (parental type)	---	---	---	---	1	58.8
$_{Ec}$AAO	---	---	---	---	---	47.5

*The total activity improvement over parental type was estimated with the FOX assay and 2 mM p-methoxybenzyl alcohol as substrate in 100 mM phosphate buffer pH 6.0.

Biochemical characterization

The FX7 variant was purified to homogeneity and characterized biochemically. Since the weak secretion of parental preαproK-AAO (0.5 U/L) in *S. cerevisiae* hindered its purification, the properties of purified FX7 were compared to that of the native AAO heterologous expressed in *E. coli* after in vitro refolding ($_{\text{Ec}}$AAO). FX7 was secreted at 2 mg/L with a specific activity for *p*-methoxybenzyl alcohol of 24 U/mg, **Table 2**. Both FX7 and $_{\text{Ec}}$AAO enzymes showed similar kinetic constants as well as pH activity profiles with all the substrates tested, although activity (k_{cat}) was lower if the enzyme is expressed in *S. cerevisiae* instead of *E. coli* Table 3, **Figure 4A, B**. The N-terminal sequencing of FX7 confirmed the correct cleavage of the chimeric preαproK leader, avoiding unwanted modifications at the N-terminus. FX7 was heavily glycosylated (~50% glycosylation), adopting a molecular mass of ~120,000 Da, yet after deglycosylation the AAO smear collapsed to a single band of around 61,000 Da, as confirmed by MALDI-TOF analysis, **Table 2**,

Supplementary Figure 1. It is well known that *S. cerevisiae* tends to hyperglycosylate heterologous proteins; possibly, a slow transit of AAO through the Golgi compartment before its packing into vesicles for exocytosis facilitates the addition of long chains of mannose moieties that can cover the protein surface as reported for many other hyperglycosylated enzymes in *S. cerevisiae* (Shuster 1991). The use of glycosylation-deficient *S. cerevisiae* strains [e.g. Δkre2 that is only capable of attaching smaller mannose oligomers, (Lussier et al. 1999)] could have lightened the strong AAO glycosylation, albeit at the possible cost of endangering secretion given that the *S. cerevisiae* strain used in our study is protease-deficient. Hyperglycosylation can exert a beneficial stability effect.

Table 2. Biochemical properties of recombinant native EcAOO and evolved AAO (FX7 mutant).

Biochemical properties	$_{Ec}$AAO	FX7 mutant
MW (Da)[1]	65,000	120,000
MW (Da)[2]	61,847[a]	61,485
MW (Da)[3]	61,088	60,934
Glycosylation degree (%)	---	50
Thermal stability, T_{50} (ºC)	47.5	64.3
pI	3.9	4.3
N-terminal end	MADFDYVVG[b]	ADFDYVVVG
Specific activity (U/mg)[4]	38	45
Secretion levels	---	2 mg/L

[1]Estimated by SDS-PAGE; [2]estimated by MALDI-TOF mass spectrometry after deglycosylation with PNGase F; [3]estimated from amino acid composition; [4]specific activity for anysil alcohol. [a]value from Ref Ruiz Dueñas et al. 2006; [b]Met1 was added to the N-terminal end for cloning in *E. coli*.

Indeed, the T_{50} (the temperature at which the enzyme retains 50 % of its initial activity after a 10 min incubation) was ~11˚C above that of $_{Ec}$AAO for all the AAO variants expressed in *S. cerevisiae*, with a further 5.5˚C increase for FX7 that must be exclusively attributed to beneficial H91N mutation (from 47.5 to 64.3˚C, **Table 1**, **Figure 5A**). This high thermostability correlated with a stronger thermoactivity (i.e. the optimum temperature for activity, T_a). Thus, the T_a of FX7 was over 80% at 80˚C where $_{Ec}$AAO conserved 22% of activity, **Figure 5B**. Notably, FX7 still maintained ~60 and 20% of activity at 90 and 100˚C, respectively, while the $_{Ec}$AAO Ta was negligible. Besides, FX7 showed a broad pH stability in the range of 3.0 to 9.0, Fig. 4C, D. After 144 h incubation, the residual FX7 activity was ~80 and 38% at pH 3 and 9, respectively, whereas the residual $_{Ec}$AAO activity at those pH values was negligible.

It is worth noting that His91 is a deviation in *P. eryngii* and *P. pulmonarious* AAO, since an Asn lies at this position in virtually all members of the GMC superfamily, including 70 putative AAO sequences from different basidiomycetes (Ferreira et al. 2015a), **Figure 6A**. Hence, restoring this consensus mutation has been crucial to improve heterologous AAO expression in yeast while enhancing thermostability, which is in excellent agreement with previous reports on ancestral library design by introducing consensus/ancestor mutations to improve the heterologous expression and thermostability of different enzymes (Khersonsky et al. 2009; Jochens et al. 2010; Zhang et al. 2010).

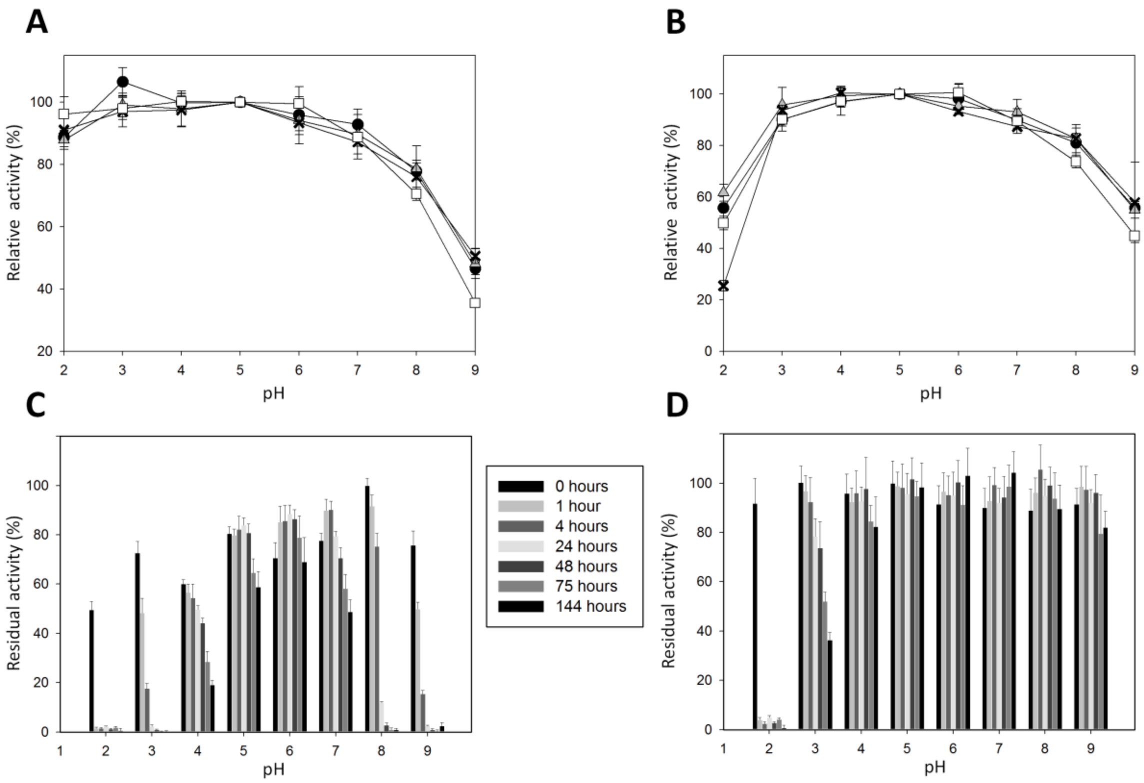

Figure 4. pH activity and stability. pH activity profiles for $_{\mathrm{Ec}}$AAO (A) and FX7 (B). Activities were measured in 100 mM citrate-phosphate-borate buffer at different pH values. Black circles (*p*-methoxybenzyl alcohol), grey triangles (veratryl alcohol), crosses (benzyl alcohol), white squares (2, 4 hexadien-1-ol). pH stability of $_{\mathrm{Ec}}$AAO (C) and the FX7 (D). Enzymes samples were incubated in 100 mM citrate-phosphate-borate buffer at different pH values and the residual activity was measured with 0.3 mM p-methoxybenzyl alcohol in 100 mM phosphate buffer pH 6.0. Results represent the mean and standard deviation of three independent experiments.

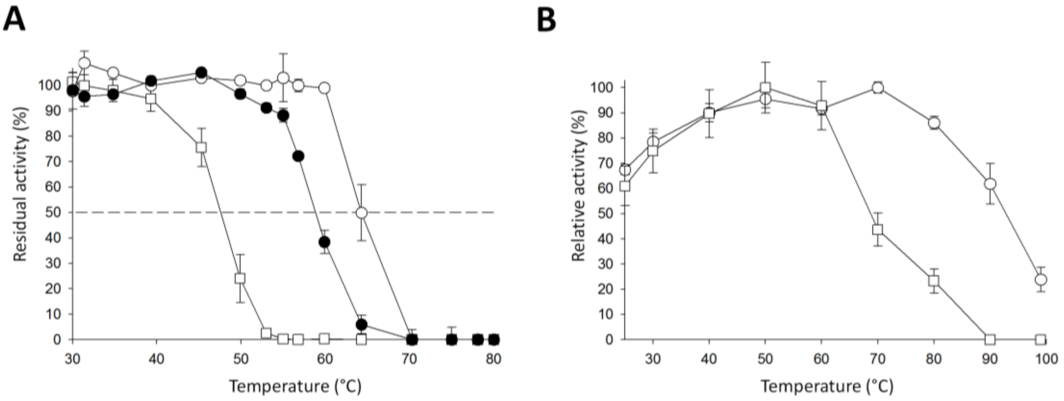

Figure 5. Thermostability of AAO variants. (B) Thermostability (T_{50}) of FX7 (white circles), preαproK-AAO parental type (black circles), and $_{Ec}$AAO (white squares). (C) Thermoactivity (T_a) of FX7 (white circles), and $_{Ec}$AAO (white squares). Each point represents the mean and standard deviation of three independent experiments.

Table 3. Kinetic parameters of native $_{Ec}$AOO and evolved AAO (FX7 mutant).

Substrate	Kinetic constant	$_{Ec}$AAO	FX7
p-methoxybenzyl alcohol	K_m (mM)	0.035 ± 0.001	0.034 ± 0.001
	k_{cat} (s^{-1})	105 ± 6	54 ± 4
	k_{cat}/K_m (s^{-1} mM^{-1})	2979 ± 66	1562 ± 44
Veratryl alcohol	K_m (mM)	0.504 ± 0.043	0.388 ± 0.023
	k_{cat} (s^{-1})	66 ± 2	28 ± 1
	k_{cat}/K_m (s^{-1} mM^{-1})	131 ± 8	71 ± 3
Benzyl alcohol	K_m (mM)	0.770 ± 0.011	0.510 ± 0.001
	k_{cat} (s^{-1})	22 ± 1	19 ± 1
	k_{cat}/K_m (s^{-1} mM^{-1})	28 ± 2	36 ± 3
2,4 hexadien-1-ol	K_m (mM)	0.087 ± 0.001	0.059 ± 0.004
	k_{cat} (s^{-1})	136 ± 3	52 ± 1
	k_{cat}/K_m (s^{-1} mM^{-1})	1555 ± 67	866 ± 53

Steady-state constants were estimated in 100 mM sodium phosphate buffer pH 6 at 24°C. All reactions were performed by triplicate.

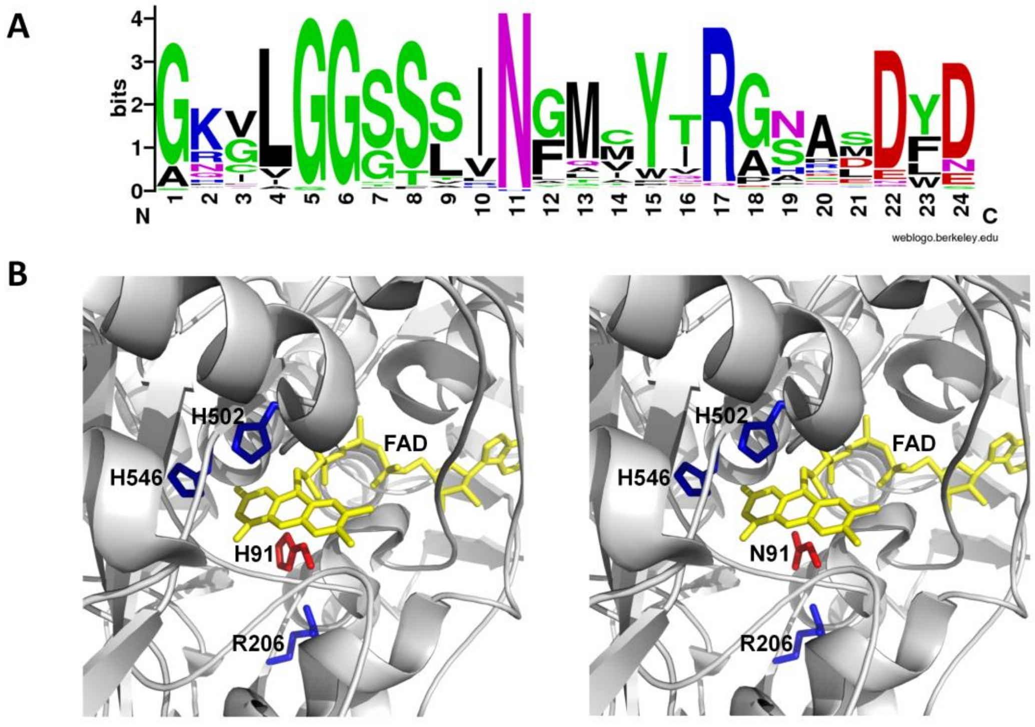

AAO wild type FX7 mutant

Figure 6. Consensus Asn91 in GMC superfamily. (A) Sequence logo of the GMC signature 1 (Prosite PS00623) in 329 GMC sequences from Genbank (http://www.ncbi.nlm.nih.gov/genbank/), JGI (http://jgi.doe.gov/) and Prosite Expasy (http://prosite.expasy.org/PS00623) including, cholesterol oxidase, choline oxidase, aryl-alcohol oxidase, pyridoxine oxidase, methanol oxidase, glucose oxidase and dehydrogenase, pyranose oxidase and dehydrogenase, cellobiose dehydrogenase, L-sorbose-1-dehydrogenase, and hydroxynitrile lyase proteins. (B) N91H mutation in FX7 variant. A molecular model using as template the P. eryngii AAO crystal structure (PDB code 3FIM) was prepared to map the mutation. The residues of the active site His502, His546 and R206 are depicted in blue, FAD in yellow and H91N mutation in red.

Indeed, the discovery of a consensus ancestor mutation by focused evolution, rather than using the consensus method based on sequence alignment or an inference phylogenetic analysis for ancestor mutations, highlights the potential of random domain mutagenesis approaches to reveal beneficial consensus/ancestor mutations. H91N lies in the flavin attachment loop region, a common motif in GMC oxidoreductases. Found on the si-face of the isoalloxazine ring, hydrophobic interactions of this residue maintain the co-factor in a bent conformation (Kiess et al. 1998). In *P. eryngii* AAO, His91 interacts with Arg206 (Arg/Lys of other GMC proteins) and it stabilizes the flavin ring conformation, **Figure 6**. The substitution of a positively charged His by a polar uncharged Asn may alter these contacts in *P. eryingii* AAO, which could aid the attachment of FAD and enhance the stability and functional expression. The two latter properties are strongly connected and it is highly likely that the improved stability allows more AAO to be secreted, as it has been described for many other proteins expressed in yeast (Shusta et al. 1999). Why the N91H substitution arose exclusively in the natural evolution of *P. eryngii* and *P. pulmonarious* AAO is unclear, yet our results suggest a possible regulation of AAO expression to reduce the inhibition of ligninolytic peroxidases mediated by H_2O_2 (Böckle et al. 1999).

3.4 CONCLUSIONS AND OUTLOOK

In this work, the AAO from *P. eryngii* was functionally expressed in *S. cerevisiae* by engineering chimeric prepro-leaders that allowed us to construct and screen mutant libraries in yeast. The particular design of an ad-hoc chimeric prepro-leader, combined with a focused-directed evolution strategy and a sensitive dual screening assay, has led to obtain an active, highly stable AAO variant that is secreted by yeast as a correctly processed enzyme.

Although hardly used, the biotechnological potential of AAO should not be underestimated. In nature, the gradual release of H_2O_2 by AAO supplies peroxidases with a continuous source of co-oxidant for lignin degradation. In vitro, this effect can be mimicked by controlling the addition of H_2O_2 with sensors and peristaltic pumps, although with limited success (Peter et al. 2014). Very recently, we introduced the FX7 variant into episomal bi-directional vectors to co-express versatile peroxidases-AAO and/or unspecific peroxygenases-AAO (unpublished material). These self-sufficient expression systems could be employed to evolve efficient enzymatic cascade reactions (e.g. for the oxidative conversion of 5-hydroxymethylfurfurals into value-added chemicals, (Carro et al. 2015). Significantly, the FX7 variant and its future offspring could also be included to design an autonomously consolidated bioprocessing yeast, with a full artificial secretome that includes the most important elements of the ligninolytic enzyme consortium. Such a microbe would have a number of potential applications in lignocellulose biorefineries for the production of fuels and commodities (Alcalde 2015), (Gonzalez-Perez and Alcalde 2014). Finally, the directed evolution platform presented here is an invaluable tool for protein engineering, which can be applied from the design of efficient stereoselective aryl secondary alcohol oxidases to the synthesis of natural flavors (Hernandez-Ortega et al. 2012a).

ACKNOWLEDGEMENTS

This work was supported by the European Commission projects Indox-FP7-KBBE-2013-7-613549 and Cost-Action CM1303-Systems Biocatalysis, and the National Projects Dewry [BIO201343407-R] and Cambios [RTC-2014-1777-3].

3.5 SUPPLEMENTARY MATERIAL

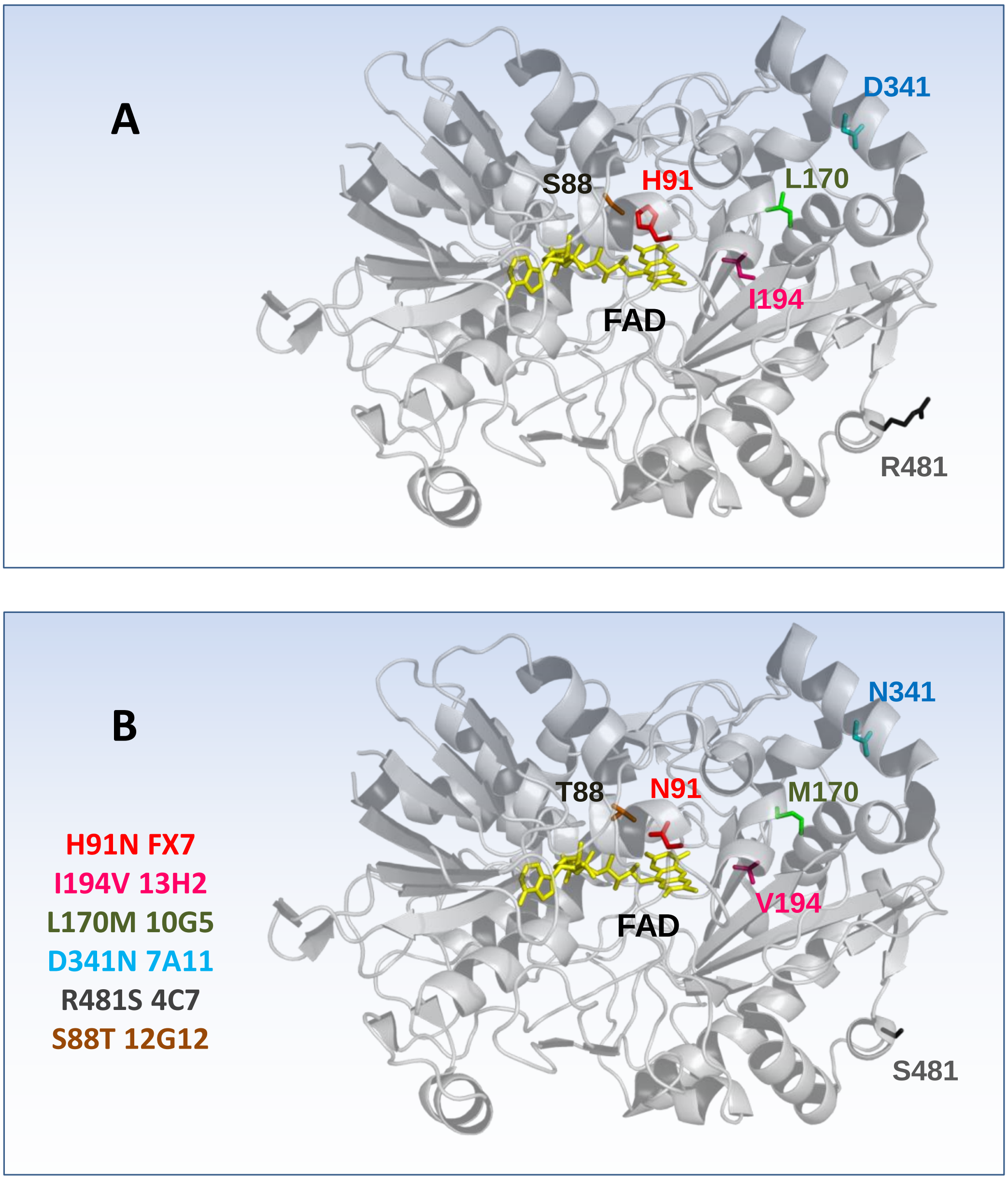
A
D341
S88
H91
L170
I194
FAD
R481
B
N341
T88
N91
M170
V194
FAD
S481
H91N FX7
I194V 13H2
L170M 10G5
D341N 7A11
R481S 4C7
S88T 12G12

Supplementary Figure 1. Structural exploration of the substitutions introduced by MORPHING. (A) Structure of the wild type AAO using as template the P. eryngii AAO crystal structure (PDB code 3FIM) (B) Mutations from each variant are depicted in different color. FX7 from library M-I-II (red), 13H2 (pink) and 10G5 (green) from library M-IV, 7A11 from library M-II (cyan), 4C7 from library M-II (dark grey) and modification in the mature protein in 12G12 from library M-I (brown).

CHAPTER IV:

Directed evolution method in *Saccharomyces cerevisiae*: Mutant library creation and screening

In this Chapter we complement the information given in Chapter III in terms of library creation methods and assays used in the different laboratory AAO evolution campaigns, including a step-by-step protocol for MORPHING method as well as the HTS blind assay.

Directed evolution method in Saccharomyces cerevisiae: Mutant library creation and screening

Javier Viña-González, David González-Pérez and Miguel Alcalde

Journal of Visualized Experiments 110: e53761.

http://doi.org/10.3791/53761

Directed evolution in *Saccharomyces cerevisiae* offers many attractive advantages when designing enzymes for biotechnological applications, a process that involves the construction, cloning and expression of mutant libraries, coupled to high frequency homologous DNA recombination in vivo. Here, we present a protocol to create and screen mutant libraries in yeast based on the example of a fungal aryl-alcohol oxidase (AAO) to enhance its total activity. Two protein segments were subjected to focused-directed evolution by random mutagenesis and in vivo DNA recombination. Overhangs of ~50 bp flanking each segment allowed the correct reassembly of the AAO-fusion gene in a linearized vector giving rise to a full autonomously replicating plasmid. Mutant libraries enriched with functional AAO variants were screened in *S. cerevisiae* supernatants with a sensitive high-throughput assay based on the Fenton reaction. The general process of library construction in *S. cerevisiae* described here can be readily applied to evolve many other eukaryotic genes, avoiding extra PCR reactions, *in vitro* DNA recombination and ligation steps.

4.1 INTRODUCTION

Directed molecular evolution is a robust, fast and reliable method to design enzymes, (Jäckel and Hilvert 2010; Bornscheuer et al. 2012). Through iterative rounds of random mutation, recombination and screening, improved versions of enzymes can be generated that act on new substrates, in novel reactions, in non-natural environments, or even to assist the cell to achieve new metabolic goals (Renata et al. 2015; Cobb et al. 2013; Abatemarco et al. 2013). Among the hosts used in directed evolution, the brewer's yeast *Saccharomyces cerevisiae* offers a repertoire of solutions for the functional expression of complex eukaryotic proteins that are not otherwise available in prokaryotic counterparts (Pourmir and Johannes 2012; Krivoruchko et al. 2011).

Used exhaustively in cell biology studies, this small eukaryotic model has many advantages in terms of post-translational modifications, ease of manipulation and transformation efficiency, all of which are important traits to engineer enzymes by directed evolution (Gonzalez-Perez et al. 2012). Moreover, the high frequency of homologous DNA recombination in *S. cerevisiae* coupled to its efficient proof-reading apparatus opens a wide array of possibilities for library creation and gene assembly in vivo, fostering the evolution of different systems from single enzymes to complex artificial pathways (Alcalde 2010; Bulter and Alcalde 2003; Ostrov et al. 2013; (Shao et al. 2009). Our laboratory has spent the past decade designing tools and strategies for the molecular evolution of different ligninases in yeast (oxidoreductases involved in the degradation of lignin during natural wood decay) (Alcalde 2015; Garcia-Ruiz et al. 2014). In this communication, we present a detailed protocol to prepare and screen mutant libraries in *S. cerevisiae* for a model flavooxidase, -aryl-alcohol oxidase (AAO) (Hernandez-Ortega et al. 2012a)-, that can be easily translated to many other enzymes. The protocol involves a focused-directed evolution method (MORPHING: Mutagenic Organized Recombination Process by Homologous in vivo Grouping) assisted by the yeast cell apparatus (Gonzalez-Perez et al. 2014), and a very sensitive screening assay based on the Fenton reaction in order to detect AAO activity secreted into the culture broth (Rhee et al. 2010).

4.2 PROTOCOL

1. **Mutant Library Construction**

1.1. Choose the regions to be subjected to MORPHING with the help of computational algorithms based on the available crystal structure or homology models (Sebestova et al. 2014).

1.1.1. Here, two regions of AAO from *Pleurotus eryngii* were targeted for random mutagenesis and recombination (Met[α1]-Val109, Phe392-Gln566), while the remainder of the gene (844 bp) was amplified by high-fidelity PCR, **Figure 1**.

Note: Several segments can be studied by MORPHING in an independent or combined manner16.

1.2. Amplify the targeted areas by mutagenic PCR. Create overlapping areas between segments (~50 bp each) by superimposing PCR reactions of the defined regions.

1.2.1. Prepare mutagenic PCR of targeted segments in a final volume of 50 µL containing DNA template (0.92 ng/µL), 90 nM oligo sense (RMLN for segment M-I and AAO-BP for segment M-II), 90 nM antisense primer (AAO-92C for segment M-I and RMLC for segment M-II) , 0.3 mM dNTPs (0.075 mM each), 3% (v/v) dimethylsulfoxide (DMSO), 1.5 mM $MgCl_2$, 0.05 mM $MnCl_2$ and 0.05 U/µL *Taq* DNA polymerase. Primers sequences are detailed in **Figure 1**.

1.2.2. Use the following PCR program: 95 °C for 2 min (1 cycle); 95 °C for 45 s, 50 °C for 45 s, 74 °C for 45 s (28 cycles); and 74 °C for 10 min (1 cycle).

1.3. Amplify the non-mutagenic regions with ultra-high fidelity polymerase and include the corresponding areas overlapping the mutagenic segments and/or linearized vector overhangs.

1.3.1. Prepare reaction mixtures in a final volume of 50 µL containing: DNA template (0.2 ng/µL), 250 nM oligo sense HFF, 250 nM oligo antisense HFR, 0.8 mM dNTPs (0.2 mM each), 3% (v/v) dimethylsulfoxide (DMSO) and 0.02 U/µL iproof DNA polymerase. Primers sequences are detailed in **Figure 1**.

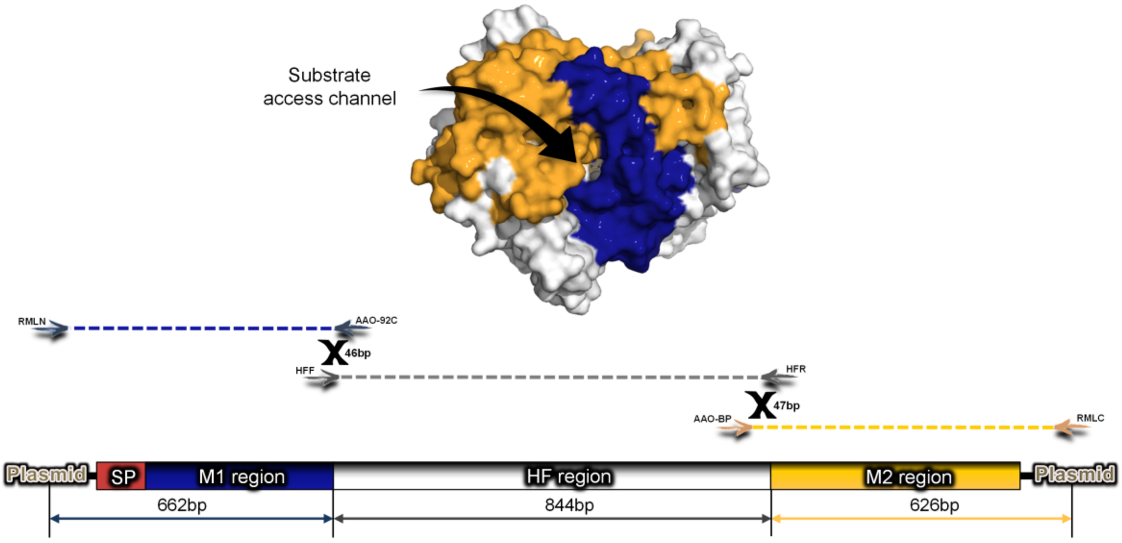

Primer name	Sequence (5'->3')	Length (bp)	Tm (°C)	PCR
RMLN	CCTCTATACTTTAACGTCAAGG	22	51.1	epPCR
AAO-92C	CCCAGTTCCATCCTTCATCGCCA	23	58.8	
HFF	TTCGATCGCTATGCGGCTGTCAC	23	58.8	HF-PCR
HFR	GGGTGGAACCATTGGTTGGAAA	22	54.8	
AAO-BP	AACTCTGCTCATTGGGAGACCATCT	25	57.7	epPCR
RMLC	GGGAGGGCGTGAATGTAAGC	20	55.9	

Figure 1. MORPHING protocol for AAO evolution. Two different regions of AAO were targeted for random mutagenesis and recombination: M1 (blue) that includes the signal peptide (SP); M2 (yellow). The HF region (grey) was amplified with high fidelity polymerases. Mutagenic regions were mapped in the crystal structure of AAO (PDB ID: 3FIM).

1.3.2. Use the following PCR program: 98 °C for 30 s (1 cycle); 98 °C for 10 s, 55 °C for 25 s, 72 °C for 45 s (28 cycles); and 72 °C for 10 min (1 cycle).

Note: With conditions described in 1.2 and 1.3 overlaps of 43 bp (plasmid-M1 region); 46 bp (M1 region-HF region); 47 bp (HF region-M2 region) and 61 bp (M2 region- plasmid) are designed (Figure 1) to favor in vivo splicing in yeast. All the PCR fragments (mutagenic and non-mutagenic) are purified by conventional agarose gel extraction.

1.4. Linearize the vector such that flanking regions of approximately 50 bp are created that are homologous to the 5´- and 3´-ends of the target gene.

1.4.1 Prepare a linearization reaction mixture containing 2 µg DNA, 7.5 U *BamHI*, 7.5 U *XhoI*, 20 µg BSA and 2 µL of Buffer NBamHI 10x in a final volume of 20 µL.

1.4.2 Incubate the reaction mixture at 37°C for 2 hours and 40 minutes. Afterwards, proceed with inactivation at 80 °C for 20 minutes.

1.5. Purify the linearized vector by agarose gel extraction to avoid contamination with the residual circular plasmid, **Figure 2**.

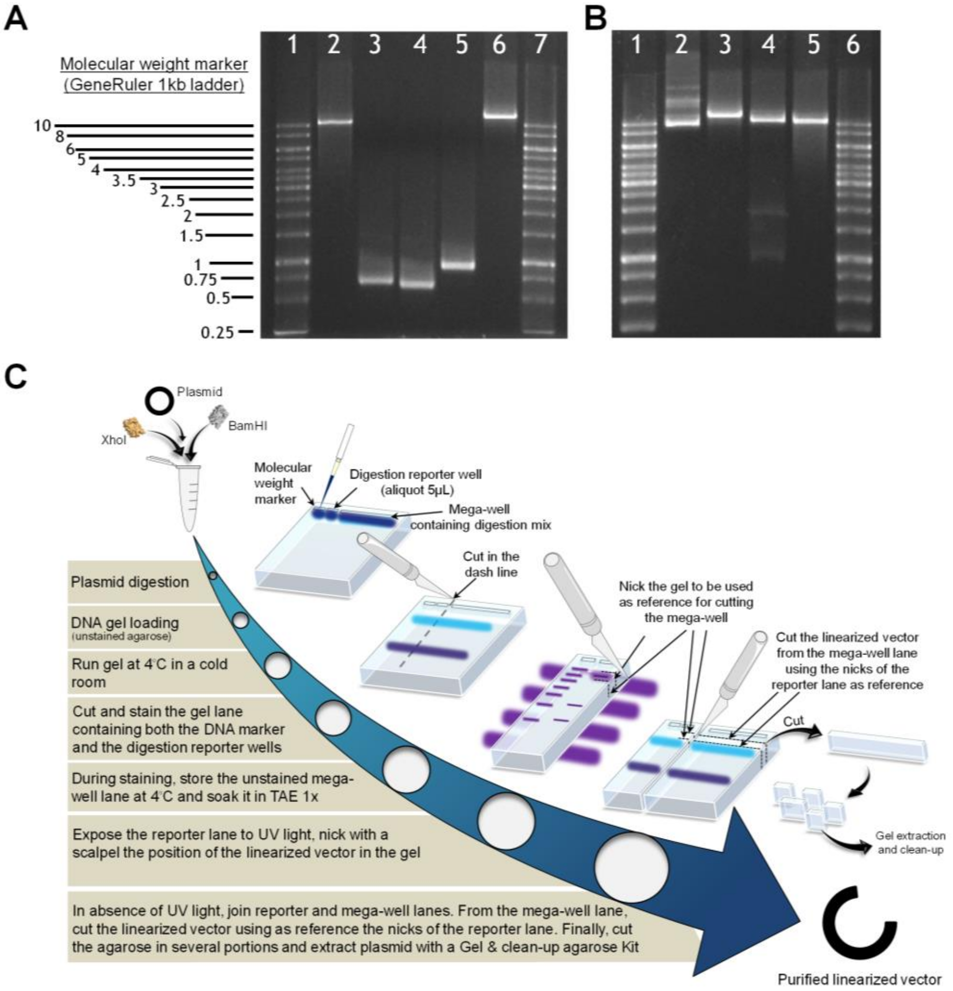
A
Molecular weight marker
(GeneRuler 1kb ladder)
10
8
6
5
4
3.5
3
2.5
2
1.5
1
0.75
0.5
0.25
1 2 3 4 5 6 7
B
1 2 3 4 5 6
C
Plasmid
XhoI
BamHI
Molecular weight marker
Digestion reporter well (aliquot 5µL)
Mega-well containing digestion mix
Cut in the dash line
Nick the gel to be used as reference for cutting the mega-well
Cut the linearized vector from the mega-well lane using the nicks of the reporter lane as reference
Cut
Gel extraction and clean-up
Plasmid digestion
DNA gel loading (unstained agarose)
Run gel at 4°C in a cold room
Cut and stain the gel lane containing both the DNA marker and the digestion reporter wells
During staining, store the unstained mega-well lane at 4°C and soak it in TAE 1x
Expose the reporter lane to UV light, nick with a scalpel the position of the linearized vector in the gel
In absence of UV light, join reporter and mega-well lanes. From the mega-well lane, cut the linearized vector using as reference the nicks of the reporter lane. Finally, cut the agarose in several portions and extract plasmid with a Gel & clean-up agarose Kit
Purified linearized vector

Figure 2. Preparation of PCR products and the linearized vector. (A) Analytical agarose gel (1 % w:v) containing a molecular weight marker (GeneRuler 1Kb ladder) in lanes 1 and 7; the *BamHI* and *XhoI* linearized vector, lane 2; PCR segment M1, lane 3; PCR segment M2, lane 4; PCR segment HF, lane 5; the in vivo reassembled vector linearized with NheI (containing the full AAO gene with regions M-I, HF and M-II), lane 6. (B) Vector linearization, lanes 1 and 6 molecular standards, 1 Kb ladder; plasmid miniprep, lane 2; plasmid linearized with NheI, lane 3; plasmid linearized with *BamHI* and *XhoI*, lane 4; linearized plasmid obtained by gel extraction and clean-up after digestion, lane 5. (C) Protocol for plasmid purification.

1.5.1. Load the digestion reaction mix into the mega-well of a semi-preparative low melting point agarose gel (0.75%, w:v) as well as an aliquot (5 µL) of the reaction mix in the adjacent well as a reporter.

1.5.2. Run DNA electrophoresis (5 V/cm between electrodes, 4 ºC) and separate the agarose gel corresponding to the mega-well and store it at 4 ºC in 1X TAE.

1.5.3. Using Gel Red, stain the lane with the molecular weight ladder and the reporter. Visualize the bands under UV light. Nick the position where the linearized vector places.

Note: As the quality of the purified linearized vector is a critical factor for successful recombination and assembly in yeast, avoid gel staining for semi-preparative DNA electrophoresis. The use of dyes and UV exposure for gel extraction may affect the stability of the DNA vector, compromising the in vivo recombination efficiency. As alternative to toxic EtBr dyes, Gel Red and SYBR dyes (main options in the market include SYBR GOLD, SYBR GREEN I, SYBR SAFE) are commonly used for gel staining.

1.5.4. In the absence of UV light, identify the linearized vector in the mega-well fragment using the guidance of the nicks in the stained reporter lane so that it can be isolated.

1.5.5. Extract the linearized vector from agarose and purify it with a commercial gel extraction kit according to manufacturer’s protocol.

Note: Use high-copy episomal shuttle vectors with antibiotic and auxotrophy markers: In this example we employed the uracil independent and ampicillin resistance pJRoC30 vector, under the control of the yeast GAL1 promoter.

1.6. Prepare an equimolar mixture of the PCR fragments and mix it with the linearized vector at a 2:1 ratio, with no less than 100 ng of linearized plasmid (test different ratios of equimolar library/open vector to achieve good transformation yields).

1.6.1. Measure the absorbance of the PCR fragments and linearized vector at 260 nm and 280 nm to determine their concentration and purity.

1.7. Transform yeast competent cells with the DNA mixture using a commercial yeast transformation kit (see Table for supplies) according to manufacturer’s instructions.

1.7.1. Here, use a protease deficient and URA3- dependent S. cerevisiae strain, BJ5465. Transform the cells with the parental circularized vector as an internal standard during screening (see below). Additionally, check the background by transforming the linearized vector in the absence of PCR fragments.

Note: In case of detecting initial low secretion levels, it is advisable to use *S. cerevisiae* protease deficient strains like BJ5465 to foster the accumulation of active protein in culture supernatants. If the target enzyme undergoes hyperglycosylation, the use of glycosylation-deficient strains (e.g. *Δkre2* that is only capable of attaching smaller mannose oligomers) could be a suitable option.

1.8. Plate the transformed cells on SC drop-out plates and incubate them at 30 °C for three days. Plate (on SC drop-out plates supplemented with uracil) URA3$^-$ *S. cerevisiae* cells lacking the plasmid as a negative control for screening (see below).

2. High-Throughput Screening Assay, Figure 3

2.1. Fill an appropriate number of sterile 96-well plates (23 plates to analyze a library of 2,000 clones) with 50 µL minimal medium per well with the help of a pipetting robot.

2.2. Pick individual colonies from the SC-drop out plates and transfer them to the 96-well plates.

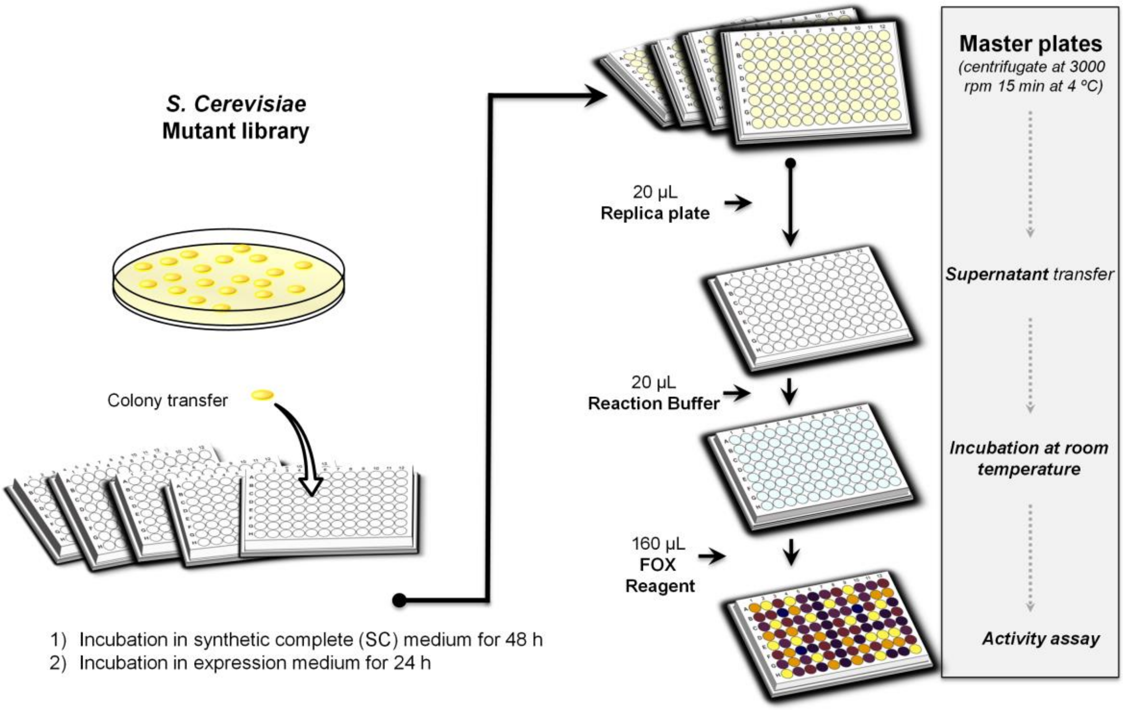
S. Cerevisiae
Mutant library
Colony transfer
1) Incubation in synthetic complete (SC) medium for 48 h
2) Incubation in expression medium for 24 h
20 µL
Replica plate
20 µL
Reaction Buffer
160 µL
FOX
Reagent
Master plates
(centrifugate at 3000 rpm 15 min at 4 °C)
Supernatant transfer
Incubation at room temperature
Activity assay

Figure 3. High-throughput screening protocol. Overview of the process.

2.2.1. In each plate, inoculate column number 6 with the parental type as an internal standard and well H1 with URA3$^-$ *S. cerevisiae* cells (in SC medium supplemented with uracil) with no plasmid as a negative control.

Note: Well H1 is filled specifically with drop-out media supplemented with uracil. A blank well containing media without cells can be also prepared as an additional sterility control.

2.3. Cover the plates with their lids and wrap them in Parafilm. Incubate plates for 48 h at 30 °C, 225 rpm and 80% relative humidity in a humid shaker.

2.4. Remove the Parafilm, add 160 µL of expression medium to each well with the help of the pipetting robot, reseal the plates and incubate them for a further 24 h.

Note: Minimal medium and expression medium are prepared as reported elsewhere (Viña-Gonzalez et al. 2015). Secretion levels may vary depending on the gene under study and accordingly, the incubation times must be optimized in each case to synchronize the cell growth in all the wells.

2.5. Centrifuge the plates (master plates) at 2,800 x g for 10 min at 4 °C.

2.6. Transfer 20 µL of the supernatant from the wells in the master plate to the replica plate using a liquid handling robotic multistation.

Note: To favor enzyme secretion it is advisable to replace the native signal peptide of the target protein by signal peptides commonly used for heterologous expression in yeast (e.g. the α factor prepro-leader, the leader of the K1 Killer toxin from *S. cerevisiae*, or even chimeric versions of both peptides (Alcalde 2015)). Alternatively, the native signal peptide can be exclusively evolved for secretion in yeast.

2.7. Add 10 µL of 2 mM *p*-methoxybenzylalcohol in 100 mM sodium phosphate buffer pH 6.0 with the help of the pipetting robot. Stir the plates briefly with a 96-well plate mixer and incubate them for 30 min at room temperature.

2.8. With the pipetting robot, add 160 µL of the FOX reagent to each replica plate and stir briefly with the mixer (final concentration of FOX mixture in the well: 100 µM xylenol orange, 250 µM $Fe(NH_4)_2(SO_4)_2$ and 25 mM H_2SO_4).

2.8.1. Add several additives to the reagent to enhance sensitivity, such as organic co-solvents (DMSO, ethanol, methanol) or sorbitol (Rhee et al. 2010). Here, amplify the response by adding sorbitol to a final concentration of 100 mM, **Figure 4**.

2.9. Read the plates (end-point mode, t_0) at 560 nm on a plate reader.

and the absorbance of the XO-Fe^{3+} complex is measured at 560 nm. Ferrous oxidation is amplified by the addition of sorbitol to the reagent mixture.

2.10. Incubate the plates at room temperature until the color develops and measure the absorption again (t_1).

2.10.1. Calculate the relative activity from the difference between the Abs value after incubation and that of the initial measurement normalized to the parental type for each plate ($\Delta t_1 - t_0$).

2.11. Subject the best mutant hits to two consecutive re-screenings to rule out false positives.

Note: Typically, re-screenings include plasmid isolation from yeast, amplification and purification in *Escherichia coli*, followed by transformation of fresh yeast cells with the plasmid (Viña-Gonzalez et al. 2015). Each selected clone is re-screened in pentaplicate.

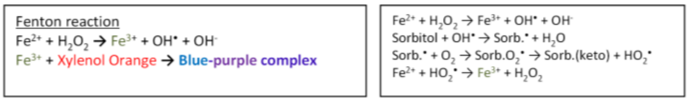
Fenton reaction
$Fe^{2+} + H_2O_2 \rightarrow Fe^{3+} + OH^{\bullet} + OH^{-}$
Fe^{3+} + Xylenol Orange → Blue-purple complex
$Fe^{2+} + H_2O_2 \rightarrow Fe^{3+} + OH^{\bullet} + OH^{-}$
$\text{Sorbitol} + OH^{\bullet} \rightarrow \text{Sorb.}^{\bullet} + H_2O$
$\text{Sorb.}^{\bullet} + O_2 \rightarrow \text{Sorb.}O_2^{\bullet} \rightarrow \text{Sorb.(keto)} + HO_2^{\bullet}$
$Fe^{2+} + HO_2^{\bullet} \rightarrow Fe^{3+} + H_2O_2$

Figure 4. The FOX method. White-rot fungi attack the cell wall of wood through a Fenton reaction that produces hydroxyl radical OH•. The FOX method couples this reaction to xylenol orange (XO).

4.3 REPRESENTATIVE RESULTS

AAO from *P. eryngii* is an extracellular flavooxidase that supplies fungal peroxidases with H_2O_2 to start attacking lignin. Two segments of AAO were subjected to focused-directed evolution by MORPHING in order to enhance its activity and its expression in *S. cerevisiae* 19. Irrespective of the foreign enzyme/s harbored by *S. cerevisiae*, the most critical issue when constructing mutant libraries in yeast concerns the engineering of specific overlapping regions to favor the splicing between fragments and their cloning into the linearized vector. In the current example, for each PCR reaction, all the fragments had overhangs of approximately 50 bp to promote in vivo splicing in yeast. The number of recombination events is dependent on the number of segments to be assembled and cloned with the linearized vector (i.e. two crossover events took place between the three PCR segments -the two mutagenic segments flanking the non-mutagenized segment- plus two additional crossovers with the linearized vector; **Figure 1**). According to our experience, overlapping sequences longer than 50 bp decrease the likelihood of internal recombination while they do not improve transformation efficiency.

Mutational loads were adjusted by sampling mutant libraries with different landscapes, calculating the number of clones with <10% of the parental enzyme activity, and further checking them by sequencing a random sample of active and non-active variants, **Figure 5A**.

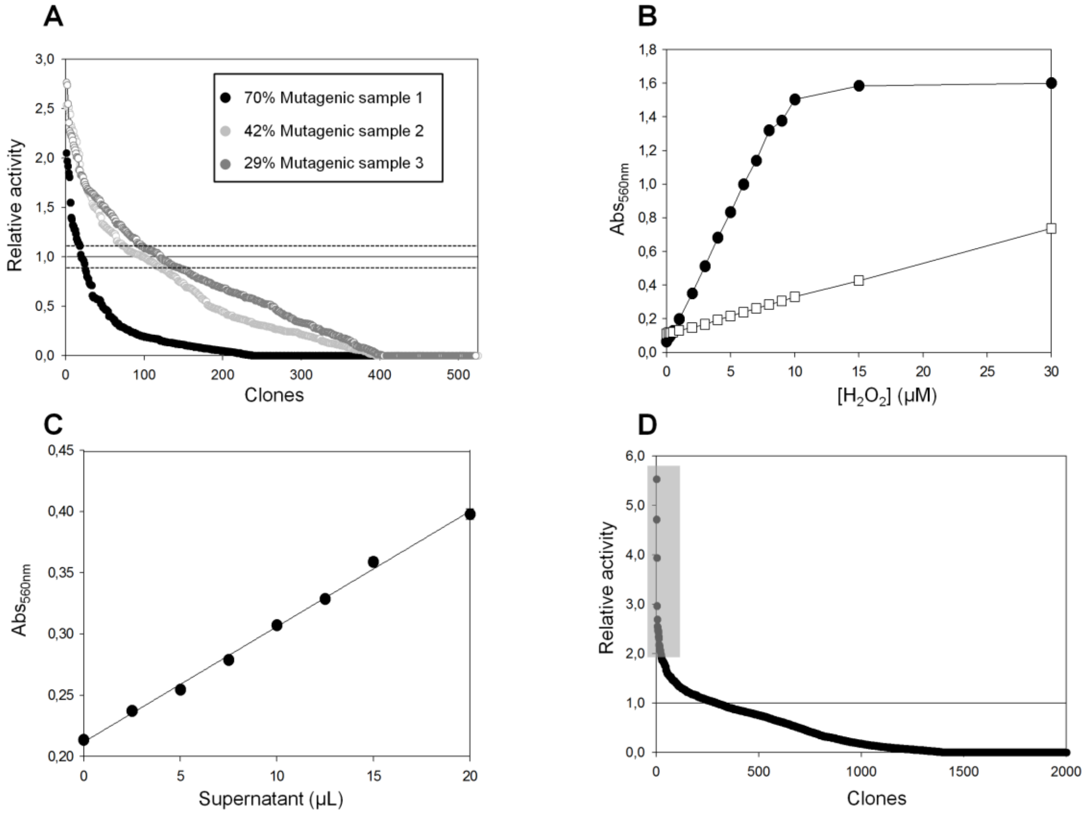

Figure 5. Mutagenic landscapes for MORPHING libraries using different error prone PCR conditions and validation of the screening assay. (A) MORPHING landscapes. Solid horizontal line shows the activity of the parental type in the assay while the dashed lines indicate the coefficient of variance of the assay. The percentages indicate the number of clones with less than 10% of the parental enzyme activity. Activities are plotted in descending order. (B) The FOX detection limit was evaluated with increasing concentrations of H_2O_2 in the presence (black circles) and absence (white squares) of sorbitol. (C) Linear correlation between AAO concentration (transformant supernatants) and Abs560nm. Each point corresponds to the average of 8 experiments and includes the standard deviation. (D) Mutant library landscape. The selected variants (shadowed square) were rescreened as reported elsewhere19. Solid line shows the activity of AAO parental type.

For the determination of the coefficient of variance *S. cerevisiae* cells were transformed with the parental AAO and plated on SC-drop out plates. Individual colonies were picked and inoculated in a 96 well-plate and the activity of the clones was evaluated from fresh preparations. Mutagenic sample 2 (*Taq*/$MnCl_2$ 0.05 mM) was chosen as the departure point for library construction and screening.

As the biological activity of AAO increases the H_2O_2 concentration in the reaction medium, we searched for a sensitive and accurate assay to quantify minor changes in H_2O_2. FOX is a chemical method based on the Fenton reaction (Gay et al. 1999), whereby oxidation by H_2O_2 drives the reaction of Fe^{3+} with xylenol orange to form a blue-purple complex (o-cresolsulfone-phthalein 3',3''-bis(methylimino)diacetate $\varepsilon_{560} = 1.5x104\ M^{-1}cm^{-1}$). The ferrous oxidation step was amplified by adding sorbitol to enhance the sensitivity of the assay, increasing the propagation of radicals with an apparent ε_{560} =2.25x105 $M^{-1}cm^{-1}$, **Figure 4**.

The detection limit of this assay (in the µM range) was calculated by the Blank determination method in a 96-well plate with standards in triplicate (0, 0.5, 1, 1.5, 2, 2.5, 3 and 4 µM H_2O_2) and using several supernatants from *S. cerevisiae* lacking the $URA3^-$ plasmid (Figure 5B). The assay was linear in the presence of sorbitol (up to 8 µM of H_2O_2), and although linearity was more persistent in the absence of this sugar (at least up to 30 µM of H_2O_2) the response was weaker (e.g., at 6 µM of H_2O_2, a 4-fold enhancement was obtained in the presence of sorbitol -deep purple- from an absorbance of 0.24 in its absence -dark orange- **Figure 5B**). The relationship between Abs and the AAO concentration was evaluated with increasing amounts of enzyme (from yeast supernatants) and a linear response was observed; R^2= 0.997, **Figure 5C**.

It is notable that the FOX signal was stable for several hours without any apparent interference by the different elements in the culture broth. The estimated sensitivity of FOX was ~ 0.4 µM of H_2O_2 produced by the AAO in the supernatant in the presence of sorbitol, and ~ 2 µM in its absence.

A mutant library of 2,000 clones was constructed and screened with this assay. Several AAO mutants were identified with notably improved secretion and activity against *p*-methoxybenzyl alcohol, **Figure 5D** (Viña-Gonzalez et al. 2015).

4.4 DISCUSSION

In this article, we have summarized most of the tips and tricks employed in our laboratory to engineer enzymes by directed evolution in *S. cerevisiae* (using AAO as an example) so that they can be adapted for use with many other eukaryotic enzyme systems by simply following the common approach described here.

In terms of library creation, MORPHING is a fast one-pot method to introduce and recombine random mutations in small protein stretches while leaving the remaining regions of the protein unaltered (Gonzalez-Perez et al. 2014). Libraries with several mutational loads can be readily prepared and recombined in vivo, along with the linearized plasmid, to generate a full autonomously replicating vector. The overlapping sequences flanking each stretch allow the fragments of the full gene to be reassembled through in vivo recombination, avoiding extra PCR reactions and in vitro ligation steps. In this protocol, the frequency of crossover events between PCR fragments can be increased by reducing the size of the overlapping regions, although this may compromise the transformation efficiency. Regardless of the DNA polymerases used for mutagenic PCR, the mutational loads can be adjusted by previously constructing and analyzing small mutant library landscapes, **Figure 5A**. If the GeneMorph II Kit is used, it is still advisable to follow this approach since in vivo DNA recombination can notably modify the mutational loads estimated by the manufacturer. In general terms, mutant landscapes in which 35-50% of the total clones screened have less than 10% of the parental activity are suitable for directed evolution campaigns, although this number varies in function of the target protein and its activity. Typically, the analysis of mutant libraries landscapes are further verified by DNA sequencing of a random sample of mutants. In the current example, the *Taq* DNA polymerase was used due to its high error rate, which is linked to the lack of 3´→5´proof-reading exonuclease activity. The mutational loads in Taq libraries were modified by the addition of different concentrations of $MnCl_2$, but the use of unbalanced dNTPs and/or the reduction in gene template concentrations are also suitable options. Inherent limitations of MORPHING come from the number of segments to be recombined. According to our experience, up to four protein blocks (five crossover events counting the recombination areas with the linearized vector) can be spliced with good transformation yields (~10^5 clones per transformation reaction). This method can be easily modified to performed multiple site-saturation mutagenesis (e.g. using NDT degenerated primers or creating degeneracy for 22 unique codons) to explore several positions simultaneously while reducing significantly the screening efforts (Reetz 2013; Mate et al. 2017).

The direct "blind" screening protocol for AAO is extremely sensitive and reliable (based on the direct detection of H_2O_2 regardless of the substrate used by the enzyme), representing a complementary assay to other well established indirect protocols to detect peroxides (mostly coupling peroxidases with colorimetric substrates). Indeed, the FOX assay has been routinely employed to measure H_2O_2 in biological fluids, and it can now be easily translated into protocols to evolve AAO and any other H_2O_2 producing enzymes (e.g., glucose oxidases, cellobiose dehydrogenases, glyoxal oxidases, methanol oxidases), particularly for activity on non-natural substrates where responses are otherwise hard to detect.

S. cerevisiae is the most adequate host for directed evolution of eukaryotic genes since it offers high transformation efficiencies (up to 1 x 10^6 transformants/µg DNA), it performs complex post-translational processing and modifications (including N- and C-terminal processing, and glycosylation) and it exports foreign proteins into the culture broth via a secretory pathway. In addition, well-established molecular biology tools are available to work with this yeast, including uni- or bi-directional episomal (non-integrative) shuttle vectors under the control of promoters of different strengths. Last but not least, its high frequency of homologous DNA recombination has allowed a range of methods to be developed to obtain DNA diversity that are currently being used to evolve single proteins, as well as more complex enzyme pathways (Gonzalez-Perez et al. 2012; Shao et al. 2009; Alcalde 2015; Chao et al. 2015). The in vivo gap repair and the proof-reading device of this yeast can be also employed to create chimeras when recombining different genes (with approx. 60% of DNA sequence identity), as well as to shuffle best offspring/mutations from a directed evolution campaign, or to bring together in vitro and in vivo recombination methods in one round of evolution, thereby enriching mutant libraries in terms of foldability and function.

ACKNOWLEDGMENTS

This work was supported by the European Commission project Indox-FP7-KBBE-2013-7-613549; a Cost-Action CM1303-Systems Biocatalysis; and the National Projects Dewry [BIO201343407-R] and Cambios [RTC-2014-1777-3].

Chapter V:

Functional expression of aryl-alcohol oxidase in *Saccharomyces cerevisiae* and *Pichia pastoris* by directed evolution.

Once the directed evolution platform was set up, we further evolved AAO while testing the combination of two different systems (*S. cerevisiae* and *P. pastoris*) for the engineering and overproduction -in bioreactor- of AAO variants.

V

CHAPTER

V

Functional expression of aryl-alcohol oxidase in *Saccharomyces cerevisiae* and *Pichia pastoris* by directed evolution.

Javier Viña-González, Katharina Elbl, Xavier Ponte, Francisco Valero and Miguel Alcalde

Biotechnology & Bioengineering. 115: 1666-1674.

https://doi.org/10.1002/bit.26585

Aryl-alcohol oxidase (AAO) plays a fundamental role in the fungal ligninolytic secretome, acting as a supplier of H_2O_2. Despite its highly selective mechanism of action, the presence of this flavooxidase in different biotechnological settings has hitherto been hampered by the lack of appropriate heterologous expression systems. We recently described the functional expression of the AAO from *Pleurotus eryngii* in *Saccharomyces cerevisiae* by fusing a chimeric signal peptide (preαproK) and applying structure-guided evolution. Here, we have obtained an AAO secretion variant that is readily expressed in *S. cerevisiae* and overproduced in *Pichia pastoris*. First, the functional expression of AAO in *S. cerevisiae* was enhanced through the *in vivo* shuffling of a panel of secretion variants, followed by the focused evolution of the preαproK peptide. The outcome of this evolutionary campaign -an expression variant that accumulated 4 mutations in the chimeric signal peptide, plus two mutations in the mature protein- showed 350-fold improved secretion (4.5 mg/L) and was stable. This secretion mutant was cloned into *P. pastoris* and fermented in a fed-batch bioreactor to enhance production to 25 mg/L. While both recombinant AAO from *S. cerevisiae* and *P. pastoris* were subjected to similar N-terminal processing and had a similar pH activity profile, they differed in their kinetic parameters and thermostability. The strong glycosylation observed in the evolved AAO from *S. cerevisiae* underpinned this effect, since when the mutant was produced in the glycosylation-deficient *S. cerevisiae* strain *Δkre2*, its kinetic parameters and thermostability were comparable to its poorly glycosylated *P. pastoris* recombinant counterpart.

5.1 INTRODUCTION

Aryl-alcohol oxidase (AAO, EC.1.1.3.7) is a monomeric extracellular flavoprotein that oxidizes a wide range of aromatic alcohols to their corresponding carbonyl compounds, concomitantly releasing H_2O_2. As a member of the glucose-methanol-choline (GMC) oxidoreductase superfamily, this FAD-dependent enzyme is secreted by different basidiomycetes involved in natural wood decay. The main role of AAO in nature is to supply ligninolytic peroxidases with H_2O_2, as well as to switch on the Fenton reaction in the combustion of lignin (Ferreira et al. 2005; Hernandez-Ortega et al. 2012a). In terms of biotechnological settings, AAO could be used in lignocellulose biorefineries to produce 2nd generation biofuels and added-value chemicals (Martinez et al. 2009; Alcalde, 2015). Moreover, and thanks to a highly enantioselective mechanism, AAO becomes very attractive for the chiral resolution of secondary alcohols aimed at obtaining valuable building blocks for pharmaceutical processes (Hernandez-Ortega et al. 2012c). Along these lines, recent findings highlight the oxidative potential of this enzyme with renewal chemicals, such as furfural derivatives for the (bio)polymer industry (Carro et al. 2015; Martinez et al. 2017). Despite these promising features, the lack of suitable heterologous functional expression systems in which the properties of AAO can be sculptured by directed evolution has precluded the use of this versatile flavooxidase in different industrial applications. We previously reported the initial functional expression of AAO from the white-rot fungus *Pleurotus eryngii* in *Saccharomyces cerevisiae* (Viña-Gonzalez et al. 2015). This was achieved by designing a chimeric signal peptide (preαproK) that fused the pre- and pro-region of the α-factor and the K1 killer toxin prepro-leaders from *S. cerevisiae*, and subsequently employing directed evolution to restricted AAO regions. We obtained a panel of AAO secretion variants that was led by the $_{Sac}$FX7 mutant, in which the consensus/ancestral substitution (H91N) was responsible for a ~100-fold improvement in total activity, as well as enhanced stability in terms of temperature and pH.

The current work describes a tandem-yeast expression system for AAO that links the directed evolution for secretion in *S. cerevisiae* to its over-production in *Pichia pastoris* on a bench-bioreactor scale. Harnessing the high frequency of homologous DNA recombination of *S. cerevisiae*, mutant libraries were constructed by shuffling $_{Sac}$FX7 with an ensemble of AAO secretion variants, while the chimeric peptide was further subjected to independent mutational loading. The resulting evolved AAO was transferred to *P. pastoris* for overproduction in a fed-batch bioreactor and characterized biochemically. To shed light on the effects exerted by hyperglycosylation in *S. cerevisiae*, the recombinant variant expressed in *P. pastoris* was further benchmarked with its counterpart secreted by a glycosylation-deficient *S. cerevisiae* strain.

5.2 MATERIAL AND METHODS

Strains and chemicals

All chemical were reagent-grade purity. Basal salts, PTM1 salts, *p*-methoxybenzyl alcohol, ABTS (2,2'-azino-bis(3-ethylbenzothiazoline-6-sulphonic acid)), horseradish peroxidase (HRP), *Taq* polymerase and the Yeast Transformation Kit were purchased from Sigma-Aldrich (SaintLouis, MO, USA). Zymoprep Yeast Plasmid Miniprep, Yeast Plasmid Miniprep Kit I and Zymoclean Gel DNA Recovery Kit were from Zymo Research (Orange, CA, USA). The P. pastoris expression vector (pPICZ B), the *P. pastoris* strain X-33 and zeocin were purchased from Invitrogen (Carlsbad, CA, USA). The protease deficient *S. cerevisiae* strain BJ5465 (MATa *ura3-52 trp1 leu2Δ1 his3Δ200 pep4::HIS3 prb1Δ1.6R can1 GAL*) was from LGC Promochem (Barcelona, Spain) whereas the glycosylation deficient S. cerevisiae strain YDR483W BY4742 (MATalpha his3*Δ*1 leu2*Δ*0 lys2*Δ*0 ura3*Δ*0 *Δ*KRE2) was from ATCC (Manassas, VA, USA). The Escherichia coli strainXL2-Blue competent cells and Phusion DNA Polymerase were obtained from Agilent Technologies (Santa Clara, CA, USA). Restriction endonucleases *BamHI, XhoI*, *XbaI*, *KpnI*, *PmeI*, the DNA Ligation Kit, the Antarctic phosphatase, EndoH and T4 DNA Ligase were purchased from New England Biolabs (Ipswich, MA, USA). Oligonucleotide primers were acquired from Isogen Life Science (Barcelona, Spain).

Culture media

Culture media for *Saccharomyces cerevisiae*: Minimal medium contained 0.67% (w:v) yeast nitrogen base, 1.92 g/L yeast synthetic drop-out medium supplement without uracil, 2% (w:v) raffinose and 25 µg/mL chloramphenicol. SC drop-out plates contained 0.67% (w:v) yeast nitrogen base, 1.92 g/L yeast synthetic drop-out medium supplement without uracil, 2% (w:v) bacto agar, 2% (w:v) D-glucose and 25 µg/mL chloramphenicol. YP medium contained 10 g yeast extract, 20 g peptone and double-distilled H_2O (ddH_2O) to 650 mL. Expression medium contained 144 mL YP 1.55x, 13.4 mL 1M KH_2PO_4 pH 6.0 buffer, 22.2 mL 20% galactose (w:v), 0.222 mL 25 µg/mL chloramphenicol and ddH_2O to 200 mL.

Culture media for Pichia pastoris: YPD medium contained 10 g/L yeast extract, 20 g/L peptone, 4 g/L D-glucose and 25 µg/mL zeocin whereas YPD plates also contained 2% (w:v) bacto agar. BMD1 medium contained 100 mM potassium phosphate buffer pH 6.0, 3.5 g/L yeast nitrogen base without amino acids, 400 µg/L biotin and 10 g/L D-glucose. BMM2 medium contained 100 mM potassium phosphate buffer pH 6.0, 3.5 g/L yeast nitrogen base without amino acids, 400 µg/L biotin and 2% methanol (v:v). BMM10 medium contained 100 mM potassium phosphate buffer pH 6.0, 3.5 g/L yeast nitrogen base without amino acids, 400 µg/L biotin and 10% methanol (v:v). BMMY medium contained 100 mM potassium phosphate buffer pH 6.0, 3.5 g/L yeast nitrogen base without amino acids, 400 µg/L biotin and 0.5% methanol (v:v). Basal salts medium contained 26.7 mL/L 85% phosphoric acid, 0.93 g/L $CaSO_4{\cdot}2H_2O$, 14.9 g/L $MgSO_4{\cdot}7H_2O$, 18.2 g/L K_2SO_4, 4.13 g/L KOH and 40 g/L glycerol.

Culture media for *Escherichia coli*: Luria-Bertani (LB) medium contained 10 g NaCl, 5 g yeast extract, 10 g peptone, 1 mL 100 mg/mL ampicillin and ddH_2O to 1 L whereas LB agar plates also contained 2% (w:v) bacto agar.

Laboratory evolution

In vivo shuffling: PCR reactions were performed separately with mutants $_{Sac}$FX7, $_{Sac}$13H2, $_{Sac}$10G5, $_{Sac}$7A11, $_{Sac}$4C7 and $_{Sac}$12G12. Reaction mixtures were prepared in a final volume of 50 µL containing DNA template (0.92 ng/µL), 90 nM oligo sense RMLN (5’-CCTCTATACTTTAACGTCAAGG-3’), 90 nM Reverse primer RMLC (5’-GGGAGGGCGTGAATGTAAGC-3’), 0.3 mM dNTPs (0.075 mM each), 3% (v:v) dimethylsulfoxide (DMSO), 1.5 mM $MgCl_2$, increasing concentrations of $MnCl_2$ (0.025, 0.05, 0.1 mM) and 0.05 U/µL Taq DNA polymerase. PCRs were performed in a thermocycler (Mycycler, Bio-Rad,Hercules, CA, USA) and parameters were: 95°C for 2 min (1 cycle); 95°C for 45 s, 50°C for 45 s, 74°C for 45 s (28 cycles); and 74°C for 10 min (1 cycle). The PCR products were mixed with the linearized episomal shuttle vector pJRoC30 (at a PCR product/linearized plasmid ratio of 6:1) and transformed into competent *S. cerevisiae* cells to promote *in vivo* DNA shuffling. The whole gene was reassembled in vivo by transformation into *S. cerevisiae*, a process facilitated by the design of ~50-bp overhangs flanking each recombination area. Transformed cells were plated on SC drop-out plates and incubated for 3 days at 30°C. Colonies containing the whole autonomously replicating vector were picked and subjected to high-throughput screening.

MORPHING library at the preαproK: The preαproK signal peptide of $_{Sac}$FX8 variant (261 bp) was used as DNA template for focused random mutagenesis technique MORPHING (Mutagenic Organized Recombination Process by Homologous IN vivo Grouping) (Gonzalez-Perez et al., 2014). Mutagenic PCR was prepared in a final volume of 50 µL containing: 90 nM RMLN, 90 nM C-ter prokiller (5´-ACGCTTGGCCACTGCTGGAAT-3’), 0.3 mM dNTPs (0.075 mM each), 3% DMSO, 0.1 mM MnCl2, 1.5 mM MgCl2, 0.05 U/µL *Taq* polymerase DNA, and 0.92 ng/µL template. The amplification parameters were 95°C for 2 min (1 cycle); 94°C for 45 s, 50°C for 45 s, and 74°C for 30 s (28 cycles); and 74°C for 10 min (1 cycle). The whole AAO gene (1701 bp) was amplified by high-fidelity PCR in a final volume of 50 µL containing: 250 nM oligo sense N-ter AAO (5'-GCCGATTTTGACTACGTTGTCGTCG-3'), 250 nM oligo antisense RMLC, 1 mM dNTPs (0.25 mM each), 3% DMSO, 0.05 U/µL Phusion DNA polymerase, and 2 ng/µL template. High-fidelity PCR was performed using the following parameters: 95°C for 2 min (1 cycle); 94°C for 30 s, 50°C for 30 s, 74°C for 2 min (30 cycles); and 74°C for 10 min (1 cycle). PCR products were mixed in equimolar amounts, 200 ng mutagenic signal peptide and 200 ng mature non-mutagenized protein, and transformed with linearized pJRoC30 (200 ng) into chemically competent cells, as described above.

High-throughput screening (HTS) assay: Individual clones were picked and cultured in sterile 96-well plates containing 50 µL of minimal medium. In each plate, column number 6 was inoculated with the parental type (internal standard) and well H1 with URA3- S. cerevisiae cells (negative control). Plates were sealed to prevent evaporation and incubated at 30°C, 225 rpm and 80% relative humidity in a humidity shaker (Minitron-INFORS, INFORS-HT, Switzerland). After 48 hours, 160 µL of expression medium were added to each well and cultured for additional 48 hours. Aliquots of 20 µL of yeast supernatants were transferred to a 96-well plate with liquid handler robotic station Freedom EVO (Tecan, Männedorf, Switzerland) and 180 µL of HRP-ABTS reagent (final concentrations of HRP-ABTS reagent in the well: 1mM p-methoxybenzyl alcohol, 2.5 mM ABTS, 1µg/mL HRP in 100 mM phosphate buffer pH 6.0) were dispensed with Multidrop™ Combi Reagent Dispenser (Thermo Scientific, Massachusetts, USA). The plates were incubated at room temperature and measured in kinetic mode at 418nm ($\varepsilon_{ABTS\bullet+}$ = 36000 M^{-1} cm^{-1}). The HTS-assay incorporated two consecutive re-screenings to rule out the selection of false positives as described elsewhere (Viña-Gonzalez et al., 2016).

AAO in *S. cerevisiae*

Shake-flask fermentation: A single colony from the S. cerevisiae clone containing the AAO fusion gene was picked from a SC drop-out plate, inoculated in minimal medium (20 mL) and incubated for 48 h at 30˚C and 220 rpm. An aliquot of cells was removed and used to inoculate minimal medium (100 mL) in a 500 mL flask (OD_{600} = 0.25). The cells completed two growth phases (6–8 h; OD_{600} = 1) and then expression medium (900 mL) was inoculated with the pre-culture (100 mL) (OD_{600} of 0.1). After incubating for 72 h at 25˚C and 220 rpm (maximal AAO activity; OD_{600} = 25–30), the cells were recovered by centrifugation at 4500 rpm and 4˚C (Avanti J-E centrifuge, Beckman Coulter Inc. CA, USA) and the supernatant was double-filtered (using both glass membrane filter and a nitrocellulose membrane of 0.45 µm pore size). The incubation for the expression in glycosylation deficient *S. cerevisiae* strain YDR483W BY4742 was stopped after 18 h to avoid proteolytic degradation of the AAO by extracellular yeast proteases.

AAO in *P. pastoris*

AAO cloning in *P. pastoris*: The coding region of the evolved AAO variant (1962 bp) was cloned into the expression vector pPICZ-B. First, pJRoC30-FX7/FX9 was used to amplify AAO variants with the primers ppKpnAAO-dir (5´- GGGGTACCATGAGATTTCCTTCAATTTTACTGC-3´) and ppAAO-rev (5´- GCTCTAGACTACTGATCAGCCTTGATAAGATCGGC-3´), the primers included targets for restriction enzymes *KpnI* and *XbaI*, respectively (underlined). The PCR reactions were prepared in a final volume of 50 µL containing 250 nM of each primer, 1 mM dNTPs (0.25 mM each), 3% DMSO, 0.05 U/µL Phusion DNA polymerase, and 2 ng/µL template. The parameters for the PCR were: 95°C for 2 min (1 cycle); 94°C for 30 s, 50°C for 30 s, 74°C for 2 min (30 cycles); and 74°C for 10 min (1 cycle). The pPICZ-B vector and the PCR product were digested with the restriction enzymes *KpnI* and *XbaI* at 37˚C for 1 h. The 5´ and 3´ends of the linearized pPICZ-B plasmid were dephosphorylated using antarctic phosphatase at 37˚C for 1 h adding 1 U of enzyme per every 200 ng of linearized vector. The PCR product and the linearized vector were loaded onto a preparative agarose gel, purified using the Zymoclean Gel DNA Recovery kit and ligated with T4 DNA ligase at room temperature for 30 min. After transformation of the pPICZ-B-AAO construct into chemically competent *E. coli* XL2-Blue cells, the plasmid was proliferated, linearized with the restriction enzyme *PmeI* at 37˚C for 1 h and transformed into electro-competent P. pastoris X-33 cells. Electro-competent P. pastoris cells were prepared and transformed with the construction as described in the protocol from Lin-Cereghino et al. (Cereghino and Cregg 2000) mixing 200 ng of linearized vector and 50 µL of competent cells. Transformants were grown on YPD plates.

Deep-well plate fermentation: *P. pastoris* colonies containing AAO under the control of the AOX1 promoter (pPICZ-B-AAO) were picked and cultivated in 96-deep-well plates containing 300 µL of BMD1 medium per well. The plates were incubated at 25˚C, 300 rpm and 80% humidity for 2 days in a humidity shaker. Afterwards, 300 µL of BMM2 medium were added per well. After 12 hours of incubation, 70 µL of BMM10 medium were added to each well repeating this addition every 24 hours for 3 days. After 142 h, the activity with *p*-methoxybenzyl alcohol was measured (final concentrations in the reaction mixture: 1mM *p*-methoxybenzyl alcohol, 2.5 mM ABTS, 1µg/mL HRP in 100 mM phosphate buffer pH 6.0).

Shake-flask fermentation: Transformants with the best activity from the deep-well plate fermentations were grown in YPD agar plates and inoculated in 3 mL of liquid YPD at 30˚C and 250 rpm. The culture reached the optical density at 600 nm at 1 after 6–7 h and was inoculated in 20 mL of BMMY medium in 100 mL shaken flasks. The cultures were incubated at 25˚C or 30˚C and they were supplemented with 250 µL of methanol every 24 h. After 3 days of methanol addition, the best clone with the highest activity was selected for the bioreactor fermentation.

Production in bioreactor: The FX9 mutant ($_{\pi}$FX9) under the control of the AOX1 promoter in the pPICZ-B-FX9 construct was produced in a 5 L vessel fermenter (Minifors, INFORS-HT, Switzerland). The bioreactor was filled with 2 L of basal salts medium (initial volume: 2 L). After sterilization, 4.35 mL/L PTM1 trace salts and 1 mL Antifoam 204 were added to the medium and the pH was adjusted with ammonium hydroxide to 5.0. The fermentation was started with the addition of 0.2 L of preculture grown on YPD medium in several baffled shaken flasks at 150 rpm and 30°C overnight (OD$_{600}$ between 6–10). According to the *Pichia* Fermentation Process Guidelines of Invitrogen the batch fermentation was run at 30°C, 600 rpm and air aeration 1 vvm. Once all the glycerol from the batch was consumed, the glycerol fed phase was initiated by the addition of 50 % (w/v) glycerol feed containing 12mL/L PTM1 trace salts to achieve higher cell density at a 21.8 mL/h feed rate. After 2 h, the glycerol feed faded out by a linear ramp 14.6-0 mL/h over 2 h and the methanol feed containing 12 mL/L PTM1 trace salts started at a 7.2 mL h^{-1} for the culture to transition and adapt to methanol. From this time on the temperature was set to 25°C and the Dissolved Oxygen (DO) above 20% with the control of the stirring speed between 600 and 1200 rpm and aeration using mixtures of air and O$_2$ within 0.7 and 1 vvm. At the end of the transition phase the methanol/PTM1 feeding was increased to 14.6 mL/h until the end of the process. Water evaporation losses were minimized during the process with an exhaust gas condenser and cooling water at 4°C. The fermentation was controlled by taking samples for biomass analysis and AAO activity: The cell concentration was monitored by measuring the optical density of cultures at 600 nm (OD$_{600}$). For wet dry weight (CDW) measurement, cells were separated from 1 mL culture broth by centrifugation at 10,000 g for 5 minutes using pre-weighed 1.5 mL tubes. The wet weight is measured immediately after all the yeast supernatant has been removed. AAO activity was measured with HRP/ABTS method with *p*-methoxybenzyl alcohol as the substrate.

AAO purification: The FX9 variants expressed in *S. cerevisiae* (protease deficient strain BJ5465 and glycosylation deficient strain YDR483W BY4742) and *P. pastoris* were purified to homogeneity as described in a former work (Viña-Gonzalez et al. 2015).

AAO biochemical characterization

N-terminal analysis and pI Determination: Purified AAO variants were subjected to SDS/PAGE, and the protein band was blotted onto PVDF membranes. The PVDF membrane was stained with Coomassie Brilliant Blue R-250, after which the enzyme band was excised and processed for N-terminal amino acid sequencing on a precise sequencer at the Protein Chemistry Service at the The Biological Research Center (Madrid, Spain). Purified FX9 (8 µg) was subjected to two-dimensional electrophoresis gel in order to determine the pI.

Determination of kinetic-thermostability (T_{50}): Appropriate dilutions of AAO were prepared for the assay. The gradient scale ranging from 30 to 80°C was established as follows: 30.0, 31.4, 34.8, 39.3, 45.3, 49.9, 53, 55, 56.8, 59.9, 64.3, 70.3, 75, 78.1 and 80°C. This gradient profile was achieved using a thermocycler. After 10 min of incubation, AAO samples were removed and chilled out on ice for 10 min and incubated further at room temperature for 5 min. Finally, samples of 20 µL were added to 180 µL volumes of 100 mM sodium phosphate pH 6.0 buffer containing 1mM *p*-methoxybenzyl alcohol and activity was measured as anisaldehyde production as absorption at 285 nm (ε_{285} = 16,950 M^{-1} cm^{-1}). Thermostability values were calculated from the ratio between the residual activities incubated at different temperature points and the initial activity at room temperature. The T_{50} value was determined by the transition midpoint of the inactivation curve of the protein as a function of temperature, which in our case was defined as the temperature at which the enzyme lost 50% of its activity following an incubation of 10 minutes. All reactions were performed by triplicate.

pH activity profile: Appropriate dilutions of enzyme samples were prepared in such a way that aliquots of 20 µL gave rise to a linear response in kinetic mode. The optimum pH activity was determined using 100 mM citrate-phosphate-borate buffer at different pH values (2.0, 3.0, 4.0, 5.0, 6.0, 7.0, 8.0 and 9.0) containing 0.3 *p*-methoxybenzyl alcohol.

Kinetic parameters: Kinetic constants for AAO were estimated in 100 mM sodium phosphate pH 6.0. Reactions were performed by triplicate and substrates oxidations were followed by measuring the absorption at 285 nm for *p*-methoxybenzyl alcohol, ε_{285} = 16,950 M^{-1} cm^{-1}; 310 nm for veratryl alcohol, ε_{310} = 9,300 M^{-1} cm^{-1}; 250 nm for benzyl alcohol, ε_{250} = 13,800 M^{-1} cm^{-1}; 280 nm for 2,4-hexadien-1-ol, ε_{280} = 30,140 M^{-1} cm^{-1}. Steady-state kinetics parameters were determined by fitting the initial reactions rates at different substrate concentrations to the Michaelis-Menten equation for one substrate, $v/e = k_{cat}.S/(K_m + S)$ where *e* represent the enzyme concentration, k_{cat} is the maximal turnover rate, S is the substrate concentration and K_m the Michaelis constant. Data were fit using SigmaPlot 10.0 (Systat. Software Inc. Richmond, CA, USA).

Protein modeling: A structural model of the AAO from *P. eryngii* crystal structure at a resolution of 2.55 Å (Protein Data Bank Europe [PDB] accession number 3FIM, (Fernandez et al. 2009) was used as scaffold for the wild type AAO model and the FX9 mutant homology model, obtained by PyMol (Schrodinger LLC.; http://www.pymol.org).

DNA sequencing: All genes were verified by DNA sequencing (BigDye Terminator v3.1 Cycle Sequencing Kit). The primers for the genes cloned in the pJRoC30 plasmid were: primers sense, RMLN and AAOsec1F 5’-GTGGATCAACAGAAGATTTCGATCG-3’ and primers antisense RMLC 5’-GCTTACATTCACGCCCTCCC-3’, AAOsec2R 5’-GTGGTTAGCAATGAGCGCGG-3’ and AAOsec3R 5’-GGAGTCGAGCCTCTGCCCCT-3’. For the AAO genes cloned in the pPICZ-B plasmid primers were: ppKpnAAO-dir and AAOsec1F as primers sense and ppAAO-rev, AAOsec2R and AAOsec3R as primers antisense.

5.3 RESULTS AND DISCUSSION

Improved secretion in *S. cerevisiae* by in vivo shuffling and MORPHING of the chimeric signal peptide

During the first evolutionary campaign to increase AAO secretion in yeast, six mutants (carrying 7 beneficial mutations) were identified with improvements in total activity that ranged from roughly 2- up to 100-fold (for $_{\text{Sac}}$FX7), **Figure 1** (Viña-Gonzalez et al. 2015). Given that most of these mutations were >20 residues from one another, they were shuffled in vivo by taking advantage of the homologous recombination machinery of *S. cerevisiae* (Gonzalez-Perez et al. 2012).

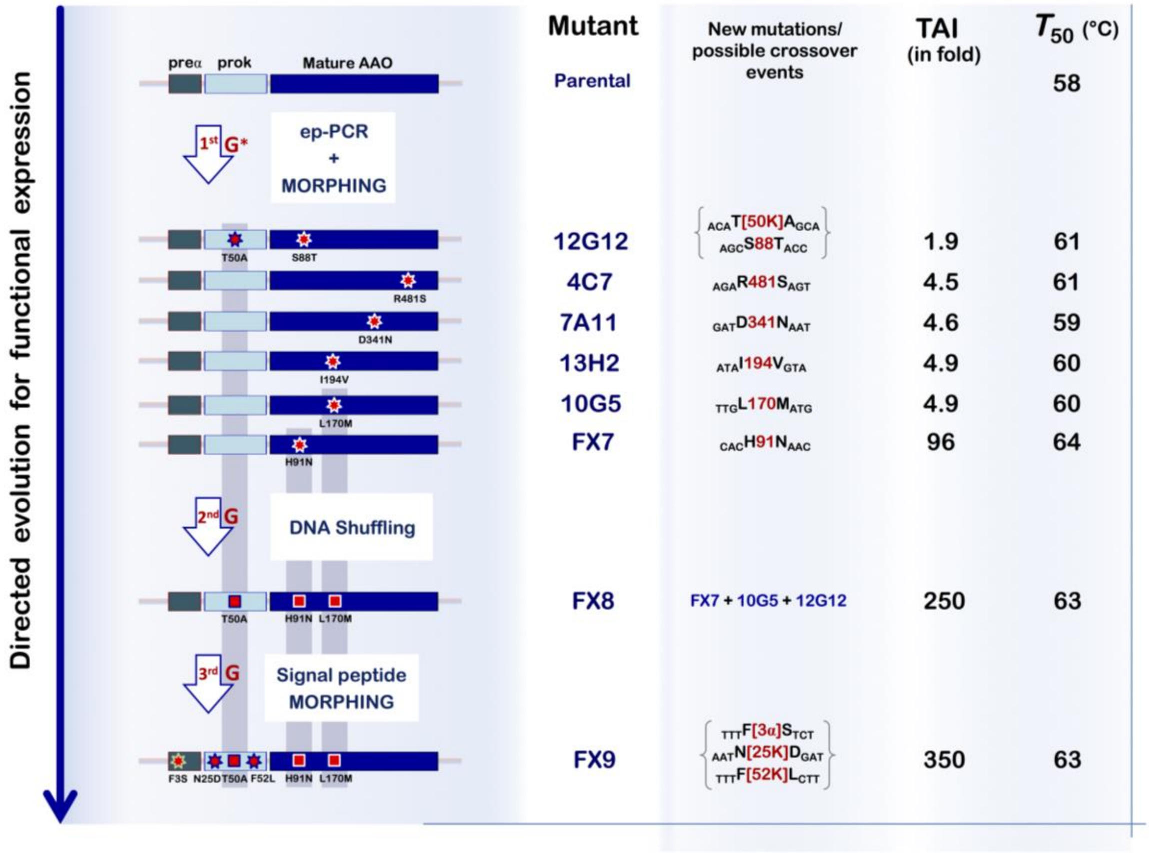
Directed evolution for functional expression
preα prok Mature AAO
1st G*
ep-PCR + MORPHING
2nd G
DNA Shuffling
3rd G
Signal peptide MORPHING
T50A S88T R481S D341N I194V L170M H91N
F3S N25D T50A F52L H91N L170M

Mutant	New mutations/ possible crossover events	TAI (in fold)	T_{50} (°C)
Parental			58
12G12	ACAT[50K]AGCA AGCS88TACC	1.9	61
4C7	AGAR481SAGT	4.5	61
7A11	GATD341NAAT	4.6	59
13H2	ATAI194VGTA	4.9	60
10G5	TTGL170MATG	4.9	60
FX7	CACH91NAAC	96	64
FX8	FX7 + 10G5 + 12G12	250	63
FX9	TTTF[3α]STCT AATN[25K]DGAT TTTF[52K]LCTT	350	63

Figure 1. Laboratory evolution of the AAO from *Pleurotus eryngii* towards functional expression in yeast. New mutations are represented as stars and accumulated mutations as squares. The preα-leader segment is depicted in green, the prok-leader segment in light blue and the mature AAO in dark blue. The TAI (total activity improvement) is the value indicating the improvement in AAO activity detected in *S. cerevisiae* supernatants relative to the parental type: *1st G, results from the first generation of variants published in Viña-Gonzalez et al. 2015.

The mutant library was screened in the HRP-ABTS assay using *p*-methoxybenzyl alcohol as the substrate as described previously (Viña-Gonzalez et al. 2015; Viña-Gonzalez et al. 2016). The best mutant from this round of DNA shuffling was $_{Sac}$FX8, which showed 2.6-fold and 250-fold improved total activity over $_{Sac}$FX7 and the parental AAO, respectively. As planned, several crossover events took place that allowed mutations from different parental types to be convened: the consensus-ancestral mutation H91N from $_{Sac}$FX7; the L170M mutation from $_{Sac}$10G5; and the T50A mutation at the K1 killer toxin pro-leader inherited from $_{Sac}$12G12, **Figure 1**. To further enhance secretion, we evolved the preαproK signal leader by MORPHING, a domain-focused mutagenesis technique that allows mutations and crossover events to be randomly introduced in defined stretches (Gonzalez-Perez et al., 2014). With this strategy 3 new mutations were included in the preαproK (F3S at the preα, and H25N- F52L at the K1 pro-leader), giving rise to the final

$_{\text{Sac}}$FX9 secretion variant with a 350-fold improvement in activity relative to the parental AAO type and with expression levels of 4.5 mg/L in flask culture.

The evolved leader sequence of $_{\text{Sac}}$FX9 derived from the DNA shuffling and the focused evolution experiments carried four substitutions relative to the original preαproK chimeric construction, **Figure 1**, **Figure 2A**.

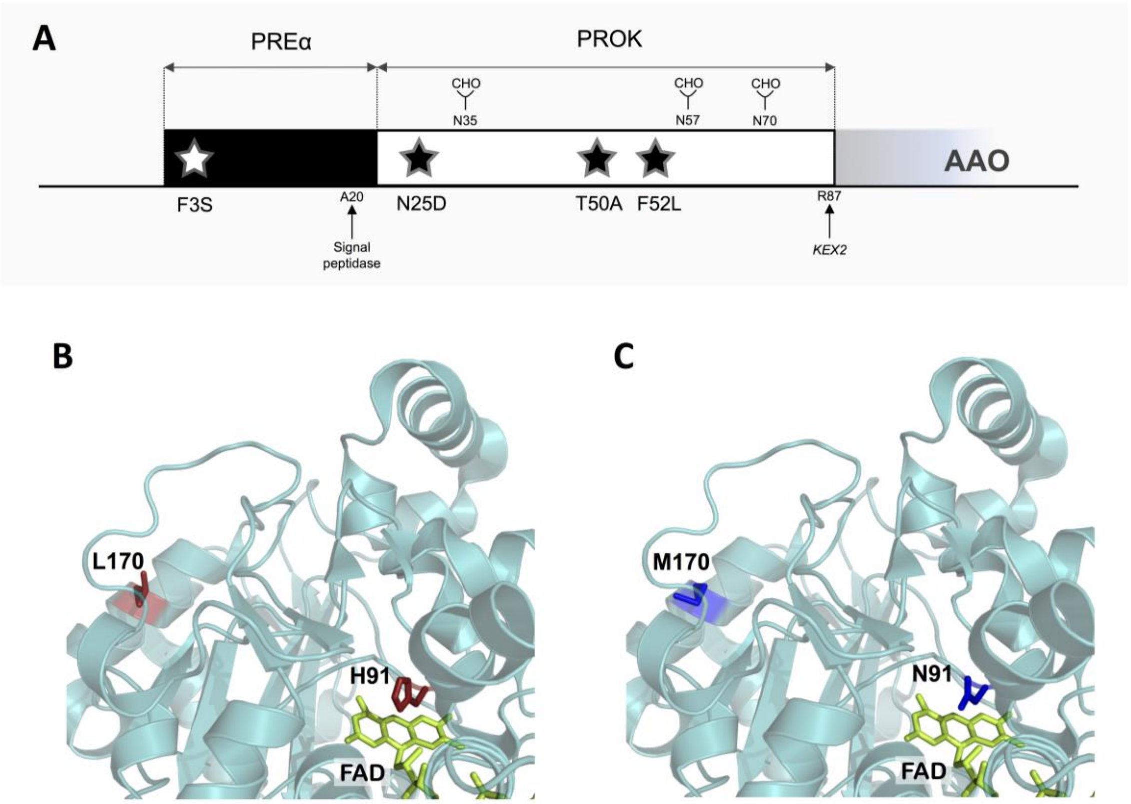

Figure 2. Mutations presented by FX9. (A) Substitutions in the chimeric preαproK signal peptide. (B and C) Molecular model using the *Pleurotus eryngii* AAO crystal structure as a template (PDB code 3FIM). (B) wild type AAO and (C) the FX9 variant. FAD is depicted in yellow and the details of the two mutations in FX9 (blue) are compared with the corresponding residues in the wild type (red).

The preα-leader segment carries the F[3α]S mutation which agrees well with substitutions at the same position (F[3α]P/L) previously found in α-factor prepro-leaders that improved antibody secretion (Rakestraw et al. 2009). An acidic residue was introduced into the proK-peptide with the new substitution N[25K]D, whereas mutation T[50K]A, inherited from parental type 12G12, together with F[52K]L increase the hydrophobic load of the middle sequence. In the mature protein, the mutation L170M from the parental 10G5 is located in an α-helix at the surface and mutation H91N from FX7 is in the catalytic pocket, **Figure 2B**, **C**. As we described previously, Asn91 is a consensus residue situated at the si-face of the FAD that stabilizes the conformation of the cofactor, thereby enhancing secretion and AAO stability (Viña-Gonzalez et al. 2015).

Functional expression of recombinant AAO in *P. pastoris* and scaling-up

The use of compatible tandem-expression systems for protein engineering and overproduction can overcome certain limitations when dealing with complex eukaryotic enzymes like AAO (Alcalde et al. 2015). In particular, combining *S. cerevisiae* as the host of choice for the directed evolution of eukaryotic ligninases with the methylotrophic yeast *P. pastoris* (currently reclassified as *Komagataella phaffii*) for overproduction offers many attractive advantages, as demonstrated recently (Mate et al. 2013a; Molina-Espeja et al. 2015). Heterologous expression in *S. cerevisiae* and *P. pastoris* falls under the lowest-common-denominator of a well-defined secretory apparatus and the ability to perform complex post-translational modifications, which frequently results in reasonable secretion of the active and stable enzyme. However, *S. cerevisiae* has a broad variety of episomal vectors, high-transformation efficiencies and a precise recombination apparatus to aid the creation and screening of mutant libraries for directed evolution. While *P. pastoris* lacks such properties, it outperforms *S. cerevisiae* in terms of protein production under the control of strong and tightly regulated promoters, reaching extremely high cell densities in bioreactors (Ahmad et al. 2014). Hence, during the heterologous expression of AAO in yeast, the question that arises is can the improvements in secretion obtained by directed evolution in *S. cerevisiae* be transferred to *P. pastoris*, or in other words, how well are the improvements in secretion preserved in both yeasts.

To assess the compatibility of these two systems, the evolved variants $_{\text{Sac}}$FX7 and $_{\text{Sac}}$FX9 were cloned into *P. pastoris* to determine if the improvements in secretion furbished by the mutations are consistent between hosts. Under the methanol inducible AOX1 promoter, transformants were grown in deep-well plate microfermentations and screened for secretion -*P. pastoris* can integrate up to six copies of the foreign gene into its genome-. Selected clones, $_{\pi}$FX7 and $_{\pi}$FX9, were then produced in 100 mL shaking flask cultures, producing total activity values of 50 and 235 U/L, respectively. Hence, the beneficial mutations for secretion in *S. cerevisiae* retained their effects in *P. pastoris* and they were even associated with an improvement in total activity from 3.6 to 4.7-fold in both the variants. To harness the high cell titers of *P. pastoris* in the bioreactor, $_{\pi}$FX9 was transferred to a 5L fed-batch fermenter and after six days, maximal volumetric activity was reached (1378 U/L) with the production of AAO (25.5 mg/L) surpassing that obtained in shaking-flask cultures roughly 6-fold. Since AAO is secreted similarly by *S. cerevisiae* and *P. pastoris,* **Table 1**, this improved production can be solely attributed to the high cell densities achieved by *P. pastoris* in the bioreactor (up to 260 g wet biomass/L; OD$_{600}$ ~ 430), **Figure 3A**.

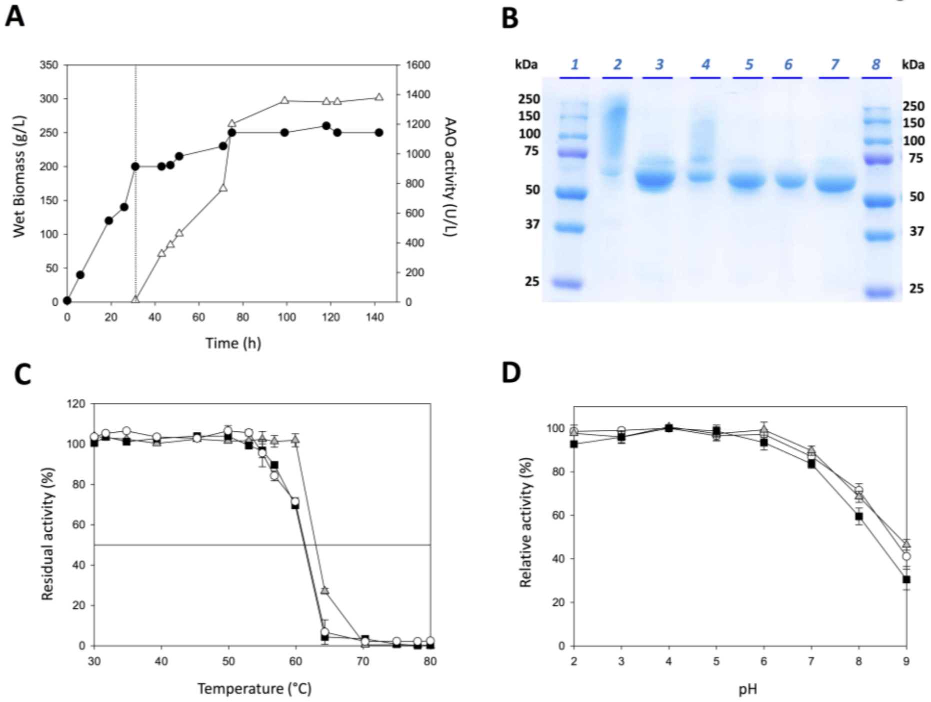

Figure 3. (A) Fermentation in a 5L bioreactor of recombinant $_{\pi}$FX9 expressed in *P. pastoris*. Fermentation was performed in four steps: glycerol-batch phase for 26 h, glycerol-fed phase for 4h, transition phase for 4 h and methanol induction phase for 112 h. The black circles represent the wet biomass, the white triangles the volumetric AAO activity and the dotted vertical line the beginning of the induction phase. (B) Molecular mass of recombinant AAO. 10% SDS-polyacrylamide gel: Lanes 1 and 8, protein markers; 2, purified $_{\text{sac}}$FX9 mutant; 3, deglycosylated $_{\text{sac}}$FX9; 4, purified $_{\Delta}$FX9; 5, deglycosylated $_{\Delta}$FX9; 6, purified $_{\pi}$FX9; 7 deglycosylated $_{\pi}$FX9. (C) Kinetic thermostability (T$_{50}$) of the recombinant variants: $_{\text{sac}}$FX9 (grey triangles), $_{\Delta}$FX9 (black squares) and $_{\pi}$FX9 (white circles). (D) pH activity profiles for $_{\text{sac}}$FX9 (grey triangles), $_{\Delta}$FX9 (black squares) and $_{\pi}$FX9 (white circles) with $_{p}$-methoxybenzyl alcohol (1 mM). Each point represents the mean and standard deviation of three independent experiments.

Influence of glycosylation on biochemical parameters

The $_{\text{Sac}}$FX9 and $_{\pi}$FX9 variants were purified to homogeneity and characterized biochemically. N-terminal sequencing confirmed the correct cleavage of the chimeric preαproK by the KEX2 protease in the Golgi compartment in both yeasts, **Table 1**. It is well known that *S. cerevisiae* produces strong glycosylation during heterologous protein expression. Indeed, as occurred with the parental $_{\text{Sac}}$FX7 (Viña-Gonzalez et al. 2015), $_{\text{Sac}}$FX9 underwent hyperglycosylation (~60% glycosylation) and the wide smear produced by the different glycoforms (ranging from ~200 to 63 kDa in SDS-PAGE) collapsed into a single 63 kDa band after deglycosylation with EndoH, **Figure 3B**, **Table 1**. By contrast, in *P. pastoris* the same variant ($_{\pi}$FX9) produced a single ~63 kDa band before and after treatment with EndoH, highlighting the weak glycosylation expected in *P.*

pastoris, Fig. 3B. The T_{50} (the temperature at which the enzyme retains 50% of its activity after a ten minute incubation) of ${}_{Sac}$FX9 was slightly higher (1.7°C) than that of ${}_{\pi}$FX9, possibly due to this hyperglycosylation, **Table 1**, **Figure 2C**.

Table 1. Biochemical properties of recombinant FX9 mutant.

Biochemical properties	**${}_{sac}$FX9**	**${}_{\Delta}$FX9**	**${}_{\pi}$FX9**
MW (Da)[1]	150,000	63,000	63,000
MW (Da)[2]	60,952	60,952	60,952
Glycosylation degree (%)	60	n.m	n.m
Thermal stability, T_{50} (°C)	63	61.2	61.3
pI	4.8	4.6	4.5
N-terminal end	ADFDYVVVG	ADFDYVVVG	ADFDYVVVG
Secretion levels (mg/L)	4.5	n.d.	4.3

[1]Estimated by SDS-PAGE; [3]estimated from amino acid composition. N.m (non-measurable); n.d. (non-determined).

As such, the kinetic thermostability of both the recombinant variants expressed by the yeasts exceeded that reported for wild type AAO expressed in *E. coli* after in vitro refolding by ~15 °C (T_{50} = 47.5 °C), emphasizing the beneficial effect of: i) natural folding and heterologous secretion in yeast; and ii) the introduction of the stabilizing consensus-ancestor mutation H91N, as described previously (Viña-Gonzalez et al. 2015). The pH activity profile of ${}_{Sac}$FX9 and ${}_{\pi}$FX9 with *p*-methoxybenzyl alcohol was similar, maintaining over 90 % of their activity from pH 2.0 to 6.0, Fig. 3D. When the steady kinetic parameters were measured for the oxidation of aromatic and aliphatic alcohols, **Table 2**, the catalytic efficiencies of ${}_{Sac}$FX9 were similar to those of the parental type ${}_{Sac}$FX7, as was the order of preference for the different substrates. By contrast, ${}_{\pi}$FX9 retained similar K_m values to that of ${}_{Sac}$FX9 but improved by ~2-fold the k_{cat} irrespective of the alcohol tested.

The discrepancies in the kinetic parameters and thermostability between ${}_{Sac}$FX9 and ${}_{\pi}$FX9 may be related to the different degrees of glycosylation in *S. cerevisiae* and *P. pastoris*. To assess this, FX9 was also cloned into the glycosylation-deficient *Δkre2 S. cerevisiae* strain. *Δkre2* is thought to attach smaller mannose oligomers than wild type strains to the 7 predicted N-glycosylation motifs (Asn-X-Ser/Thrs) in AAO (i.e. N62, N138, N151, N222, N303, N325 and N369). After production and purification, the variant secreted by *Δkre2* (${}_{\Delta}$FX9) was characterized biochemically. As predicted, noticeable lower glycosylation was evident by SDS-PAGE, resolving to a smooth smear with a concentration of the protein at ~63 kDa, and it unequivocally tightened into a single band upon deglycosylation, **Figure 3B**, **Table 1**. The ${}_{\Delta}$FX9 variant displayed a similar pH activity profile to its AAO counterparts together with a T_{50} value identical to that of $_{\pi}$FX9 (i.e. 1.7°C lower than $_{Sac}$FX9), **Figure 3C**, **D**. To complete the breakdown of the biochemical properties of the recombinant AAOs, the kinetic parameters of $_{\Delta}$FX9 were measured. As expected, they came close to those of $_{\pi}$FX9 due to the ~1.5-fold enhancement in the k_{cat} while the K_m was maintained, **Table 2**. Together, the expression of FX9 in *Δkre2* confirmed that the variation in kinetics and thermostability between $_{Sac}$FX9 and $_{\pi}$FX9 were produced by the distinct degree of glycosylation.

Table 2. Kinetic parameters for yeast-recombinant AAO variants.

Substrate	Kinetic constants	$_{sac}$FX7*	$_{sac}$FX9	$_{\Delta}$FX9	$_{\pi}$FX9
***p*-methoxybenzyl alcohol**	K_m (mM)	0.034 ± 0.001	0.023 ± 0.002	0.022 ± 0.001	0.037 ± 0.004
	k_{cat} (s^{-1})	54 ± 4	41 ± 0.6	56.9 ± 0.6	70 ± 2
	k_{cat}/K_m (mM^{-1} s^{-1})	1562	1782	2586	1909
Veratryl alcohol	K_m (mM)	0.38 ± 0.02	0.34 ± 0.02	0.36 ± 0.01	0.41 ± 0.01
	k_{cat} (s^{-1})	28 ± 1	24.6 ± 0.7	36.8 ± 0.3	56.9 ± 0.6
	k_{cat}/K_m (mM^{-1} s^{-1})	71	72.3	102.2	138.8
Benzyl alcohol	K_m (mM)	0.51 ± 0.01	0.37 ± 0.01	0.38 ± 0.03	0.44 ± 0.02
	k_{cat} (s^{-1})	19 ± 1	15.1 ± 0.2	23.4 ± 0.6	34.4 ± 0.5
	k_{cat}/K_m (mM^{-1} s^{-1})	36	40.8	61.6	78.3
2,4-hexadien-1-ol	K_m (mM)	0.059 ± 0.004	0.096 ± 0.009	0.095 ± 0.006	0.106 ± 0.001
	k_{cat} (s^{-1})	52 ± 1	47 ± 1	62 ± 1	89 ± 3
	k_{cat}/K_m (mM^{-1} s^{-1})	866	456.3	652.6	839.6

AAO kinetic constants were estimated in 100 mM phosphate buffer pH 6.0 at 25°C. All reactions were performed by triplicate. * Kinetic values from Viña-Gonzalez et al., 2015.

5.4 CONCLUSIONS

This study shows how to harness a tandem-yeast expression system to engineer a fungal AAO by directed evolution and overproduce it in a bioreactor. The properties acquired during the evolution cycles in *S. cerevisiae* are easily decoded by *P. pastoris*, which can produce the recombinant enzyme while retaining its improved catalytic properties and general stability. As a natural progression, future studies could focus on the production of the recombinant enzyme at the g/L scale in other strong industrial hosts like *Trichoderma* or *Aspergillus sp.* Certainly, the findings presented here invite a further exploration and extension of the biotechnological potential of AAO, for example tailoring its activity to oxidize secondary alcohols and resolve chiral mixtures, or tuning the AAO catalysis to furfural-derivative cascade reactions (Hernandez-Ortega et al. 2012c; Carro et al. 2015; Martinez et al., 2017).

ACKNOWLEDGEMENTS

This research was supported by the EU project FP7-KBBE-2013-7-613549-INDOX and by the Spanish Government project BIO2016-79106-R-Lignolution.

Chapter VI:

Structure-Guided Evolution of Aryl-Alcohol Oxidase from *Pleurotus eryngii* for the Selective Oxidation of Secondary Benzyl Alcohols

Among the most attractive applications of AAO in organic synthesis is arising its possible use for racemic resolution of chiral secondary alcohols. Here, we designed the first artificial AAO for such challenging processes, combining structure-guided evolution with computational analysis at the atomic level.

CHAPTER
VI

CHAPTER

VI

Structure-Guided Evolution of Aryl Alcohol Oxidase from *Pleurotus eryngii* for the Selective Oxidation of Secondary Benzyl Alcohols

Javier Viña-Gonzalez, Diego Jimenez-Lalana, Ferran Sancho, Ana Serrano, Angel T. Martinez, Victor Guallar and Miguel Alcalde

Advanced Synthesis & Catalysis. 2019, 361, 1 – 13.

https://10.1002/adsc.201900134

Aryl alcohol oxidase (AAO) is a fungal flavoenzyme capable of oxidizing aromatic primary alcohols into their correspondent aldehydes through a stereoselective hydride abstraction. Unfortunately, this enzyme does not act on secondary benzyl alcohols in racemic mixtures due to the strict control of substrate diffusion and positioning at the active site restricted to primary benzyl alcohols. Here we describe the engineering of AAO from *Pleurotus eryngii* to oxidize chiral benzyl alcohols with high enantioselectivity. The secondary benzyl alcohol oxidase was remodeled at the active site through four cycles of structure-guided evolution, including a final step of in vivo site-directed recombination to address the positive epistatic interactions between mutations. The final variant, with five substitutions and a renovated active site, was characterized at biochemical and computational level. The mutational sculpting helped position the bulkier (S)-1-(*p*-methoxyphenyl)-ethanol, improving the mutant´s catalytic efficiency by three orders of magnitude relative to the native enzyme while showing a high enantioselectivity (ee > 99%). As a promising candidate for racemic resolution, this evolved secondary benzyl alcohol oxidase maintained its natural stereoselective mechanism while displaying activity on several secondary benzyl alcohols.

6.1 INTRODUCTION

With global annual sales of $ 1 trillion, an increasingly important challenge in drug development that the pharmaceutical sector must overcome is that posed by chiral chemistry. Indeed, enantiopure building blocks are in strong demand to produce drugs with particular biological activities, while they are also paramount for the production of fine chemicals (Caldwell 2001; Sekhon 2013; Chhabra et al. 2013). Biocatalysis has found an important niche in the field of chiral technology, with enzymatic and whole-cell biotransformations offering stereo-, regio- and chemio-selectivity under mild reaction conditions. Classically, two fundamental approaches are followed in the industrial production of chiral molecules: enantioselective synthesis and racemic mixture separation. While asymmetrical synthesis involves complex and expensive processes (Maier et al. 2001), dynamic kinetic resolution (DKR) is currently one of the most efficient sources of chiral molecules, in which separation is coupled to the in situ re-racemization of one of the enantiomers. Another recently described transformative source of enantiomers is cyclic de-racemization. Based on cyclic oxidation-reduction sequences, after the selective oxidation of one of the enantiomers, the achiral intermediate (ketone or imine) is non-selectively reduced to the racemic initial material. After a certain number of cycles, a theoretical 100% yield of the non-reactive enantiomer can be accumulated (Faber 2001; Pàmies and Bäckvall 2004; Turner 2004). The core step in racemic separation, kinetic resolution, has been achieved for secondary alcohols using either whole-cell systems (Fantin et al. 1993; Li et al. 2010; Voss et al. 2008) or isolated enzymes, such as alcohol dehydrogenases (Matsuda et al. 2009), lipases (Ghanem and Aboul-Enein 2005; Qin et al. 2016) and particularly, oxidases (Escalettes and Turner 2008; Musa et al. 2007). This latter solution is the simplest means to prepare optically pure secondary benzyl alcohols, given their trivial requirements (only needing O_2 from the air) and high enantioselectivity (Escalettes and Turner 2008; Kroutil et al. 2004; van Hellemond et al. 2009; Dijkman et al. 2015)

Among these enzymes, aryl alcohol oxidase (AAO, EC 1.1.3.7) is a promising candidate for the enantioselective oxidation of chiral benzyl alcohols. AAO is a flavoenzyme belonging to the GMC (glucose-methanol-choline) superfamily of oxidoreductases and it is naturally secreted as a part of the fungal enzymatic consortium involved in lignin degradation (Ruiz-Dueñas et al. 2006). Accepting a variety of aromatic alcohols as substrates, the activity of AAO is initially divided into two half-reactions. The first reductive half-reaction involves highly enantioselective hydride transfer from the alcohol's α-C to the FAD co-factor. This process yields the corresponding aldehyde, such that the FAD can then be reoxidized by O_2, releasing H_2O_2 as a by-product of the second oxidative half of the reaction (Ferreira et al. 2009). Unfortunately, the active site of AAO is buried under a hydrophobic constriction formed by residues Tyr92, Phe397 and Phe501. As a result, substrates bulkier than primary aromatic alcohols cannot easily be accommodated, reducing the enzyme's activity on chiral molecules to a residual trace. Until recently the failure to functionally express AAO in a heterologous host had prevented its directed evolution. However, fusing the enzyme to a chimeric signal prepro-leader has enabled this protein to be successfully evolved for secretion by yeast (Viña-Gonzalez et al. 2015; Viña-Gonzalez et al. 2018).

Taking advantage of this expression system, here we have combined different laboratory evolution strategies to unlock the activity of AAO on secondary aromatic alcohols. We first carried out a carefully structure-guided campaign of evolution using chiral 1-(*p*-methoxyphenyl)-ethanol as the substrate, thereby generating a palette of secondary benzyl alcohol oxidase mutants. Employing in vivo site-directed recombination approaches, mutations were curated by comparing them with their correspondent parental reversions. The differential oxidation of secondary benzyl alcohols by the final benzyl alcohol oxidase variant was characterized, while the rationale behind these changes was analyzed computationally at the atomic level.

6.2 MATERIALS AND METHODS

Materials

All chemicals were reagent-grade purity. Benzyl alcohol, *p*-chlorobenzyl alcohol, 3,4-dimethoxybenzyl alcohol, *p*-Methoxybenzyl alcohol, 1-phenylethanol, 1-phenylpropanol, 1-(*p*-methoxyphenyl)-ethanol, 4-fluoro-α-methylbenzyl alcohol, (R)-4-fluoro-α-methylbenzyl alcohol, (S)-4-fluoro-α-methylbenzyl alcohol, 2,4-hexadien-1-ol, cinnamyl alcohol, Horseradish peroxidase (HRP), *Taq* polymerase and the Yeast Transformation Kit were purchased from Sigma (Madrid, Spain). Amplex® Red reagent (10-acetyl-3,7-dihydroxyphenoxazine) was obtained from Biogen (Madrid, Spain). Zymoprep Yeast Plasmid Miniprep, Yeast Plasmid Miniprep Kit I and Zymoclean Gel DNA Recovery Kit were from Zymo Research (Orange, CA, USA). Restriction enzymes *BamHI* and *XhoI* were from New England Biolabs (Hertfordshire, UK). I-Proof high-fidelity DNA polymerase was from Biorad (Hercules, CA, USA). The episomal shuttle vector pJRoC30 was from the California Institute of Technology (CALTECH, USA). *E. coli* XL2-Blue competent cells were from Stratagene (La Jolla, CA, USA). Primers were acquired from Isogen Life Science (Barcelona, Spain) and are included in **Table S1**.

Culture media

Minimal medium SC contained 100 mL 6.7% (w:v) sterile yeast nitrogen base, 100 mL 19.2 g/L sterile yeast synthetic drop-out medium supplement without uracil, 100 mL sterile 20% raffinose (w:v), 700 mL sddH$_2$O and 1 mL 25 g/L chloramphenicol. YP medium contained 10 g yeast extract, 20 g peptone and sddH$_2$O to 650 mL whereas YPD medium also contained 20% glucose (w:v). AAO expression medium contained 144 mL YP 1.55x, 13.4 mL 1 M KH$_2$PO$_4$ pH 6.0 buffer, 22.2 mL 20% galactose (w:v), 0.222 mL 25 g/L chloramphenicol and ddH$_2$O to 200 mL. Luria Broth (LB) medium contained 10 g sodium chloride, 5 g yeast extract, 10 g peptone, 1 mL 100 mg/mL ampicillin and sddH$_2$O to 1 L. AAO selective expression medium (SEM) contained 100 mL 6.7% (w:v) sterile yeast nitrogen base, 100 mL 19.2 g/L sterile yeast synthetic drop-out medium supplement without uracil, 100 mL sterile 20% galactose (w:v), 100 mL 1 M KH$_2$PO$_4$ pH 6.0, 600 mL sddH$_2$O and 1 mL 25 g/L chloramphenicol.

Construction of variants I500A, F501A and I500A-F501A

All the PCR products were cleaned, concentrated, loaded onto a preparative agarose gel (1%, w:v) and purified using the Zymoclean Gel DNA Recovery kit before being cloned into the shuttle vector pJRoC30 under the control of the GAL1 promoter. *BamHI* and *XhoI* were used to linearize the plasmid pJRoC30 and to remove the parent gene. FX9 variant was amplified from pJRoC30-FX9 (Viña-Gonzalez et al. 2018) with two PCR reactions for each mutant containing overhang segments for the whole plasmid to be reassembled in the yeast. PCR reactions were carried out in a final volume of 50 µL containing 3% DMSO, 0.8 mM dNTPs (0.2 mM each), 0.03 U/µL Iproof DNA polymerase, and 0.2 ng/µL template. The oligos used for each PCR reaction were: For I500A, PCR1 (oligo sense RMLN and oligo antisense I500Ar), PCR2 (oligo sense I500Af and oligo antisense RMLC). For F501A, PCR1 (RMLN and oligo antisense F501Ar), PCR2 (oligo sense F501Af and RMLC). For double mutant I500A-F501A, PCR1 (RMLN and oligo antisense DM500-1Ar), PCR2 (oligo sense DM500-1Af and RMLC). Amplification reactions were carried out in a thermal cycler MycyclerTM (BIO-RAD, USA) with the following PCR program: 98°C for 30 seconds (1 cycle); 98°C for 10 seconds, 50°C for 25 seconds and 72°C for 60 seconds (28 cycles); and 72°C for ten minutes (1 cycle). After purification, PCR products (400 ng each) were mixed with the linearized pJRoC30 (100 ng; ratio PCR product: vector = 4:1) and transformed in yeast (Yeast transformation kit) for the recombination and in vivo cloning. 176 colonies were picked, expressed and screened as described below. Each construct was recovered and its sequence confirmed by DNA sequencing.

Directed evolution

First generation: combinatorial saturation mutagenesis at positions Ile500 and Phe501: Two PCR reactions were carried out in a final volume of 50 µL containing 3% DMSO, 0.8 mM dNTPs (0.2 mM each), 0.03 U/µL iproof DNA polimerase, and 0.2 ng/µL FX9 template and different primers according to the 22-trick protocol (Kille et al. 2012). PCR1 contained 0.25 µM RMLN and 0.25 µM mix of reverse primers: 22c1R, 22c2R, 22c3R, 22c4R, 22c5R, 22c6R, 22c7R, 22c8R and 22c9R. PCR2 contained 0.25 µM RMLC and 0.25 µM mix of forward primers: 22c1F, 22c2F, 22c3F, 22c4F, 22c5F, 22c6F, 22c7F, 22c8F and 22c9F. Amplification reactions were carried out in a thermal cycler MycyclerTM (BIO-RAD, USA) with the following PCR program: 98°C for 30 seconds (1 cycle); 98°C for 10 seconds, 50°C for 25 seconds and 72°C for 60 seconds (28 cycles); and 72°C for ten minutes (1 cycle). After purification, PCR products (400 ng each) were mixed with the linearized pJRoC30 (100 ng; ratio PCR product: vector = 4:1) and transformed in yeast for in vivo cloning. According to the 22-trick protocol, a library of 3066 individual colonies was screened as described below.

Second generation: MORPHING: The 15G12 variant was used as the parental template for focused random mutagenesis technique MORPHING (Mutagenic Organized Recombination Process by Homologous IN vivo Grouping) (Gonzalez-Perez et al. 2014). Three libraries were constructed independently targeting 3 protein blocks: MA, MB, and MC. Additionally, a mutagenic library subjecting the whole AAO fusion was prepared by error prone PCR (ep-PCR). Primers were designed to create homologous overlapping areas of ~50 bp for the whole gene to be reassembed in vivo upon transformation in *S. cerevisiae*. i) ep-PCR for MORPHING blocks and whole AAO gene were carried out in a final volume of 50 µL containing: 90 nM oligo sense (FM1 for MA block, FM2 for MB block, FM3 for MC block and RMLN for whole gene amplification), 90 nM oligo antisense (RM1 for fragment MA, RM2 for fragment MB, RM3 for fragment MC and RMLC for whole gene amplification), 0.3 mM dNTPs (0.075 mM each), 3% DMSO, 0.05 or 0.01 mM $MnCl_2$, 1.5 mM $MgCl_2$, 0.05 U/ µL Taq polymerase DNA, and 0.92 ng/ µL 15G12 template. The amplification parameters were 95°C for 2 min (1 cycle); 95°C for 45 s, 50°C for 45 s, and 74°C for 2 min (28 cycles); and 74°C for 10 min (1 cycle). Concentrations of 0.05 and 0.01 mM $MnCl_2$ were used for MORPHING and full gene ep-PCR, respectively, to adjust the mutational rate to 1-3 mutations per gene. ii) High-fidelity PCRs for MORPHING were carried out in a final volume of 50 µL containing 3% DMSO, 0.8 mM dNTPs (0.2 mM each), 0.03 U/µL iproof DNA polimerase, 0.25 µM oligo sense (RMLN for HA1, HB1 and HC fragments, FHF1 for HA2 and FHF2 for HB2), 0.25 µM oligo antisense (RHF1 for HA1, RHF2 for HB1, RHF3 for MC and RMLC for HA2 and HB2 fragments) and 0.2 ng/µL template. High-fidelity PCR was performed using the following parameters: 98°C for 30 s (1 cycle); 94°C for 10 s, 48°C for 30 s, 72°C for 30 s (30 cycles); and 72°C for 10 min (1 cycle). The assembly of the fragments for the different libraries is described in Figure 1B. PCR products were cleaned, concentrated, loaded onto a preparative agarose gel, purified, mixed in equimolar amounts, (200 ng mutagenic fragment and 200 ng non-mutagenic fragment) and transformed with linearized pJRoC30 (200 ng) into chemically competent cells, as described above.

Third generation: mutagenic shuffling: ep-PCR reactions were performed separately with mutants 3F10, 11H2, 12D2 and 6G3. Reaction mixtures were prepared in a final volume of 50 µL containing DNA template (0.92 ng/µL), 90 nM oligo sense RMLN (5'-CCTCTATACTTTAACG TCAAGG-3'), 90 nM Reverse primer RMLC (5'-GGGAGGGCGTGAATGTAAGC-3'), 0.3 mM dNTPs (0.075 mM each), 3% (v:v) dimethylsulfoxide (DMSO), 1.5 mM $MgCl_2$, 0.1 mM $MnCl_2$ and 0.05 U/µL Taq DNA polymerase. PCRs were performed in a thermocycler (Mycycler, Bio-Rad, Hercules, CA, USA) and parameters were: 95°C for 2 min (1 cycle); 95°C for 45 s, 50°C for 45 s, 74°C for 45 s (28 cycles); and 74°C for 10 min (1 cycle). The PCR products were mixed with linearized pJRoC30 (at a PCR product/linearized plasmid ratio of 4:1) and transformed into competent S. cerevisiae cells to promote in vivo DNA shuffling. Transformed cells were plated on SC (synthetic complete) drop-out plates and incubated for 3 days at 30°C. Colonies containing the whole autonomously replicating vector were picked and subjected to high-throughput screening as described below.

Fourth generation: site-directed recombination: The 3C11 variant was used as template and primers were designed for the 10 selected mutations (E39G, I76V, A77V, R80C, M83I, V90A, Q174R, F332L, V340A, and Q466R) for the in vivo site-directed recombination of mutations vs. corresponding reversions at each position of the combinatorial library. A total of 6 PCR reactions were performed. Reactions were carried out in a final volume of 50 µL containing 3% DMSO, 0.8 mM dNTPs (0.2 mM each), 0.03 U/µL iproof DNA polimerase, and 0.2 ng/µL 3C11 with 0.25 µM of the following oligos: PCR1 used oligo sense RMLN and oligo antisense R116 (containing position 39). PCR2 was performed with oligo sense F116 (containing position 39) and oligo antisense R5 (containing positions 76, 77, 80, 83 and 90). PCR3 used oligo sense F5 (containing positions 76, 77, 80, 83 and 90) and oligo antisense R521 (containing position 174). PCR4 used oligo sense F521 (containing position 174) and oligo antisense R9419 (containing positions 332 and 340). PCR5 was performed with oligo sense F9419 (containing positions 332 and 340) and oligo antisense R1397 (containing position 466). PCR6 was performed with oligo sense F1397 (containing position 466) and oligo antisense RMLC, (Figure S1, Table S1). For the in vivo assembly of the whole gene, the fragments were designed with overhangs of around 40 bp between them. Amplification reactions were carried out in a thermal cycler and the PCR program was: 98°C for 30 seconds (1 cycle); 98°C for 10 seconds, 50°C for 25 seconds and 72°C for 30 seconds (28 cycles); and 72°C for ten minutes

(1 cycle). After purification, PCR products (400 ng each) were mixed with the linearized pJRoC30 (100 ng; ratio PCR product: vector = 4:1) and transformed in yeast for in vivo cloning. A library of 3070 individual colonies was screened as described below.

High-throughput screening (HTS) assay

Transformed cells were plated in SC drop-out plates and incubated for 3 days at 30°C, individual clones were fermented in sterile 96-well plates containing 200 µL of SEM medium. Plates were sealed and incubated at 30°C, 225 rpm and 80% relative humidity in a humidity shaker (Minitron-INFORS, Biogen, Spain) for 72 hours. Aliquots of 20 µL of yeast supernatants were transferred to a 96-well plate using a robotic station for liquid handling Freedom EVO (Tecan, Männedorf, Switzerland) and 180 µL of HRP-Amplex Red reagent for secondary alcohol activity detection. The final concentrations in the well were 5 mM 1-(p-methoxyphenyl)-ethanol, 70 µM Amplex Red, 3 µg/mL HRP in 100 mM phosphate buffer pH 6.0. Reagents were dispensed with Multidrop™ Combi Reagent Dispenser (Thermo Scientific, Massachusetts, USA). The plates were incubated at room temperature and activity with the chiral alcohol was determined as H_2O_2 production coupled to the oxidation of Amplex Red reagent by the HRP and measured at 563nm ($\varepsilon_{resorufin}$ 563 = 56000 M^{-1} cm^{-1}). Reaction mixture with p-methoxybenzyl alcohol (1 mM final concentration) was also prepared to determine activity with a primary alcohol. One unit of AAO activity is defined as the amount of enzyme that converts 1 µmol of alcohol to aldehyde or ketone with the stoichiometric formation of H_2O_2 per min under the reaction conditions. The HTS-assay incorporated two consecutive re-screenings to rule out the selection of false positives as described in previous work (Viña-Gonzalez et al. 2015).

Protein production and purification

The native AAO, heterologously expressed in E. coli and in vitro refolded (wtAAO), was produced and purified as described elsewhere (Ruiz-Dueñas et al. 2006). Evolved variants were produced in yeast (Viña-Gonzalez et al. 2015) and purified by cationic exchange chromatography, anion exchange chromatography and size-exclusion chromatography (ÄKTA purifier, GE Healthcare, WI, US). The crude extract from *S. cerevisiae* cultures was concentrated and dialyzed in 20 mM sodium phosphate/citrate at pH 3.3 (buffer A) by tangential ultrafiltration (Pellicon; Millipore, USA) through a 10-kDa-pore-size membrane (Millipore, USA) by means of a peristaltic pump (Masterflex easy load; Cole-Parmer, USA). The sample was filtered and loaded onto a strong cation-exchange column (HiTrap SP FF; GE Healthcare) pre-equilibrated with buffer A and coupled to the ÄKTA purifier system. The proteins were eluted with a linear gradient of buffer P (20 mM piperazine buffer pH 5.5) + 1M NaCl in two phases at a flow rate of 1 ml/min: from 0 to 50 % during

15 min and from 50 to 100% in 2 min. Fractions with AAO activity were pooled, dialyzed against buffer P, concentrated and loaded onto a high-resolution resin, strong-anion-exchange column (Biosuite MonoQ 10 cm; Waters, USA) pre-equilibrated in buffer P. The proteins were eluted with a linear gradient from 0 to 0.5 M of NaCl in two phases at a flow rate of 1 ml/min: from 0 to 50 % during 20 min and from 50 to 100% in 2 min. Fractions with AAO activity were pooled, dialyzed against 20 mM phosphate buffer pH 6.0, concentrated and further purified by a Superose 12 HR 10/30 molecular exclusion column (Amersham Bioscience; Amersham, UK) pre-equilibrated with 150 mM NaCl in 20 mM phosphate buffer pH 6.0 at a flow rate of 0.5 ml/min. The fractions with AAO activity were pooled, dialyzed against buffer 20 mM phosphate buffer pH 6.0, concentrated and stored.

Biochemical characterization

Steady-state kinetic constants: Alcohol oxidation kinetics for 1-(*p*-methoxyphenyl)-ethanol, *p*-methoxybenzyl alcohol and 2,4-hexadien-1-ol were measured in 100 mM phosphate buffer pH 6.0 at 25°C in air-saturated conditions (0.256 mM O_2 concentration). Reactions were performed by triplicate and substrates oxidations were followed by measuring the absorption at 285 nm for *p*-methoxybenzyl alcohol, ε_{285} = 16,950 M^{-1} cm^{-1} and at 280 nm for 2,4-hexadien-1-ol, ε_{280} = 30,140 M^{-1} cm^{-1}. The oxidation of 1-(*p*-methoxyphenyl)-ethanol was measured indirectly coupled with saturated conditions of HRP and Amplex Red substrate (4.5 U/mL HRP and 75 µg/mL Amplex Red final concentrations) following activity at 563nm (ε_{563} = 56000 M^{-1} cm^{-1}).

HPLC analysis and optical rotation: The enantioselectivity of LanDo variant was analyzed by chiral HPLC with equipment consisting of a tertiary pump (Varian/AgilentTechnologies) coupled to an autosampler (Merck Millipore) and a Lux 5 µm Cellulose-1 column (Phenomenex). For the mobile phase hexane and isopropanol in a ratio 9:1 was used. The separation of the enantiomers was performed at a flow rate of 1.0 mL/min. The rotary polarization was measured with a JASCO P-2000 polarimeter. After full conversion, a reaction mixture with the remaining alcohol (1mg/mL of 1-(p-methoxyphenyl)-ethanol) was extracted with ethyl acetate and dissolved in methanol. The measurement was made at 25 °C with a sodium lamp at 589 nm.

Protein modeling: A structural model of the AAO from P. eryngii crystal structure at a resolution of 2.55 Å (Protein Data Bank Europe [PDB] accession number 3FIM (Fernandez et al. 2009), was used as scaffold for the wild type AAO model and the homology models for different mutants were made from 3FIM by PyMol (Schrodinger LLC.; http://www.pymol.org).

DNA sequencing: All genes were verified by DNA sequencing (BigDye Terminator v3.1 Cycle Sequencing Kit) using the following primers: primers sense, RMLN and AAOsec1F and primers antisense RMLC, AAOsec2R, and AAOsec3R.

Computational methods

The diffusion and binding of the secondary alcohol (S)-1-(*p*-methoxyphenyl)-ethanol were studied using the new adaptive-PELE (Protein Energy Landscape Exploration) software (Lecina et al. 2017). This adaptive protocol offers improved sampling by running multiple and consecutive short PELE simulations (epochs), setting the initial conditions of each epoch following a reward function that favours sampling of unexplored areas. Even though the ligands were parameterized based on the OPLS2005 force field, the electrostatic charges were derived from the electrostatic potential obtained through quantum calculations at the M06/6-31G* level with Jaguar (Bochevarov et al. 2013), and its rotamer library was built with Macromodel (Murphy et al. 2000; Sastry et al. 2013). Similarly, the FAD cofactor was optimized with a mixed QM/MM calculation at the same level of theory using Qsite.

A single adaptive-PELE simulation was enough to explore the diffusion and binding of (S)-1-(p-methoxyphenyl)-ethanol for the native protein and the different variants. The ligand was initially placed between residues Gly52 and Asn56 in all cases. Each simulation used 192 processors, producing 60 epochs of 20 PELE steps each. During the simulation, ligand perturbations (rotations and translations) are coupled with the backbone perturbation to allow protein flexibility. This is achieved by using an anisotropic network model (Atilgan et al. 2001) applied to every Cα atom, while all sidechain conformations within 6 Å of the ligand were predicted each step. An epsilon value of 0.2 was used in the adaptive protocol, meaning that 20% of the processors started each epoch from the structure with the best ligand-FAD distance.

6.3 RESULTS AND DISCUSSION

Laboratory evolution

First generation: Unlocking activity for secondary aromatic alcohols

The departure point of this study was a secretion mutant of the AAO from Pleurotus eryngii named FX9. This mutant is the product of several rounds of directed evolution aimed to promote functional expression in *Saccharomyces cerevisiae* (Viña-Gonzalez et al. 2015; Viña-Gonzalez et al. 2018). In this FX9 variant, the AAO is fused to a chimeric prepro-leader (preα-factor-proKiller) that enhanced secretion by introducing the F[3α]S, N[25proK]D, T[50proK]A and

F[52proK]L mutations into the pre-α and pro-Killer leaders. In addition, two substitutions were included in the mature AAO: L170M in an α-helix situated at the protein surface, and the consensus, ancestral mutation H91N in the FAD attachment loop. These latter mutations enhanced stability and improved production by *S. cerevisiae* to 4.5 mg/L and by *Pichia pastoris* in bioreactor to 25.5 mg/L, while conserving the general biochemical features of the native AAO (Viña-Gonzalez et al. 2018)..

As a substrate for the screening assay we chose 1-(*p*-methoxyphenyl)-ethanol, a chiral molecule with similar structure to the natural *p*-methoxybenzyl alcohol substrate, the oxidation of which by AAO can be rapidly assessed in a coupled Amplex Red/HRP assay (see Experimental Section for details). As the activity of AAO on secondary alcohols is irrelevant, no response was detected with 1-(*p*-methoxyphenyl)-ethanol when the parental FX9 was screened in microtiter fermentations of the supernatant (i.e. cultures in 96 well plates). As indicated previously, AAO's failure to oxidize secondary alcohols is due to steric perturbation of the residues forming the catalytic cavity when trying to accommodate bulkier, chiral molecules. Specifically, Phe501 is thought to be a steric liability at the active site, particularly given the very weak but detectable activity on 1-(*p*-methoxyphenyl)-ethanol of a F501A variant expressed in *E. coli* after in vitro refolding (Hernandez-Ortega et al. 2012c). A more recent rational attempt to achieve secondary alcohol oxidation based on PELE (Protein Energy Landscape Exploration) suggested Ile500 was another possible obstacle for ligand diffusion. Indeed, the I500A substitution conferred better transit of the substrate to the active site due to channel broadening (Serrano et al. 2019).

To ensure that the activity on secondary benzyl alcohol could be measured at the start of the laboratory evolution campaign, we first prepared three mutants from the FX9 secretion variant: I500A, F501A and 500A-F501A (**Figure S2 A**, **B**). When isolated from yeast supernatants these variants did not appear to act on 1-(*p*-methoxyphenyl)-ethanol. Hence, we performed combinatorial saturation mutagenesis of the Ile500-Phe501 residues and we found several clones with activity on 1-(*p*-methoxyphenyl)-ethanol, which were scaled up to a 100 mL flask to estimate the overall improvement in activity. Of these, the I500Q-F501W, I500L-F501I, I500M-F501V and I500M-F501W mutants presented a 5-, 15-, 30- and 160-fold enhancement in activity relative to the parental FX9, respectively. The activity of the I500M-F501W mutant (named 15G12) was further tested against a panel of primary and secondary alcohols, **Table 1**. Its specific activity on primary alcohols was dramatically reduced depending on the chemical nature of the molecule, with practically no activity on *p*-methoxybenzyl alcohol (c.a. 0.5% of that of the parental FX9 variant). By contrast, the activity of the 15G12 variant on secondary aromatic alcohols rose from undetectable levels, to weak yet evident activity on 1-phenyl ethanol and 4-fluoro-α-methylbenzyl alcohol, and up to 1.5 U/L activity on 1-(*p*-methoxyphenyl)-ethanol, **Table 1**. Given that hydride abstraction of *p*-methoxybenzyl alcohol to the flavin of AAO occurs exclusively from the pro-R position, in deracemization reactions of secondary alcohols R-hydrogen abstraction should produce S enantioselective oxidation of the alcohol to the corresponding ketone. To confirm this, reactions were performed with the optically pure (R) and (S)-4-fluoro-α-methylbenzyl alcohol enantiomers, and as expected, only activity on the latter was detected (Hernandez-Ortega et al. 2012c)

Table1. Activity of AAO variants with primary and secondary alcohols.

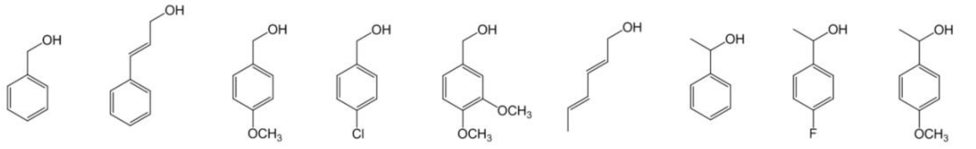

	Benzyl alcohol	Cinnamyl alcohol	*p*-Methoxy benzyl alcohol	*p*-Chloro benzyl alcohol	3,4-Dimethoxy benzyl alcohol	2,4-Hexadien -1-ol	1-Phenyl ethanol	*p*-Fluoro-α-methyl benzyl alcohol	1-(*p*-Methoxyphenyl)-ethanol
FX9 (U/mg)	15.6	41.1	46.6	26.6	22.2	43.4	n.d.	n.d.	2.2×10^{-3}
15G12 (U/mg)	0.6	18.4	0.3	0.6	0.03	13	6×10^{-3}	6×10^{-3}	0.3

Specific activities were estimated in 100 mM phosphate buffer pH 6.0 containing 5 mM of each alcohol. Each reaction was performed by triplicate and substrate conversion was followed by measuring the absorption at 563nm (ε_{563} = 56000 M^{-1} cm^{-1}) using the HRP/Amplex red coupled assay as described in the experimental section.

Paradoxically, while the initial search for a wider space for secondary aromatic alcohol accommodation focused on the I500A-F501A mutations, the bulky alcohol would appear to be much better oxidized in a narrower catalytic pocket following the substitution of Ile500 and Phe501 by the more expansive Met and Trp, respectively (**Figure S2 C**, **D**). Thus, these two mutations at the active site reposition the secondary alcohol, favouring catalysis, as confirmed by computational analysis (see below).

Second and third generations: Searching for new beneficial mutations

After unlocking the activity on secondary benzyl alcohols, different protein segments of the 15G12 mutant were targeted for random mutagenesis and DNA recombination by MORPHING, with a view to further optimize its activity on secondary alcohols. This focused structural evolution tool allows the protein to be divided into defined mutagenic areas, each of which can be interrogated in conjunction with the in vivo recombination of the different DNA fragments in *S. cerevisiae* (Gonzalez-Perez et al. 2014). This approach has already been successfully applied during the evolution of AAO towards functional expression in yeast (Viña-Gonzalez et al. 2015) and on this occasion, the design involved the study of three protein blocks in independent libraries, **Figure 1A**, **B**. The first of these was the MA block at the N-terminus (Leu48-Thr100), which is associated with the access channel and the FAD-binding domain, and that contains important determinants like Pro79, Asn91, Tyr92 and Val90. The second MB block (Leu310-Ile417) covers the wall of the catalytic pocket and it contains the aromatic Phe397, a residue implicated in substrate positioning and product release. The third MC block (Glu490-Gln566) is situated in the C-terminal region, and it contains the catalytic His502 and several amino acids related to substrate positioning (Met500, Trp501 and His546). Together, these three blocks encompass the complete active site and the aromatic bottleneck formed by Tyr92, Phe397 and Trp501, **Figure 1C** (Fernandez et al. 2009; Hernandez-Ortega et al 2011a; Ferreira et al. 2006; Hernandez-Ortega et al. 2012a; Carro et al. 2018)

We carried out the three independent libraries of MORPHING; besides, we prepared a conventional error-prone PCR (epPCR) mutagenic library that targeted the whole AAO gene (in total over 4,000 clones were screened). From the pool of libraries, seven mutants with stronger activity on the secondary 1-(*p*-methoxyphenyl)-ethanol were selected for further analysis, ranging from a 1.4 to 2.2-fold enhancement over 15G12, **Figure 2**. The most successful MORPHING corresponded to the MA block, with five of the seven improved AAO variants from this library. Interestingly, all the mutations identified were located within a 14 amino acid span, from Ile76 to Val90. The mutations carried by the best variant (3F10) were I76V and M83I, which in conjunction with the rest of the substitutions in this stretch (A77V, R80C, I76V and V90A) highlight the importance of the access channel in modulating oxidative activity. Indeed, it should be noted that the R80C substitution was also found in the triple 6G3 mutant from the whole gene epPCR library, together with two superficial substitutions: E39G and Q466R, **Figure 2**. The MORPHING method was also successful in fragment MB, where the 12D12 variant presented two mutations at the surface: F332L and V340A. Applying focused mutagenesis to the area corresponding to the catalytic pocket, the MC block, was ineffective since variants with improvements were not detected.

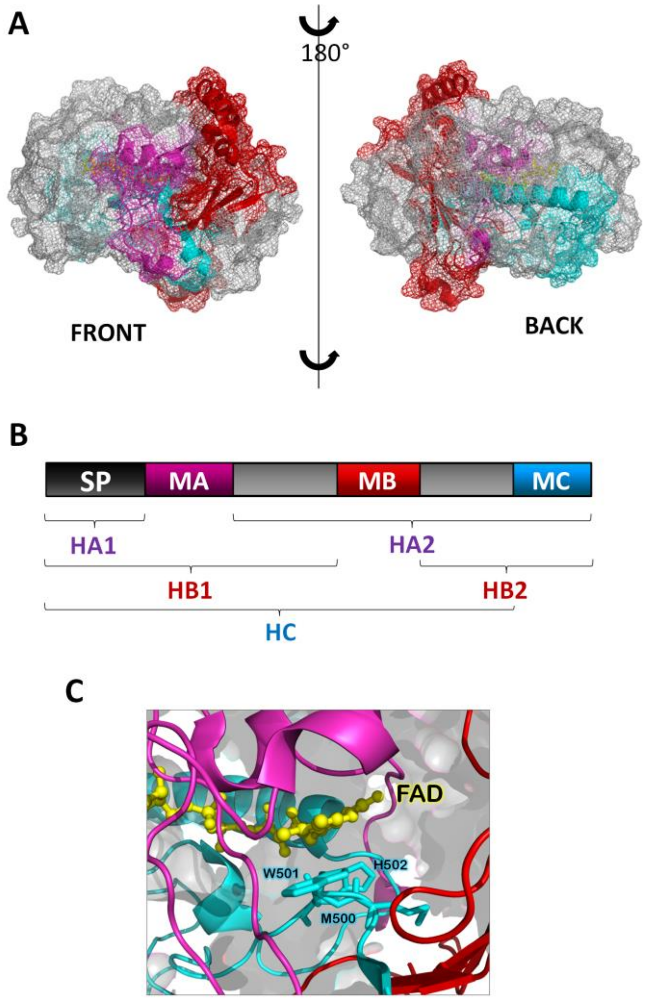

Figure 1. MORPHING fragments for focused evolution. (A) Front and back views of AAO, with the MA, MB and MC MORPHING blocks shown in purple, red and blue, respectively. (B) The dark grey box corresponds to the signal peptide, and the three mutagenic fragments considered for MORPHING are shown as purple, red and blue boxes. For the first MORPHING library, mutagenic block MA was in vivo assembled with high-fidelity fragments HA1 and HA2. For the second library, mutagenic fragment MB was recombined from high-fidelity fragments HB1 and HB2. The third library was constructed with the assembly of mutagenic block MC and high-fidelity fragment HC. (C) The catalytic pocket of AAO with the contribution of the MORPHING blocks MA, MB and MC (purple, red and blue, respectively). Model prepared with the crystal structure of the AAO from *P. eryngii* (PDB 3FIM).

To further enhance secondary alcohol oxidation, the best variants from each library were submitted to epPCR and in vivo shuffling in *S. cerevisiae*: 3F10 and 11H2 from the MA library, the 12D2 variant from the MB library, and the 6G3 variant obtained through whole-gene mutagenic amplification. From this third generation, the 3C11 variant was seen to enhance the activity roughly 1.2-fold compared to 3F10 (412-fold relative to the FX9 parental type), retaining the I76V mutation from 3F10 and acquiring the V90A change, also previously detected in the 9F2 variant, as well as incorporating the new Q174R substitution, **Figure 2**.

Fourth generation: Mutational polishing by site-directed recombination

After careful evaluation of the mutations obtained in the second and third generations, **Table 2**, we decided to undertake a final round of evolution to assess whether there were any positive epistatic effects among the mutations. We constructed a combinatorial library by in vivo site-directed recombination, such that the 10 mutations and their corresponding reversions could be rapidly combined in an one-pot transformation reaction, evaluating the library in order to obtain the optimal combination of substitutions for the oxidation of chiral alcohols, **Figure S1**. From this ensemble of mutations, the three best variants identified shared the same backbone of substitutions: A77V-R80C-V340A. The third best variant was the 24H3 mutant that carried the A77V-R80C-Q174R-F332L-V340A-Q466R mutations, displaying activity more than 420-fold better than the FX9 parental type. In the case of 4D3, the only difference from the 24H3 variant was the absence of the Q174R mutation, which translated into a 480-fold increase in activity, highlighting a detrimental effect of Q174R within this mutational context. The further purging of Q466R and F332L gave rise to the LanDo variant that carried the A77V-R80C-V340A mutations in conjunction with I500M-F501W and the 6 secretion mutations of FX9, this variant representing the best performer with a total 800-fold enhancement of activity relative to the parental type, **Figures 2, 3**.

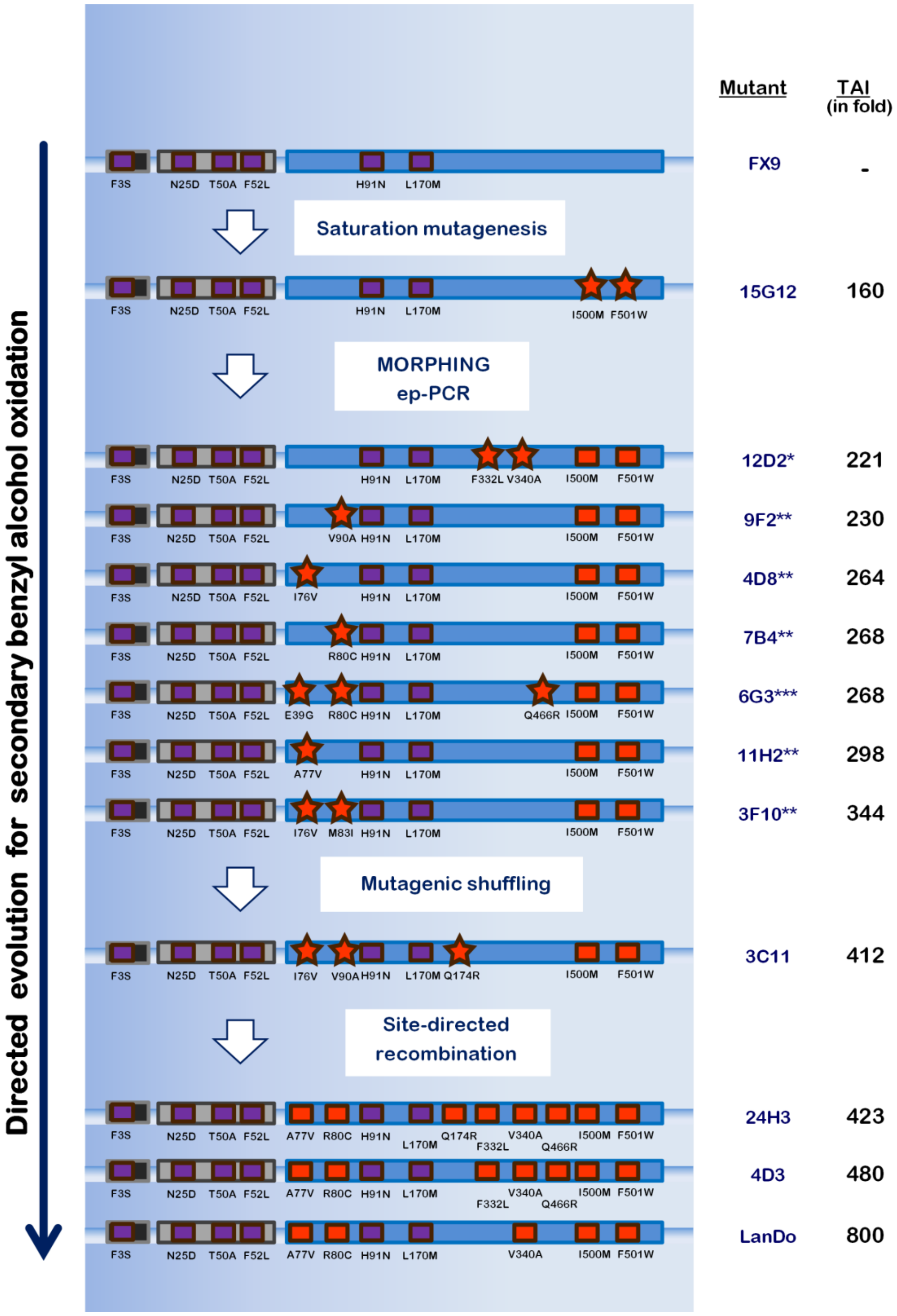
Directed evolution for secondary benzyl alcohol oxidation
Mutant
TAI (in fold)
F3S N25D T50A F52L H91N L170M
FX9
-
Saturation mutagenesis
F3S N25D T50A F52L H91N L170M I500M F501W
15G12
160
MORPHING ep-PCR
F3S N25D T50A F52L H91N L170M F332L V340A I500M F501W
12D2*
221
F3S N25D T50A F52L V90A H91N L170M I500M F501W
9F2**
230
F3S N25D T50A F52L I76V H91N L170M I500M F501W
4D8**
264
F3S N25D T50A F52L R80C H91N L170M I500M F501W
7B4**
268
F3S N25D T50A F52L E39G R80C H91N L170M Q466R I500M F501W
6G3***
268
F3S N25D T50A F52L A77V H91N L170M I500M F501W
11H2**
298
F3S N25D T50A F52L I76V M83I H91N L170M I500M F501W
3F10**
344
Mutagenic shuffling
F3S N25D T50A F52L I76V V90A H91N L170M Q174R I500M F501W
3C11
412
Site-directed recombination
F3S N25D T50A F52L A77V R80C H91N L170M Q174R F332L V340A Q466R I500M F501W
24H3
423
F3S N25D T50A F52L A77V R80C H91N L170M F332L V340A Q466R I500M F501W
4D3
480
F3S N25D T50A F52L A77V R80C H91N L170M V340A I500M F501W
LanDo
800

Figure2. Laboratory evolution of AAO for the oxidation of secondary benzyl alcohol. New mutations are represented as stars and accumulated mutations as squares. The chimeric prepro-leader is depicted in grey and the mature AAO in blue. The TAI (total activity improvement) refers to the fold improvement of AAO activity with 1-(*p*-methoxyphenyl)-ethanol as a substrate and it was estimated relative to the FX9 parental type from S. cerevisiae supernatants: *Mutants from the MB library; **Mutants from the MA library; ***Mutant from the epPCR library.

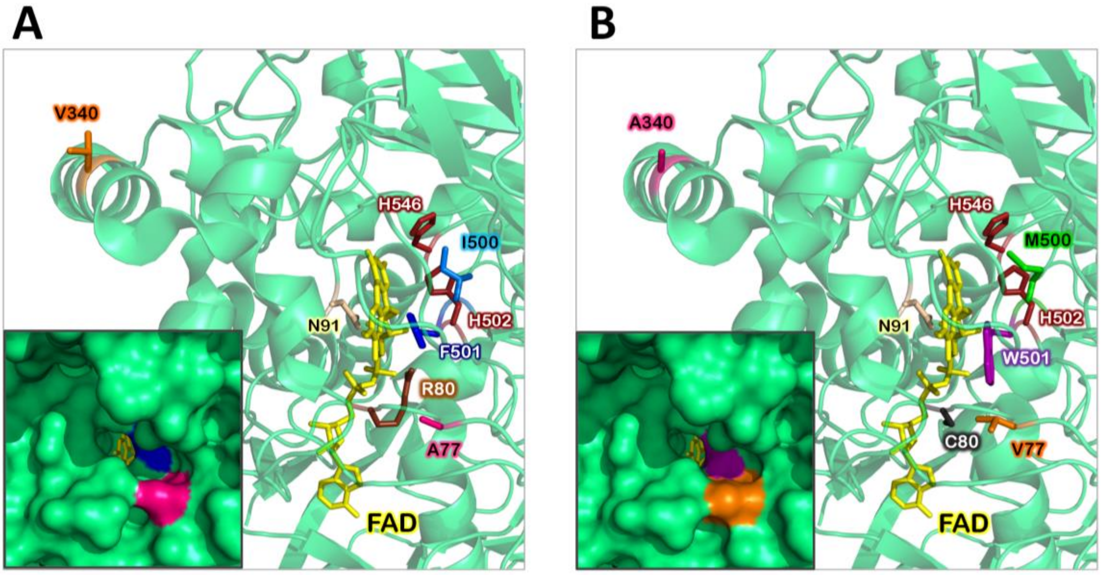

Figure 3. Location of the mutations in the evolved secondary benzyl-alcohol oxidase. (A) FX9 parental type and (B) LanDo mutant. The FAD molecule is represented in yellow, the catalytic base His502 and His546 is depicted in red, and the consensus ancestral mutation Asn91 is in light pink. A77V, R80C, V340A, I500M and F501W are represented following a color code (before and after mutation). The mutation L170M at the surface of the enzyme is not present in the fragment represented. The inset shows a detail of the protein surface at the access channel. The model was prepared with a crystal structure of the AAO from P. eryngii (PDB 3FIM).

Biochemical characterization

To characterize the LanDo mutant and the FX9 parental variant, they were produced and purified to homogeneity. To determine the enantioselectivity of the LanDo variant, transformation of the racemic 1-(*p*-methoxyphenyl)-ethanol was followed by chiral-HPLC, **Figure 4** and 100% conversion with an enantiomeric excess (ee) >99% was achieved after a two hour reaction. The configuration of the remaining alcohol in the reaction was confirmed by optical rotation, **Figure S3**; **Table S2**, the positive rotation corresponding to the R enantiomer meaning the natural oxidation of the S enantiomer by AAO was maintained after evolution (Hernandez-Ortega et al. 2012c).

Table 2. Selected mutations for site-directed recombination.

Mutation	Variant	Library	Secondary motif
$_{GAG}$E39G$_{GGG}$	6G3	*ep*-PCR	Loop
$_{ATT}$I76V$_{GTT}$	3F10, 4D8	MA	Loop
$_{GCG}$A77V$_{GTG}$	11H2	MA	Loop
$_{CGC}$R80C$_{TGC}$	6G3, 7B4	*ep*-PCR, MA	Loop
$_{ATG}$M83I$_{ATA}$	3F10	MA	Loop
$_{GTT}$V90A$_{GCT}$	9F2	MA, mutagenic shuffling	Loop
$_{CAA}$Q174R$_{CGA}$	3C11	Mutagenic Shuffling	Alpha helix
$_{TTC}$F332L$_{CTC}$	12D2	MB	Alpha helix
$_{GTT}$V340A$_{GCT}$	12D2	MB	Alpha helix
$_{CAA}$Q466R$_{CGA}$	6G3	*ep*-PCR	Loop

Despite the remarkably specific activity for the secondary 1-(*p*-methoxyphenyl)-ethanol (2.9 U/mg), the five new mutations carried by the LanDo variant did not negatively affect its secretion (4.6 mg/L). The activity of LanDo with secondary alcohols was tested against available commercial secondary (aromatic) alcohols that were representative of the structural scope of the AAO. The initial turnover rates of the LanDo variant relative to the wildtype AAO (wtAAO, heterologous expressed in *E. Coli* after in vitro refolding) increased 30, 20 and 100-fold times for 1-(*p*-methoxyphenyl)-ethanol, *p*-fluoro-α-methylbenzyl alcohol and 1-phenylethanol, respectively. Indeed, the LanDo variant even showed activity on 1-phenylpropanol, a substrate not oxidized by wtAAO, **Table 3**. The kinetic parameters were measured under air-saturated conditions for 1-(*p*-methoxyphenyl)-ethanol, and for the primary alcohols p-methoxybenzyl alcohol and 2,4-

hexadien-1-ol. LanDo displayed an outstanding increase in the catalytic efficiency for enantioselective oxidation of 1-(*p*-methoxyphenyl)-ethanol, three orders of magnitude.

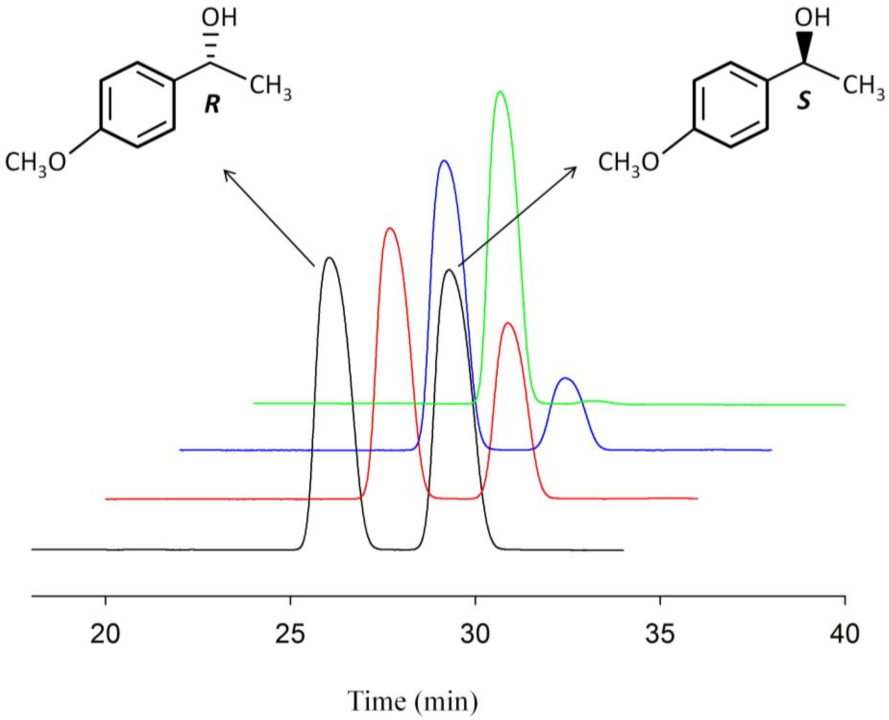

Figure 4. Chiral HPLC analysis. HPLC elution profiles after the reaction of the AAO variant LanDo (1 µM) with racemic 1-(p-methoxyphenyl)-ethanol (2.5 mM). Reactions were performed at room temperature in 100 mM phosphate buffer pH 6.0 with continuous shaking and the aliquots were analyzed by chiral HPLC at different times. The separation of the R and S enantiomers in the negative control is represented in black, whereas the 15, 45, and 90 min reactions are represented in red, blue and green, respectively.

Table 3. Initial turnover rates for secondary alcohols.

	***p*-Fluoro-α-methylbenzyl alcohol**	**1-Phenylethanol**	**1-Phenylpropanol**
wtAAO	0.35 ± 0.01	0.10 ± 0.03	n.m.
LanDo	7.3 ± 0.1	10 ± 0.5	1 ± 0.1

Turnover rates (min^{-1}) were estimated in 100 mM phosphate buffer pH 6.0 containing 5 mM of each secondary alcohol with the exception of 1-phenylpropranol (2.5 mM). Each reaction was performed by triplicate and substrate conversion was followed by measuring the absorption at 563nm (ε_{563} = 56000 M^{-1} cm^{-1}) using the HRP/Amplex red coupled assay as described in the experimental section.

Interestingly, the activity on primary alcohols that was dramatically reduced after inserting the I500M-F501W pair in the first cycle of evolution in 15G12 variant, **Table 1**; **Figure 2**, was recovered to a considerable extent for *p*-methoxybenzyl alcohol and the aliphatic 2,4-hexadien-1-ol. This result indicates the beneficial effect that A77V, R80C and V340A exerted on LanDo´s overall activity.

Table 4. Kinetic parameters for AAO variants.

Substrate	Kinetic constants	wtAAO**	LanDo
1-(*p*-methoxyphenyl)-ethanol	K_m (mM)*	24.9 ± 1.1	0.65 ± 0.1
	k_{cat} (s^{-1})	0.18 ± 0.002	4.9 ± 0.1
	k_{cat}/K_m (mM^{-1} s^{-1})	0.007	7.5
p*-methoxybenzyl alcohol*	K_m (mM)	0.027 ± 0.004	0.02 ± 0.003
	k_{cat} (s^{-1})	142 ± 5	72 ± 3
	k_{cat}/K_m (mM^{-1} s^{-1})	5233	3600
2,4-hexadien-1-ol**	K_m (mM)	0.094 ± 0.005	0.095 ± 0.006
	k_{cat} (s^{-1})	119 ± 2	40.9 ± 0.7
	k_{cat}/K_m (mM^{-1} s^{-1})	1271	430.5

AAO kinetic constants were measured in 100 mM phosphate buffer pH 6.0 at 25°C. All reactions were performed by triplicate. *Referred to the S enantiomer, as 50% of the racemic mixture. **Calculated for wtAAO previously (Ferreira et al. 2005).

Computational analysis

In order to rationalize the effect of the mutations identified, PELE simulations were run for wtAAO and the variants obtained in the different rounds of directed evolution. The oxidation of alcohols by AAO involves a non-synchronous concerted reaction, where both proton transfer from the hydroxyl group to the catalytic base His502 and hydride abstraction from the benzylic position by the flavin are taking place at the same reaction step (Ferreira et al. 2009). PELE results were plotted placing both catalytic distances in the X and Y axis, and the interaction energy between the protein and the ligand was represented by colors, **Figure 5**.

No significant differences were evident between the wtAAO and the secretion mutant FX9 (H91N-L170M) in these plots, consistent with the experimental evidence that this variant does not improve the activity on secondary alcohols but does increase expression and stability. The 15G12 variant included the I500M and F501W mutations on top of the previous ones, accumulating a total of 4 mutations in the mature protein. In this case, the plot shows how the ligand can reach catalytic positions 2.5 Å away from both the FAD and the histidine at the same time, producing better catalytic constants than those of the wtAAO. In addition, a minimum could be seen where the ligand-histidine distance was ~2.2 Å, although the interaction energies were much higher and they were therefore less accessible.

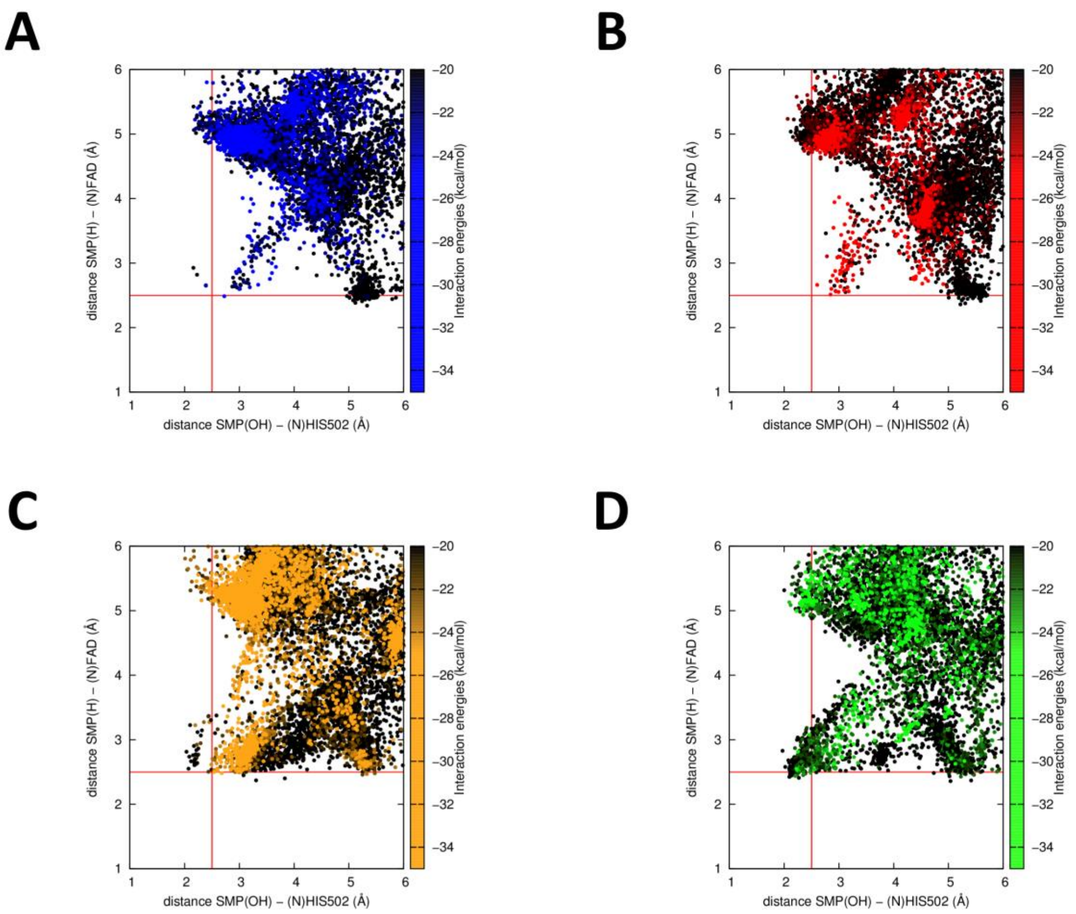

Figure 5. Substrate diffusion computational PELE simulations. Plots represent the PELE simulations relating catalytic distances (X and Y) and interaction energies (color scheme, right Y axis) for different AAO variants: (A) wtAAO; (B) the FX9 secretion mutant; (C) the 15G12 mutant; (D) the final evolved benzyl-alcohol oxidase, LanDo mutant.

The largest improvement came after introducing an additional three mutations in the LanDo variant: A77V, R80C, and V340A. These three substitutions allow the ligand to achieve even smaller catalytic distances, up to ~2 Å for the histidine and 2.4 Å for the FAD, with reasonable interaction energies. Considering that closer catalytic distances imply a decrease in energy barriers, this agreed well with the higher kinetic constants. Moreover, the increase in the number of structures with good catalytic distances could reflect the ease with which the ligand can find catalytic positions, explaining the lower K_m values for this variant.

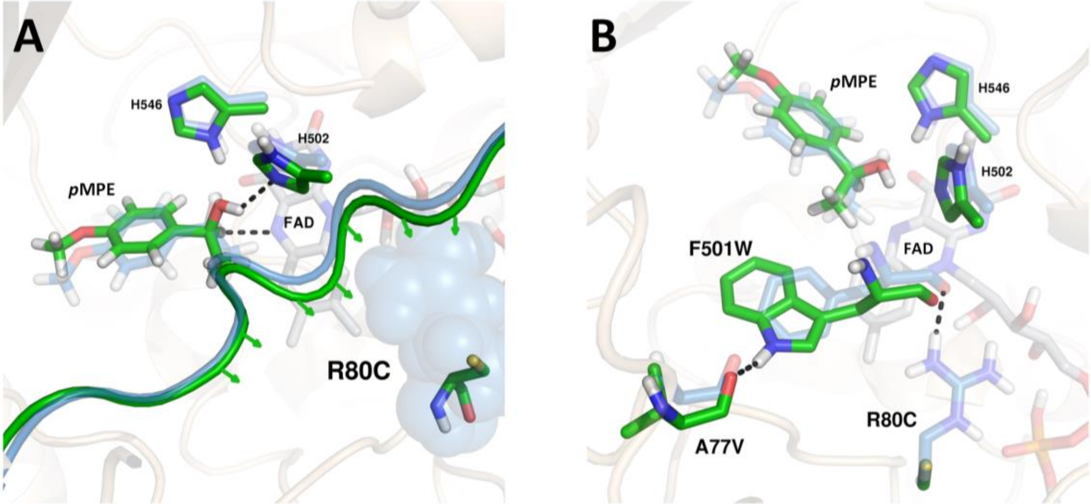

Figure 6. Conformational changes at the catalytic pocket of AAO. (A) Backbone displacement (green) to better position (S)- 1-(p-methoxyphenyl)-ethanol (pMPE). (B) Interruption of the interaction of Arg80 with the backbone of residue 501, and the formation of a hydrogen bond between Val77 and Trp501.

Despite the large number of mutations in LanDo (7 in total, excluding the mutations in the chimeric prepro-leader), there are no major conformational changes in the protein or in the positioning of the ligand. Nevertheless, we did note subtle modifications that were sufficient to improve the catalytic position of (S)-1-(*p*-methoxyphenyl)-ethanol. In particular, the R80C mutation was found repeatedly in independent libraries during evolution, **Figure 2** and it created an empty space at the top of the FAD cofactor. Consequently, the backbone containing H502 shifts in that direction, **Figure 6A**. Moreover, Arg80 interacts with the oxygen of the backbone of residue 501, such that this mutation frees Trp501 to form a hydrogen bond with the oxygen backbone of Val77, **Figure 6B**. All these subtle adjustments allow the ligand to adopt conformations with better catalytic distances, **Figures 5**, **6**.

6.4 CONCLUSIONS

Focusing evolution on structural elements made it possible to identify mutations in the catalytic pocket and access channel that allowed an AAO to be designed that acts on different secondary benzyl alcohols. This final secondary-benzyl alcohol oxidase variant maintained strong enantioselectivity, providing a potential catalyst for chiral de-racemization. The complex enzyme-substrate relationships of this enzyme were highlighted by an enhancement of three orders of magnitude in the catalytic efficiency, an effect produced by a combination of bulky substitutions in the catalytic cavity and other unpredicted changes. Paradoxically, a steric problem appeared to be resolved by introducing bulkier residues, something difficult to anticipate from a rational point of view. It is worth noting that the resolution of molecules like 1-phenylpropanol could be of use to obtain moiety precursors of serotonin/norepinephrine reuptake inhibitors like Fluoxetine or Atmoxetine (Matsuda et al. 2009). The results obtained here also highlight the importance and efficacy of S. cerevisiae as a platform for both the functional expression of eukaryotic genes and as a molecular tool-box to generate DNA libraries for directed evolution campaigns. The data presented open new opportunities for the evolution of AAO, which include the oxidation of furfural derivatives for the synthesis of biopolymers or the in situ production of H_2O_2 in cascade oxyfunctionalization reactions by peroxygenases (Carro et al. 2018b).

ACKNOWLEDGEMENTS

This research was supported by the EU project FP7-KBBE-2013-7-613549-INDOX, by the Spanish Government projects BIO2016-79106-R-Lignolution, CTQ2016-74959-R (MINECO/FEDER, EU) and by the Comunidad de Madrid project Y2018/BIO4738-EVOCHIMERA.

6.5 SUPPLEMENTARY MATERIAL

Supplementary Table 1. List of primers

Oligo	Sequence
RMLN	5’-CCTCTATACTTTAACGTCAAGG-3’
RMLC	5’-GGGAGGGCGTGAATGTAAGC-3’
I500Af	5’- GAGACAACGCCAACACG*GCT*TTCCACCCAGTTGGAACGGC -3’
I500Ar	5’- GCCGTTCCAACTGGGTG*GAA*AGCCGTGTTGGCGTTGTCTC -3’
F501Af	5’-GAGACAACGCCAACACGATT*GCT*CACCCAGTTGGAACGGC -3’
F501Ar	5’- GCCGTTCCAACTGGGTGAGC*AAT*CGTGTTGGCGTTGTCTC -3’
DM5001Af	5’- GAGACAACGCCAACACG*GCTGCT*CACCCAGTTGGAACGGC -3’
DM5001Ar	5’- GCCGTTCCAACTGGGTG*AGCAGC*CGTGTTGGCGTTGTCTC -3’
22c1F	5’-GAGACAACGCCAACACG*NDTNDT*CACCCAGTTGGAAC-3’
22c1R	5’-GTTCCAACTGGGTG*AHNAHN*CGTGTTGGCGTTGTCTC-3’
22c2F	5’-GAGACAACGCCAACACG*NDTVHG*CACCCAGTTGGAAC-3’
22c2R	5’-GTTCCAACTGGGTG*CDBAHN*CGTGTTGGCGTTGTCTC-3’
22c3F	5’-GAGACAACGCCAACACG*NDTTGG*CACCCAGTTGGAAC-3’
22c3R	5’-GTTCCAACTGGGTG*CCAAHN*CGTGTTGGCGTTGTCTC-3’
22c4F	5’-GAGACAACGCCAACACG*VHGNDT*CACCCAGTTGGAAC-3’
22c4R	5’-GTTCCAACTGGGTG*AHNCDB*CGTGTTGGCGTTGTCTC-3’
22c5F	5’-GAGACAACGCCAACACG*VHGVHG*CACCCAGTTGGAAC-3’
22c5R	5’-GTTCCAACTGGGTG*CDBCDB*CGTGTTGGCGTTGTCTC-3’
22c6F	5’-GAGACAACGCCAACACG*VHGTGG*CACCCAGTTGGAAC-3’
22c6R	5’-GTTCCAACTGGGTG*CCACDB*CGTGTTGGCGTTGTCTC-3’
22c7F	5’-GAGACAACGCCAACACG*TGGNDT*CACCCAGTTGGAAC-3’
22c7R	5’-GTTCCAACTGGGTG*AHNCCA*CGTGTTGGCGTTGTCTC-3’
22c8F	5’-GAGACAACGCCAACACG*TGGVHG*CACCCAGTTGGAAC-3’
22c8R	5’-GTTCCAACTGGGTG*CDBCCA*CGTGTTGGCGTTGTCTC-3’

22c9F	5’-GAGACAACGCCAACACG*TGGTGG*CACCCAGTTGGAAC-3’
22c9R	5’-GTTCCAACTGGGTG*CCACCA*CGTGTTGGCGTTGTCTC-3’
RHF1	5’-GGAACAAGGCCGGGCGCAAG-3’
FM1	5’-TAGGGGCAGAGGCTCCACTC-3’
RM1	5’-GCATAGCGATCGAAATCTTC-3’
FHF-1	5’-TCATGATGCGTGGATCAACA-3’
RHF-2	5’-AGGAGCAAATGGTCGGATAG-3’
FM2	5’-ATCCTAGCGTAGGCCGAAAC-3’
RM2	5’-TCTCCGCGAGCTACAGGAGA-3’
FHF-2	5’-TTATGAGTGTTACAAACGCGTTGATT-3’
RHF-3	5’-GTTGGCGTTGTCTCTAATGTACGACTC-3’
FM3	5’-CGACGGACGATGCTGCTATC-3’
F116	5’-ACGTGTCCGTCTTGGTCCTAGAGGCGGGTGTATCAGAT*GRG*AA-‘3
R116	5’-TCTGCCCCTAATACATT*CYC*A-‘3
F5	5’-CA*RTTGYG*TATCCT*YGC*GGCCGT*ATR*CTAGGGGGGTCTAGCTCT*GYT*AA-‘3
R5	5’-TT*ARC*AGAGCTAGACCCCCCTAG*YAT*ACGGCC*GCR*AGGATA*CRCAAY*TG-‘3
F521	5’- GCGTCATGGCCACGACG*CRA*GAGCAAA-‘3
R521	5`- GTCGGGATTGAAGAAGAACTCTTCGCTTTGCTC*TYG*CGTCGTGG -‘3
F9419	5’-ATAACATC*YTC*AGAGACTCGTCCGAGTTCAAC*GYT*GATTTA-‘3
R9419	5’-TAAATC*ARC*GTTGAACTCGGACGAGTCTCT*GAR*GATGTTAT-‘3
F1397	5’-TTCGTTTCCTCTCTGGT*CRA*GC-‘3
R1397	5’-GTATAACGAAGTCCGCCCACGC*TYG*ACC-’3
AAOsec1F	5’-GTGGATCAACAGAAGATTTCGATCG-3’
AAOsec2R	5’-GTGGTTAGCAATGAGCGCGG-3’
AAOsec3R	5’-GGAGTCGAGCCTCTGCCCCT-3’

Codon substitutions are shown in italics (where N = A/T/C/G; D = no C; V =no T, H = no G; B = no A; R = A/G; Y = C,T).

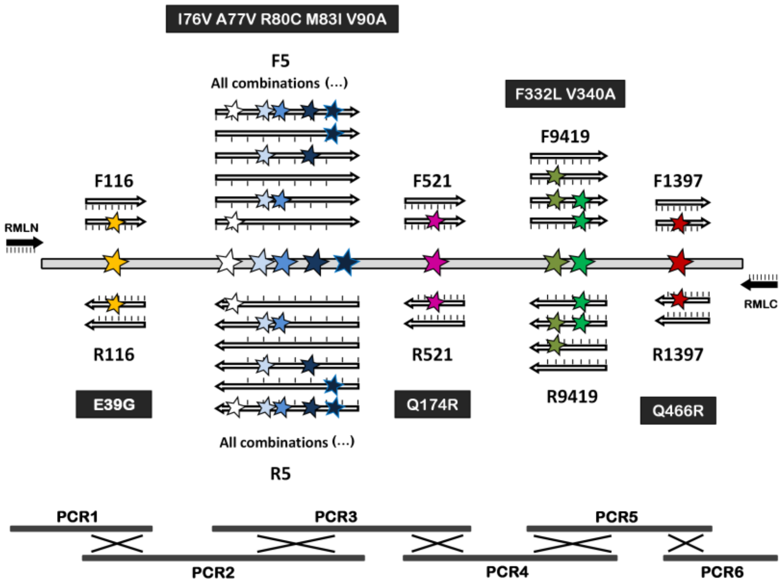
I76V A77V R80C M83I V90A
F5
All combinations (...)
F332L V340A
F9419
F116
F521
F1397
RMLN
RMLC
R116
R521
R1397
R9419
E39G
Q174R
Q466R
All combinations (...)
R5
PCR1
PCR3
PCR5
PCR2
PCR4
PCR6

Figure S1. Method for *in vivo* site-directed recombination. Primers designed to be used in the site-directed recombination experiment for the PCR amplification of the selected mutated positions (in black). For each mutation, adjacent sense and antisense primers were synthesized that were 50% mutated at the sites of interest. Six PCR reactions were performed with ~40 bp homologous sequences at each end to foster *in vivo* recombination (7 crossover events). The PCR fragments were assembled by transformation into yeast with the linearized vector to yield a library of all combinations of the mutations/reversions in one-pot

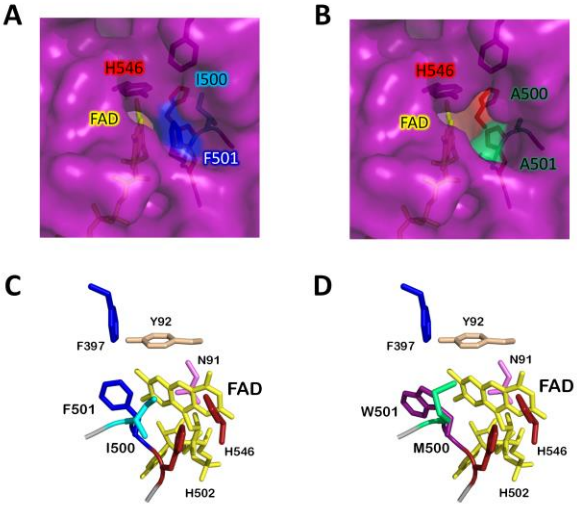
A
H546
I500
FAD
F501
B
H546
A500
FAD
A501
C
F397
Y92
N91
FAD
F501
I500
H546
H502
D
F397
Y92
N91
FAD
W501
M500
H546
H502

Figure S2. The access channel and catalytic pocket before and after mutation. The channel giving access to the active site in the FX9 (**A**) and I500A-F501A (**B**) mutants: the FAD molecule is depicted in yellow, the Phe501 and Ile500 residues in the parental type are in blue and light blue, the Ala500 and Ala501 mutations are in green, and histidine 546 at the catalytic pocket is in red. Catalytic pocket in the FX9 (**C**) and 15G12 (**D**) variants: His502 and His546 at the active site are depicted in red, FAD is depicted in yellow, ancestral/consensus mutation Asn91 is in pink, Phe397 and Phe501 are in blue, Ile500 in light blue, Tyr92 is depicted in white, whereas the new Trp501 and Met500 substitutions are depicted in purple and light green, respectively. The models were prepared from the crystal structure of *P. eryngii* AAO (PDB 3FIM).

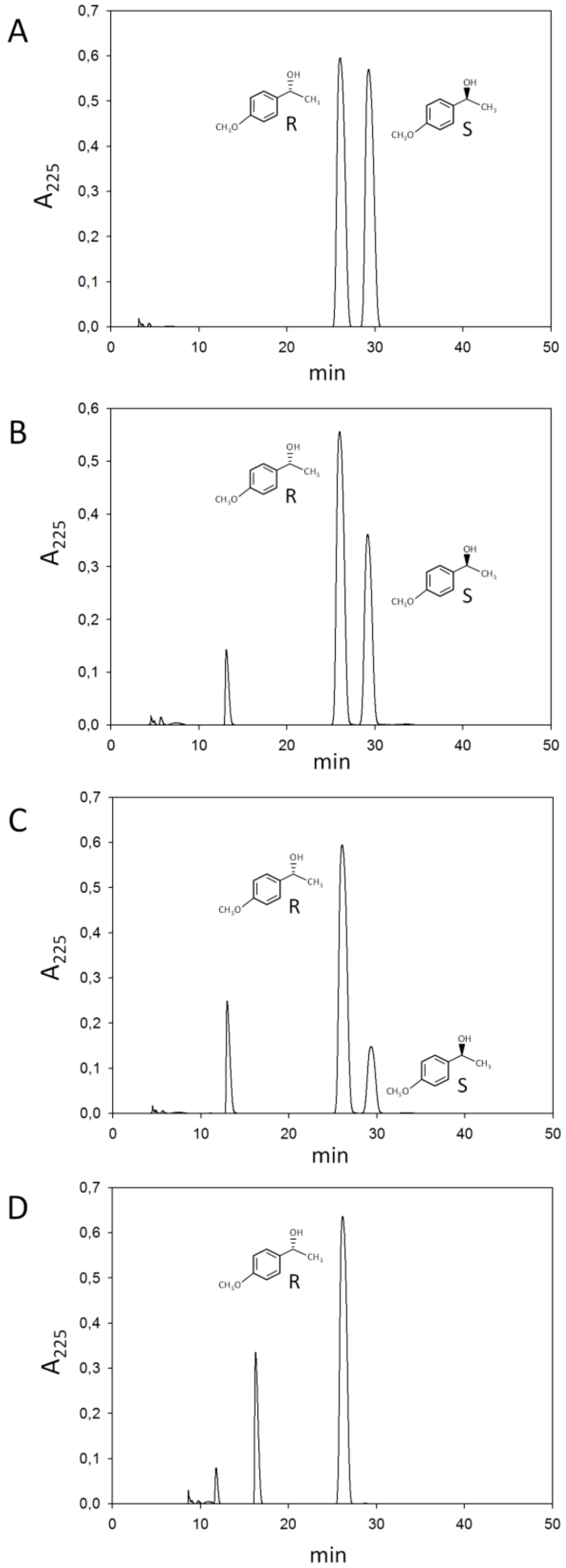
A
B
C
D
A225
min
0,0
0,1
0,2
0,3
0,4
0,5
0,6
0,7
0
10
20
30
40
50
OH
CH3
CH3O
R
S

Figure S3. **Full chiral HPLC chromatograms**. Elution profiles of the reaction of LanDo variant (1 µM) with racemic 1-(p-methoxyphenyl)-ethanol (2.5 mM). Negative control (A), after 15 minutes reaction (B), after 45 min raction (C) and after 90 min reaction (D).

PMT Voltage[V]	Temperature[C]	Optical Rotation Monitor
353	24.96	0.0592
353	24.95	0.0601
353	24.96	0.0593
354	24.96	0.0602
353	24.98	0.0586
353	24.99	0.0603
354	25.01	0.0600
354	25.03	0.0589

Supplementary Table 2. Polarimeter measurements for the LanDo variant reaction with 1-(p-methoxyphenyl)-ethanol (correspondent to the remaining R-enantiomer). Number of cycles: 8 with 1 sec cycle iterval. Path length 100mm.

CHAPTER
VI

Chapter VII:

Sequential oxidations of 5-hydroxymethyl furfural to furan-2,5-dicarboxylic acid by an evolved aryl-alcohol oxidase

The synthesis of biobased polymers from furfural derivatives is a long-pursued application whereby GMC oxidases (including AAO and HMFO) could participate. In this Chapter, we have harnessed the AAO evolution system to engineer a new active variant that complete the synthetic route from HMF to FDCA.

CHAPTER

VII

CHAPTER

VII

Sequential oxidations of 5-hydroxymethyl furfural to furan-2,5-dicarboxylic acid by an evolved aryl-alcohol oxidase

Javier Viña-Gonzalez, Angel T. Martínez, and Miguel Alcalde

.

Furan-2,5-dicarboxylic acid (FDCA) is a building block precursor of biodegradable plastics to replace those derived from fossil carbon sources. In recent years, much interest has been attracted to the synthesis of FDCA from the bio-based 5-hydroxymethylfurfural (HMF) by enzymatic cascade reactions. Aryl-alcohol oxidase (AAO) and 5-hydroxymethylfurfural oxidase (HMFO) are GMC flavoenzymes that may be used for the production of FDCA from HMF through three sequential oxidations, without the assistance of auxiliary enzymes. Such challenging process is dependent on the hydration degree of forming aldehydes, with the rate-limiting step in the final oxidation of intermediate 5-formyl-furancarboxylic acid (FFCA) to FDCA. While HMFO does accept FCCA as final substrate in the HMF reaction pathway, AAO hardly recognizes it. Here, we have engineered AAO by bringing together structural-alignment with HMFO and directed evolution for the stepwise oxidation of HMF to FDCA. With a 3-fold enhanced catalytic efficiency for HMF and a 6-fold improved overall conversion, the evolved AAO mutant completed the three consecutive 2-electron oxidations required in the synthesis of FDCA from HMF, becoming a new attractive blueprint for upcoming biobased industries.

7.1 INTRODUCTION

5-Hydroxymethylfurfural (HFM) is a renewable platform chemical that can be obtained from biomass-derived carbohydrates. Considered a highly valuable building block, HMF is conventionally produced from the acid-catalyzed dehydration of fructose, ideally from sucrose and inulin hydrolysates (Moreau et al. 2004). The result of three consecutive oxidations from HMF is furan-2,5-dicarboxylic acid (FDCA), classified as one of the most promising value added chemicals from biomass to be used in the polymer industry (Werpy and Petersen 2004). Indeed, biobased molecules are widely welcome for a more sustainable chemical industry, with the FDCA family of polymers comprising aliphatic and aromatic polyesters and polyamides. Among the most appealing applications, the synthesis of PEFs (poly(ethylene-2,5-furandicarboxylates)) from FDCA copolymerization with diols highlights as a renewable alternative to traditional polyesters based on petrochemical terephthalic acid, such as poly(ethylene-terephthalates), PETs. Leaving aside other furan derivatives like 5-(butoxymethyl)furfural and 5-(methoxymethyl)-2-furfural, HMF is the main material source for the production of FDCA monomers, which can be synthesized with catalytic nanoparticles, electrocatalytic oxidation or via enzymatic processes using lipases or, as seen in recent studies, dehydrogenases and oxidases (Sousa et al. 2015). Thus, the preferred process for an environmental-friendly transformation of HMF into FDCA is via enzymatic oxidation, either using single enzymes or whole microorganisms.

The transformation of HMF by flavooxidases has been hitherto studied for two members of the glucose-methanol-choline (GMC) superfamily of oxidoreductases that share a N-terminal FAD-binding domain: the aryl-alcohol oxidase from *Pleurotus eryngii* (AAO, EC 1.1.3.7) and the 5-hydroxymethylfurfural oxidase from *Methylovorus sp.* strain MP688 (HMFO, EC 1.1.3.47) (Carro et al., 2015; Dijkman et al., 2014). The general catalytic cycle of both enzymes comprises dehydrogenative oxidations mediated by two-half reactions, the reductive reaction in which the reducing substrate is 2-electron oxidized by the FAD and the oxidative reaction where H_2O_2 is produced after the reduction of O_2 by the FAD which in turn, returns to its oxidized resting state.

In the FDCA synthetic pathway from HMF, up to three consecutive 2-electron oxidations -6 electrons in total- could take place, generating two furanic intermediates, DFF (2,5-diformylfuran) and FFCA (5-formyl-furancarboxilyc acid), **Figure 1**. While the physiological roles of AAO and HMFO are distant, their reaction mechanisms and substrate tastes, ranging from primary aromatic alcohols to conjugated aliphatic systems, place them -from a functional point of view- as true alcohol oxidases. Accordingly, aldehydes *`sensum stricto´* are not substrates of these flavoenzymes, but only their hydrated *gem*-diols. This is particularly relevant for the FDCA route, in which the poor degree of spontaneous hydration of carbonyl groups (with *gem*-diols formation of 29 and 1.8% for DFF and FFCA, respectively (Dijkman et al., 2014)) diminish or even abolish enzyme reactivity. As such, the rate-limiting step of the whole pathway is found at the oxidation of FFCA, with a scarce *gem*-diol presence and a hypothesized need for re-accommodating the molecule in a proper catalytic distance to the FAD cofactor (Carro et al, 2015). Together, it makes the final oxidation step from FFCA to FDCA inefficient, with barely detectable traces of FDCA in the case of AAO and/or weak final conversion yields, in the case of native HMFO. Although the direct transformation of FFCA into FDCA by the AAO does seem to be possible (Karich et al., 2018), it has yet to be proved the full cascade of oxidative reactions using HMF as the departure substrate. Such bottleneck in the catalytic performance of AAO has been so far bypassed adding fungal peroxygenases in the final conversion of FFCA into FDCA (Carro et al. 2015), while the pioneering work of Fraaije group has disclosed several HMFO variants with improved activity for FFCA (Dijkman et al. 2014, Dijkman et al. 2015, Martin et al., 2018).

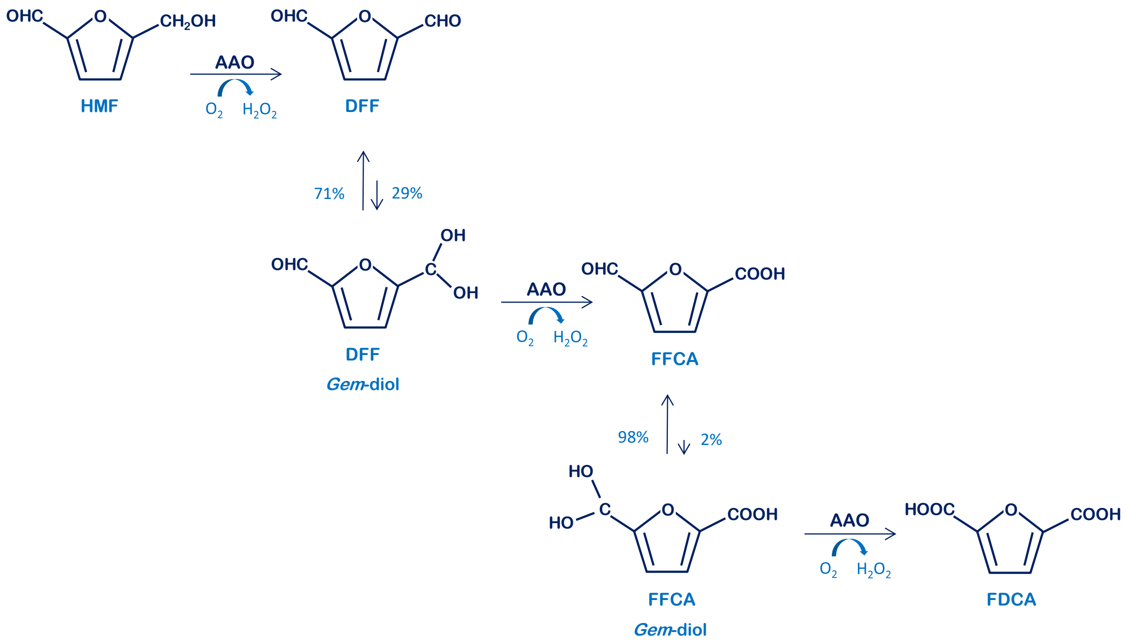

Figure 1. AAO/FDCA route *via* alcohol/*gem*-diol oxidation.

Particularly, HMFO mutations for the enantioselective oxidation of secondary alcohols, also conferred a striking 1000-fold improvement in the catalytic efficiency for FFCA. As both secondary alcohols and *gem*-diols have bulky substituents on the α-carbon compared to natural primary alcohols, the introduction of less constraining amino acids helped to relax the catalytic cavity, increasing the activity for FFCA (Dijkman et al. 2015). Similarly, we recently performed a directed AAO evolution campaign for the selective oxidation of secondary benzyl alcohols (Viña-Gonzalez et al. 2019). Paradoxically, rather than enhancing the active site cleft as happened for HMFO variants, our bulkier mutations allowed the substrate to be placed at a better catalytic distance (Viña-Gonzalez et al., 2019). Given the structural similarities and mechanism of action between AAO and HMFO, it is reasonable to think that mutations responsible for unlocking the oxidation of secondary alcohols in AAO, could be a suitable departing point to enhance FFCA oxidation, as described for HMFO (Dijkman et al., 2015).

Up to date, HMFO was the only GMC oxidase known to perform the three oxidations required to transform HMF into FDCA. In the current study we prove that an evolved AAO can also complete this challenging synthetic route. Through structural alignment between HMFO and AAO, mutant libraries were constructed and screened for the oxidation of HMF and FFCA, the best variant of this process was biochemically characterized and the role of mutations asigned within the FDCA route.

7.2 RESULTS AND DISCUSSION

Laboratory evolution of the AAO for the synthesis of FDCA

Before starting directed evolution, we benchmarked a set of AAO mutants from our previous evolutionary campaigns for heterologous expression and oxidation of secondary alcohols (Viña-Gonzalez et al., 2015, Viña-Gonzalez et al., 2018, Viña-Gonzalez et al., 2019). The final two candidates for the FDCA route were the FX9 and 15G12 variants. FX9 is a highly stable expression mutant that carries mutations H91N-L170M (H91N is a back-to-ancestor/consensus mutation at the si-face of the FAD that stabilizes the cofactor, whereas L170M is placed in a superficial α-helix, far from the active site) (Viña-Gonzalez et al. 2018). The 15G12 mutant harbors the two mutations of FX9 plus I500M-F501W substitutions, placed at the catalytic cavity and involved in unlocking the activity for secondary aromatic alcohols (Viña-Gonzalez et al. 2019) **Figure 2A, B**. It is worthy to note that secretion in yeast for both variants is further promoted by an evolved chimeric prepropeptide (preαfactor-proKiller) that is cleavaged upon exocytosis (Viña-Gonzalez et al. 2015). Yeast´s supernatants of FX9 and 15G12 variants from microtiter fermentations (*i.e.* the high-throughput screening -HTS- format needed for AAO evolution) were assessed in the oxidation of HMF and FFCA by the HRP-ABTS/Amplex red assay (see Methods section for details). While none of the two mutants showed reliable response against FFCA in HTS format, the activity of FX9 with HMF was roughly 33 times higher (0.3 U/L) compared to that of 15G12 (0.009 U/L). Since the bulky substitutions I500M-F501W at the catalytic site of 15G12 dramatically affected the activity against HMF, we considered logical to study those positions in search of positive epistatic effects. As explained in the introduction, our reasoning connects with previous HMFO mutant designs for secondary-alcohol oxidation, which also showed improved activity *vs*. FFCA (Dijkman et al., 2015). Accordingly, we constructed a combinatorial saturation mutagenesis (CSM) library on positions 500 and 501 which was subjected to a dual HTS assay with HMF and FFCA. No active variants against FFCA were found whereas ~95% of the clones of the mutagenic landscapes for HMF were inactive, indicating that positions 500 and 501 are highly sensitive to modifications, **Figure 2C**. Nevertheless, a few clones did show roughly 2 to 3-fold increase activity for HMF compared to the FX9 parental type. Interestingly, all of then harbored the single mutation F501W (named henceforth Bantha mutant), which was already present in 15G12, while reverting to the original Ile500 **Figure. 2D**.

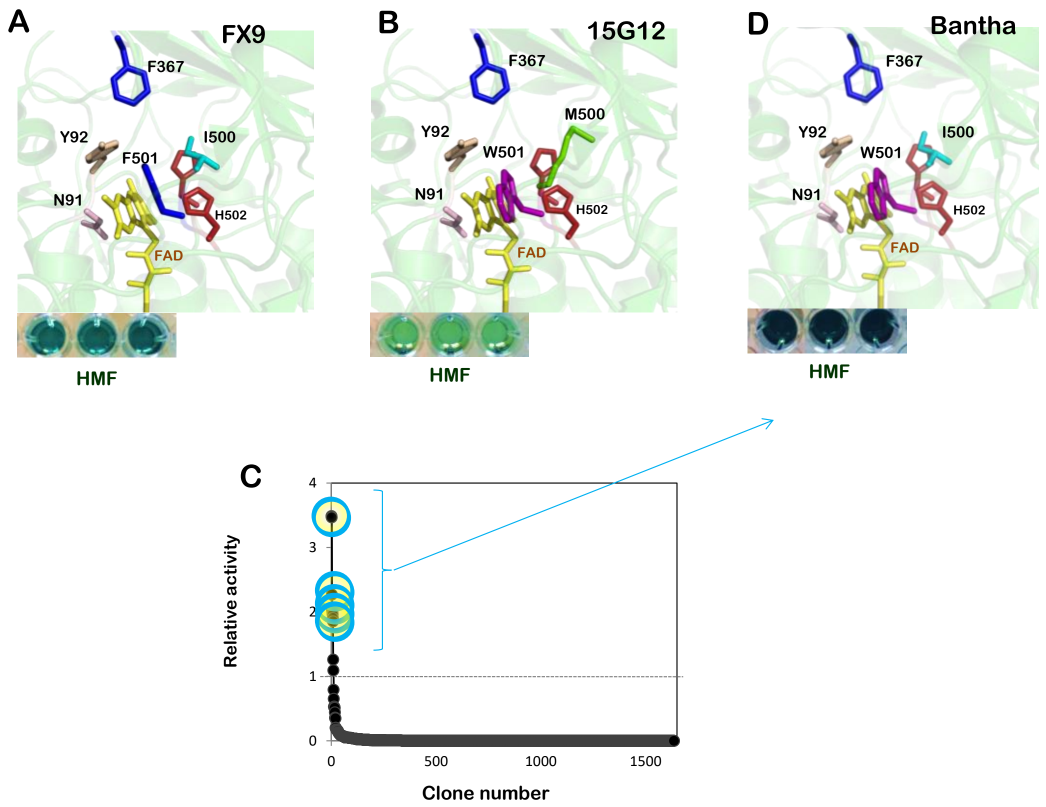

Figure 2. Mutations in AAO evolved variants. After several cycles of evolution for functional expression, FX9 variant (**A**) maintained the same residues as the wildtype AAO (wtAAO) at the re-side of the FAD in the catalytic pocket plus the H91N mutation (in pink). The mutant 15G12 (**B**) acquired the substitutions I500M-F501W for secondary alcohol oxidation and decreased activity for HMF (inset). The Bantha variant (**D**), with substitutions H91N, F501W and M500I reversion, increased activity with HMF (inset). (**C**) Mutational landscape of the combinatorial library. Activity of clones is plotted in descending order. Horizontal line shows the activity of the parental type *vs*. HMF. Insets in A, B, D show the activity response in HTS format for HMF.

The unambiguous relationship between the substrate scopes of AAO and HMFO, along with the similar effect on HMF for mutations involved in secondary alcohol oxidation led us to explore other structural determinants that may be transferred between the catalytic sites of both enzymes. Although the sequence identity between AAO and HMFO is rather low (~30%), the structural alignment of the catalytic sites revealed other potentially relevant substrate-enzyme interaction positions **Figure 3**. Using Bantha variant as template, a new CSM library was constructed targeting positions Tyr92 and His465. The Tyr92 residue is related to the substrate diffusion and positioning on the active site whereas His465 contributes for a proper catalytic location of the alcohol in front of the FAD cofactor. These residues correspond to the Met103 and Asn511 in the HMFO structure, respectively. Unfortunately, no improved variants were identified in this library.

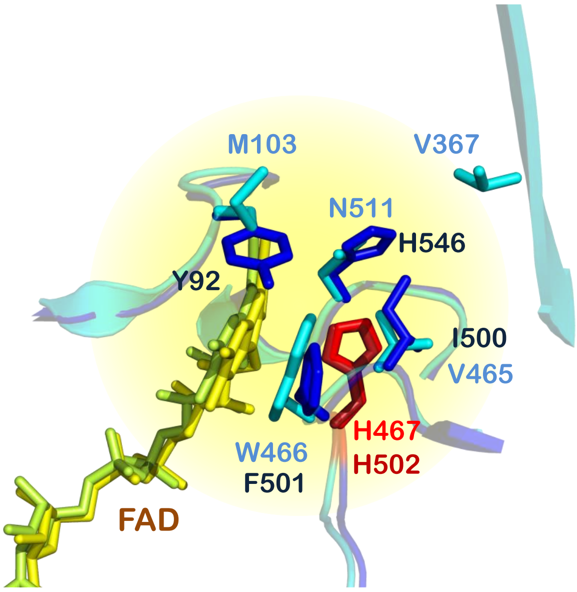

Figure 3.Structural alignment of the catalytic pockets of AAO and HMFO. Residues from the AAO (PDB accession number 3FIM (Fernández et al. 2009)) are depicted in dark blue while residues of the HMFO (PDB accession number 4UDP (Dijkman et al. 2015)) are depicted in light blue.

Accordingly, the Bantha mutant and the parental FX9 were produced, purified to homogeneity and biochemically characterized. Steady kinetic constants were measured with HMF, **Table 1**. The K_m values were hardly affected by the F501W substitution and therefore the increased catalytic efficiency was exclusively depended on a 3-fold enhanced in the k_{cat}. When compared Bantha with wildtype AAO -wtAAO, heterologous expressed in *E. coli* after *in vitro* refolding-, the k_{cat} improved 26-fold whereas the K_m increased ~8-fold with a concomitant 3-fold enhancement in the k_{cat}/K_m. The higher K_m values found in the *S. cerevisiae* variants may be caused by the high glycosylation degree (~50%) of evolved mutants.

Table 1. Kinetic parameters for Bantha and FX9 variants.

	Kinetic constant	Bantha	FX9	wtAAO*
HMF	K_m (mM)	12,4 ± 0,8	13 ± 2	1,6 ± 0,2
	k_{cat} (s^{-1})	9,4 ± 0,5	3,4 ± 0,3	0,36 ± 0,001
	k_{cat}/K_m (mM^{-1} s^{-1})	0,76	0,26	0,23

AAO kinetic constants were measured in 100 mM phosphate buffer pH 6.0 at 25°C. All reactions were performed by triplicate. Values were corrected considering that two H_2O_2 molecules are formed when two successive oxidations convert HMF into FFCA**.** * Calculated for wtAAO as described previously (Carro et al., 2015).

Even though some promiscuous activity for FDCA has been detected with FFCA as substrate (Karich et al. 2018), the oxidation of HMF into FDCA to complete the whole cascade reaction, is yet to be reported for the AAO. The weak equilibrium between the aldehyde group of FFCA and its scarce *gem*-diol, along with the need of re-positioning the furanic ring of FFCA in the active pocket for the third oxidation step are supposed to be the reasons behind this lack of activity (Carro et al., 2015). We analyzed by HPLC the possible production of FDCA from FFCA in a 20 h reaction, observing a conspicuous 7-fold improved conversion of Bantha *vs*. wtAAO (and in a lesser extent for FX9 -roughly half of the Bantha´s activity-)**.** Then, we measured the production of FDCA from HMF achieving a ~6-fold improved conversion together with low but noticeable yields of 3 % for the Bantha mutant. Although the minor traces of conversion of FDCA from HMF in wtAAO (0.5%) were previously assigned to the oxidative power of H_2O_2 released from consecutive oxidations from HMF through FFCA (Carro et al., 2015), we cannot rule out that it actually comes from the latent activity of wtAAO for FFCA that has been now widened by directed evolution.

Table 2. Production of FDCA by wtAAO and Bantha mutant.

Substrate	[Mm]	Enzyme	[µM]	Time (h)	Conv. (%)	FDCA yield (%)
HMF	2	Bantha	3.3	48	100	3
HMF	2	wtAAO	3.3	48	100	0.5
FFCA	2.5	Bantha	3.3	20	7	7
FFCA	2.5	wtAAO	3.3	20	1	1

Reactions were performed at room temperature in phosphate buffer 100 mM pH 8.0 and analyzed by HPLC-PDA.

It is worth noting that in our study no reaction optimization was performed (*e.g* by FAD and/or catalase supply to bypass possible enzyme inactivation, increasing substrate and/or enzyme load, testing different reaction pH or temperatures); however, our results unequivocally show that evolved AAO (without any reaction engineering optimization) converts HMF into FDCA via three sequential oxidation steps, using the different reaction intermediates (including FFCA) as new substrates to complete the whole route. Both F501W and H91N mutations of Bantha mutant concords with the same residues in native HMFO (Trp466 and Asn102 according to HMFO numbering), addressing a strong structure-function relationship between both enzymes. While the ancestor-consensus mutation H91N widens the promiscuous activity for FFCA, the substitution F501W enhanced the activity HMF, **Figure 4**.

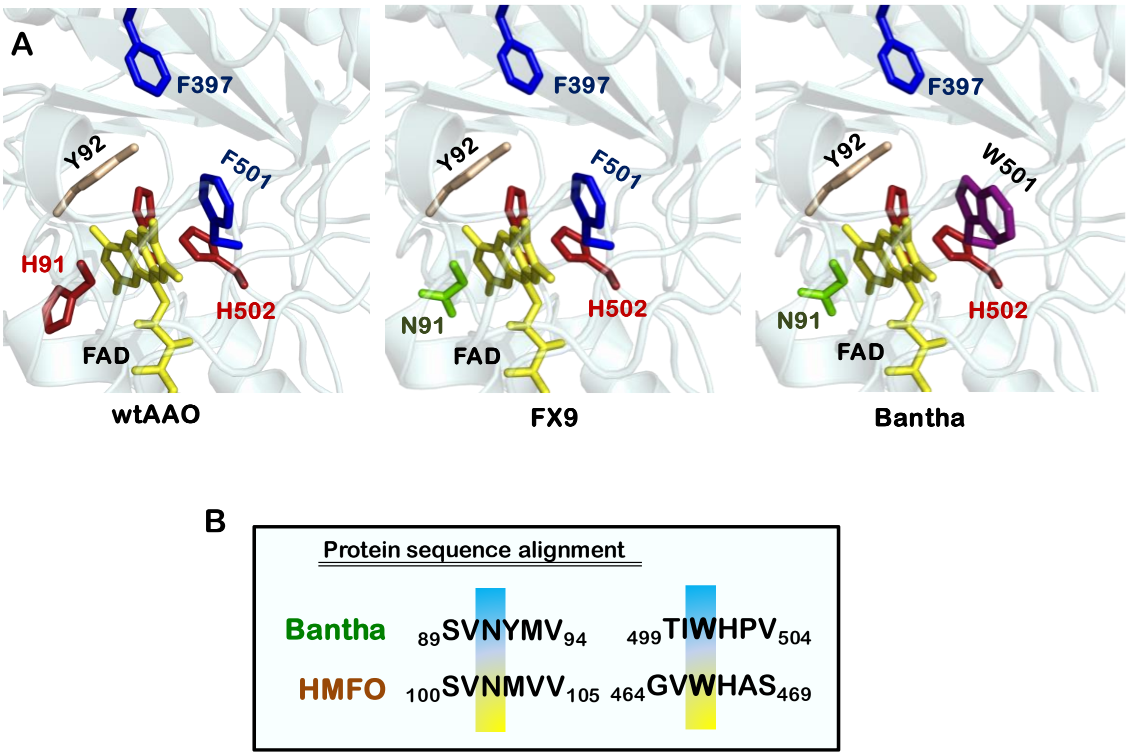
A
F397
Y92
F501
H91
H502
FAD
wtAAO
F397
Y92
F501
N91
H502
FAD
FX9
F397
Y92
W501
N91
H502
FAD
Bantha
B
Protein sequence alignment
Bantha
89SVNYMV94
499TIWHPV504
HMFO
100SVNMVV105
464GVWHAS469

Figure 4. (A) Structural details of wtAAO, FX9 and Bantha mutants. (B) Sequence alignment of the Bantha variant with the HMFO highlighting the acquired mutations in the AAO corresponding to native residues on the HMFO.

7.3 CONCLUSIONS

Significant efforts are being carried out to fully develop the biotechnological potential of the GMC oxidases. In the case of the AAO and the HMFO, the production of FDCA is hampered by the chemoselectivity of the alcohol/aldehyde oxidation rates. In the present study, the oxidation of FFCA into FDCA by AAO was targeted by laboratory evolution. As a result, the AAO variant Bantha, introducing a Trp next to the catalytic base, and carrying the H91N consensus-ancestor mutation increased the overall activity on the furfural derivatives for the whole conversion of HMF into FDCA showing, for the first time, the ability of this flavoenzyme to perform the entire cascade of three consecutive oxidations. Therefore, this study widens the repertoire of potential biocatalysts for the HMF cascade reaction into FDCA.

7.4 MATERIAL AND METHODS

Materials

All chemical were reagent-grade purity. 5-Hydroxymethylfurfural was obtained from AVABIOCHEM (Zug, Switzerland), 5-formyl-furancarboxilyc acid and furan-2,5-dicarboxylic acid were obtained from TCI chemicals (Zwijndrecht, Belgium). ABTS (2,2'-azino-bis(3-ethylbenzothiazoline-6-sulphonic acid)), Horseradish peroxidase (HRP), the Yeast Transformation Kit was purchased from Sigma (Madrid, Spain). Amplex® Red reagent (10-acetyl-3,7-dihydroxyphenoxazine) was obtained from Biogen (Madrid, Spain). Zymoprep Yeast Plasmid Miniprep, Yeast Plasmid Miniprep Kit I and Zymoclean Gel DNA Recovery Kit were from Zymo Research (Orange, CA). Restriction enzymes *Bam*HI, *Xho*I, were from New England Biolabs (Hertfordshire, UK). I-Proof high fidelity DNA polymerase was from Biorad (Hercules, CA, USA). The episomal shuttle vector pJRoC30 was from the California Institute of Technology (CALTECH, USA). *E. coli* XL2-Blue competent cells were from Stratagene (La Jolla, CA, USA). The protease deficient S. *cerevisiae* strain BJ5465 was from LGC Promochem (Barcelona, Spain). Primers were acquired from Isogen Life Science (Barcelona, Spain) and are included in Table S1.

Culture media for *Saccharomyces cerevisiae*

Minimal medium contained 0.67% (w:v) yeast nitrogen base, 1.92 g/L yeast synthetic drop-out medium supplement without uracil, 2% (w:v) raffinose and 25 µg/mL chloramphenicol. SC drop-out plates contained 0.67% (w:v) yeast nitrogen base, 1.92 g/L yeast synthetic drop-out medium supplement without uracil, 2% (w:v) bacto agar, 2% (w:v) D-glucose and 25 µg/mL chloramphenicol. YP medium contained 10 g yeast extract, 20 g peptone and double-distilled H_2O (ddH_2O) to 650 mL. AAO expression medium contained 144 mL YP 1.55x, 13.4 mL 1M KH_2PO_4 pH 6.0 buffer, 22.2 mL 20% galactose (w:v), 0.222 mL 25 µg/mL chloramphenicol and ddH_2O to 200 mL. AAO selective expression medium (SEM) contained 100 mL 6.7% (w:v) sterile yeast nitrogen base, 100 mL 19.2 g/L sterile yeast synthetic drop-out medium supplement without uracil, 100 mL sterile 20% galactose (w:v), 100 mL 1 M KH2PO4 pH 6.0, 600 mL sddH2O and 1 mL 25 g/L chloramphenicol.

Culture media for *Escherichia coli*

Luria Broth (LB) medium contained 10 g sodium chloride, 5 g yeast extract, 10 g peptone, 1 mL 100 mg/mL ampicillin and ddH_2O to 1 L.

Laboratory evolution of AAO

First generation: Combinatorial saturation mutagenesis at positions Ile500 and Phe501: The FX9 variant (261 bp) was used as DNA template for saturation mutagenesis technique at position 500 and 501 at the active site of the AAO. Two PCR reactions were carried out in a final volume of 50 µL containing 3% DMSO, 0.8 mM dNTPs (0.2 mM each), 0.03 U/µL iproof DNA polimerase, and 0.2 ng/µL FX9 template and different primers according to the 22-trick protocol (Kille et al. 2012). PCR1 contained 0.25 µM RMLN and 0.25 µM mix of reverse primers: 22c1R, 22c2R, 22c3R, 22c4R, 22c5R, 22c6R, 22c7R, 22c8R and 22c9R. PCR2 contained 0.25 µM RMLC and 0.25 µM mix of forward primers: 22c1F, 22c2F, 22c3F, 22c4F, 22c5F, 22c6F, 22c7F, 22c8F and 22c9F. Amplification reactions were carried out in a thermal cycler MycyclerTM (BIO-RAD, USA) with the following PCR program: 98°C for 30 seconds (1 cycle); 98°C for 10 seconds, 50°C for 25 seconds and 72°C for 60 seconds (28 cycles); and 72°C for ten minutes (1 cycle). After purification, PCR products (400 ng each) were mixed with the linearized pJRoC30 (100 ng; ratio PCR product: vector = 4:1) and transformed in yeast for in vivo cloning. According to the 22-trick protocol, a library of 1700 individual colonies was screened as described below.

Second generation: Combinatorial saturation mutagenesis at positions Tyr92 and His546: Three PCR reactions were carried out in a final volume of 50 µL containing 3% DMSO, 0.8 mM dNTPs (0.2 mM each), 0.03 U/µL iproof DNA polimerase, and 0.2 ng/µL Bantha template and different primers according to the 22-trick protocol. PCR1 contained 0.25 µM RMLN and 0.25 µM mix of reverse primers: 92RAHN, 92RCDB and 92RCCA. PCR2 contained 0.25 µM mix of forward primers 92FNDT, 92FVHG and 92FTGG 0.25 µM mix of reverse primers: 546RAHN, 546RCDB and 546RCCA. PCR2 contained 0.25 µM mix of forward primers 546FNDT, 546FVHG and 546FTGG and reverse primer RMLC. Amplification reactions were carried out in a thermal cycler MycyclerTM (BIO-RAD, USA) with the following PCR program: 98°C for 30 seconds (1 cycle); 98°C for 10 seconds, 50°C for 25 seconds and 72°C for 60 seconds (28 cycles); and 72°C for ten minutes (1 cycle). After purification, PCR products (400 ng each) were mixed with the linearized pJRoC30 (100 ng; ratio PCR product: vector = 4:1) and transformed in yeast for in vivo cloning. According to the 22-trick protocol, a library of more than 1700 individual colonies was screened as described below.

High-throughput screening (HTS) assay: Transformed cells were plated in SC drop-out plates and incubated for 3 days at 30°C, individual clones were fermented in sterile 96-well plates containing 200 µL of SEM medium. Plates were sealed and incubated at 30°C, 225 rpm and 80% relative humidity in a humidity shaker (Minitron-INFORS, Biogen, Spain) for 72 hours. Aliquots of 20 µL of yeast supernatants were transferred to a 96-well plate using a robotic station for liquid handling Freedom EVO (Tecan, Männedorf, Switzerland) and 180 µL of HRP-ABTS reagent for 5-hydroxymetylfurfural activity detection or 180 µL of HRP-Amplex red reagent for 5-formyl-furancarboxilyc acid activity detection. The final concentrations for the HRP-ABTS mixture in the well were 5 mM 5-hydroxymethylfurfural, 2.5 mM ABTS, 3 µg/mL HRP in 100 mM phosphate buffer pH 6.0. The final concentrations for the HRP-Amplex red mix in the well were 5 mM 5-formyl-furancarboxilyc acid, 70 µM Amplex Red, 3 µg/mL HRP in 100 mM phosphate buffer pH 6.0. Reagents were dispensed with Multidrop™ Combi Reagent Dispenser (Thermo Scientific, Massachusetts, USA). The plates were incubated at room temperature and activity with the furfural derivative was determined as H_2O_2 production coupled to the oxidation of reagent by the HRP and measured at 418 ($\varepsilon_{ABTS\bullet}$ 418 = 36000 M^{-1} cm^{-1}) for ABTS or at 563nm ($\varepsilon_{resorufin}$ 563 = 56000 M^{-1} cm^{-1}) for Amplex Red. One unit of AAO activity is defined as the amount of enzyme that converts 1 µmol of substrate with the stoichiometric formation of H_2O_2 per min under the reaction conditions. The HTS-assay incorporated two consecutive re-screenings to rule out the selection of false positives as described in previous work (Viña-Gonzalez et al. 2015).

Protein production and purification of AAO

The FX9 and Bantha variants expressed in *S. cerevisiae* were produced and purified to homogeneity as described in a former work (Viña-Gonzalez et al., 2015). The native AAO, heterologously expressed in *E. coli* and in vitro refolded (wtAAO), was produced and purified as described elsewhere, (Ruiz-Dueñas et al. 2006).

Biochemical characterization of AAO

Steady-state kinetic constants: 5-hydroxymethylfurfural oxidation kinetics were measured in 100 mM phosphate buffer pH 6.0. The oxidation 5-hydroxymethylfurfural was follow indirectly coupled with saturated conditions of HRP and Amplex Red substrate (4.5 U/mL HRP and 75 µg/mL Amplex Red final concentrations) following activity at 563nm (ε_{563} = 56000 M^{-1} cm^{-1}).

HPLC analysis: FDCA production for the different AAOs was analysed by HPLC with equipment consisting of a tertiary pump (Varian/Agilent Technologies, CA, USA) coupled to an autosampler (Merck Millipore, MA, USA) and a Ultrabase C8 column from Análisis Vínicos (Ciudad Real, Spain) . For the mobile phase 12 mM phosphate buffer pH 7 (A) and acetonitrile (B) at a flow rate of 1.2 min^{-1} were used and detection was done at 268 nm. After 1 min with 100% A, B was increased for 3.5 min to 5% and then to 40% in 2.5 min. After maintaining 40% B for 0.5 min, A was returned to 100% in 0.5 min and maintained for 2 min. FFCA and FDCA had a retention time of 2.1 and 1 min respectively. Calibration curve was prepared with 0.05, 0.1, 0.2 and 0.4 mM of FDCA.

Protein modeling: A structural model of the AAO from P. eryngii crystal structure at a resolution of 2.55 Å (Protein Data Bank Europe [PDB] accession number 3FIM (Fernández et al. 2009), was used as scaffold for the wild type AAO model and the homology models for different mutants were made from 3FIM by PyMol (Schrodinger LLC.; http://www.pymol.org).

DNA sequencing: All genes were verified by DNA sequencing (BigDye Terminator v3.1 Cycle Sequencing Kit) using the following primers: primers sense, RMLN and AAOsec1F and primers antisense RMLC and AAOsec2R.

ACKNOWLEDGEMENTS

This research was supported by the EU project H2020-BBI-PPP-2015-2-720297-ENZOX2, by the Spanish Government projects BIO2016-79106-R-Lignolution, and by the Comunidad de Madrid project Y2018/BIO4738-EVOCHIMERA.

7.5 SUPPLEMENTARY MATERIAL

Supplementary Table 1. List of primers

Oligo	**Sequence**
RMLN	5’-CCTCTATACTTTAACGTCAAGG-3’
RMLC	5’-GGGAGGGCGTGAATGTAAGC-3’
22c1F	5’-GAGACAACGCCAACACG*NDTNDT*CACCCAGTTGGAAC-3’
22c1R	5’-GTTCCAACTGGGTG*AHNAHN*CGTGTTGGCGTTGTCTC-3’
22c2F	5’-GAGACAACGCCAACACG*NDTVHG*CACCCAGTTGGAAC-3’
22c2R	5’-GTTCCAACTGGGTG*CDBAHN*CGTGTTGGCGTTGTCTC-3’
22c3F	5’-GAGACAACGCCAACACG*NDTTGG*CACCCAGTTGGAAC-3’
22c3R	5’-GTTCCAACTGGGTG*CCAAHN*CGTGTTGGCGTTGTCTC-3’
22c4F	5’-GAGACAACGCCAACACG*VHGNDT*CACCCAGTTGGAAC-3’
22c4R	5’-GTTCCAACTGGGTG*AHNCDB*CGTGTTGGCGTTGTCTC-3’
22c5F	5’-GAGACAACGCCAACACG*VHGVHG*CACCCAGTTGGAAC-3’
22c5R	5’-GTTCCAACTGGGTG*CDBCDBC*GTGTTGGCGTTGTCTC-3’
22c6F	5’-GAGACAACGCCAACACG*VHGTGG*CACCCAGTTGGAAC-3’
22c6R	5’-GTTCCAACTGGGTG*CCACDB*CGTGTTGGCGTTGTCTC-3’
22c7F	5’-GAGACAACGCCAACACG*TGGNDT*CACCCAGTTGGAAC-3’
22c7R	5’-GTTCCAACTGGGTG*AHNCCA*CGTGTTGGCGTTGTCTC-3’
22c8F	5’-GAGACAACGCCAACACG*TGGVHG*CACCCAGTTGGAAC-3’
22c8R	5’-GTTCCAACTGGGTG*CDBCCA*CGTGTTGGCGTTGTCTC-3’
22c9F	5’-GAGACAACGCCAACACG*TGGTGG*CACCCAGTTGGAAC-3’
22c9R	5’-GTTCCAACTGGGTG*CCACCA*CGTGTTGGCGTTGTCTC-3’
92FNDT	5’-GGTCTAGCTCTGTTAAC*NDT*ATGGTCATGATGCGTG-3’
92FVHG	5’-GGTCTAGCTCTGTTAAC*VHG*ATGGTCATGATGCGTG-3’
92FTGG	5’-GGTCTAGCTCTGTTAAC*TGG*ATGGTCATGATGCGTG-3’
92RAHN	5’-CACGCATCATGACCAT*AHN*GTTAACAGAGCTAGACC-3’
92RCDB	5’-CACGCATCATGACCAT*CDB*GTTAACAGAGCTAGACC-3’
92RCCA	5’-CACGCATCATGACCAT*CCA*GTTAACAGAGCTAGACC-3’
546FNDT	5’-CCTTCGCGCCCAACGCA*NDT*ACCCAAGGACCGATATA-3’

546FVHG	5’-CCTTCGCGCCCAACGCA*VHG*ACCCAAGGACCGATATA-3’
546FTGG	5’-CCTTCGCGCCCAACGCA*TGG*ACCCAAGGACCGATATA-3’
546RAHN	5’-TATATCGGTCCTTGGGT*AHN*TGCGTTGGGCGCGAAGG-3’
546RCDB	5’-TATATCGGTCCTTGGGT*CDB*TGCGTTGGGCGCGAAGG-3’
546RCCA	5’-TATATCGGTCCTTGGGT*CCA*TGCGTTGGGCGCGAAGG-3’
AAOsec1F	5’-GTGGATCAACAGAAGATTTCGATCG-3’
AAOsec2R	5’-GTGGTTAGCAATGAGCGCGG-3’

Codon substitutions are shown in italics (where N = A/T/C/G; D = no C; V =no T, H = no G; B = no A; R = A/G; Y = C,T).

CHAPTER

VII

Chapter VIII:

GLOBAL DISCUSSION

CHAPTER
VIII

8.1 Directed evolution platform for AAO

In the past couple of decades, we have witnessed the multiple efforts taken to elucidate the structural and mechanistic aspects of the AAO. Even though rational approaches were applied in the first attempts to modulate the enzyme's activity, it has to be a powerful methodology like directed evolution the force needed to drive the AAO performance to biotechnological settings. Certainly, the proper engineering of the enzyme implicates the set-up of an evolutionary platform governed by suitable expression host together with the development of screening activity assays to sort out the mutant variants in a high-throughput format. As detailed in **Chapter III**, the starting point of the present Doctoral studies was the functional expression (secretion) of the AAO in *S. cerevisiae* and the design of a HTS-assay for the detection of AAO activities in yeast supernatants.

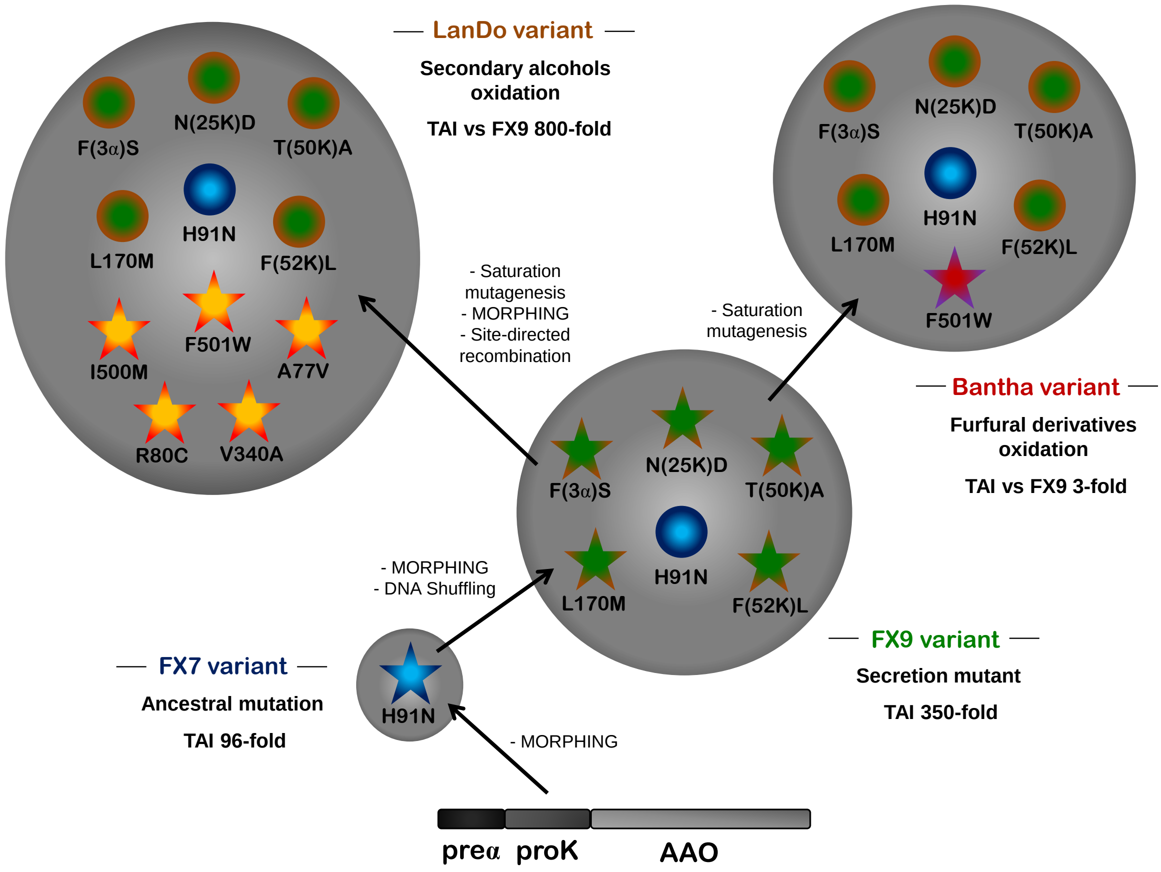
LanDo variant
Secondary alcohols oxidation
TAI vs FX9 800-fold
F(3α)S
N(25K)D
T(50K)A
H91N
L170M
F(52K)L
F501W
I500M
A77V
R80C
V340A
- Saturation mutagenesis
- MORPHING
- Site-directed recombination
- Saturation mutagenesis
F(3α)S
N(25K)D
T(50K)A
H91N
L170M
F(52K)L
F501W
Bantha variant
Furfural derivatives oxidation
TAI vs FX9 3-fold
F(3α)S
N(25K)D
T(50K)A
H91N
L170M
F(52K)L
- MORPHING
- DNA Shuffling
FX9 variant
Secretion mutant
TAI 350-fold
FX7 variant
Ancestral mutation
TAI 96-fold
H91N
- MORPHING
preα
proK
AAO

Figure 8.1. Different evolutive routes followed during the engineering of the AAO in the present Doctoral Thesis. Stars indicate new acquired mutations while circles depict accumulated substitutions. TAI (Total Activity Improvements) were calculated with *p*-methoxybenzyl alcohol in the evolution for secretion, with 1-(*p*-methoxyphenyl)-ethanol in the evolution for secondary alcohol oxidation and with 5-HMF in the evolution for the synthesis of FDCA.

8.1.1 Functional expression in *Saccharomyces cerevisiae*

In order to set up a reliable directed evolution platform within the context of a high-throughput experiment, it is essential for enzymes to be functionally expressed in a proper host organism. In the case of fungal enzymes like the AAO, the budding yeast *S. cerevisiae* is the go-to organism for directed evolution campaigns. This ascomycete can express foreign eukaryotic proteins performing correct folding and post-translational modifications that include glycosylation, disulfide bond formation, N- and C-terminal processing. Additionally, episomal vectors are available for this yeast, with high-transformation efficiencies, and there is a substantial tool-box for its genetic manipulation (Pourmir and Johannes 2012; Gonzalez-Perez et al. 2012). However, missing chaperones, prosthetic groups, some post-translational modifications and a not-fully understood secretory pathway are some of the few possible constraints when trying to reach appropriate heterologous expression levels (Delic et al. 2013). Also, yeast growth is strongly limited by oxygen availability, and considering that library construction is typically performed in microtiter plates, the expression may also be limited in such conditions. The most straightforward strategy to overcome these shortcomings is the directed evolution of the signal sequences, such that the transit and processing of the exogenous polypeptide adapt to the subtleties of the secretory pathway. To achieve functional expression, the native signal sequence can be replaced by common yeast prepro-leaders, such as those from the mating α-factor, the invertase, the acid phosphatase and the killer K1 toxin (Bitter et al. 1984; Chang et al. 1986; Cartwright et al. 1992; Hashimoto et al. 1998) or even by synthetic preproleaders designed by sequence-based semi rational approaches (Kjeldsen et al. 1997). In addition to the evolution of signal peptides, the accumulation of secretion mutations in the mature protein could also be a profitable strategy to circumvent folding and post-translational related hurdles. Secretion mutations foster solubility, stability and also, the kinetics and thermodynamics of intermediate protein states (Roodveldt et al. 2005).

8.1.2 Chimeric fusion genes for yeast expression

Widely used in biotechnology, *S. cerevisiae* is the optimal host organism to express fungal enzymes for *in vitro* evolution experiments. For years our laboratory has successfully used the prepro-leader sequence of the mating α-factor of *S. cerevisiae* to lead the secretion in yeast of ligninases. An alternative to secret foreign protein can be offered by the prepro-leader sequence of the K1 toxin, much less explored but proven useful to express ß-lactamase (Cartwright et al. 1992; Zhu et al. 1993). This peptide is formed by the prepro(δ) sequence (with similar processing as the prepro-leader of the α-factor) fused to a truncated version of the γ-segment with 3 glycosylation sites. As such, to expand the repertory of signal sequences, we fused the AAO gene to the α-factor prepro-leader (α-AAO), the K1 toxin prepro-leader (K-AAO) and shuffled variants presenting the preα sequence and the K1 γ-segment (preαproK-AAO) and the prepro(δ) sequence with the proα sequence (preKproα-AAO). For these constructs, prepro(δ) fragment was tailored by site-directed mutagenesis modifying the residues Pro43-Arg44 to a more efficient KR recognition site for protease KEX2 (Brenner and Fuller, 1992). The four fusion genes reported detectable levels of AAO activity in the presence of aromatic substrate veratryl alcohol. In flask supernatants, the secretion levels hierarchy between the corresponding constructs was as follows: α-AAO, (1.5 U/L); preαproK-AAO (0.5 U/L); preKproα-AAO (0.35 U/L) and K-AAO (0.06 U/L). With all the fusions successfully processed and exported by *S. cerevisiae*, the engineering of these chimeric leaders opens novel strategies to secrete foreign proteins so that they could be tested with other eukaryotic genes (*e.g.* recent studies in our laboratory with fungal peroxygenases expand the use of such fusion peptides, unpublished material).

8.1.3 Dual high-throughput screening for AAO activity

The detection of new enzyme variants is a pivotal step to set about in the plan of action for any evolutionary process. As previously commented, a good host organism for *in vitro* evolution must be easily adapted to a high-throughput screening format (HTS). While dozens of HTS assays have been developed for such purposes, establishing reliable protocols in terms of sensitivity, reproducibility, coefficients of variation, linearity is not an easy task. Accordingly, robust HTS assays must be available to select ligninolytic enzyme mutants with improved secretion, activity, stability, redox potential, shifted pH profile and much more. (García-Ruiz et al. 2010; Gonzalez-Perez et al. 2014; Mate et al. 2017). Inherent to the exploration of mutant libraries for the desired enzymatic traits, adequate secretion must first be achieved to obtain a steady signal before improving other relevant biochemical attributes. As already discussed, this is the first bottleneck that researchers must overcome when starting a directed evolution project with a new ligninase. As such, in most cases the HTS protocol employed must detect variants with Total

Activity Improvements (TAI: the product of specific activity and secretion) in the first few rounds of evolution (Alcalde 2015; Mate et al. 2017).

AAO activity implicates a H_2O_2 concentration increase in the yeast supernatants. To quantify minor changes of peroxide, FOX assay is a sensitive and accurate chemical method based on the Fenton reaction. After being oxidized by H_2O_2, Fe^{3+} reacts with xylenol orange forming a blue-purple complex. The Fe^{2+} oxidation step can be propagated with the addition of sorbitol enhancing the Fe^{3+} concentration and therefore, the sensitivity of the assay. When tested against *S. cerevisiae* supernatants, FOX signal was linear and stable without noticeable interferences and with a sensitivity limit of ~0.4 µM in the presence of sorbitol. Additionally, a dual HTS-assay was set up by adding the indirect method of coupling the H_2O_2 production with the activity of horseradish peroxidase (HRP) oxidizing colorimetric reporter ABTS. Being based on the H_2O_2 release by the AAO, the dual HTS-assay can be applied to explore libraries regardless of the substrate oxidized. Hence, this platform opens many paths for the evolution of the enzyme, like the oxidation of secondary alcohols or furfural derivatives.

8.1.4 Finding ancestral mutation H91N by directed evolution

The construct preαproK-AAO was selected as the departure point for the evolutionary journey of the AAO. With this parental type, it is avoided a possible inefficient processing by rather scarce STE13 protease (proK segment only depends on KEX2 activity). Even though detectable levels of the enzyme were observed with the initial constructs, the enhancement of activity and secretion levels was the demanded first step in the directed evolution of the AAO. For that purpose, a whole gene error-prone PCR (*ep*PCR) was explored together with focused mutagenesis by MORPHING (González-Perez et al. 2014). This structural-based tool allows directing the mutational load to specific areas of the protein while maintaining the remaining residues unchanged. To be afterwards assembled by the homologous DNA recombination machinery of *S. cerevisiae*, two mutagenic regions were selected based on structural determinants: (i) M-I segment (Met[α1]-Val109) including the preproleader and residues from the access channel and catalytic site and (ii) M-II segment (Phe392-Gln566) comprising the catalytic pocket. More than 5000 clones were tested being part of the *ep*PCR library and the single and combined MORPHING libraries. While several variants presented up to 5-fold improvements in total activity compared with preαproK-AAO, the FX7 variant showed a striking 96-fold enhancement in activity thanks to the consensus/ancestral substitution H91N. This mutation is placed in contact with the *si*-side of the FAD cofactor at the catalytic pocket. The most conserved residues from a group of homologous proteins can be singled out with multiple sequence alignments (MSA) of their amino acid distribution. Then, the introduction of consensus residues can assist the stabilization of enzymes and increase secretion levels without affecting catalytic performance (Porebski and Buckle, 2016). Moreover, ancestral enzymes can be reconstructed based on phylogenetic inference. Resurrecting such ancient enzymes in the laboratory can provide protein engineering with robust and promiscuous scaffolds, and giving the results obtaining in this current study, the extant AAO is a promising blueprint for future `resurrection´experiments (Ayuso-Fernández et al. 2017; Gomez-Fernandez et al. 2018). With secretion levels of 2 mg/L, the FX7 variant was correctly processed and presented a similar kinetic performance as the native $_{EC}$AAO (expressed and refolded in *E. coli*). FX7 was expressed with heavy glycosylation (~50%), a characteristic with possible stabilization effects. Certainly, not only the mutant presented broad pH stability but also a T_{50} value (temperature at which 50% of the initial activity is retained after 10 min incubation) 11°C higher than the $_{EC}$AAO. In conclusion, the FX7 variant made an optimal template for the following cycles of evolution.

8.2 Tandem-yeast expression system for AAO

As detailed in **Chapter V**, in the specific case of ligninolytic enzymes, which must be engineered and over-produced for industrial uses, it has recently been proposed a tandem yeast expression system where the enzyme could be modified at the *scientist taste* by directed evolution in *S. cerevisiae* and subsequently produced in higher titers in methylotrophic yeast *Pichia pastoris (Komagataella phaffii)* (Molina-Espeja et al. 2015). Wide known and well developed as an industrial host organism, *P. pastoris* is capable of using rather inexpensive reduced one-carbon methanol as carbon source and has a preference for respiratory growth achieving much higher cell densities than *S. cerevisiae* in fed-batch bioreactor. Multiple copies of genes, under a strong promoter derived from the alcohol oxidase 1 gene (AOX1), can be integrated in the yeast genome creating stable strains for protein production. Being easy to manipulate and culture, low secretion rates of endogenous proteins facilitate downstream processing for enzymatic preparations (Daly and Hearn 2005; Molina-Espeja et al. 2015).

8.2.1 Enhanced secretion by DNA shuffling and MORPHING at the signal peptide

The evolutive strategy to further increase secretion started with the selection of the best variants from the previous cycle, six mutants presenting improvements from 2 to 96-fold. Since most of the correspondent substitutions, T[50K]A, S88T, H91N, L170M, D341N and R481S, are placed at >20 residues of distance, there was a promising scenario for an *in vivo* DNA Shuffling library (Kevin et al. 1997). Variant FX8 was the result of, at least, two recombination events between variant 12G12, with mutation T50A at the proK segment; variant 10G5 with mutation L170M at the surface of the protein; and variant FX7 that harbors the ancestral H91N. When compared with the latter, the FX8 showed 2.5-fold improvements in total activity. To further improve secretion levels, the next strategy was to construct a `*smart*´ library directing the mutational load to the signal peptide by MORPHING. FX9 mutant acquired F[3α]S substitution in the preα segment in addition to N[25K]D and F[52K]L in the proK segment. These mutations together with T[50K]A, L170M and H91N increased secretion levels up to 4.5 mg/L with a total 350-fold improvements compared to preαproK-AAO. The FX9 variant was chosen to explore the secretion possibilities of the AAO in *P. pastoris*.

8.2.2 Functional expression in *Pichia pastoris*

Within the goal of expressing the AAO in *P. pastoris*, it was of special interest to determine the potential correspondence on the *Pichia* system of the secretion improvements observed in *S. cerevisiae*. For that purpose, the FX7 and FX9 variants were cloned in *P. pastoris* and the selected transformants, $_{\pi}$FX7 and $_{\pi}$FX9, were expressed in 100 mL shaken flasks. When compared with the enhancements in total activity calculated for the variants expressed in *S. cerevisiae*, $_{sac}$FX7 and $_{sac}$FX9, the value happened to even increase from 3.6 to 4.5-fold. In this way, it was shown that the effects of the beneficial mutations were in tight correlation between both yeasts systems. Moreover, to test the capability of the *Pichia* system to express the AAO, the $_{\pi}$FX9 variant was produced in a 5L fed-batch fermenter in collaboration with Prof. Francisco Valero from the Autonomous University of Barcelona. With around 260 g/L of wet biomass, the secretion levels reached up to 25.5 g/L of AAO, that is 6-fold times the secretion observed in flask. Considering these results as the first step for the industrial production of the AAO, several strategies can be followed to further increment secretion levels (i) the use of different strong promoters (*e.g.* PCAT1); (ii) the use of MutS (Methanol utilization slow) or glyco-engineered *P. pastoris* strains; (iii) integrating a higher number of gene copies with different selection markers (Ahmad et al. 2014). During the present doctoral studies such research started on a stay at Graz University (Austria) under the supervision of Prof. Anton Glieder (unpublished material).

8.2.3 The glycosylation effect on the AAO

To further elucidate the effects of glycosylation, the $_{sac}$FX9 was biochemically characterized together with $_{\pi}$FX9 and with $_{\Delta}$FX9, the FX9 expressed in glycosylation-deficient *S. cerevisiae* strain *Δkre2*. As expected, $_{sac}$FX9 was hyperglycosylated (~60%) while lower and very weak glycosylation were present in $_{\Delta}$FX9 and $_{\pi}$FX9 respectively. $_{sac}$FX9 presented similar kinetic values as the parental $_{sac}$FX7, hence all the collected mutations improved only secretion levels not affecting overall activity. There was a clear effect on the catalytic performance for the different glycoforms, the $_{\Delta}$FX9 and $_{\pi}$FX9 presented higher k_{cat} values, around 2-fold, irrespective of the substrate tested while maintain a similar K_m. It was yet to be established to which extent glycosylation was responsible for the 15°C difference on the kinetic thermostability (T_{50} value) of $_{sac}$FX9 when compared with the native enzyme expressed in *E.coli* after *in vitro* folding. The T_{50} of $_{sac}$FX9 (63°C) was only around 2°C higher than the values estimated for $_{\Delta}$FX9 and $_{\pi}$FX9, that is, the AAO was mostly stabilized by natural folding and the ancestral mutation H91N, addressing the poor stability of the *in vitro* refolded AAO counterpart.

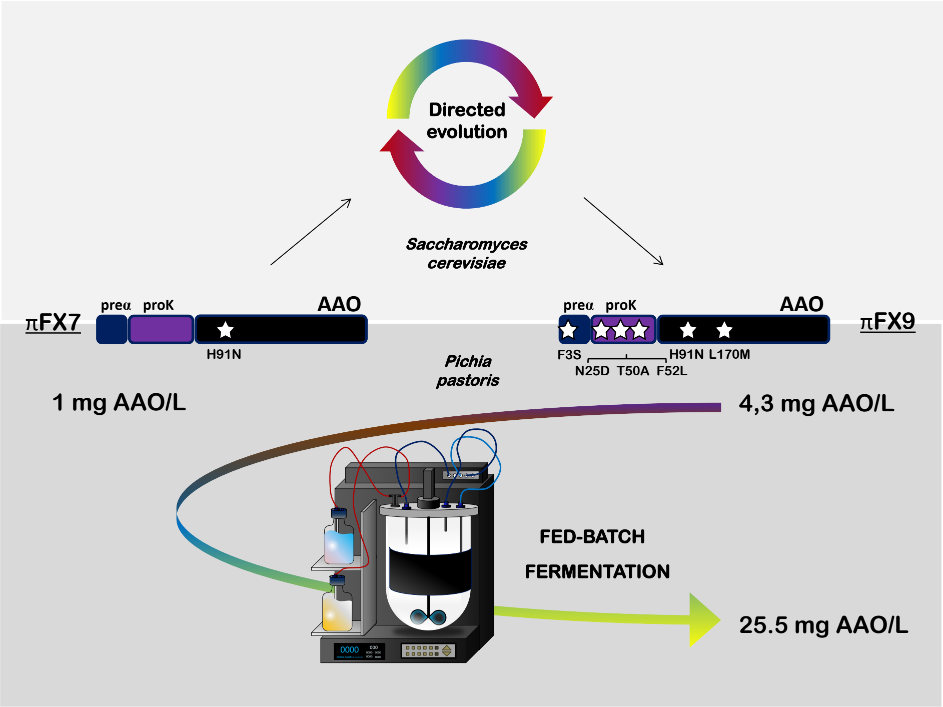
Directed evolution
Saccharomyces cerevisiae
πFX7
preα
proK
AAO
H91N
Pichia pastoris
preα
proK
AAO
πFX9
F3S
H91N L170M
N25D T50A F52L
1 mg AAO/L
4,3 mg AAO/L
FED-BATCH
FERMENTATION
25.5 mg AAO/L

Figure 8.2. AAO expression in *Pichia pastoris*.

8.3 Secondary benzyl-alcohol oxidase by directed evolution

As commented in **Chapter VI**, the characteristic enantioselective mechanism of AAO could be used to obtain optically pure chiral alcohols as molecules of interest for organic synthesis. With an already developed yeast expression system and a substrate-`*blind*´ HTS-assay, several evolutive strategies were applied to boost the residual activity on secondary benzyl-alcohols. The final variant went under extensive biochemical characterization and the gathered mutations were interpreted with computational tools.

8.3.1 Atypical activity with secondary alcohols by saturation mutagenesis

The selected scaffold to engineer activity with secondary alcohols was the secretion variant FX9. The followed strategy was to focus efforts on the active site, with the aim of not affecting the secretion or stability of the enzyme but modulating activity. Computational studies pointed at Ile500 and Phe501 as main steric obstacles in the accommodation of bulkier 1-(*p*-methoxyphenyl)-ethanol (Hernandez-Ortega et al. 2012c; Serrano et al. 2019). Following that direction, site-directed mutagenesis was applied to construct on FX9 the variants I500A, F501A and I500A-F501A. Unfortunately, none of the microfermentations from those mutants presented activity with the secondary alcohol. Hoping to find a better amino acid configuration at those key positions, a combinatorial saturation mutagenesis library was prepared targeting positions Ile500 and Phe501. Surprisingly, variant 15G12 was the best performer with 160-fold improvements oxidizing 1-(*p*-methoxyphenyl)-ethanol while presenting bulkier substitutions I500M-F501W. According to the modified activity profile, 15G12 lost most activity with AAO's natural substrate, *p*-methoxybenzyl alcohol, and was able to oxidize secondary substrates *p*-fluoro-α-methylbenzyl alcohol and 1-phenylethanol.

8.3.2 Further mutational benefits by MORPHING

Once the residual activity on the secondary alcohol was unveiled, the next plan of action was to amplify the structural search for improving mutations. The MORPHING method had been previously applied in **Chapter III** and **Chapter IV** to enhance secretion and total activity. Here, the one-pot focused mutagenesis tool left the signal peptide unaltered (avoiding preproleader-related secretion effects) and was stricter targeting segments of the mature protein. Mutagenic blocks MA (Leu48-Thr100), MB (Leu310-Ile417) and MC (Glu490-Gln566) came together covering the access channel and catalytic pocket of the 15G12 variant. The approach was particularly successful uncovering the importance of block MA, comprising the access channel and FAD-binding domain, with around 70% of the selected mutations placed on the block at a 14 residues distance: I76V, A77V, R80C, M83I and V90A.

8.3.3 Site-directed *in vivo* recombination to polish mutational load

The improvements oxidizing 1-(*p*-methoxyphenyl)-ethanol observed in the second and third cycles (*i.e.* MORPHING, *ep*PCR and a subsequent DNA Shuffling) ranged from 220 to 140-fold compared with FX9 variant. To explore the possible epistatic effects of the panel of substitutions across the mutant collection, a site-directed recombination library was constructed with 10 selected mutations. The site-directed recombination methodology creates genetic diversity when the selected mutations and their correspondent reversions are studied in a combinatorial manner. The positive and detrimental epistatic events were clear when the best variant LanDo, with A77V-R80C-V340A-I500M-F501W (plus the secretion mutations) and 800-fold improvements compared with FX9, became the second best mutant with the addition of Q466R and F332L (negative epistasis), with 480-fold improvements, and the third best combination with the further addition of Q174R (negative epistasis) to show 430-fold enhancements.

8.3.4 Biochemical and computational analysis of LanDo variant

With a specific activity of 2.9 U/mL for 1-(*p*-methoxyphenyl)-ethanol, LanDo showed and striking increase of three orders of magnitude in catalytic efficiency when compared with the wild type expressed in *E. coli* after *in vitro* refolding. Additionally the initial turnover rates for *p*-fluoro-α-methylbenzyl alcohol and 1-phenylethanol were increased 20 and 100-fold times and LanDo showed activity towards 1-phenylpropanol, undetectable with the native enzyme. Also, it was worth noticing the recovery of the activity for *p*-methoxybenzyl alcohol, a trait almost totally lost in 15G12. The essential characteristic to resolve chiral mixtures, beyond total activity with secondary alcohols, is a high preference for one of the alcohol enantiomers. To determine the enantioselectivity of LanDo, the transformation of the racemic 1-(*p*-methoxyphenyl)-ethanol was studied by chiral-HPLC. The enantiomeric excess when the reaction was completed was >99%, corresponding to the R enantiomer, after two hours reaction. This result implicates that the natural selectivity of the AAO was maintained throughout the evolution cycles.

A computational interpretation of the previous results was carried outin collaboration Prof. Victor Guallar from the Barcelona Supercomputing Center (BSC). PELE (Protein Energy Landscape Exploration) is a method based on the Monte Carlo algorithm part of the *in silico* toolbox to model protein dynamics and protein-ligand interactions (Monza et al. 2017). Measuring favorable positioning, in the case of parental 15G12 the ligand (*S*)-1-(*p*-methoxyphenyl)-ethanol, could reach better catalytic distances (2.5 Å) to the FAD and the catalytic base than the wild type and secretion variant FX9. In the case of LanDo, these values were even smaller with 2 Å to the catalytic histidine and 2.4 Å to the cofactor. At the atomic level, particularly R80C created an empty space on top of the FAD; in addition, since Arg80 interacts with the backbone of Trp501, the introduction of the Cys80 allows Trp501 to form a hydrogen bond with Val77. In LanDo, minor conformational changes were responsible for a remarkably improved catalytic performance making this variant a promising catalyst for the resolution of racemic mixtures of benzyl alcohols.

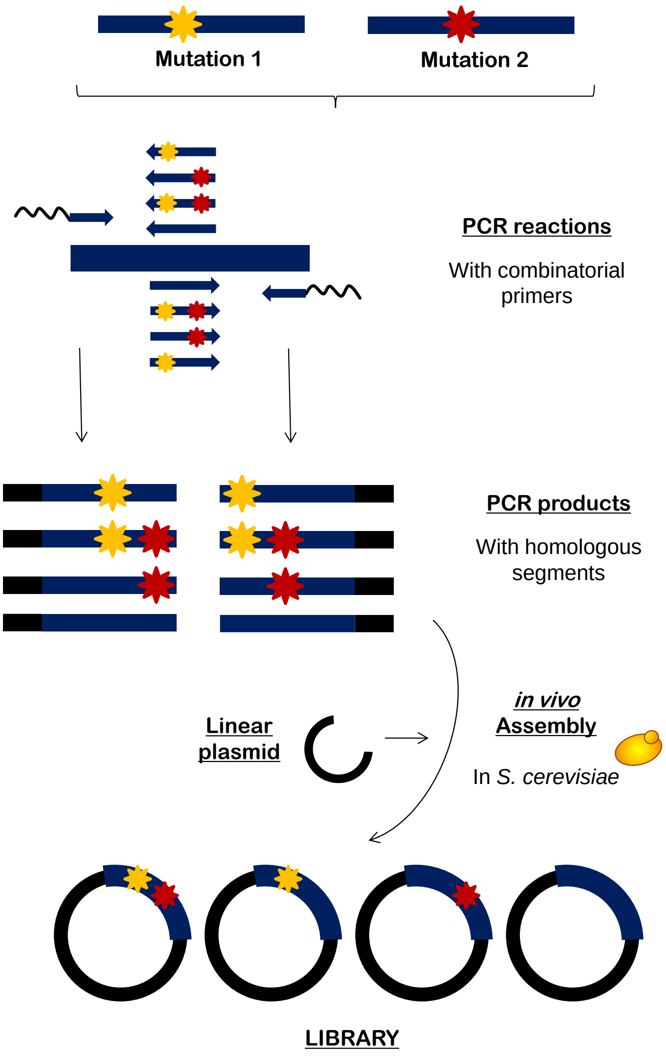
Mutation 1
Mutation 2
PCR reactions
With combinatorial primers
PCR products
With homologous segments
Linear plasmid
in vivo Assembly
In S. cerevisiae
LIBRARY

Figure 8.3. Site directed recombination method.

8.4 Directed evolution to increase FFCA oxidation with AAO

As indicated in **Chapter VII**, FDCA is a bio-based platform chemical of relevant interest in polymer industry. The enzymatic production of FDCA from renewable HMF consists of a cascade reaction of three consecutive 2 e^- oxidations. The activity of the AAO with this family of furan-derived heterocycles was recently examined by Carro et al (2014). It was described that the AAO catalyzes the transformation of HMF into FFCA via DFF oxidation since the enzyme lacks activity with the product of the HMF carbonyl group oxidation, the 5-hydroxymethylfurancarboxylic acid (HMFCA). Apparently not active with FFCA, the full conversion into FDCA was achieved by coupling AAO with the unspecific peroxygenase (UPO) from *Agrocybe aegerita* in a self-sufficient enzymatic cascade. This system comprises the transformation of HMF into FFCA by the AAO producing the H_2O_2 to supply UPO with the necessary co-substrate for the oxidation of the formyl group of the FFCA to finally obtain FDCA (Carro et al. 2015). By contrast, in other experiments with three different AAOs, the native enzymes from *Pleurotus eryngii*, *Pleurotus ostreatus* and *Bjerkandera adusta* did show a moderate direct transformation of FFCA into FDCA but failing to achieve FDCA production when HMF was the starting substrate (Karich et al. 2018). In the case of the HMFO, the FFCA oxidation has been explored by the group of Prof. Marco Fraaije (University of Groningen). For a better production of FDCA with the HMFO system, a double variant V367R-W466F, positions surrounding the active site where His467 is the catalytic base, was constructed by site directed mutagenesis with an increase in the catalytic efficiency for FFCA of three orders of magnitude. Still, the k_{cat} of the new variant was one order of magnitude lower than that of the native enzyme with HMF (Dijkman et al. 2015).

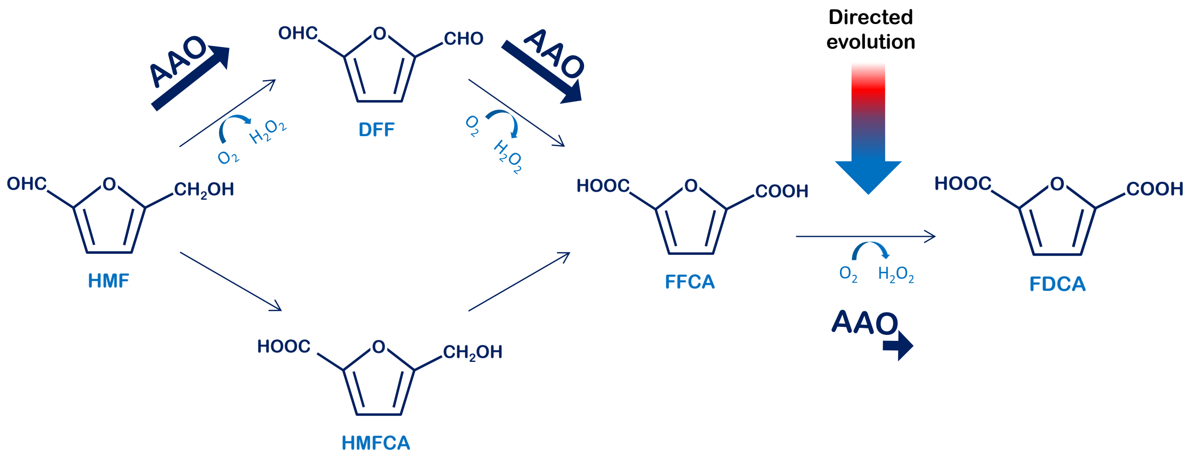

Figure 8.4. Oxidative pathways for the transformation of HMF into FDCA

8.4.1 Directed evolution of AAO for HMF and FFCA oxidation

Given that all reaction intermediates of the FDCA route have to be accepted as substrates, the first plan of action for the evolution of the AAO was the benchmarking of variants FX9 (**Chapter V**) and 15G12 (**Chapter VI**) to establish their capacity to oxidize both departing HMF and the final intermediate FFCA. As expected for AAO variants, no activity was detected with FFCA in HTS format. Interestingly, the volumetric activity of FX9 using HMF (0.3 U/L) was more than 30-fold higher than the activity of 15G12 (the enzyme from the secondary alcohol oxidation campaign). Indeed, it was evident that positions 500 and 501 were determinant on the activity with the furfural derivate, as it was similarly reported in the case of HMFO studies (Dijkman et al. 2015). The strategy followed consisted of saturating these positions and other structurally related residues (after alignment with HMFO) by combinatorial saturation mutagenesis (CSM) to find a better catalyst for the reaction than FX9. After several CSM experiments, only one combination of amino acids improved (3-fold times) the HMF oxidation, the Bantha mutant with substitution F501W. Certainly, the kinetic parameters calculation showed a 60-fold enhanced k_{cat} for Bantha. With improved catalytic efficiency with HMF, we wondered whether or not the new variant could complete the whole cascade reaction from HMF to FDCA with increased activity on FFCA. The production of FDCA from HMF and FFCA by Bantha and FX9 were analyzed by HPLC and compared with the wild type expressed in *E. coli* after re-folding ($_{Ec}$AAO). After 24 hours incubation, Bantha transformed FFCA 7-fold more efficiently than the $_{Ec}$AAO while FX9 also performed the whole route, but in a lesser extent. Moreover, on a 48 hours reaction, after both enzymes transformed HMF totally into FFCA, the posterior oxidation into FDCA was 6 times more efficient for Bantha. This way, it was shown for the first time the capability of AAO to complete the whole cascade of three consecutive oxidations.

8.4.2 Mutational analysis for the Bantha variant

The AAO variant Bantha carries two substitutions that are paramount to complete the FDCA route: H91N and F501W. The back-to-consensus ancestor mutation H91N, was responsible to broaden the promiscuity towards FFCA (as this activity was already observed for the FX9 variant carrying H91N). Conversely, the F501W substitution was behind the overall improved activity from HMF by helping to place O_2 for a better reactivity. In fact, a Trp residue can be found at the homologous position in other AAOs like the enzyme from *Bjerkandera adusta* (Hernandez-Ortega et al 2011b). It is worth noticing that the HMFO also presents a Trp in the correspondent position (W466) as well as an Asn at position 102 equivalent to the ancestral/consensus mutation H91N acquired in the evolutive campaign for functional expression (**Chapter III**), and this enzyme did complete the whole FDCA route in its native form.

Paradoxically, in the improved HMFO variant V367R-W466F from Fraaije studies, the opposite substitution creates a wider space better accommodating the hydrated aldehyde form of FFCA, something that is difficult to be rationalized albeit the introduction of bulkier residues in the catalytic site of AAO was also beneficial for secondary alcohol oxidation.

Still far from being an optimal process, these substitutions discovered during the evolution of the AAO add up to the enzymatic toolbox for FDCA preparation.

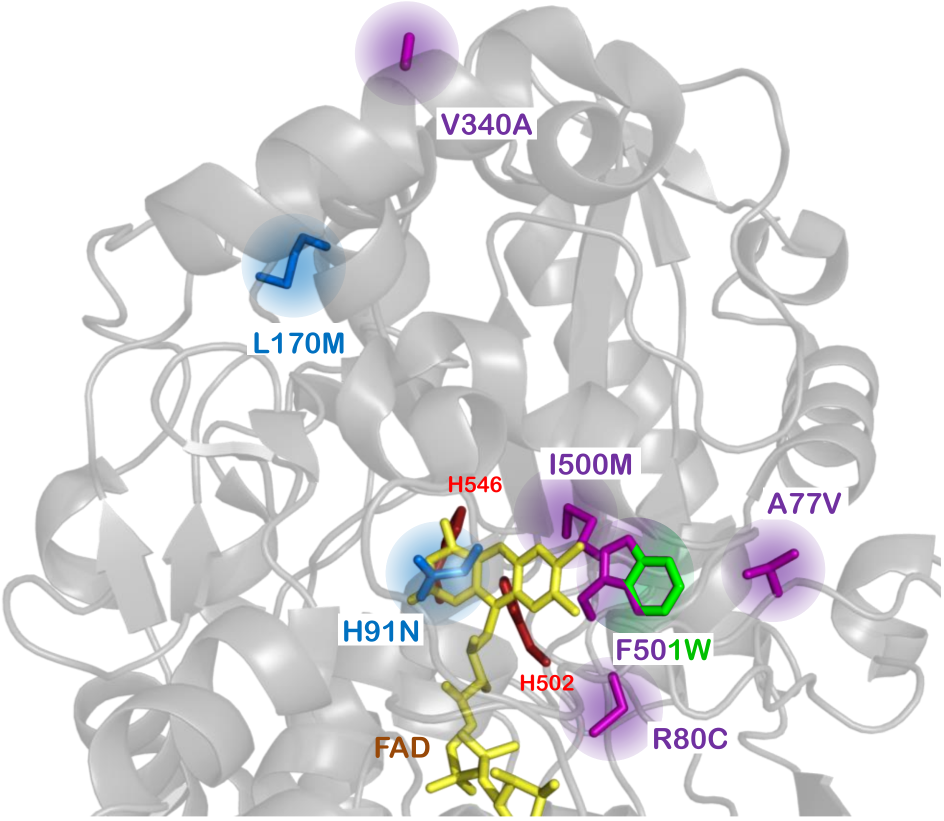

Figure 8.5. Identified mutations in the AAO throughout the directed evolution campaigns. FAD is depicted in yellow, catalytic histidines are depicted in red. Mutations corresponding to the secretion evolution are in blue, mutations from the evolution for secondary alcohol oxidation are in purple while mutation corresponding to the furfural derivatives oxidation evolution is depicted in green (please notice that H91N mutation opens substrate promiscuity for the FDCA route).

CHAPTER VIII

Chapter IX:

CONCLUSIONS

CHAPTER IX

CHAPTER IX

9.1 CONCLUSIONS

1. The AAO from *Pleurotus eryngii* has been functionally expressed in *S. cerevisiae* by using different signal peptides: the mating α-factor preproleader, the killer K1 toxin preproleader and their chimeric combinatorial fusions.
2. A high-throughput screening assay to detect H_2O_2 based on the Fenton reaction (FOX assay) was developed. FOX assay presented a stable linear response with detection limits as low as 0.4 µM.
3. The preαproK-AAO fusion was subjected to directed evolution to enhance total activity values in yeast. Mutant libraries were constructed including a classical mutagenic PCR and focused libraries by MORPHING method, covering key structural determinants of the enzyme.
4. The intermediate variant FX7, with enhacements in total activity of almost 100-fold (expression levels of 2 mg/L) and high stability, harbored the single mutation H91N. This substitution introduces an ancestral/consensus residue at the *si*-side of the FAD cofactor.

5. Further rounds of evolution for heterologous expression led to the final secretion variant FX9, the result of recombining the best beneficial mutations from the previous offspring while targeting the mutational loading at the chimeric preproleader. FX9 improved secretion up to 4.5 mg/L, showing similar biochemical properties as FX7, including kinetic values, stability and glycosylation levels

6. A tandem-yeast expression system was set up with the cloning and expression of FX9 in *Pichia pastoris*. The scaling-up of the production in a 5L fermented increase the production levels up to 25.5 mg/L.

7. The activity of the FX9 variant for secondary alcohols was unlocked by remodeling the active site of the enzyme through structure-guided evolution along with a a polishing step of site-directed recombination *in vivo*. The ultimate variant (named LanDo) carried bulky substitutions in the catalytic cavity that opened the substrate promiscuity and it was computationally rationalized at atomic level. LanDo was active with several chiral alcohols and increased the catalytic efficiency towards 1-(*p*-methoxyphenyl)-ethanol in 1000-fold with 99 %ee (corresponding to the R-enantiomer) being a promising platform for racemic resolution.

8. Structure-guided evolution of AAO was performed to complete the stepwise oxidation from HMF to FDCA. Taking advantage of the unlocked promiscuity of AAO evolved variants, the catalytic site of AAO was sculptured to bypass the limiting step of the HMF pathway.

9.2 CONCLUSIONES

9. La AAO de *Pleurotus eryngii* ha sido expresada funcionalmente en *S. cerevisiae* con el uso de distintos péptidos señales: el péptido señal del factor-α, la secuencia preproleader de la toxina killer K1 y sus fusiones quiméricas combinatoriales.
10. Se desarrolló un ensayo de cribado de alta capacidad para detectar H_2O_2 basado en la reacción de Fenton (ensayo FOX). El ensayo FOX presentó una respuesta estable y linear con límites de detección de 0.4 µM.
11. La fusion preαproK-AAO fue sometida a evolución dirigida para mejorar los niveles totales de actividad en levadura. Se construyeron librerías mutantes incluyendo una clásica amplificación mutagénica y el método focalizado MORPHING cubriendo importantes determinantes estructurales de la enzima.

12. La variante intermedia FX7, con una mejora en actividad total de casi 100 veces (niveles de expresión de 2 mg/L) y alta estabilidad, adquirió la mutación H91N. Esta sustitución introduce un residuo ancestral/consenso en el lado *si* del cofactor FAD.

13. Rondas de evolución adicionales para expresión heteróloga llevaron a la variante FX9, resultante de la recombinación de las mutaciones más beneficiosas de la anterior generación y de la focalización de carga mutagénica en el péptido señal chimérico. FX9 mejoró la secreción hasta niveles de 4.5 mg/L, presentando similares propiedades bioquímicas a FX7 incluyendo valores cinéticos, de estabilidad y de glicosilación.

14. Se puso a punto un sistema en tándem de expresión en levaduras con el clonaje y la expresión de FX9 en *Pichia pastoris*. El escalado de la producción en fermentador de 5L incrementó los niveles de secreción hasta 25.5 mg/L.

15. Se reveló la actividad de FX9 con alcoholes secundarios remodelando el bolsillo catalítico de la enzima por medio de evolución guiada por la estructura junto a un pulido mutagénico por reversión al parental combinatorial. La variante final LanDo, con sustituciones voluminosas en el sitio activo que abrieron la promiscuidad de sustrato, fue analizado con herramientas computacionales a nivel atómico. LanDo presentó actividad con distintos alcoholes quirales e incrementó la eficiencia catalítica hacia 1-(*p*-methoxyphenyl)-ethanol en 1000 veces con 99% ee (correspondiente al enantiómero R) siendo una prometedora plataforma para resoluciones racémicas.

16. Se llevó a cabo evolución focalizada en la estructura de la AAO para completar la oxidación de HMF en FDCA. Haciendo uso de la desvelada promiscuidad de las variantes de AAO, se remodeló el bolsillo catalítico de la enzima para mejorar el paso limitante de dicha conversión.

Chapter X:

REFERENCES

CHAPTER

X

10 REFERENCES

Abatemarco, J., Hill, A., & Alper, H. S. (2013). Expanding the metabolic engineering toolbox with directed evolution. *Biotechnol J, 8*(12), 1397-1410.

Ahmad, M., Hirz, M., Pichler, H., & Schwab, H. (2014). Protein expression in Pichia pastoris: recent achievements and perspectives for heterologous protein production. *Applied microbiology and biotechnology, 98*(12), 5301-5317.

Alcalde, M. (2010). Mutagenesis protocols in Saccharomyces cerevisiae by in vivo overlap extension. *Methods Mol Biol, 634*, 3-14. doi:10.1007/978-1-60761-652-8_1

Alcalde, M. (2015). Engineering the ligninolytic enzyme consortium. *Trends Biotechnol, 33*(3), 155-162. doi:10.1016/j.tibtech.2014.12.007

Arnold, F. H., & Georgiou, G. (2003). Directed evolution library creation. *Methods in molecular biology, 231*, 231.

Asada, Y., Watanabe, A., Ohtsu, Y., & Kuwahara, M. (1995). Purification and characterization of an aryl-alcohol oxidase from the lignin-degrading basidiomycete Phanerochaete chrysosporium. *Bioscience, biotechnology, and biochemistry, 59*(7), 1339-1341.

Atilgan, A. R., Durell, S., Jernigan, R. L., Demirel, M., Keskin, O., & Bahar, I. (2001). Anisotropy of fluctuation dynamics of proteins with an elastic network model. *Biophysical journal, 80*(1), 505-515.

Ayuso-Fernández, I., Martínez, A. T., & Ruiz-Dueñas, F. J. (2017). Experimental recreation of the evolution of lignin-degrading enzymes from the Jurassic to date. *Biotechnology for biofuels, 10*(1), 67.

Bitter, G. A., Chen, K. K., Banks, A. R., & Lai, P. H. (1984). Secretion of foreign proteins from Saccharomyces cerevisiae directed by alpha-factor gene fusions. *Proceedings of the National Academy of Sciences of the United States of America, 81*(17), 5330-5334.

Bloom, J. D., & Arnold, F. H. (2009). In the light of directed evolution: pathways of adaptive protein evolution. *Proceedings of the National Academy of Sciences, 106*(Supplement 1), 9995-10000.

Bochevarov, A. D., Harder, E., Hughes, T. F., Greenwood, J. R., Braden, D. A., Philipp, D. M., . . . Friesner, R. A. (2013). Jaguar: A high-performance quantum chemistry software program with strengths in life and materials sciences. *International Journal of Quantum Chemistry, 113*(18), 2110-2142.

Böckle, B., Martínez, M. J., Guillén, F., & Martínez, Á. T. (1999). Mechanism of Peroxidase Inactivation in Liquid Cultures of the Ligninolytic Fungus *Pleurotus pulmonarius*. *Applied and Environmental Microbiology, 65*(3), 923.

Bornscheuer, U., Huisman, G., Kazlauskas, R., Lutz, S., Moore, J., & Robins, K. (2012). Engineering the third wave of biocatalysis. *Nature, 485*(7397), 185.

Bou, R., Codony, R., Tres, A., Decker, E. A., & Guardiola, F. (2008). Determination of hydroperoxides in foods and biological samples by the ferrous oxidation–xylenol orange method: A review of the factors that influence the method's performance. *Analytical biochemistry, 377*(1), 1-15.

Bourbonnais, R., & Paice, M. G. (1988). Veratryl alcohol oxidases from the lignin-degrading basidiomycete Pleurotus sajor-caju. *Biochemical Journal, 255*(2), 445-450.

Brake, A. J. (1990). [34] α-Factor leader-directed secretion of heterologous proteins from yeast *Methods Enzymol* (Vol. 185, pp. 408-421): Elsevier.

Brenner, C., & Fuller, R. S. (1992). Structural and enzymatic characterization of a purified prohormone-processing enzyme: secreted, soluble Kex2 protease. *Proceedings of the National Academy of Sciences, 89*(3), 922-926.

Bulter, T., & Alcalde, M. (2003). Preparing libraries in Saccharomyces cerevisiae. *Methods Mol Biol, 231*, 17-22.

Caldwell, J. (2001). Do single enantiomers have something special to offer? *Human Psychopharmacology: Clinical and Experimental, 16*(S2), S67-S71.

Camarero, S., Pardo, I., Cañas, A. I., Molina, P., Record, E., Martínez, A. T., . . . Alcalde, M. (2012). Engineering Platforms for Directed Evolution of Laccase from *Pycnoporus cinnabarinus*. *Applied and Environmental Microbiology, 78*(5), 1370-1384. doi:10.1128/aem.07530-11

Carro, J., Amengual-Rigo, P., Sancho, F., Medina, M., Guallar, V., Ferreira, P., & Martínez, A. T. (2018). Multiple implications of an active site phenylalanine in the catalysis of aryl-alcohol oxidase. *Scientific reports, 8*.

Carro, J., Ferreira, P., Rodríguez, L., Prieto, A., Serrano, A., Balcells, B., . . . Ullrich, R. (2015). 5-hydroxymethylfurfural conversion by fungal aryl-alcohol oxidase and unspecific peroxygenase. *The FEBS journal, 282*(16), 3218-3229.

Carro, J., Serrano, A., Ferreira, P., & Martínez, A. T. (2016). Fungal aryl-alcohol oxidase in lignocellulose degradation and bioconversion *Microbial Enzymes in Bioconversions of Biomass* (pp. 301-322): Springer.

Cartwright, C. P., Zhu, Y. S., & Tipper, D. J. (1992). Efficient secretion in yeast based on fragments from K1 killer preprotoxin. *Yeast, 8*(4), 261-272.

Cavener, D. R. (1992). GMC oxidoreductases: a newly defined family of homologous proteins with diverse catalytic activities. *Journal of molecular biology, 223*(3), 811-814.

Chang, C. N., Matteucci, M., Perry, L. J., Wulf, J. J., Chen, C. Y., & Hitzeman, R. A. (1986). *Saccharomyces cerevisiae* secretes and correctly processes human interferon hybrid proteins containing yeast invertase signal peptides. *Molecular and Cellular Biology, 6*(5), 1812-1819.

Chao, R., Yuan, Y., & Zhao, H. (2015). Recent advances in DNA assembly technologies. *FEMS Yeast Res, 15*(1), 1-9.

Chhabra, N., Aseri, M. L., & Padmanabhan, D. (2013). A review of drug isomerism and its significance. *International journal of applied and basic medical research, 3*(1), 16.

Cobb, R. E., Chao, R., & Zhao, H. (2013). Directed Evolution: Past, Present and Future. *AIChE J, 59*(5), 1432-1440.

Cortassa, S., Aon, J. C., & Aon, M. A. (1995). Fluxes of carbon, phosphorylation, and redox intermediates during growth of Saccharomyces cerevisiae on different carbon sources. *Biotechnology and bioengineering, 47*(2), 193-208.

Couturier, M., Mathieu, Y., Li, A., Navarro, D., Drula, E., Haon, M., . . . Berrin, J.-G. (2016). Characterization of a new aryl-alcohol oxidase secreted by the phytopathogenic fungus *Ustilago maydis*. *Applied microbiology and biotechnology, 100*(2), 697-706.

Daly, R., & Hearn, M. T. (2005). Expression of heterologous proteins in Pichia pastoris: a useful experimental tool in protein engineering and production. *Journal of Molecular Recognition: An Interdisciplinary Journal, 18*(2), 119-138.

Delic, M., Valli, M., Graf, A. B., Pfeffer, M., Mattanovich, D., & Gasser, B. (2013). The secretory pathway: exploring yeast diversity. *FEMS Microbiol Rev, 37*(6), 872-914.

Dijkman, W. P., Binda, C., Fraaije, M. W., & Mattevi, A. (2015). Structure-based enzyme tailoring of 5-hydroxymethylfurfural oxidase. *ACS catalysis, 5*(3), 1833-1839.

Dijkman, W. P., & Fraaije, M. W. (2014). Discovery and characterization of a 5-hydroxymethylfurfural oxidase from Methylovorus sp. strain MP688. *Appl. Environ. Microbiol., 80*(3), 1082-1090.

Dijkman, W. P., Groothuis, D. E., & Fraaije, M. W. (2014). Enzyme-catalyzed oxidation of 5-hydroxymethylfurfural to furan-2, 5-dicarboxylic acid. *Angewandte Chemie International Edition, 53*(25), 6515-6518.

Dym, O., & Eisenberg, D. (2001). Sequence-structure analysis of FAD-containing proteins. *Protein Science, 10*(9), 1712-1728.

Escalettes, F., & Turner, N. J. (2008). Directed evolution of galactose oxidase: generation of enantioselective secondary alcohol oxidases. *ChemBioChem, 9*(6), 857-860.

Faber, K. (2001). Non-sequential processes for the transformation of a racemate into a single stereoisomeric product: proposal for stereochemical classification. *Chemistry–A European Journal, 7*(23), 5004-5010.

Fantin, G., Fogagnolo, M., Medici, A., Pedrini, P., Poli, S., & Sinigaglia, M. (1993). Kinetic resolution of 1-aryl-and 1-heteroaryl ethanols by oxidation with Baker's yeast. *Tetrahedron letters, 34*(5), 883-884.

Farmer, V., Henderson, M. E., & Russell, J. (1960). Aromatic-alcohol-oxidase activity in the growth medium of *Polystictus versicolor*. *Biochemical Journal, 74*(2), 257.

Fernández, I. S., Ruiz-Duenas, F. J., Santillana, E., Ferreira, P., Martínez, M. J., Martínez, Á. T., & Romero, A. (2009). Novel structural features in the GMC family of oxidoreductases revealed by the crystal structure of fungal aryl-alcohol oxidase. *Acta Crystallographica Section D: Biological Crystallography, 65*(11), 1196-1205.

Ferreira, P., Carro, J., Serrano, A., & Martínez, A. T. (2015a). A survey of genes encoding H2O2-producing GMC oxidoreductases in 10 Polyporales genomes. *Mycologia, 107*(6), 1105-1119.

Ferreira, P., Hernández-Ortega, A., Herguedas, B., Martínez, Á. T., & Medina, M. (2009). Aryl-alcohol oxidase involved in lignin degradation: a mechanistic study based on steady and pre-steady state kinetics and primary and solvent isotope effects with two alcohol substrates. *Journal of Biological Chemistry*, jbc. M109. 011593.

Ferreira, P., Hernández-Ortega, A., Herguedas, B., Rencoret, J., Gutiérrez, A., Martínez, M. J., . . . Martínez, Á. T. (2010). Kinetic and chemical characterization of aldehyde oxidation by fungal aryl-alcohol oxidase. *Biochemical Journal, 425*(3), 585-593.

Ferreira, P., Hernández-Ortega, A., Lucas, F., Carro, J., Herguedas, B., Borrelli, K. W., . . . Medina, M. (2015b). Aromatic stacking interactions govern catalysis in aryl-alcohol oxidase. *The FEBS journal, 282*(16), 3091-3106.

Ferreira, P., Medina, M., Guillén, F., Martínez, M. J., Van Berkel, W. J., & Martínez, Á. T. (2005). Spectral and catalytic properties of aryl-alcohol oxidase, a fungal flavoenzyme acting on polyunsaturated alcohols. *Biochemical Journal, 389*(3), 731-738.

Ferreira, P., Ruiz-Dueñas, F. J., Martínez, M. J., Van Berkel, W. J., & Martínez, A. T. (2006). Site-directed mutagenesis of selected residues at the active site of aryl-alcohol oxidase, an H_2O_2-producing ligninolytic enzyme. *The FEBS journal, 273*(21), 4878-4888.

Galperin, I., Javeed, A., Luig, H., Lochnit, G., & Rühl, M. (2016). An aryl-alcohol oxidase of *Pleurotus sapidus*: heterologous expression, characterization, and application in a 2-enzyme system. *Applied microbiology and biotechnology, 100*(18), 8021-8030.

Garcia-Ruiz, E., Gonzalez-Perez, D., Ruiz-Duenas, F. J., Martinez, A. T., & Alcalde, M. (2012). Directed evolution of a temperature-, peroxide- and alkaline pH-tolerant versatile peroxidase. *Biochemical Journal, 441*(1), 487-498.

García-Ruiz, E., Maté, D., Ballesteros, A., Martinez, A. T., & Alcalde, M. (2010). Evolving thermostability in mutant libraries of ligninolytic oxidoreductases expressed in yeast. *Microbial cell factories, 9*(1), 17.

Garcia-Ruiz, E., Mate, D. M., Gonzalez-Perez, D., Molina-Espeja, P., Camarero, S., Martínez, A. T., . . . Alcalde, M. (2014). Directed evolution of ligninolytic oxidoreductases: from functional expression to stabilization and beyond. *Cascade biocatalysis*, 1-22.

Gay, C., Collins, J., & Gebicki, J. M. (1999). Hydroperoxide assay with the ferric–xylenol orange complex. *Analytical biochemistry, 273*(2), 149-155.

Ghanem, A., & Aboul-Enein, H. Y. (2005). Application of lipases in kinetic resolution of racemates. *Chirality: The Pharmacological, Biological, and Chemical Consequences of Molecular Asymmetry, 17*(1), 1-15.

Goetghebeur, M., Brun, S., Galzy, P., & Nicolas, M. (1993). Benzyl alcohol oxidase and laccase synthesis in *Botrytis cinerea*. *Bioscience, biotechnology, and biochemistry, 57*(8), 1380-1381.

Gomez-Fernandez, B. J., Garcia-Ruiz, E., Martin-Diaz, J., de Santos, P. G., Santos-Moriano, P., Plou, F. J., . . . Risso, V. A. (2018). Directed-in vitro-evolution of Precambrian and extant Rubiscos. *Scientific reports, 8*(1), 5532.

Gonzalez-Perez, D., & Alcalde, M. (2014). Assembly of evolved ligninolytic genes in *Saccharomyces cerevisiae*. *Bioengineered, 5*(4), 254-263.

Gonzalez-Perez, D., Garcia-Ruiz, E., & Alcalde, M. (2012). Saccharomyces cerevisiae in directed evolution: An efficient tool to improve enzymes. *Bioengineered bugs, 3*(3), 172-177.

Gonzalez-Perez, D., Garcia-Ruiz, E., Ruiz-Dueñas, F. J., Martinez, A. T., & Alcalde, M. (2014b). Structural determinants of oxidative stabilization in an evolved versatile peroxidase. *ACS catalysis, 4*(11), 3891-3901.

Gonzalez-Perez, D., Molina-Espeja, P., Garcia-Ruiz, E., & Alcalde, M. (2014). Mutagenic Organized Recombination Process by Homologous In Vivo Grouping (MORPHING) for Directed Enzyme Evolution. *PLoS ONE, 9*(3), e90919.

Guillén, F., Martinez, A. T., & Martínez, M. J. (1990). Production of hydrogen peroxide by aryl-alcohol oxidase from the ligninolytic fungus *Pleurotus eryngii*. *Applied microbiology and biotechnology, 32*(4), 465-469.

Guillén, F., Martínez, A. T., & Martínez, M. J. (1992). Substrate specificity and properties of the aryl-alcohol oxidase from the ligninolytic fungus Pleurotus eryngii. *European Journal of Biochemistry, 209*(2), 603-611.

Hashimoto, Y., Koyabu, N., & Imoto, T. (1998). Effects of signal sequences on the secretion of hen lysozyme by yeast: construction of four secretion cassette vectors. *Protein Engineering, 11*(2), 75-77.

Hernández-Ortega, A., Borrelli, K., Ferreira, P., Medina, M., Martínez, A. T., & Guallar, V. (2011a). Substrate diffusion and oxidation in GMC oxidoreductases: an experimental and computational study on fungal aryl-alcohol oxidase. *Biochemical Journal, 436*(2), 341-350.

Hernández-Ortega, A., Ferreira, P., & Martínez, A. T. (2012a). Fungal aryl-alcohol oxidase: a peroxide-producing flavoenzyme involved in lignin degradation. *Applied Microbiology and Biotechnology, 93*(4), 1395-1410. doi:10.1007/s00253-011-3836-8

Hernández-Ortega, A., Lucas, F., Ferreira, P., Medina, M., Guallar, V., & Martínez, A. T. (2011b). Modulating O_2 reactivity in a fungal flavoenzyme: involvement of aryl-alcohol oxidase Phe-501 contiguous to catalytic histidine. *Journal of Biological Chemistry*, jbc. M111. 282467.

Hernández-Ortega, A., Lucas, F. t., Ferreira, P., Medina, M., Guallar, V., & Martínez, A. T. (2012b). Role of active site histidines in the two half-reactions of the aryl-alcohol oxidase catalytic cycle. *Biochemistry, 51*(33), 6595-6608.

Hernández-Ortega, A., Ferreira, P., Merino, P., Medina, M., Guallar, V., & Martínez, A. T. (2012c). Stereoselective hydride transfer by aryl-alcohol oxidase, a member of the GMC superfamily. *ChemBioChem, 13*(3), 427-435.

Isikgor, F., & Becer, R. (2015). *Lignocellulosic Biomass: A Sustainable Platform for Production of Bio-Based Chemicals and Polymers* (Vol. 6).

Iwahara, S., Nishihara, T., Jomori, T., Kuwahara, M., & Higuchi, T. (1980). Enzymic oxidation of α, β-unsaturated alcohols in the side chains of lignin-related aromatic compounds. *Journal of fermentation technology, 58*(3), 183-188.

Jäckel, C., & Hilvert, D. (2010). Biocatalysts by evolution. *Current opinion in biotechnology, 21*(6), 753-759.

Jochens, H., Aerts, D., & Bornscheuer, U. T. (2010). Thermostabilization of an esterase by alignment-guided focussed directed evolution. *Protein Engineering, Design & Selection, 23*(12), 903-909.

Karich, A., Kleeberg, S. B., Ullrich, R., & Hofrichter, M. (2018). Enzymatic preparation of 2, 5-furandicarboxylic acid (FDCA)—a substitute of terephthalic acid—by the joined action of three fungal enzymes. *Microorganisms, 6*(1), 5.

Kersten, P., & Cullen, D. (2007). Extracellular oxidative systems of the lignin-degrading Basidiomycete Phanerochaete chrysosporium. *Fungal Genet Biol, 44*(2), 77-87. doi:10.1016/j.fgb.2006.07.007

Kevin R, O., Vo, K. T., Michaelis, S., & Paddon, C. (1997). Recombination-mediated PCR-directed plasmid construction in vivo in yeast. *Nucleic acids research, 25*(2), 451-452.

Khersonsky, O., Rosenblat, M., Toker, L., Yacobson, S., Hugenmatter, A., Silman, I., . . . Tawfik, D. S. (2009). Directed evolution of serum paraoxonase PON3 by family shuffling and ancestor/consensus mutagenesis, and its biochemical characterization. *Biochemistry, 48*(28), 6644-6654.

Kiess, M., Hecht, H. J., & Kalisz, H. M. (1998). Glucose oxidase from Penicillium amagasakiense: Primary structure and comparison with other glucose-methanol-choline (GMC) oxidoreductases. *European Journal of Biochemistry, 252*(1), 90-99.

Kille, S., Acevedo-Rocha, C. G., Parra, L. P., Zhang, Z.-G., Opperman, D. J., Reetz, M. T., & Acevedo, J. P. (2012). Reducing codon redundancy and screening effort of combinatorial protein libraries created by saturation mutagenesis. *ACS synthetic biology*, 2(2), 83-92.

Kim, S. J., Suzuki, N., Uematsu, Y., & Shoda, M. (2001). Characterization of Aryl Alcohol Oxidase Produced by Dye-Decolorizing Fungus, *Geotrichum candidum* Dec1. *Journal of bioscience and bioengineering, 91*(2), 166-172.

Kjeldsen, T., Pettersson, A. F., Hach, M., Diers, I., Havelund, S., Hansen, P. H., & Andersen, A. S. (1997). Synthetic leaders with potential BiP binding mediate high-yield secretion of correctly folded insulin precursors from *Saccharomyces cerevisiae*. *Protein Expression and Purification, 9*(3), 331-336.

Klose, T., Herbst, D. A., Zhu, H., Max, J. P., Kenttämaa, H. I., & Rossmann, M. G. (2015). A mimivirus enzyme that participates in viral entry. *Structure, 23*(6), 1058-1065.

Krivoruchko, A., Siewers, V., & Nielsen, J. (2011). Opportunities for yeast metabolic engineering: Lessons from synthetic biology. *Biotechnology Journal, 6*(3), 262-276.

Kroutil, W., Mang, H., Edegger, K., & Faber, K. (2004). Biocatalytic oxidation of primary and secondary alcohols. *Advanced Synthesis & Catalysis, 346*(2-3), 125-142.

Kumar, K. A., Reddy, T. C., Reddy, G. V., Reddy, D., Mahipal, S., Sinha, S., . . . Reddanna, P. (2011). High-throughput screening assays for cyclooxygenase-2 and 5-lipoxygenase, the targets for inflammatory disorders. *Indian Journal of Biochemistry and Biophysics*. 48(4):256-61.

Lapadatescu, C., Giniès, C., Le Quéré, J.-L., & Bonnarme, P. (2000). Novel Scheme for Biosynthesis of Aryl Metabolites from l-Phenylalanine in the Fungus *Bjerkandera adusta*. *Applied and Environmental Microbiology, 66*(4), 1517-1522.

Leitner, C., Volc, J., & Haltrich, D. (2001). Purification and characterization of pyranose oxidase from the white rot fungus *Trametes multicolor*. *Applied and Environmental Microbiology, 67*(8), 3636-3644.

Li, Y.-L., Xu, J.-H., & Xu, Y. (2010). Deracemization of aryl secondary alcohols via enantioselective oxidation and stereoselective reduction with tandem whole-cell biocatalysts. *Journal of Molecular Catalysis B: Enzymatic, 64*(1-2), 48-52.

Lussier, M., Sdicu, A.-M., & Bussey, H. (1999). The KTR and MNN1 mannosyltransferase families of *Saccharomyces cerevisiae*. *Biochimica et Biophysica Acta (BBA)-General Subjects, 1426*(2), 323-334.

Maier, N. M., Franco, P., & Lindner, W. (2001). Separation of enantiomers: needs, challenges, perspectives. *Journal of Chromatography A, 906*(1-2), 3-33.

Martínez, A. T., Ruiz-Duenas, F. J., Martínez, M. J., Del Rio, J. C., & Gutierrez, A. (2009). Enzymatic delignification of plant cell wall: from nature to mill. *Current Opinion in Biotechnology, 20*(3), 348-357.

Martínez, A. T., Speranza, M., Ruiz-Duenas, F. J., Ferreira, P., Camarero, S., Guillen, F., . . . del Rio, J. C. (2005). Biodegradation of lignocellulosics: microbial, chemical, and enzymatic aspects of the fungal attack of lignin. *International Microbiology, 8*(3), 195-204.

Mate, D., Garcia-Burgos, C., Garcia-Ruiz, E., Ballesteros, A. O., Camarero, S., & Alcalde, M. (2010). Laboratory evolution of high-redox potential laccases. *Chemistry & Biology, 17*(9), 1030-1041.

Mate, D. M., Garcia-Ruiz, E., Camarero, S., Shubin, V. V., Falk, M., Shleev, S., . . . Alcalde, M. (2013). Switching from blue to yellow: altering the spectral properties of a high redox potential laccase by directed evolution. *Biocatalysis and Biotransformation, 31*(1), 8-21.

Mate, D. M., Gonzalez-Perez, D., Mateljak, I., de Santos, P. G., Vicente, A. I., & Alcalde, M. (2017). The pocket manual of directed evolution: Tips and tricks *Biotechnology of Microbial Enzymes* (pp. 185-213): Elsevier.

Matsuda, T., Yamanaka, R., & Nakamura, K. (2009). Recent progress in biocatalysis for asymmetric oxidation and reduction. *Tetrahedron: Asymmetry, 20*(5), 513-557.

Molina-Espeja, P., Garcia-Ruiz, E., Gonzalez-Perez, D., Ullrich, R., Hofrichter, M., & Alcalde, M. (2014). Directed Evolution of Unspecific Peroxygenase from Agrocybe aegerita. *Applied and Environmental Microbiology, 80*(11), 3496-3507.

Molina-Espeja, P., Ma, S., Mate, D. M., Ludwig, R., & Alcalde, M. (2015). Tandem-yeast expression system for engineering and producing unspecific peroxygenase. *Enzyme and microbial technology, 73*, 29-33.

Molina-Espeja, P., Viña-González, J., Gomez-Fernández, B. J., Martín-Diaz, J., Garcia-Ruiz, E., & Alcalde, M. (2016). Beyond the outer limits of nature by directed evolution. *Biotechnology Advances, 34*(5), 754-767.

Monza, E., Acebes, S., Lucas, M. F., & Guallar, V. (2017). Molecular Modeling in Enzyme Design, Toward In Silico Guided Directed Evolution *Directed Enzyme Evolution: Advances and Applications* (pp. 257-284): Springer.

Moreau, C., Belgacem, M. N., & Gandini, A. (2004). Recent catalytic advances in the chemistry of substituted furans from carbohydrates and in the ensuing polymers. *Topics in Catalysis, 27*(1-4), 11-30.

Murphy, R. B., Philipp, D. M., & Friesner, R. A. (2000). A mixed quantum mechanics/molecular mechanics (QM/MM) method for large-scale modeling of chemistry in protein environments. *Journal of Computational Chemistry, 21*(16), 1442-1457.

Ostrov, N., Wingler, L. M., & Cornish, V. W. (2013). Gene assembly and combinatorial libraries in *S. cerevisiae* via reiterative recombination. *Methods in Molecular Biology, 978*, 187-203.

Pàmies, O., & Bäckvall, J.-E. (2004). Chemoenzymatic dynamic kinetic resolution. *Trends in Biotechnology, 22*(3), 130-135.

Peter, S., Karich, A., Ullrich, R., Gröbe, G., Scheibner, K., & Hofrichter, M. (2014). Enzymatic one-pot conversion of cyclohexane into cyclohexanone: Comparison of four fungal peroxygenases. *Journal of Molecular Catalysis B: Enzymatic, 103*, 47-51.

Porebski, B. T., & Buckle, A. M. (2016). Consensus protein design. *Protein Engineering, Design and Selection, 29*(7), 245-251.

Pourmir, A., & Johannes, T. W. (2012). Directed evolution: selection of the host organism. *Computational and Structural Biotechnology Journal, 2*, e201209012.

Qin, S., Zhao, Y., Wu, B., & He, B. (2016). A calcium-ion-stabilized lipase from Pseudomonas stutzeri ZS04 and its application in resolution of chiral aryl alcohols. *Applied biochemistry and biotechnology, 180*(7), 1456-1466.

Rakestraw, J. A., Sazinsky, S. L., Piatesi, A., Antipov, E., & Wittrup, K. D. (2009). Directed evolution of a secretory leader for the improved expression of heterologous proteins and full-length antibodies in *Saccharomyces cerevisiae*. *Biotechnol Bioeng, 103*(6).

Reetz, M. T. (2013). Biocatalysis in organic chemistry and biotechnology: past, present, and future. *J Am Chem Soc, 135*(34), 12480-12496.

Regalado, V., Perestelo, F., Rodriguez, A., Carnicero, A., Sosa, F., De la Fuente, G., & Falcon, M. (1999). Activated oxygen species and two extracellular enzymes: laccase and aryl-alcohol oxidase, novel for the lignin-degrading fungus Fusarium proliferatum. *Applied microbiology and biotechnology, 51*(3), 388-390.

Renata, H., Wang, Z. J., & Arnold, F. H. (2015). Expanding the enzyme universe: accessing non-natural reactions by mechanism-guided directed evolution. *Angewandte Chemie International Edition in English, 54*(11), 3351-3367.

Rhee, S. G., Chang, T.-S., Jeong, W., & Kang, D. (2010). Methods for detection and measurement of hydrogen peroxide inside and outside of cells. *Molecules and cells, 29*(6), 539-549.

Romanos, M. A., Scorer, C. A., & Clare, J. J. (1992). Foreign gene expression in yeast: a review. *Yeast, 8*(6), 423-488.

Romero, E., Ferreira, P., Martínez, Á. T., & Martínez, M. J. (2009). New oxidase from Bjerkandera arthroconidial anamorph that oxidizes both phenolic and nonphenolic benzyl alcohols. *Biochimica et Biophysica Acta (BBA)-Proteins and Proteomics, 1794*(4), 689-697.

Roodveldt, C., Aharoni, A., & Tawfik, D. S. (2005). Directed evolution of proteins for heterologous expression and stability. *Current Opinion in Structural Biology 15*(1), 50-56.

Ruiz-Dueñas, F. J., Ferreira, P., Martínez, M. J., & Martínez, A. T. (2006). In vitro activation, purification, and characterization of *Escherichia coli* expressed aryl-alcohol oxidase, a unique H_2O_2-producing enzyme. *Protein Expression and Purification, 45*(1), 191-199.

Ruiz-Dueñas, F. J., & Martínez, Á. T. (2009). Microbial degradation of lignin: how a bulky recalcitrant polymer is efficiently recycled in nature and how we can take advantage of this. *Microbial Biotechnology, 2*(2), 164-177.

Sannia, G., Limongi, P., Cocca, E., Buonocore, F., Nitti, G., & Giardina, P. (1991). Purification and characterization of a veratryl alcohol oxidase enzyme from the lignin degrading basidiomycete *Pleurotus ostreatus*. *Biochimica et Biophysica Acta (BBA)-General Subjects, 1073*(1), 114-119.

Sastry, G. M., Adzhigirey, M., Day, T., Annabhimoju, R., & Sherman, W. (2013). Protein and ligand preparation: parameters, protocols, and influence on virtual screening enrichments. *Journal of computer-aided molecular design, 27*(3), 221-234.

Schmitt, M. J., & Breinig, F. (2006). Yeast viral killer toxins: lethality and self-protection. *Nature Reviews Microbiology, 4*(3), 212.

Sebestova, E., Bendl, J., Brezovsky, J., & Damborsky, J. (2014). Computational tools for designing smart libraries. Methods in Molecular Biology*, 1179*, 291-314.

Sekhon, B. S. (2013). Exploiting the power of stereochemistry in drugs: an overview of racemic and enantiopure drugs. *Journal of Modern Medicinal Chemistry, 1*, 10-36.

Serrano, A., Sancho, F., Viña-González, J., Carro, J., Alcalde, M., Guallar, V., & Martínez, A. T. (2019). Switching the substrate preference of fungal aryl-alcohol oxidase: towards stereoselective oxidation of secondary benzyl alcohols. *Catalysis Science & Technology, 9*(3), 833-841.

Shao, Z., & Zhao, H. (2012). DNA assembler: a synthetic biology tool for characterizing and engineering natural product gene clusters. *Methods in Enzymology, 517*, 203-224.

Shao, Z., Zhao, H., & Zhao, H. (2009). DNA assembler, an in vivo genetic method for rapid construction of biochemical pathways. *Nucleic Acids Research, 37*(2), e16.

Shrivastava, A., & Gupta, V. B. (2011). Methods for the determination of limit of detection and limit of quantitation of the analytical methods. *Chronicles of young scientists, 2*(1), 21.

Shusta, E. V., Kieke, M. C., Parke, E., Kranz, D. M., & Wittrup, K. D. (1999). Yeast polypeptide fusion surface display levels predict thermal stability and soluble secretion efficiency. Journal of Molecular Biology*, 292*(5), 949-956.

Shuster, J. R. (1991). Gene expression in yeast: protein secretion. *Current opinion in biotechnology, 2*(5), 685-690.

Sigoillot, C., Camarero, S., Vidal, T., Record, E., Asther, M., Pérez-Boada, M., . . . Colom, J. F. (2005). Comparison of different fungal enzymes for bleaching high-quality paper pulps. *Journal of Biotechnology, 115*(4), 333-343.

Sousa, A. F., Vilela, C., Fonseca, A. C., Matos, M., Freire, C. S., Gruter, G.-J. M., . . . Silvestre, A. J. (2015). Biobased polyesters and other polymers from 2, 5-furandicarboxylic acid: a tribute to furan excellency. *Polymer chemistry, 6*(33), 5961-5983.

Turner, N. J. (2004). Enzyme catalysed deracemisation and dynamic kinetic resolution reactions. *Current Opinion in Chemical Biology, 8*(2), 114-119.

Turner, N. J. (2009). Directed evolution drives the next generation of biocatalysts. *Nature Chemical Biology, 5*, 567.

Van Hellemond, E. W., Vermote, L., Koolen, W., Sonke, T., Zandvoort, E., Heuts, D. P., . . . Fraaije, M. W. (2009). Exploring the biocatalytic scope of alditol oxidase from *Streptomyces coelicolor*. *Advanced Synthesis & Catalysis, 351*(10), 1523-1530.

Van Putten, R.-J., Van der Waal, J. C., De Jong, E., Rasrendra, C. B., Heeres, H. J., & de Vries, J. G. (2013). Hydroxymethylfurfural, a versatile platform chemical made from renewable resources. *Chemical reviews, 113*(3), 1499-1597.

Van Schie, M. M., de Almeida, T. P., Laudadio, G., Tieves, F., Fernández-Fueyo, E., Noël, T., . . . Hollmann, F. (2018). Biocatalytic synthesis of the Green Note trans-2-hexenal in a continuous-flow microreactor. *Beilstein journal of organic chemistry, 14*, 697.

Varela, E., Böckle, B., Romero, A., Martínez, A. T., & Martínez, M. a. J. (2000). Biochemical characterization, cDNA cloning and protein crystallization of aryl-alcohol oxidase from *Pleurotus pulmonarius*. *Biochimica et Biophysica Acta (BBA)-Protein Structure and Molecular Enzymology, 1476*(1), 129-138.

Varela, E., Guillén, F., Martínez, Á. T., & Martínez, M. a. J. (2001). Expression of Pleurotus eryngii aryl-alcohol oxidase in *Aspergillus nidulans*: purification and characterization of the recombinant enzyme. *Biochimica et Biophysica Acta (BBA)-Protein Structure and Molecular Enzymology, 1546*(1), 107-113.

Varela, E., Martínez, A. T., & Jesús, M. (1999). Molecular cloning of aryl-alcohol oxidase from the fungus Pleurotus eryngii, an enzyme involved in lignin degradation. *Biochemical Journal, 341*(1), 113-117.

Viña-González, J., Elbl, K., Ponte, X., Valero, F., & Alcalde, M. (2018). Functional expression of aryl-alcohol oxidase in *Saccharomyces cerevisiae* and *Pichia pastoris* by directed evolution. *Biotechnology & Bioengineering, 115*(7), 1666-1674.

Viña-González, J., Gonzalez-Perez, D., & Alcalde, M. (2016). Directed evolution method in *Saccharomyces cerevisiae*: mutant library creation and screening. *Journal of visualized experiments: JoVE*(110).

Viña-González, J., González-Perez, D., Ferreira, P., Martínez, A. T., & Alcalde, M. (2015). Focused Directed Evolution of Aryl-Alcohol Oxidase in Saccharomyces cerevisiae by Using Chimeric Signal Peptides. *Applied and Environmental Microbiology, 81*(18), 6451-6462.

Viña-González, J., Jimenez-Lalana, D., Sancho, F., Serrano, A., Martinez, A. T., Guallar, V., & Alcalde, M. (2019). Structure-Guided Evolution of Aryl Alcohol Oxidase from *Pleurotus eryngii* for the Selective Oxidation of Secondary Benzyl Alcohols. *Advanced Synthesis & Catalysis*, 361, 1–13.

Voss, C. V., Gruber, C. C., & Kroutil, W. (2008). Deracemization of secondary alcohols through a concurrent tandem biocatalytic oxidation and reduction. *Angewandte Chemie International Edition, 47*(4), 741-745.

Werpy, T., & Petersen, G. (2004). *Top value added chemicals from biomass: volume I--results of screening for potential candidates from sugars and synthesis gas*.

Wongnate, T., & Chaiyen, P. (2013). The substrate oxidation mechanism of pyranose 2-oxidase and other related enzymes in the glucose–methanol–choline superfamily. *The FEBS journal, 280*(13), 3009-3027.

Yu, Z., Wang, J., Zhou, N., Zhao, C., & Qiu, J. (2013). A highly sensitive method for quantitative determination of L-amino acid oxidase activity based on the visualization of ferric-xylenol orange formation. *PLoS ONE, 8*(12), e82483.

Zhang, Z.-G., Yi, Z.-L., Pei, X.-Q., & Wu, Z.-L. (2010). Improving the thermostability of Geobacillus stearothermophilus xylanase XT6 by directed evolution and site-directed mutagenesis. *Bioresource Technology, 101*(23), 9272-9278.

Zhou, C. H., Xia, X., Lin, C. X., Tong, D. S., & Beltramini, J. (2011). Catalytic conversion of lignocellulosic biomass to fine chemicals and fuels. *Chemical Society Reviews, 40*(11), 5588-5617.

Zhu, Y. S., Kane, J., Zhang, X. Y., Zhang, M., & Tipper, D. J. (1993). Role of the γ component of preprotoxin in expression of the yeast K1 killer phenotype. *Yeast, 9*(3), 251-266.

Zsebo, K., Lu, H., Fieschko, J., Goldstein, L., Davis, J., Duker, K., . . . Bitter, G. (1986). Protein secretion from *Saccharomyces cerevisiae* directed by the prepro-alpha-factor leader region. *Journal of Biological Chemistry, 261*(13), 5858-5865.

Chapter XI:

ANNEX

CHAPTER

XI

11 ANNEX

CHAPTER
XI

11.1 Publications from the Doctoral Thesis

Viña-Gonzalez, J., Gonzalez-Perez, D., Ferreira, P., Martinez, A.T. and Alcalde, M. (2015). Focused directed evolution of aryl-alcohol oxidase in yeast by using chimeric signal peptides. *Applied and Environmental Microbiology* 81: 6451-6462.

Viña-Gonzalez, J., Gonzalez-Perez, D. and Alcalde, M. (2016). Directed evolution method in *Saccharomyces cerevisiae*: Mutant library creation and screening. *Journal of Visualized Experiments* 110: e53761. and see the experiments at http://www.jove.com/video/53761.

Viña-Gonzalez, J., Elbl, K., Ponte, X., Valero, F.and Alcalde, M. (2018). Functional expression of aryl-alcohol oxidase in *Saccharomyces cerevisiae* and *Pichia pastoris* by directed evolution. *Biotechnology & Bioengineering*. 115: 1666-1674.

Serrano, A., Sancho, F., Viña-Gonzalez, J., Carro, J., Alcalde, M., Guallar, V. and Martinez, A.T. (2019). Switching the substrate preference of fungal aryl-alcohol oxidase: towards stereoselective oxidation of secondary benzyl alcohols. *Catalysis Science and Technology* 9: 833-841.

Viña-Gonzalez, J., Jimenez-Lalana, D., Sancho, F., Serrano, A., Martinez, A.T., Guallar, V. and Alcalde, M. (2019). Structure-guided evolution of aryl alcohol oxidase from *Pleurotus eryingii* for the selective oxidation of secondary benzyl alcohols. *Advanced Synthesis and Catalysis*. 361: 1 – 13.

11.2 Other publications from the author

Viña-Gonzalez, J. and Alcalde, M. (2019). Directing the evolution of the fungal ligninolytic secretome. In: Protein Engineering: Tools and Applications. Zhao, H. Ed. Wiley-VCH, Weinheim, Germany. *In press*.

Vicente, A.I., Viña-Gonzalez, J., Mateljak, I., Monza, E., Lucas, F., Guallar, V. and Alcalde, M. (2019). Enhancing Thermostability by Modifying Flexible Surface Loops in an Evolved High-Redox Potential Laccase. AiChE journal. *Submitted*.

CHAPTER XI

Vicente, A.I., Viña-Gonzalez, J., Santos-Moriano, P., Marquez-Alvarez, C., Ballesteros, O. and Alcalde, M. (2016). Evolved alkaline fungal laccase secreted by *Saccharomyces cerevisiae* as useful tool for the synthesis of C-N heteropolymeric dye. Journal of Molecular Catalysis B: Enzymatic 134: 323-330.

Molina-Espeja, P., Viña-Gonzalez, J., Gomez, B.J., Martin-Diaz, J., Garcia-Ruiz, E., and Alcalde, M. (2016). Beyond the outer limits of nature by directed evolution. Biotechnology Advances. 34: 754-767.

11.3 Copy of the publications from the doctoral thesis

AEM
Journals.ASM.org

Focused Directed Evolution of Aryl-Alcohol Oxidase in *Saccharomyces cerevisiae* by Using Chimeric Signal Peptides

Javier Viña-Gonzalez,[a] David Gonzalez-Perez,[a] Patricia Ferreira,[b] Angel T. Martinez,[c] Miguel Alcalde[a]

Department of Biocatalysis, Institute of Catalysis, CSIC, Madrid, Spain[a]; Departamento de Bioquímica y Biología Molecular y Celular, Facultad de Ciencias, Universidad de Zaragoza, and Instituto de Biocomputación y Física de Sistemas Complejos, Zaragoza, Spain[b]; Centro de Investigaciones Biológicas, CSIC, Madrid, Spain[c]

Aryl-alcohol oxidase (AAO) is an extracellular flavoprotein that supplies ligninolytic peroxidases with H_2O_2 during natural wood decay. With a broad substrate specificity and highly stereoselective reaction mechanism, AAO is an attractive candidate for studies into organic synthesis and synthetic biology, and yet the lack of suitable heterologous expression systems has precluded its engineering by directed evolution. In this study, the native signal sequence of AAO from *Pleurotus eryngii* was replaced by those of the mating α-factor and the K_1 killer toxin, as well as different chimeras of both prepro-leaders in order to drive secretion in *Saccharomyces cerevisiae*. The secretion of these AAO constructs increased in the following order: preproα-AAO > preαproK-AAO > preKproα-AAO > preproK-AAO. The chimeric preαproK-AAO was subjected to focused-directed evolution with the aid of a dual screening assay based on the Fenton reaction. Random mutagenesis and DNA recombination was concentrated on two protein segments (Met[α1]-Val109 and Phe392-Gln566), and an array of improved variants was identified, among which the FX7 mutant (harboring the H91N mutation) showed a dramatic 96-fold improvement in total activity with secretion levels of 2 mg/liter. Analysis of the N-terminal sequence of the FX7 variant confirmed the correct processing of the preαproK hybrid peptide by the KEX2 protease. FX7 showed higher stability in terms of pH and temperature, whereas the pH activity profiles and the kinetic parameters were maintained. The Asn91 lies in the flavin attachment loop motif, and it is a highly conserved residue in all members of the GMC superfamily, except for *P. eryngii* and *P. pulmonarius* AAO. The *in vitro* involution of the enzyme by restoring the consensus ancestor Asn91 promoted AAO expression and stability.

Aryl-alcohol oxidase (AAO; EC 1.1.3.7) is a flavoenzyme of the GMC (glucose-methanol-choline) oxidoreductase superfamily, the members of which share a N-terminal FAD-binding domain containing the canonical ADP-binding motif. Secreted by several white-rot fungi, this monomeric flavoprotein plays an essential role in natural lignin degradation (1). Accordingly, AAO oxidizes lignin-derived compounds and aromatic fungal metabolites, releasing H_2O_2 that is required by ligninolytic peroxidases to attack the plant cell wall (2). Moreover, the H_2O_2 produced by AAO is an efficient vehicle to generate highly reactive hydroxyl radicals through the Fenton reaction ($Fe^{2+} + H_2O_2 \rightarrow OH^{\cdot} + OH^{-} + Fe^{3+}$), such that $OH^{\cdot}$ can act as a diffusible electron carrier to depolymerize plant polymers. AAO oxidizes a variety of aromatic benzyl (and some aliphatic polyunsaturated) alcohols to the corresponding aldehydes. In addition, AAO participates in the oxidation of aromatic aldehydes to the corresponding acids and also has activity on furfural derivatives (3).

The past few years have witnessed an intense effort to discern the basis and mechanism of action underlying AAO catalysis (3–10). The AAO catalytic cycle involves dehydrogenative oxidation mediated by two half-reactions: (i) the reductive half-reaction in which the donor alcohol is two-electron oxidized by the FAD cofactor, the latter receiving one of the alcohol's α-Hs through a hydride transfer process that yields the aldehyde product and the reduced flavin, and (ii) the oxidative half-reaction, in which O_2 is two-electron reduced by the FAD, releasing H_2O_2 and the reoxidized flavin (5).

Directed molecular evolution is by far the best strategy currently available to design enzymes to industrial standards (11–14). However, AAO has not been subjected to directed evolution, probably due to the lack of appropriate functional expression systems. Indeed, AAO has only been heterologous expressed in *Aspergillus nidulans* (15), an unsuitable host for directed evolution experiments (16), and in *Escherichia coli* after the *in vitro* refolding of inclusion bodies, an approach incompatible with directed evolution campaigns (17).

In the present study, the native signal peptide of AAO was replaced by two different signal sequences to drive its functional expression in *Saccharomyces cerevisiae*: (i) the signal prepro-leader of the mating α-factor of *S. cerevisiae*, which has been used widely to evolve different ligninases (18–23), and (ii) the signal prepro(δ)-leader and the γ-spacer segment of the K_1 killer toxin, which have been seen to be useful in boosting β-lactamase secretion in yeast (24, 25). For the first time, chimeric versions of these leaders were designed by combining the different pre- and pro-regions, and these constructs were subjected to conventional and focused-directed evolution using a very sensitive dual high-throughput screening (HTS) assay based on the Fenton reaction. The best mutant identified dramatically improved the total activ-

Received 12 June 2015 **Accepted** 3 July 2015

Accepted manuscript posted online 10 July 2015

Citation Viña-Gonzalez J, Gonzalez-Perez D, Ferreira P, Martinez AT, Alcalde M. 2015. Focused directed evolution of aryl-alcohol oxidase in *Saccharomyces cerevisiae* by using chimeric signal peptides. Appl Environ Microbiol 81:6451–6462. doi:10.1128/AEM.01966-15.

Editor: A. A. Brakhage

Address correspondence to Miguel Alcalde, malcalde@icp.csic.es.

Supplemental material for this article may be found at http://dx.doi.org/10.1128/AEM.01966-15.

Copyright © 2015, American Society for Microbiology. All Rights Reserved.

doi:10.1128/AEM.01966-15

ity and stability being readily secreted by yeast. Indeed, this active, highly stable and soluble AAO variant is a promising point of departure for new engineering goals.

MATERIALS AND METHODS

All chemicals were of reagent-grade purity. Ferrous ammonium sulfate, xylenol orange, sorbitol, benzyl alcohol, *p*-methoxybenzyl alcohol, veratryl (3,4-dimethoxybenzyl) alcohol, 2,4-hexadien-1-ol, ABTS [2,2′azino-bis(3-ethylbenzthiazolinesulfonic acid)], horseradish peroxidase (HRP), *Taq* polymerase, and a yeast transformation kit were purchased from Sigma (Madrid, Spain). Zymoprep yeast plasmid miniprep, yeast plasmid miniprep kit I, and a Zymoclean gel DNA recovery kit were obtained from Zymo Research (Orange, CA). Restriction enzymes BamHI and XhoI were from New England BioLabs (Hertfordshire, United Kingdom). I-Proof high-fidelity DNA polymerase was from Bio-Rad (USA). The episomal shuttle vector pJRoC30 was from the California Institute of Technology (Caltech) and plasmids pRE1219 and pJRoC30-δγN2C1 were kindly donated by S. Camarero (CIB-CSIC, Madrid, Spain). *E. coli* XL2-Blue competent cells were from Stratagene (La Jolla, CA), whereas the protease-deficient *S. cerevisiae* strain BJ5465 (MATa *ura3-52 trp1 leu2Δ1 his3Δ200 pep4*::*HIS3 prb1Δ1.6R can1 GAL*) was obtained from LGC Promochem (Barcelona, Spain).

Culture media. Minimal medium SC contained 100 ml of 6.7% (wt/vol) sterile yeast nitrogen base, 100 ml of a 19.2-g/liter sterile yeast synthetic dropout medium supplement without uracil, 100 ml of sterile 20% (wt/vol) raffinose, 700 ml of sterile double-distilled H_2O (sddH_2O), and 1 ml of chloramphenicol at 25 g/liter. YP medium contained 10 g of yeast extract, 20 g of peptone, and ddH_2O to 650 ml, whereas YPD medium also contained 20% (wt/vol) glucose. AAO expression medium contained 144 ml of 1.55× YP, 13.4 ml of 1 M KH_2PO_4 (pH 6.0) buffer, 22.2 ml of 2% (wt/vol) galactose, 0.222 ml of chloramphenicol at 25 g/liter, and ddH_2O to 200 ml. Luria broth (LB) medium contained 10 g of sodium chloride, 5 g of yeast extract, 10 g of peptone, 1 ml of ampicillin at 100 mg/ml, and ddH_2O to 1 liter.

Fusion genes and signal chimeric leaders. AAO mature protein was fused both to the α-factor prepro-leader (preproα-AAO, construct i) and to the prepro(δ)-γ regions of the prepro-toxin K$_1$ killer (preproK-AAO, construct ii). In addition, two chimeric signal peptides were constructed and attached to the AAO: the α-factor pre-leader fused to the γ segment of the K$_1$ killer toxin (preαproK-AAO, construct iii) and the prepro(δ)-signal sequence of the K$_1$ killer toxin fused to the α-factor pro-leader (preKproα-AAO, construct iv). The design of overlapping areas of $\sim$40 bp between adjacent fragments allowed the *in vivo* fusion of the different genetic elements using the *S. cerevisiae* homologous recombination machinery.

AAO was amplified from pflag1AAO vector (17) using oligonucleotide sense AAO/N-ter primer (5′-GCCGATTTTGACTACGTTGTCGTCG-3′) and oligonucleotide antisense AAO/C-ter/pJRo-overhang primer (5′-CATAACTAATTACATGATGCGGCCCTCTAGATGCATGCTCGAGCGGCCGCCTACTGATCAGCCTTGATAAGATCGGCT-3′; the overhang for pJRoC30 is underlined). The α-factor prepro-leader (89 residues, including the STE13 cleavage site EAEA) was obtained from pJRoC30-αVP (20) using oligonucleotide sense RMLN primer (5′-CCTCTATACTTTAACGTCAAGG-3′) and oligonucleotide antisense αC-ter/AAO-overhang primer (5′-CCGCGTTCCCCGCCCCGACGACAACGTAGTCAAAATCGGCAGCTTCAGCCTCTCTTTTCTC-3′; the overhang for AAO is underlined). The preα fragment, used to create preαproK-AAO, was amplified from pJRoC30-αVP with oligonucleotide sense RMLN and oligonucleotide antisense preαC-ter/proK-overhang (5′-AGTCGTTAGCTGGGAGTATACTAATACCATGTTCATTTAAGTTGACTGGAGCAGCTAATG-3′; the overhang for the proK is underlined) primers; this fragment was designed to include the 19 residues of the α-pre-leader plus the first four residues—APVN—of the α-pro-leader. The proα fragment (66 residues and the STE13 cleavage site) used to create preKproα-AAO was obtained from pJRoC30-αVP with the oligonucleotide sense proα/N-ter primer (5′-GCTCCAGTCAACACTACAAC-3′) and the oligonucleotide antisense αC-ter/AAO-overhang. Prepro(δ)-leader from the K$_1$ killer toxin, used as the preK-leader (47 residues long, including the C-terminal EAP acid environment) with different overhangs (for subsequent assembly in yeast to give rise to different chimeras), was obtained from two independent PCRs from plasmid pRE1219, which contains the prepro(δ) region (1 to 44 residues) and the alpha-toxin subunit (45 to 149 residues): (i) to be fused in preproK-AAO with the oligonucleotide sense primer preKN-ter/pJRo-overhang (5′-TATACTTTAACGTCAAGGAGAAAAAACTATAGGATCATAGGATCCATGACGAAGCCAACCCAAGTATTA-3′; the overhang for pJRoC30 is underlined) and the oligonucleotide antisense primer preKC-ter/proK-overhang (5′-AGTCGTTAGCTGGGAGTATACTAATACCATGTTCATTTAACGGCGCTTCACGTTTTAGTAATGACACTGGT-3′; the overhang for proK is underlined) and (ii) with preKN-ter/pJRo-overhang as the oligonucleotide sense primer and preKC-ter/proα-overhang (5′-TTTGTGCCGTTTCATCTTCTGTTGTAGTGTTGACTGGAGCCGGCGCTTCACGTTTTAGTAATGACACTGGT-3′; the overhang for proα is underlined) as the antisense primer to be part of the preKproα-AAO. The truncated γ-spacer-segment from the K$_1$ killer toxin (64 residues), the proK segment in both preproK-AAO and preαproK-AAO, was obtained from pJRoC30-δγN2C1 with the oligonucleotide sense proKN-ter primer (5′-TTAAATGAACATGGTATTAGTATACTCCCA-3′) and the antisense primer proKC-ter/AAO-overhang (5′-CCGCGTTCCCCGCCCCGACGACAACGTAGTCAAAATCGGCACGCTTGGCCACTGCTGGAAT-3′; the overhang for AAO is underlined).

pJRoC30 was linearized with BamHI and XhoI. PCRs were performed in a final volume of 50 μl containing a 250 nM concentration of each primer, 10 ng of template, deoxynucleoside triphosphates (dNTPs) at 200 μM each, 3% (vol/vol) dimethyl sulfoxide (DMSO), and 0.02 U of iProof high-fidelity polymerase/liter. The amplification reactions were carried out in a thermal cycler Mycycler (Bio-Rad). The PCR cycles were as follows: 98°C for 30 s (1 cycle); 98°C for 10 s, 50°C for 25 s, and 72°C for 60 s (28 cycles); and 72°C for 10 min (1 cycle). PCR fragments and the linearized vector were loaded onto a preparative agarose gel (0.75% [wt/vol]) and purified using a Zymoclean gel DNA recovery kit. PCR products (400 ng of each) were mixed with the linearized vector (100 ng; PCR product/vector ratio of 4:1) and transformed in yeast (yeast transformation kit), promoting the recombination and cloning *in vivo*. Transformed cells were plated in SC (synthetic complete) dropout plates, followed by incubation for 3 days at 30°C; individual clones were fermented in 96-well plates and screened for AAO activity. For each positive construct, the plasmids were extracted and sequenced. Fusions were retransformed into yeast and fermented in 100-ml flasks while monitoring cell growth and activity (using HRP-ABTS and FOX [ferrous oxidation by xylenol orange] assays [see below]) over time.

Focused-directed AAO evolution. All of the PCR products were cleaned, concentrated, loaded onto a low melting-point preparative agarose gel (0.75% [wt/vol]) and purified using a Zymoclean gel DNA recovery kit before being cloned into pJRoC30. The plasmid was linearized with BamHI and XhoI. pJRoC30-preαproK-AAO variant was used as DNA template for focused random mutagenesis. The preαproK-AAO fusion was split into three different segments for MORPHING (Mutagenic Organized Recombination Process by Homologous *IN vivo* Grouping) (26). Amplified by PCR, each fragment included homologous overlapping overhangs of $\sim$50 bp so that the whole gene could be reassembled *in vivo* by transformation into *S. cerevisiae*. Mutagenic regions M-I and M-II (590 and 528 bp, respectively, excluding the recombination areas) were subjected to *Taq*/$MnCl_2$ amplification, and the remaining segment (844 bp) was amplified by high-fidelity PCR. To adjust the mutagenic loads, small mutant libraries (around 500 clones each) were created with equal concentrations of DNA template and different $MnCl_2$ concentrations (0.025, 0.05, and 0.01 mM combining both segments and with 0.05 mM in segment M-I and 0.025 mM in segment M-II). The percentage of inactive clones (with $<$10% of the parent activity) was calculated to estimate mutational loads. Four mutant libraries were created. Two mutagenic libraries (~1,000 clones each) were prepared targeting segment M-I or segment M-II independently for random mutagenesis. The third library (~1,000 clones, library M-I-II) was constructed by assembling mutagenic segments (M-I and M-II) flanking a nonmutagenic amplification in the middle of the gene. Finally, the whole preαproK-AAO fusion was subjected to *Taq*/$MnCl_2$ amplification (library M-IV), adjusting the mutational rate to 1 to 3 mutations per gene (~2,000 clones). Concentrations of 0.05 and 0.01 mM $MnCl_2$ were used for MORPHING and full gene random mutagenesis, respectively.

(i) Mutagenic PCR of targeted segments. Reaction mixtures were prepared in a final volume of 50 μl containing DNA template (0.92 ng/μl), 90 nM oligonucleotide sense primer (RMLN for segment M-I and AAOMBP [5′-AACTCTGCTCATTGGGAGACCATCT-3′] for segment M-II), 90 nM reverse primer (AAO92C [5′-CCCAGTTCCATCCTTCATCGCCA-3′] for segment M-I and RMLC [5′-GGGAGGGCGTGAATGTAAGC-3′] for segment M-II), 0.3 mM dNTPs (0.075 mM each), 3% (vol/vol) DMSO, 1.5 mM $MgCl_2$, increasing concentrations of $MnCl_2$ (0.025, 0.05, and 0.1 mM), and 0.05 U of *Taq* DNA polymerase/μl. Mutagenic PCRs parameters were as follows: 95°C for 2 min (1 cycle); 95°C for 45 s, 50°C for 45 s, and 74°C for 45 s (28 cycles); and 74°C for 10 min (1 cycle).

(ii) High-fidelity PCR. Reaction mixtures were prepared in a final volume of 50 μl containing DNA template (0.2 ng/μl), 250 nM oligonucleotide sense HFF (5′-TTCGATCGCTATGCGGCTGTCAC-3′), and 250 nM oligonucleotide antisense HFR (5′-GGGTGGAACCATTGGTTGGAAAAG-3′). High-fidelity PCRs were performed using the following parameters: 98°C for 30 s (1 cycle); 98°C for 10 s, 55°C for 25 s, and 72°C for 45 s (28 cycles); and 72°C for 10 min (1 cycle).

(iii) Whole-gene reassembly. The whole gene was cloned and recombined *in vivo* by transformation into *S. cerevisiae*. PCR products were mixed in equimolar amounts (400 ng) and transformed with linearized plasmid (200 ng) into chemically competent cells. Transformed cells were plated on SC dropout plates and incubated for 3 days at 30°C. Colonies containing the whole autonomously replicating vector were picked and screened for activity.

HTS assay. Individual clones were picked and cultured in sterile 96-well plates containing 50 μl of minimal medium (SC). In each plate, column 6 was inoculated with the parental type (internal standard) and well H1 with $URA3^-$ *S. cerevisiae* cells (negative control). Plates were sealed to prevent evaporation and incubated at 30°C, 225 rpm, and 80% relative humidity in a humidity shaker (Minitron-INFORS; Biogen, Spain). After 48 h, 160 μl of expression medium was added to each well, followed by culture for an additional 48 h. Finally, 20-μl portions of the supernatants were screened for activity with the FOX and HRP-ABTS assays using veratryl or *p*-methoxybenzyl alcohol as the substrate as described below. One unit of AAO activity is defined as the amount of enzyme that converts 1 μmol of alcohol to aldehyde with the stoichiometric formation of H_2O_2 per min under the reaction conditions.

Chemical (direct) FOX assay. Aliquots of 20 μl of yeast supernatants were transferred with liquid handler robotic station Freedom EVO (Tecan, Männedorf, Switzerland) and incubated with 20 μl of substrate (2 mM *p*-methoxybenzyl alcohol or 10 mM veratryl alcohol in 100 mM phosphate buffer [pH 6.0]) for 30 min at room temperature, and then 160 μl of FOX reagent was added with a Multidrop Combi-Reagent dispenser (Thermo Scientific, Waltham, MA) to assess the AAO H_2O_2 production [final concentration of FOX mixture in the well: 100 μM xylenol orange, 250 μM $Fe(NH_4)_2(SO_4)_2$, and 25 mM H_2SO_4] (27). Plates were recorded in endpoint mode at 560 nm using a spectrophotometer SpectraMax 384 Plus (Molecular Devices, Sunnyvale, CA); it required ~20 min of incubation to develop an intense and stable colorimetric response. The relative activities were calculated from the difference between the absorbance value after incubation to that of the initial measurement normalized to the parental type for each plate. To enhance method sensitivity, several additives may be added to the reagent, such as organic cosolvents (DMSO, ethanol, and methanol) or sorbitol (28). In our case, the response was amplified by adding a final concentration of 100 mM sorbitol, which acts as chain amplifier generating additional ferric ions to increase the response of the method (29). The assay was validated by determining the coefficient of variance, the linearity of the response and the detection limit. The detection limit was calculated by the blank determination method on a 96-well plate with triplicate standards (0, 0.5, 1, 1.5, 2, 2.5, 3, and 4 μM H_2O_2) and several portions of supernatants from *S. cerevisiae* $URA3^-$ lacking plasmid (30). FOX signal stability was tested with different H_2O_2 concentrations (0, 2, 4, 6, 8, 10, 15, and 18 μM) for 300 min at 24°C.

Enzymatic (indirect) HRP-ABTS assay. Aliquots of 20 μl of yeast supernatants were added to 180 μl of HRP-ABTS reagent (final concentrations of HRP-ABTS reagent in the well: 1 mM *p*-methoxybenzyl alcohol or 5 mM veratryl alcohol, 2.5 mM ABTS, 1 μg of HRP/ml in 100 mM phosphate buffer [pH 6.0]) dispensed with a Multidrop Combi-Reagent dispenser. The plates were incubated at room temperature and measured in endpoint or kinetic mode at 418 nm ($\varepsilon_{ABTS^{\cdot+}} = 36{,}000\ M^{-1}\ cm^{-1}$).

The dual HTS assay incorporated two consecutive rescreenings to rule out the selection of false positives.

(i) First rescreening. Aliquots of 5 μl of the best clones of the screening were transferred to new sterile 96-well plates with 50 μl of minimal medium per well. Columns 1 and 12 plus rows A and H were not used to prevent the appearance of false positives. After 24 h of incubation at 30°C and 225 rpm, 5-μl portions were transferred to the adjacent wells, followed by further incubation for 24 h. Finally, 160 μl of expression medium was added, and the plates were incubated for 48 h. Accordingly, each mutant was grown in four independent wells. The parental type was subjected to the same procedure (lane D, wells 7 to 11). Plates were assessed according to the same HTS protocol of the screening described above.

(ii) Second rescreening. An aliquot from the best clones from the first rescreening was inoculated in 3 ml of YPD medium, followed by incubation at 30°C for 24 h at 225 rpm. The plasmids from these cultures were recovered with a Zymoprep yeast plasmid miniprep kit I. Since the product of the Zymoprep was impure and the DNA extracted was very low concentrated, the shuttle vectors were transformed into supercompetent *E. coli* XL2-Blue cells and plated onto LB-ampicillin (LB-amp) plates. Single colonies were selected to inoculate 5 ml of LB-amp medium and incubated overnight at 37°C and 225 rpm. The plasmids from the best mutants and the parental type were extracted (NucleoSpin plasmid kit) and transformed into *S. cerevisiae*. Five colonies for each mutant were picked and rescreened as described above.

AAO production and purification. (i) Production of recombinant AAO variants in *S. cerevisiae*. A single colony from the *S. cerevisiae* clone containing the AAO fusion gene was picked from a SC dropout plate, inoculated in SC medium (20 ml) and incubated for 48 h at 30°C and 220 rpm (Minitron-INFORS, Biogen Spain). An aliquot of cells was removed and used to inoculate minimal medium (100 ml) in a 500-ml flask (optical density at 600 nm [OD_{600}] = 0.25). The cells completed two growth phases (6 to 8 h; OD_{600} = 1), and then expression medium (900 ml) was inoculated with the preculture (100 ml; OD_{600} of 0.1). After incubation for 72 h at 25°C and 220 rpm (maximal AAO activity; OD_{600} = 25 to 30), the cells were recovered by centrifugation at 4,500 rpm and 4°C (Avanti J-E centrifuge; Beckman Coulter, Inc., Brea, CA), and the supernatant was double filtered (using both a glass membrane filter and a nitrocellulose membrane [0.45-μm pore size]).

(ii) Purification of AAO mutant. AAO (FX7 variant) was purified by FPLC (ÄKTA purifier; GE Healthcare, United Kingdom). The crude extract was concentrated and dialyzed in 20 mM piperazine buffer (buffer P [pH 5.5]) by tangential ultrafiltration (Pellicon; Millipore, Temecula, CA) through a 10-kDa-pore-size membrane (Millipore) by means of a peristaltic pump (Masterflex Easy Load; Cole-Parmer, Vernon Hills, IL). The sample was filtered and loaded onto a weak anion-exchange column (HiTrap Q FF; GE Healthcare) preequilibrated with buffer P and coupled to the ÄKTA purifier system. The proteins were eluted with a linear gradient of buffer *P* + 1 M NaCl in two phases at a flow rate of 1 ml/min: from 0 to 50% in 15 min and from 50 to 100% in 2 min. Fractions with AAO activity

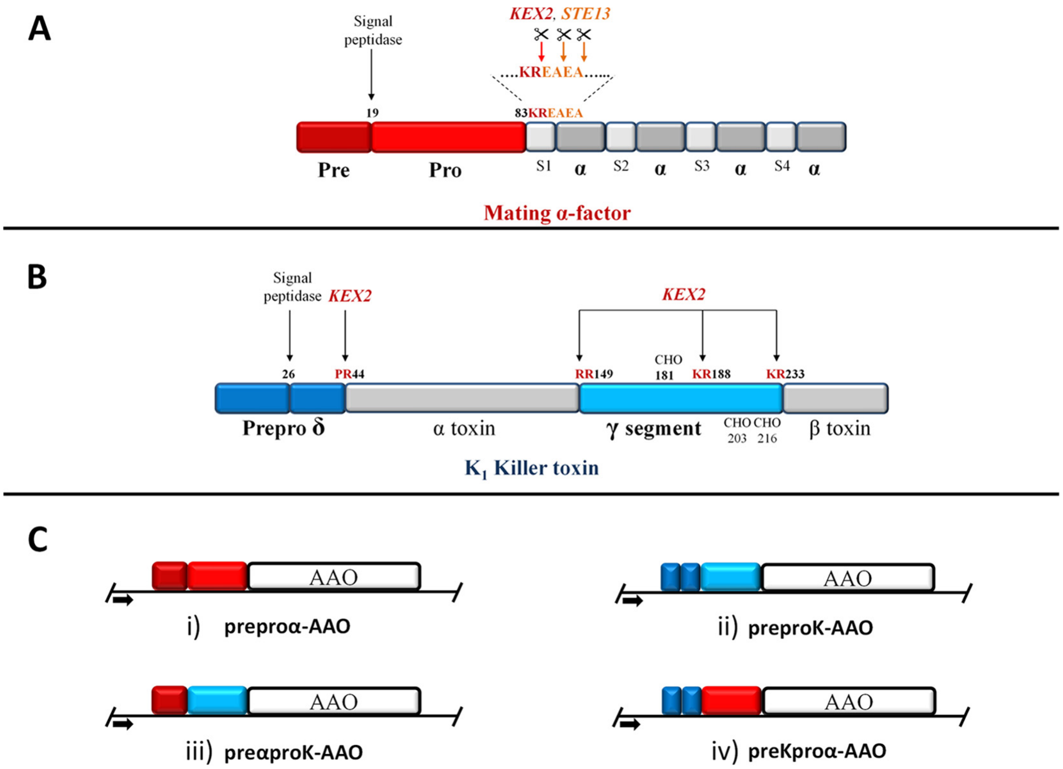

FIG 1 Prepro-leaders used and chimeric signal peptides engineered for functional AAO expression in *S. cerevisiae*. (A) Mating α-factor; (B) K1 killer prepro-toxin; (C) AAO fusions for functional expression. The different processing sites for the KEX2 and STE13 signal peptidases are indicated in each case. The yeast mating pheromone α prepro-polyprotein precursor contains a hydrophobic N-terminal pre-sequence (dark red), followed by an N-glycosylated pro-sequence (red). The K1 killer toxin is derived from a 316 residue prepro-toxin. The unprocessed precursor consists of a prepro(δ) sequence (dark blue) that contains a 26-residue signal peptide. The γ segment (light blue) separating the alpha- and beta-toxin subunits was also used to engineer the chimeras.

were pooled, dialyzed against buffer P, concentrated, and loaded onto a high-resolution resin, strong-anion-exchange column (Biosuite MonoQ 10 cm; Waters, Milford, MA) preequilibrated in buffer P. The proteins were eluted with a linear gradient from 0 to 0.5 M NaCl in two phases at a flow rate of 1 ml/min: from 0 to 50% in 20 min and from 50 to 100% in 2 min. Fractions with AAO activity were pooled, dialyzed against buffer 20 mM phosphate buffer (pH 6.0), concentrated, and further purified by high-pressure liquid chromatography with a Superose 12 HR 10/30 molecular exclusion column (Amersham Bioscience) preequilibrated with 150 mM NaCl in phosphate buffer (pH 6.0) at a flow rate of 0.5 ml/min. The fractions with AAO activity were pooled, dialyzed against buffer (20 mM phosphate buffer [pH 6.0]), concentrated, and stored at −20°C. Throughout the purification protocol the fractions were analyzed by SDS-PAGE on 10% gels in which the proteins were stained with Protoblue Safe (National Diagnostics, USA). All protein concentrations were calculated using Bio-Rad protein assay reagent and bovine serum albumin (BSA) as the standard for the protein concentration.

(iii) Production and purification of native AAO from *E. coli*. Native heterologous AAO expressed in *E. coli* after *in vitro* refolding ($_{Ec}$AAO) was produced and purified as described elsewhere (17).

Biochemical characterization. (i) MALDI-TOF-MS analysis and pI determination. The matrix-assisted laser desorption ionization–time of flight mass spectrometry (MALDI-TOF-MS) experiments were performed on an Autoflex III MALDI-TOF-TOF instrument with a Smartbeam laser (Bruker Daltonics). The spectra were acquired using a laser power just above the ionization threshold, and the samples were analyzed in the positive-ion detection and delayed extraction linear mode. Typically, 1,000 laser shots were summed into a single mass spectrum. External calibration was performed using the BSA from Bruker, covering the range from 15,000 to 70,000 Da. Purified FX7 (8 μg) was subjected to two-dimensional electrophoresis gel in order to determine the pI.

(ii) N-terminal analysis. Purified AAO was subjected to SDS-PAGE, and the protein band was blotted onto polyvinylidene difluoride (PVDF) membranes. The PVDF membrane was stained with Coomassie brilliant blue R-250, and then the enzyme band was excised and processed for N-terminal amino acid sequencing on a precise sequencer at the core facilities of the Helmholtz Centre for Infection Research, Germany.

(iii) Determination of kinetic thermostability (T_{50}). Appropriate dilutions of purified FX7 and $_{Ec}$AAO were prepared for the assay, while the samples of parental preαproK-AAO were obtained from the crude supernatants. A temperature gradient scale ranging from 30 to 80°C was established as follows: 30.0, 31.4, 34.8, 39.3, 45.3, 49.9, 53, 55, 56.8, 59.9, 64.3, 70.3, 75, 78.1, and 80°C. This gradient profile was achieved using a thermocycler (Mycycler). After 10 min of incubation, FX7 and $_{Ec}$AAO samples were removed and chilled on ice for 10 min, followed by further incubation at room temperature for 5 min. Finally, 20-μl samples were added to 180-μl volumes of 100 mM sodium phosphate buffer (pH 6.0) containing 1 mM *p*-methoxybenzyl alcohol, and the activity was measured as anisaldehyde production by determining the absorption at 285 nm (ε_{285} = 16,950 M^{-1} cm^{-1}). In the case of parental preαproK-AAO supernatants, the samples were subjected to an HRP-ABTS assay described above for the screening. Thermostability values were calculated from the ratio between the residual activities incubated at different temperature points and the initial activity at room temperature. The T_{50} value was determined by the transition midpoint of the inactivation curve of the protein as a function of temperature, which in our case was defined as the temperature at which the enzyme lost 50% of its activity after an incubation of 10 min. All reactions were performed by triplicate.

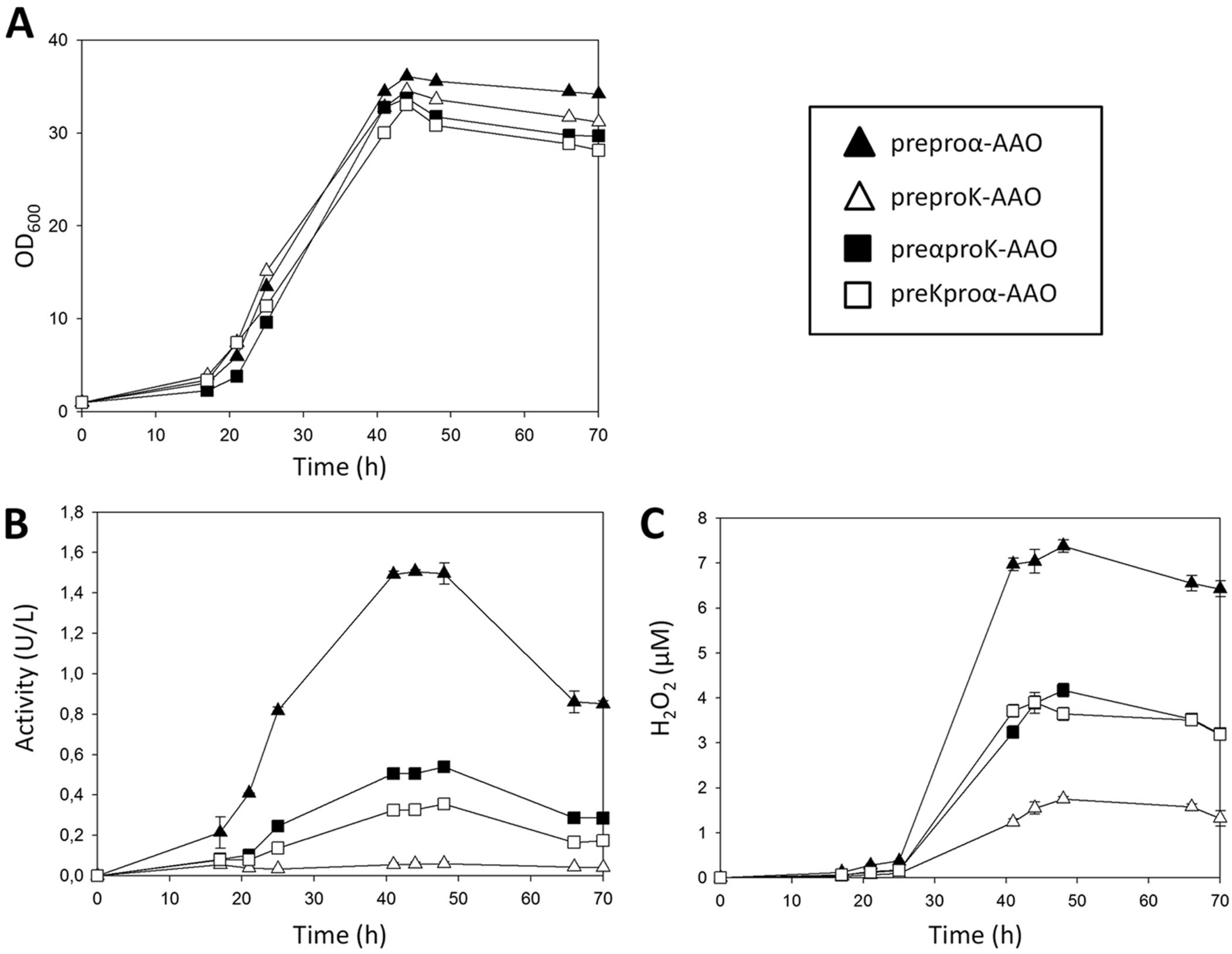

FIG 2 Expression of the AAO fusions in *S. cerevisiae*. (A) Shake flask fermentation growth curves; (B) AAO activity measured in an HRP-ABTS assay; (C) H_2O_2 production measured in a FOX assay. The preproα-AAO fusion achieved the highest yields in terms of cell growth and enzymatic activity (OD$_{600}$ = 36; 1.5 U/liter after 44 h), followed by the preαproK-AAO, preKproα-AAO, and preproK-AAO fusions. Clone activity and H_2O_2 production were evaluated in triplicate, and each point includes the standard deviation.

(iv) Thermoactivity (T_a). Enzyme dilutions of purified FX7 (33 nM, final concentration) and $_{Ec}$AAO (18 nM, final concentration) were prepared in such a way that aliquots of 20 μl gave rise to a linear response in kinetic mode. The optimum temperature for activity was estimated in prewarmed 96-well reading plates (Labnet VorTemp 56 Shaking Incubator; Labnet International, USA) with 100 mM sodium phosphate (pH 6.0) containing 1 mM *p*-methoxybenzyl alcohol at various corresponding temperatures (25, 30, 40, 50, 60, 70, 80, 90, and 99°C), followed by incubation in an Eppendorf Thermomixer Comfort apparatus (Thermo Fisher Scientific). Reactions were performed by triplicate and *p*-methoxybenzyl alcohol oxidation, followed by aldehyde production at 285 nm.

(v) Kinetic parameters. Kinetic constants for AAO were estimated in 100 mM sodium phosphate (pH 6.0). The final enzyme concentrations used were as follows: with *p*-methoxybenzyl alcohol, 33 and 18 nM for FX7 and $_{Ec}$AAO, respectively; with veratryl alcohol, 38 and 32 nM for FX7 and $_{Ec}$AAO, respectively; with benzyl alcohol, 62 and 47 nM for FX7 and $_{Ec}$AAO, respectively; and with 2,4-hexadien-1-ol, 15 and 4 nM for FX7 and $_{Ec}$AAO, respectively. Reactions were performed in triplicate, and substrate oxidations were monitored by measuring the absorption at 285 nm for *p*-methoxybenzyl alcohol (ε_{285} = 16,950 M^{-1} cm^{-1}), 310 nm for veratryl alcohol (ε_{310} = 9,300 M^{-1} cm^{-1}), 250 nm for benzyl alcohol (ε_{250} = 13,800 M^{-1} cm^{-1}), and 280 nm for 2,4-hexadien-1-ol (ε_{280} = 30,140 M^{-1} cm^{-1}). Steady-state kinetic parameters were determined by fitting the initial reactions rates at different substrate concentrations to the Michaelis-Menten equation for one substrate, $v/e = k_{cat} \cdot S/(K_m + S)$, where e represents the enzyme concentration, k_{cat} is the maximal turnover rate, S is the substrate concentration, and K_m is the Michaelis constant. The data were fit using SigmaPlot 10.0 (Systat Software, Inc., Richmond, CA).

(vi) pH activity and stability profiles. Appropriate dilutions of enzyme samples were prepared in such a way that aliquots of 20 μl yielded a linear response in kinetic mode. The optimum pH activity was determined using 100 mM citrate-phosphate-borate buffer at different pH values (2.0, 3.0, 4.0, 5.0, 6.0, 7.0, 8.0, and 9.0) containing the corresponding alcohol concentration (0.3, 5, 9, and 1.2 mM for *p*-methoxybenzyl alcohol, veratryl alcohol, benzyl alcohol, and 2,4-hexadien-1-ol, respectively). To measure pH stability, enzyme samples were incubated at different times over a range of pH values. The residual activity was deduced from the activity before and after incubation with 0.3 mM *p*-methoxybenzyl alcohol in 100 mM phosphate buffer (pH 6.0).

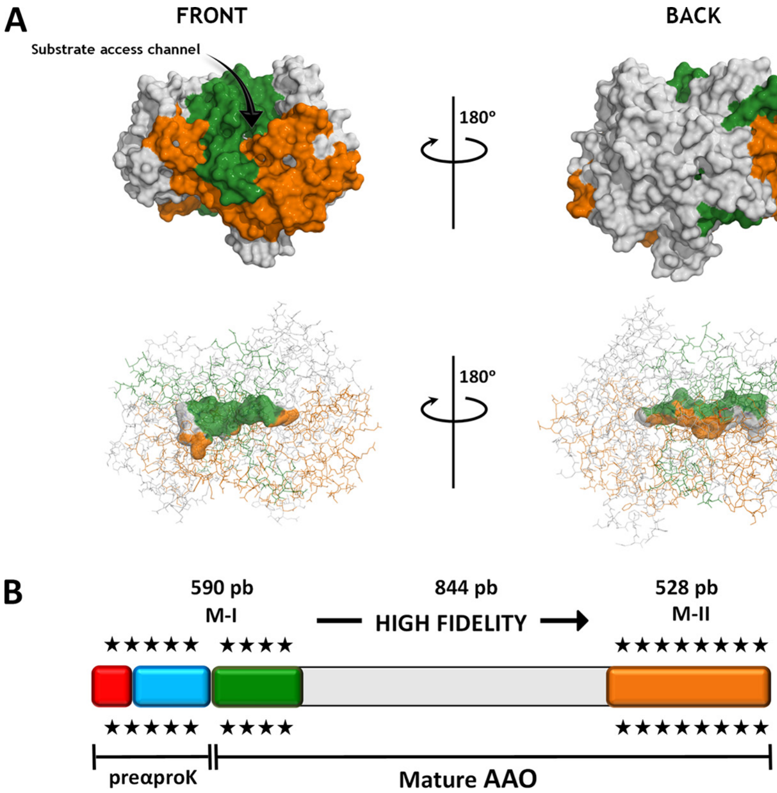

FIG 3 AAO segments for focused directed evolution. (A) The AAO structure is shown in front and back views as a surface mode (upper part), along with a detailed view of the FAD cavity (lower part). The mutagenic regions M-I and M-II are highlighted in green and orange, respectively. The gray region corresponds to the mutation-free segment. (B) The fusion gene preαproK-AAO is shown in color boxes (red and blue). Mutagenic region M-I contains preα (red box)-proK (blue box) signal peptide and the first 109 amino acid residues of mature AAO (green box). The mutagenic region M-II is shown as an orange box, and in gray is the region amplified with high-fidelity polymerase. Stars indicate the mutagenic regions in the fusion gene.

(vii) Protein modeling. The crystal structure of the AAO from *P. eryngii* at a resolution of 2.55 Å (Protein Data Bank Europe [PDB] accession number 3FIM [31]) was used for the FX7 mutant homology model, obtained by PyMol (Schrodinger, LLC [http://www.pymol.org]).

(viii) DNA sequencing. All genes were verified by DNA sequencing (using a BigDye Terminator v3.1 cycle sequencing kit). The primers used were common to the four constructions: sense primers RMLN and AAOsec1F (5′-GTGGATCAACAGAAGATTTCGATCG-3′) and antisense primers RMLC (5′-GCTTACATTCACGCCCTCCC-3′), AAOsec2R (5′-GTGGTTA GCAATGAGCGCGG-3′), and AAOsec3R (5′-GGAGTCGAGCCTCTGCC CCT-3′).

RESULTS AND DISCUSSION

Construction of chimeric signal prepro-leaders. In terms of yeast expression, the replacement of native signal peptides to foster foreign protein secretion has been used widely for years. Recently, the directed evolution of the α-factor prepro-leader permitted the functional expression of antibodies (32) and different classes of ligninases (including high-redox potential laccases, versatile peroxidases, and unspecific peroxygenases) (18–22). In the present study, the prepro-leaders from the mating α-factor and the K_1 killer toxin, along with their chimeric combinations, were tailored and attached to the native AAO for functional expression and directed evolution. The mating α-factor signal sequence is formed by 19 and 64 amino acids from the pre- and pro-leaders, respectively (33–35) (Fig. 1A). The pre-leader initiates endoplasmic reticulum translocation, and it is finally removed by the action of a signal peptidase that cuts between residues 19 and 20. The pro-leader contains three Asn-linked glycosylation sites, and it is thought to be involved in the folding and maturation of the protein before it is packed into vesicles for exocytosis. The pro-leader is processed in the Golgi compartment by the action of the KEX2, STE13, and KEX1 proteases, although the latter is not needed for heterologous protein secretion. The K_1 killer prepro-toxin is preceded by a prepro-sequence of 44 residues, prepro(δ), that undergoes similar processing as the α-factor prepro-leader, albeit without the requirement of STE13 and KEX1 activity (24, 25, 36) (Fig. 1B). The prepro-toxin contains an internal γ-segment of 85 residues with three extra KEX2 recognition sites for processing in the Golgi compartment. Bearing in mind the common features of these two prepro-leaders in terms of processing and secretion, the following four fusion constructs were attached to the mature AAO (Fig. 1C): (i) the preproα-AAO containing the full α-factor prepro-leader, (ii) the preproK-AAO formed by the prepro(δ) of K_1 toxin connected to a truncated version (64 residues) of the γ-segment known to be important for correct processing (the truncated segment stretched from positions 169 to 233 and preserved the three N-glycosylation sites: N181, N203, and N216 [24]), (iii) the chimeric preαproK-AAO comprising the α-factor pre-leader fused to the truncated γ-segment, and (iv) the chimeric preKproα-AAO formed by the prepro(δ) of the K_1 toxin linked to the α-factor pro-leader. In addition, we modified the prepro(δ)-containing constructs, fusions ii and iv, by site-directed mutagen-

TABLE 1 Selected mutants of preαproK-AAO libraries

Variant	Library	Mutation	Location	Secondary motif	Total activity improvement (fold)[a]	T_{50} (°C)
FX7	M-I-II	${}_{\mathrm{CAC}}\mathrm{H91N}_{\mathrm{AAC}}$	FAD-binding domain	Loop	96	64.3
13H2	M-IV	${}_{\mathrm{ATA}}\mathrm{I194V}_{\mathrm{GTA}}$	Substrate-binding domain	Loop	4.9	60.8
10G5	M-IV	${}_{\mathrm{TTG}}\mathrm{L170\ M}_{\mathrm{ATG}}$	Substrate-binding domain	Alpha helix	4.9	60.5
7A11	M-II	${}_{\mathrm{GAT}}\mathrm{D341N}_{\mathrm{AAT}}$	Substrate-binding domain	Alpha helix	4.6	59.3
4C7	M-II	${}_{\mathrm{AGA}}\mathrm{R481S}_{\mathrm{AGT}}$	Substrate-binding domain	Loop	4.5	61.5
12G12	M-I	${}_{\mathrm{ACA}}\mathrm{T[50K]A}_{\mathrm{GCA}}\ {}_{\mathrm{AGC}}\mathrm{S88T}_{\mathrm{ACC}}$	Signal peptide; FAD-binding domain	Loop	1.9	61.8
PreαproK-AAO (parental type)					1	58.8
${}_{Ec}$AAO						47.5

[a] The total activity improvement over parental type was estimated with 2 mM *p*-methoxybenzylalcohol as the substrate in 100 mM phosphate buffer (pH 6.0).

esis to modify the P43-R44 KEX2 recognition site to K43-R44, since this substitution was associated with a 50-fold enhancement in KEX2 catalytic efficiency (37).

The fusion constructs were spliced in *S. cerevisiae*, and taking advantage of the high frequency of *in vivo* homologous DNA recombination of this yeast overlapping areas of ~50 bp guaranteed correct DNA assembly of the different genetic elements and the linearized plasmid without altering the open reading frame (38). The activity of each AAO construct against veratryl alcohol was assayed in microscale fermentations (96-well plates), and the four fusions produced detectable AAO activity in the culture broth, which was consistent in the two colorimetric assays used (see below). The secretion driven by the corresponding constructs was as follows: preproα-AAO > preαproK-AAO > preKproα-AAO > preproK-AAO. We verified by DNA sequencing that the constructs did not incorporate mutations in the mature protein or in the prepro-sequences (apart from the aforementioned P43K substitution) and that all of the elements were properly assembled *in vivo* as intended. Fermentations were translated from the high-throughput format to larger volumes (10 ml) for each construct studied. Irrespective of the substrate (*p*-methoxybenzyl or veratryl alcohol), the hierarchy of activity of the fusion genes was maintained: preproα-AAO (1.5 U/liter), preαproK-AAO (0.5 U/liter), preKproα-AAO (0.35 U/liter), and preproK-AAO (0.06 U/liter) (Fig. 2). We tried to enhance the membrane permeability of the yeast by adding ethanol to the expression medium, and yet the activity detected was 5-fold lower, which was probably due to growth inhibition as a consequence of changes in yeast physiology and the redox balance of the medium (39).

TABLE 2 Biochemical properties of recombinant native ${}_{Ec}$AAO and evolved AAO (FX7 mutant)

Biochemical properties	${}_{Ec}$AAO	FX7 mutant
Molecular mass (Da)[a]		
SDS-PAGE	65,000	120,000
MALDI-TOF-MS	61,847[c]	61,485
Amino acid composition	61,088	60,934
Glycosylation degree (%)		50
Thermal stability (T_{50} [°C])	47.5	64.3
pI	3.9	4.3
N-terminal end sequence	MADFDYVVG[d]	ADFDYVVVG
Sp act (U/mg)[b]	74	24
Secretion level (mg/liter)		2

[a] Masses were estimated based on SDS-PAGE, MALDI-TOF-MS after deglycosylation with PNGase F, or the amino acid composition.

[b] That is, the specific activity for *p*-methoxybenzyl alcohol.

[c] This information was obtained from reference 17.

[d] Met1 (M) was added to the N-terminal end for cloning in *E. coli*.

Directed evolution of preαproK-AAO. Of the four AAO constructs, the preproα-AAO produced the highest secretion, although the risk of inefficient processing of the α-pro-leader by STE13 ruled out its use. Given that little STE13 is found in the Golgi apparatus, the secreted heterologous protein maintains an extra EAEA spacer dipeptide at the N terminus, as previously demonstrated in the evolution of other oxidoreductases fused to preproα (laccases and peroxidases) (18, 20, 40). This problem may be circumvented by (i) suppressing the cleavage site for STE13, (ii) enhancing the expression of STE13, or (iii) deleting the whole α-factor pro-leader. However, this may drive the intracellular accumulation and/or the secretion of partially processed forms, no matter the strategy used (41). It is worth noting that the N-terminal of AAO interacts with the FAD molecule through a network of H bonds, such that an extra-N-terminal sequence could modify these contacts, jeopardizing catalysis (30, 42). Since a correct processing is crucial to conserve the integrity and orientation of the attached FAD cofactor in the tertiary structure of AAO, the preαproK-AAO construct, in which the proK fragment is exclusively processed by the abundant KEX2, was chosen as the point of departure for engineering.

To enhance the activity and secretion of the preαproK-AAO in yeast several mutant libraries were constructed by conventional and guided-directed evolution. The latter was performed by MORPHING, a one-pot focused domain mutagenesis method supported by the *in vivo* gap repair mechanism of *S. cerevisiae* (26). By MORPHING, we can direct random mutations and recombination events to short sequences, while keeping the remaining parts of the gene unaltered. Two protein segments of the preαproK-AAO (M-I, Met[α1]-Val109; M-II, Phe392-Gln566) were studied simultaneously through this approach (Fig. 3). The M-I segment includes the preαproK (to evolve the chimeric leader for secretion) plus a region of the mature AAO (Ala1-Val109) that contains the FAD-binding domain at its N terminus, along with several structural determinants in the nearby substrate access channel: Val54, Pro55, His91, Tyr92, Pro79, and Val90 (4, 6, 30). The M-II segment contains the catalytic pocket, including the His546 involved in substrate positioning, the catalytic base His502, and the aromatic residues Phe397 and Phe501. These latter amino acids create a hydrophobic gate in conjunction with Tyr92 of the M-I segment, thereby blocking access to the active channel (1, 4, 30). A total of three focused mutant libraries were

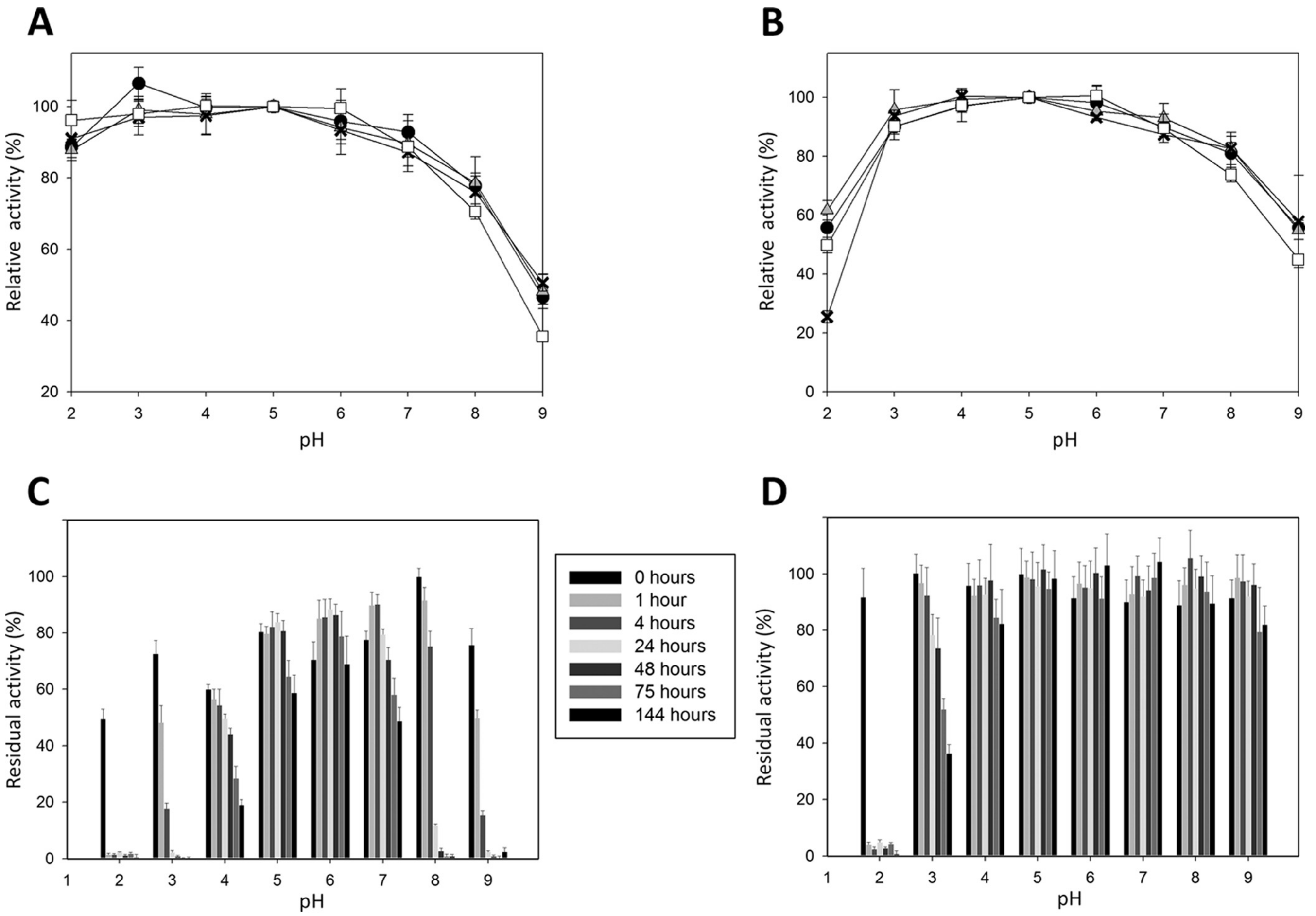

FIG 4 pH activity and stability. (A and B) pH activity profiles for $_{Ec}$AAO (A) and FX7 (B). Activities were measured in 100 mM citrate-phosphate-borate buffer at different pH values. Symbols: black circles, *p*-methoxybenzyl alcohol; gray triangles, veratryl alcohol; crosses, benzyl alcohol; white squares, 2,4-hexadien-1-ol. (C and D) pH stability of $_{Ec}$AAO (C) and FX7 (D). Enzymes samples were incubated in 100 mM citrate-phosphate-borate buffer at different pH values, and the residual activity was measured with 0.3 mM *p*-methoxybenzyl alcohol in 100 mM phosphate buffer (pH 6.0). The results represent the means and standard deviations of three independent experiments.

constructed (single M-I and M-II, as well as M-I-II combined), in addition to one conventional mutant library (targeting the full preαproK-AAO by random mutation and DNA recombination; M-IV). Mutational loads were adjusted to introduce 1 to 3 amino acid changes per protein, and the four libraries were explored with a highly sensitive dual HTS system to detect AAO activity irrespective of the substrate. This method coupled a standard HRP-ABTS indirect colorimetric assay to a direct chemical method (FOX) based on the Fenton reaction in order to detect H_2O_2. The latter is typically used to measure H_2O_2 in biological fluids, and more recently to determine L-amino acid oxidase and lipoxygenase activities (27, 28, 43, 44), but to our best knowledge it has never been used to evolve H_2O_2-producing enzymes. The limit of sensitivity of the FOX assay was 2 μM H_2O_2, and it was further shifted to 0.4 μM H_2O_2 through the inclusion of sorbitol to propagate the response (see Materials and Methods for details). Two consecutive rescreenings were carried out to avoid the selection of false positives. After exploring ~5,000 clones, we identified five mutants with a total activity improvement over the parental type ranging from 2- to 5-fold and, significantly, the FX7 variant (H91N) from the combined M-I-II MORPHING displayed a dramatic 96-fold improvement in total activity with respect to the parental type (Table 1). The remaining mutations found in these variants (i.e., T[$K_1$50]A, S88T, L170M, I194V, D341N, and R481S) are located at a distance of >20 residues from one another, making them suitable candidates for future DNA shuffling studies or to be evaluated by site-directed recombination (see Fig. S1 in the supplemental material).

Biochemical characterization. The FX7 variant was purified to homogeneity and characterized biochemically. Since the weak secretion of parental preαproK-AAO (0.5 U/liter) in *S. cerevisiae* hindered its purification, the properties of purified FX7 were compared to that of the native AAO heterologous expressed in *E. coli* after *in vitro* refolding ($_{Ec}$AAO). FX7 was secreted at 2 mg/liter with a specific activity for *p*-methoxybenzyl alcohol of 24 U/mg (Table 2). Both FX7 and $_{Ec}$AAO enzymes showed similar kinetic constants, as well as pH activity profiles, with all of the substrates tested (Fig. 4A and B), although turnover rates (k_{cat}) were lower if the enzyme is expressed in *S. cerevisiae* instead of *E. coli* (Table 3). The N-terminal sequencing of FX7 confirmed the correct cleavage of the chimeric preαproK-leader, avoiding unwanted modifications at the N terminus. FX7 was heavily glycosylated (~50% gly-

TABLE 3 Kineticparameters of native $_{Ec}$AAO and evolved AAO (FX7 mutant)[a]

		$_{Ec}$AAO		FX7	
Substrate	Kinetic constant	Mean	SEM	Mean	SEM
p-Methoxybenzyl alcohol	K_m (mM)	0.035	0.001	0.034	0.001
	k_{cat} (s^{-1})	105	6	54	4
	k_{cat}/K_m (s^{-1} mM^{-1})	2979	66	1562	44
Veratryl alcohol	K_m (mM)	0.504	0.043	0.388	0.023
	k_{cat} (s^{-1})	66	2	28	1
	k_{cat}/K_m (s^{-1} mM^{-1})	131	8	71	3
Benzyl alcohol	K_m (mM)	0.770	0.011	0.510	0.001
	k_{cat} (s^{-1})	22	1	19	1
	k_{cat}/K_m (s^{-1} mM^{-1})	28	2	36	3
2,4-Hexadien-1-ol	K_m (mM)	0.087	0.001	0.059	0.004
	k_{cat} (s^{-1})	136	3	52	1
	k_{cat}/K_m (s^{-1} mM^{-1})	1555	67	866	53

[a] Steady-state constants were estimated in 100 mM sodiumphosphate buffer (pH 6) at 24°C. All reactions were performed intriplicate.

cosylation), adopting a molecular mass of ~120,000 Da, and yet after deglycosylation the AAO smear collapsed to a single band of around 61,000 Da, as confirmed by MALDI-TOF analysis (Table 2 and see Fig. S2 in the supplemental material). It is well known that *S. cerevisiae* tends to hyperglycosylate heterologous proteins; possibly, a slow transit of AAO through the Golgi compartment before its packing into vesicles for exocytosis facilitates the addition of long chains of mannose moieties that can cover the protein surface as reported for many other hyperglycosylated enzymes in *S. cerevisiae* (34). The use of glycosylation-deficient *S. cerevisiae* strains (e.g., a Δ*kre2* mutant that is only capable of attaching smaller mannose oligomers [45]) could have lightened the strong AAO glycosylation, albeit at the possible cost of endangering secretion, given that the *S. cerevisiae* strain used in our study is protease deficient. Hyperglycosylation can exert a beneficial stability effect. Indeed, the T_{50} (the temperature at which the enzyme retains 50% of its initial activity after a 10-min incubation) was ~11°C above that of $_{Ec}$AAO for all of the AAO variants expressed in *S. cerevisiae*, with a further 5.5°C increase for FX7 that must be exclusively attributed to beneficial H91N mutation (from 47.5 to 64.3°C) (Table 1 and Fig. 5A). This high thermostability correlated with a stronger thermoactivity (i.e., the optimum temperature for activity [T_a]). Thus, the T_a of FX7 was over 80% at 80°C, whereas $_{Ec}$AAO conserved 22% activity at the same temperature (Fig. 5B). Notably, FX7 still maintained ~60 and 20% activities at 90 and 100°C, respectively, whereas the $_{Ec}$AAO T_a was negligible. Moreover, FX7 showed a broad pH stability in the range of 3 to 9 (Fig. 4C and D). After 144 h of incubation, the residual FX7 activities were ~80 and 38% at pH 3 and 9, respectively, whereas the residual $_{Ec}$AAO activities at those pH values were negligible.

It is worth noting that His91 is a deviation in *P. eryngii* and *P. pulmonarius* AAO, since an Asn lies at this position in virtually all members of the GMC superfamily, including 70 putative AAO sequences from different basidiomycetes (10) (Fig. 6A). Hence, restoring this consensus mutation has been crucial to improve heterologous AAO expression in yeast while enhancing thermostability, which is in excellent agreement with previous reports on ancestral library design by introducing consensus/ancestor mutations to improve the heterologous expression and thermostability of different enzymes (46–48). Indeed, the discovery of a consensus mutation by focused evolution, rather than using the consensus method based on sequence alignment or an inference phylogenetic analysis for ancestor mutations, highlights the potential of random domain mutagenesis approaches to reveal beneficial consensus/ancestor mutations. H91N lies in the flavin attachment loop region, a common motif in GMC oxidoreductases. Found on the *si*-face of the isoalloxazine ring, hydrophobic interactions of this residue maintain the cofactor in a bent conformation (49). In *P. eryngii* AAO, His91 interacts with Arg206 (Arg/Lys of other GMC proteins), and it stabilizes the flavin ring conformation (Fig. 6). The substitution of a positively charged His by a polar uncharged Asn may alter these contacts in *P. eryingii* AAO, which could aid the attachment of FAD and enhance the stability and functional expression. The two latter properties are strongly connected, and it is highly likely that the improved stability allows more AAO to be secreted, as it has been described for many other proteins expressed in yeast (50). Why the N91H substitution arose exclusively in the natural evolution of *P. eryngii* and *P. pulmonarius* AAO is unclear, and yet our results suggest a possible reg-

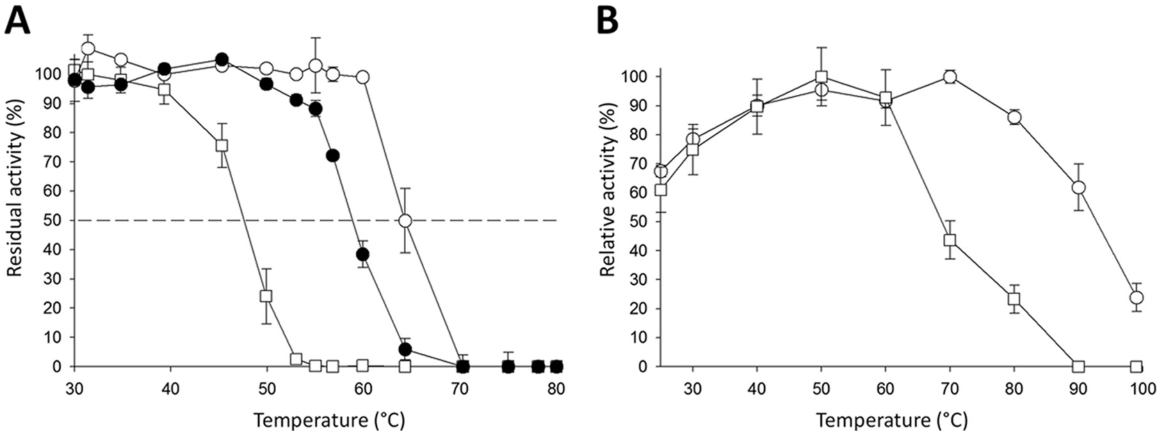

FIG 5 Thermostability and thermoactivity of AAO variants. (A) Thermostability (T_{50}) of FX7 (○), preαproK-AAO parental type (●), and $_{Ec}$AAO (□). (B) Thermoactivity (T_a) of FX7 (○), and $_{Ec}$AAO (□). Each point represents the means and standard deviations of three independent experiments.

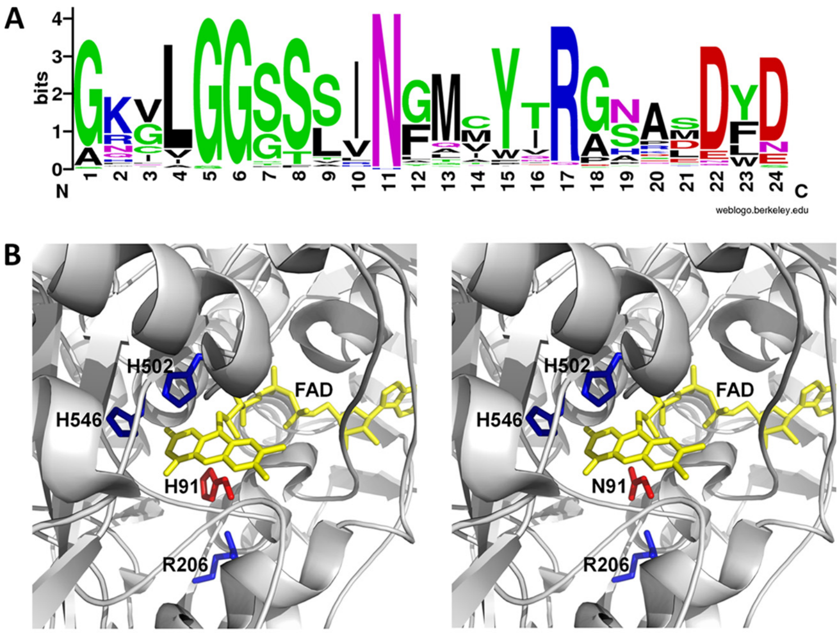

AAO wild type

FX7 mutant

FIG 6 (A) Consensus Asn91 in GMC superfamily. Sequence logo of the GMC signature 1 (prosite PS00623) in 329 GMC sequences from GenBank (http://www.ncbi.nlm.nih.gov/GenBank/), JGI (http://jgi.doe.gov/), and Prosite Expasy (http://prosite.expasy.org/PS00623), including cholesterol oxidase, choline oxidase, aryl-alcohol oxidase, pyridoxine oxidase, methanol oxidase, glucose oxidase and dehydrogenase, pyranose oxidase and dehydrogenase, cellobiose dehydrogenase, L-sorbose-1-dehydrogenase, and hydroxynitrile lyase proteins. (B) N91H mutation in FX7 variant. A molecular model using as the template the *P. eryngii* AAO crystal structure (PDB code 3FIM) was prepared to map the mutation. The residues of the active site His502, His546, and R206 are depicted in blue, FAD is depicted in yellow, and the H91N mutation is depicted in red.

ulation of AAO expression to reduce the inhibition of ligninolytic peroxidases by H_2O_2 (51).

Conclusions and outlook. In this study, the AAO from *P. eryngii* was functionally expressed in *S. cerevisiae* by engineering chimeric prepro-leaders that allowed us to construct and screen mutant libraries in yeast. The particular design of an *ad hoc* chimeric prepro-leader, combined with a focused-directed evolution strategy and a sensitive dual screening assay, has led to obtain an active, highly stable AAO variant that is secreted by yeast as a correctly processed enzyme.

Although hardly used, the biotechnological potential of AAO should not be underestimated. In nature, the gradual release of H_2O_2 by AAO supplies peroxidases with a continuous source of cooxidant for lignin degradation. *In vitro*, this effect can be mimicked by controlling the addition of H_2O_2 with sensors and peristaltic pumps, although with limited success (52). Very recently, we introduced the FX7 variant into episomal bidirectional vectors to coexpress versatile peroxidase-AAO and/or unspecific peroxygenase-AAO (unpublished data). These self-sufficient expression systems could be used to evolve efficient enzymatic cascade reactions (e.g., for the oxidative conversion of 5-hydroxymethylfurfurals into value-added chemicals [53]). Significantly, the FX7 variant and its future offspring could also be included to design an autonomously consolidated bioprocessing yeast, with a full artificial secretome that includes the most important elements of the ligninolytic enzyme consortium. Such a microbe would have a number of potential applications in lignocellulose biorefineries for the production of fuels and commodities (22, 54). Finally, the directed evolution platform presented here is an invaluable tool for protein engineering, which can be applied from the design of efficient stereoselective aryl secondary alcohol oxidases to the synthesis of natural flavors (1).

ACKNOWLEDGMENTS

This study was supported by the European Commission projects Indox-FP7-KBBE-2013-7-613549 and Cost-Action CM1303-Systems Biocatalysis and by the National Projects Dewry (BIO201343407-R) and Cambios (RTC-2014-1777-3).

REFERENCES

1. **Hernandez-Ortega A, Ferreira P, Martinez AT.** 2012. Fungal aryl-alcohol oxidase: a peroxide-producing flavoenzyme involved in lignin degradation. Appl Microbiol Biotechnol **93:**1395–1410. http://dx.doi.org/10.1007/s00253-011-3836-8.
2. **Ruiz-Dueñas FJ, Martinez AT.** 2009. Microbial degradation of lignin: how a bulky recalcitrant polymer is efficiently recycled in nature and how we can take advantage of this. Microb Biotechnol **2:**164–177. http://dx.doi.org/10.1111/j.1751-7915.2008.00078.x.
3. **Ferreira P, Hernandez-Ortega A, Herguedas B, Rencoret J, Gutierrez A, Martinez MJ, Jimenez-Barbero J, Medina M, Martinez AT.** 2010. Kinetic and chemical characterization of aldehyde oxidation by fungal aryl-alcohol oxidase. Biochem J **425:**585–593. http://dx.doi.org/10.1042/BJ20091499.
4. **Ferreira P, Ruiz-Dueñas FJ, Martinez MJ, van Berkel WJH, Martinez AT.** 2006. Site-directed mutagenesis of selected residues at the active site of aryl-alcohol oxidase, an H_2O_2-producing enzyme. FEBS J **273:**4878–4888. http://dx.doi.org/10.1111/j.1742-4658.2006.05488.x.
5. **Ferreira P, Hernandez-Ortega A, Herguendas B, Martinez AT, Medina M.** 2009. Aryl-alcohol oxidase involved in lignin degradation: a mechanistic study based on steady and pre-steady-state kinetics and primary and solvent isotope effects with two different alcohol substrates. J Biol Chem **284:**24840–24847. http://dx.doi.org/10.1074/jbc.M109.011593.
6. **Hernandez-Ortega A, Lucas F, Ferreira P, Medina M, Guallar V, Martinez AT.** 2011. Modulating O_2 reactivity in a fungal flavoenzyme: in-

volvement of aryl-alcohol oxidase Phe-501 contiguous to catalytic histidine. J Biol Chem **286:**41105–41114. http://dx.doi.org/10.1074/jbc.M111.282467.

7. **Hernandez-Ortenga A, Borreli K, Ferreira P, Medina M, Martinez AT, Guallar V.** 2011. Substrate diffusion and oxidation in GMC oxidoreductases: an experimental and computational study on fungal aryl-alcohol oxidase. Biochem J **436:**341–350. http://dx.doi.org/10.1042/BJ20102090.
8. **Hernandez-Ortega A, Ferreira P, Merino P, Medina M, Guallar V, Martinez AT.** 2012. Stereoselective hydride transfer by aryl-alcohol oxidase, a member of the GMC superfamily. Chembiochem **13:**427–435. http://dx.doi.org/10.1002/cbic.201100709.
9. **Hernandez-Ortega A, Lucas F, Ferreira P, Medina M, Guallar V, Martinez AT.** 2012. Role of active site histidines in the two half reactions of the aryl-alcohol oxidase catalytic cycle. Biochemistry **51:**6595–6608. http://dx.doi.org/10.1021/bi300505z.
10. **Ferreira P, Hernandez-Ortega A, Lucas F, Carro J, Herguedas B, Borreli KW, Guallar V, Martinez AT, Milagros M.** 2015. Aromatic stacking interactions govern catalysis in aryl-alcohol oxidase. FEBS J http://dx.doi.org/10.1111/febs.13221.
11. **Bloom JD, Arnold FH.** 2009. In the light of directed evolution: pathways of adaptive protein evolution. Proc Natl Acad Sci U S A **106:**9995–10000. http://dx.doi.org/10.1073/pnas.0901522106.
12. **Turner NJ.** 2009. Directed evolution drives the next generation of biocatalysts. Nat Chem Biol **5:**567–573. http://dx.doi.org/10.1038/nchembio.203.
13. **Jackel C, Hilvert D.** 2010. Biocatalysts by evolution. Curr Opin Biotechnol **21:**753–759. http://dx.doi.org/10.1016/j.copbio.2010.08.008.
14. **Bornscheuer UT, Huisman GW, Kazlauskas RJ, Lutz S, Moore JC, Robins K.** 2012. Engineering the third wave of biocatalysis. Nature **485:**185–194. http://dx.doi.org/10.1038/nature11117.
15. **Varela E, Guillen F, Martinez AT, Martinez MJ.** 2001. Expression of *Pleurotus eryngii* aryl-alcohol oxidase in *Aspergillus nidulans*: purification and characterization of the recombinant enzyme. Biochim Biophys Acta **1546:**107–113. http://dx.doi.org/10.1016/S0167-4838(00)00301-0.
16. **Pourmir A, Johannes TW.** 2012. Directed evolution selection of the host organism. Comp Struct Biotechnol J **2:**e201209012. http://dx.doi.org/10.5936/csbj.201209012.
17. **Ruiz Dueñas FJ, Ferreira P, Martínez MJ, Martínez AT.** 2006. *In vitro* activation, purification, and characterization of *Escherichia coli* expressed aryl-alcohol oxidase, a unique H_2O_2-producing enzyme. Prot Expr Purif **45:**191–199. http://dx.doi.org/10.1016/j.pep.2005.06.003.
18. **Mate D, Garcia-Burgos C, Garcia-Ruiz E, Ballesteros AO, Camarero S, Alcalde M.** 2010. Laboratory evolution of high redox potential laccases. Chem Biol **17:**1030–1041. http://dx.doi.org/10.1016/j.chembiol.2010.07.010.
19. **Camarero S, Pardo I, Cañas AI, Molina P, Record E, Martinez AT, Martinez MJ, Alcalde M.** 2012. Engineering platforms for directed evolution of laccase from *Pycnoporus cinnabarinus*. Appl Environ Microbiol **78:**1370–1384. http://dx.doi.org/10.1128/AEM.07530-11.
20. **Garcia-Ruiz E, Gonzalez-Perez D, Ruiz-Dueñas FJ, Martinez AT, Alcalde M.** 2012. Directed evolution of a temperature, peroxide and alkaline pH tolerant versatile peroxidase. Biochem J **441:**487–498. http://dx.doi.org/10.1042/BJ20111199.
21. **Molina-Espeja P, Garcia-Ruiz E, Gonzalez-Perez D, Ullrich R, Hofrichter M, Alcalde M.** 2014. Directed evolution of unspecific peroxygenase from *Agrocybe aegerita*. Appl Environ Microbiol **80:**3496–3507. http://dx.doi.org/10.1128/AEM.00490-14.
22. **Alcalde M.** 2015. Engineering the ligninolytic enzyme consortium. Trends Biotechnol **33:**155–162. http://dx.doi.org/10.1016/j.tibtech.2014.12.007.
23. **Garcia-Ruiz E, Mate DM, Gonzalez-Perez D, Molina-Espeja P, Camarero S, Martinez AT, Ballesteros AO, Alcalde M.** 2014 Directed evolution of ligninolytic oxidoreductases: from functional expression to stabilization and beyond, p 1–18. *In* Fessner R (ed), Cascade biocatalysis. Wiley-VCH, Weinheim, Germany.
24. **Cartwright C, Zhu Y, Tipper DJ.** 1992. Efficient secretion in yeast based on fragments from K1 killer preprotoxin. Yeast **8:**261–272. http://dx.doi.org/10.1002/yea.320080404.
25. **Zhu Y, Kane J, Zhang X, Zhang M, Tipper DJ.** 1993. Role of the γ component of the preprotoxin in expression of the yeast K1 killer phenotype. Yeast **9:**251–266. http://dx.doi.org/10.1002/yea.320090305.
26. **Gonzalez-Perez D, Molina-Espeja P, Garcia-Ruiz E, Alcalde M.** 2014. Mutagenic organized recombination process by homologous in vivo grouping (MORPHING) for directed enzyme evolution. PLoS One **9:**e90919. http://dx.doi.org/10.1371/journal.pone.0090919.
27. **Gay C, Collins J, Gebicki JM.** 1999. Hydroperoxide assay with the ferric-xylenol orange complex. Anal Biochem **273:**149–155. http://dx.doi.org/10.1006/abio.1999.4208.
28. **Rhee SG, Chang T, Jeong W, Kang D.** 2010. Methods for detection and measurement of hydrogen peroxide inside and outside of cells. Mol Cells **29:**539–549. http://dx.doi.org/10.1007/s10059-010-0082-3.
29. **Bou R, Codony R, Tres A, Decker EA.** 2008. Determination of hydroperoxides in foods and biological samples by the ferrous oxidation-xylenol orange method: a review of the factors that influence the method's performance. Anal Biochem **337:**1–15.
30. **Shrivastava A, Gupta VB.** 2011. Methods for the determination of limit of detection and limit of quantitation of the analytical methods. Chron Young Sci **2:**21–25. http://dx.doi.org/10.4103/2229-5186.79345.
31. **Fernandez IS, Ruiz-Dueñas FJ, Santillana E, Ferreira P, Martinez MJ, Martinez AT, Romero A.** 2009. Novel structural features in the GMC family of oxidoreductases revealed by the crystal structure of fungal aryl-alcohol oxidase. Acta Crystallogr D Biol Crystallogr **65:**1196–1205. http://dx.doi.org/10.1107/S0907444909035860.
32. **Rakestraw JA, Sazinsky SL, Piatesi A, Antipov E, Wittrup KD.** 2009. Directed evolution of a secretory leader for the improved expression of heterologous proteins and full-length antibodies in *Saccharomyces cerevisiae*. Biotechnol Bioeng **103:**1192–1201. http://dx.doi.org/10.1002/bit.22338.
33. **Zsebo KM, Lu HS, Fieschko JC, Goldstein L, Davis J, Duker K, Suggs SV, Lai PH, Bitter GA.** 1986. Protein secretion from *Saccharomyces cerevisiae* directed by the prepro-α-factor leader region. J Biol Chem **261:**5858–5865.
34. **Shuster JR.** 1991. Gene expression in yeast: protein secretion. Curr Opin Biotechnol **2:**685–690. http://dx.doi.org/10.1016/0958-1669(91)90035-4.
35. **Romanos MA, Scorer CA, Clare JJ.** 1992. Foreign gene expression in yeast: a review. Yeast **8:**423–488. http://dx.doi.org/10.1002/yea.320080602.
36. **Schmitt MJ, Breinig F.** 2006. Yeast viral killer toxins: lethality and self-protection. Nat Rev Microbiol **4:**212–221.
37. **Brenner C, Fuller SR.** 1992. Structural and enzymatic characterization of a purified prohormone-processing enzyme: secreted, soluble Kex2 protease. Proc Natl Acad Sci U S A **89:**922–926. http://dx.doi.org/10.1073/pnas.89.3.922.
38. **Gonzalez-Perez D, Garcia-Ruiz E, Alcalde M.** 2012. *Saccharomyces cerevisiae* in directed evolution: an efficient tool to improve enzymes. Bioengineered **3:**1–6. http://dx.doi.org/10.4161/bbug.3.1.19011.
39. **Cortassa S, Aon JC, Aon MA.** 1995. Fluxes of carbon, phosphorylation, and redox intermediates during growth of *Saccharomyces cerevisiae* on different carbon-sources. Biotechnol Bioeng **47:**193–208. http://dx.doi.org/10.1002/bit.260470211.
40. **Mate D, Garcia-Ruiz E, Camarero S, Shubin V, Falk M, Shleev S, Alcalde M.** 2013. Switching from blue to yellow: altering the spectral properties of a high redox potential laccase by directed evolution. Biocatal Biotransformation **31:**8–21. http://dx.doi.org/10.3109/10242422.2012.749463.
41. **Brake AJ.** 1990. α-Factor leader-directed secretion of heterologous proteins from yeast. Methods Enzymol **185:**408–421. http://dx.doi.org/10.1016/0076-6879(90)85036-N.
42. **Dym O, Eisenberg D.** 2001. Sequence-structure analysis of FAD-containing proteins. Protein Sci **10:**1712–1728. http://dx.doi.org/10.1110/ps.12801.
43. **Zu Z, Wang J, Zhou N, Zhao C, Qiu J.** 2013. A highly sensitive method for quantitative determination of L-amino acid oxidase activity based on the visualization of ferric-xylenol orange formation. PLoS One **8:**e82483. http://dx.doi.org/10.1371/journal.pone.0082483.
44. **Kumar KA, Reddy TC, Reddy GV, Reddy DBK, Mahipal SVK, Sinha S, Gaikwad AN, Reddanna P.** 2011. High-throughput screening assays for cycloxygenase-2 and 5-lipoxygenase, the targets for inflammatory disorders. Indian J Biochem Biotechnol **48:**256–261.
45. **Lussier M, Sdicu AM, Bussey H.** 1999. The KTR and MNN1 mannosyltransferase families of *Saccharomyces cerevisiae*. Biochim Biophys Acta **1426:**323–334. http://dx.doi.org/10.1016/S0304-4165(98)00133-0.
46. **Khersonsky O, Rosenblat M, Toker L, Yacobson S, Hugenmatter A, Silman I, Sussman JL, Aviram M, Tawfik D.** 2009. Directed evolution of serum paraoxonase PON3 by family shuffling and ancestor/consensus mutagenesis, and its biochemical characterization. Biochemistry **48:**6644–6654. http://dx.doi.org/10.1021/bi900583y.
47. **Jochens H, Aerts D, Bornscheuer UT.** 2010. Thermostabilization of an

esterase by alignment-guided focused directed evolution. Protein Eng Des Sel **23:**903–909. http://dx.doi.org/10.1093/protein/gzq071.

48. **Zhang ZG, Yi ZL, Pei XQ, Wu ZL.** 2010. Improving the thermostability of *Geobacillus stearothermophilus* xylanase XT6 by directed evolution and site-directed mutagenesis. Bioresour Technol **101:**9272–9278. http://dx.doi.org/10.1016/j.biortech.2010.07.060.
49. **Kiess M, Hecht HJ, Kalisz HM.** 1998. Glucose oxidase from *Penicillium amagasakiense*: primary structure and comparison with other glucose-methanol-choline (GMC) oxidoreductases. Eur J Biochem **252:**90–99.
50. **Shusta EV, Kieke MC, Parke E, Kranz DM, Wittrup KD.** 1999. Yeast polypeptide fusion surface display levels predict thermal stability and soluble secretion efficiency. J Mol Biol **292:**949–956. http://dx.doi.org/10.1006/jmbi.1999.3130.
51. **Böckle B, Martinez MJ, Guillen F, Martinez A.** 1999. Mechanism of peroxidase inactivation in liquid cultures of the ligninolytic fungus *Pleurotus pulmonarius*. Appl Environ Microbiol **65:**923–928.
52. **Peter S, Karich A, Ullrich R, Gröbe G, Scheibner K, Hofrichter M.** 2014. Enzymatic one-pot conversion of cyclohexane into cyclohexanone: comparison of four fungal peroxygenases. J Mol Catal B Enzymol **103:**47–51. http://dx.doi.org/10.1016/j.molcatb.2013.09.016.
53. **Carro J, Ferreira P, Rodriguez L, Prieto A, Serrano A, Balcells B, Arda A, Jimenez-Barbero J, Gutierrez A, Ullrich R, Hofrichter M, Martinez AT.** 2014. 5-Hydroxymethylfurfural conversion by fungal aryl-alcohol oxidase and unspecific peroxygenase. FEBS J http://dx.doi.org/10.1111/febs.13177.
54. **Gonzalez-Perez D, Alcalde M.** 2014. Assembly of evolved ligninolytic genes in *Saccharomyces cerevisiae*. Bioengineered **5:**254–263. http://dx.doi.org/10.4161/bioe.29167.

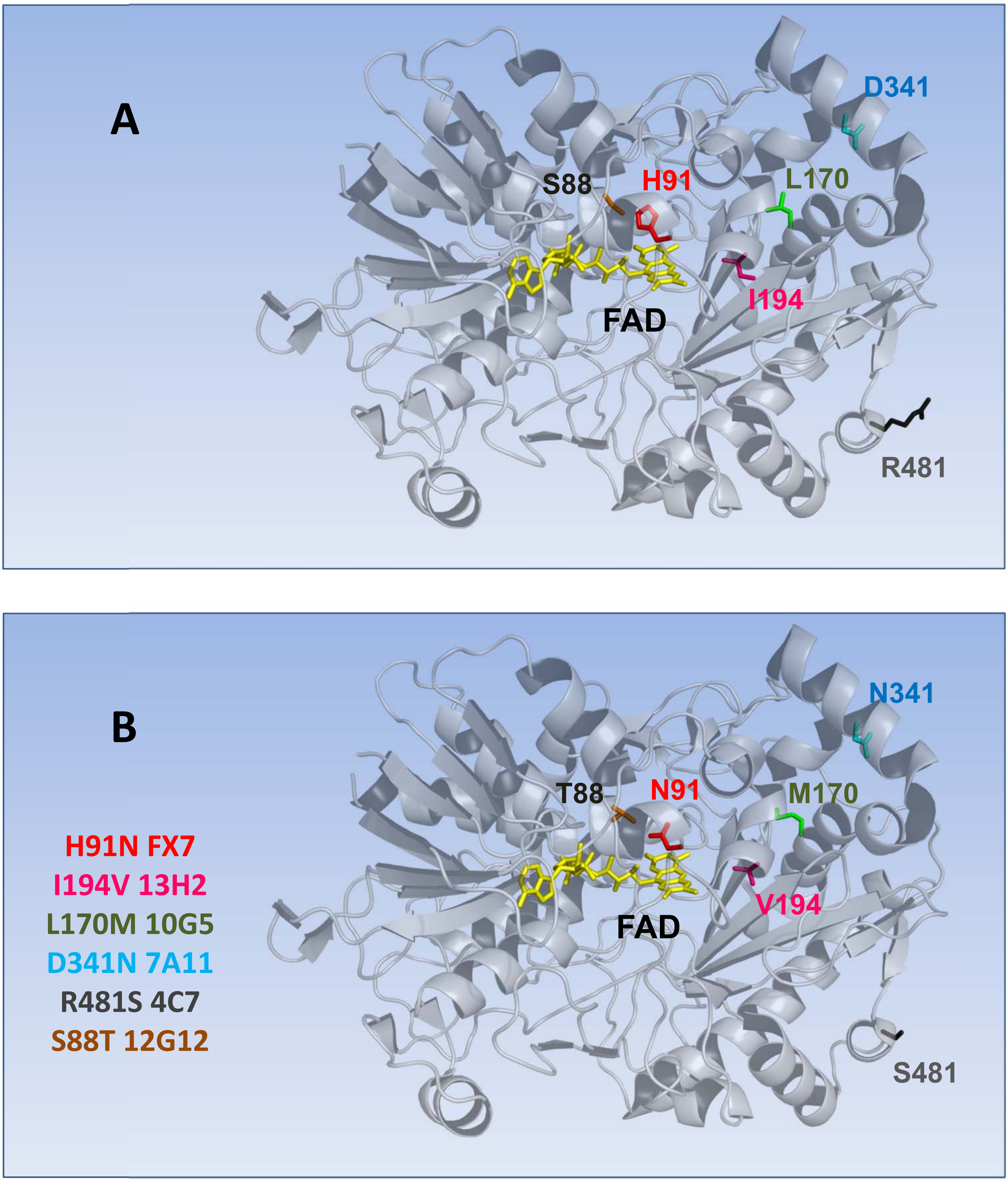
A
D341
S88
H91
L170
I194
FAD
R481
B
N341
T88
N91
M170
V194
FAD
S481
H91N FX7
I194V 13H2
L170M 10G5
D341N 7A11
R481S 4C7
S88T 12G12

Supplementary Figure 1. Structural exploration of the substitutions introduced by MORPHING. (A) Structure of the wild type AAO using as template the *P. eryngii* AAO crystal structure (PDB code 3FIM) **(B)** Mutations from each variant are depicted in different color. FX7 from library M-I-II (red), 13H2 (pink) and 10G5 (green) from library M-IV, 7A11 from library M-II (cyan), 4C7 from library M-II (dark grey) and modification in the mature protein in 12G12 from library M-I (brown).

Video Article

Directed Evolution Method in *Saccharomyces cerevisiae*: Mutant Library Creation and Screening

Javier Viña-Gonzalez[1], David Gonzalez-Perez[1], Miguel Alcalde[1]

[1]Department of Biocatalysis, Institute of Catalysis, CSIC

Correspondence to: Miguel Alcalde at malcalde@icp.csic.es

URL: http://www.jove.com/video/53761
DOI: doi:10.3791/53761

Keywords: Directed evolution, *Saccharomyces cerevisiae*, *in vivo* DNA recombination, focused-random mutagenesis, high-throughput screening.

Date Published: 1/20/2016

Citation: Viña-Gonzalez, J., Gonzalez-Perez, D., Alcalde, M. Directed Evolution Method in *Saccharomyces cerevisiae*: Mutant Library Creation and Screening. *J. Vis. Exp.* (), e53761, doi:10.3791/53761 (2016).

Abstract

Directed evolution in *Saccharomyces cerevisiae* offers many attractive advantages when designing enzymes for biotechnological applications, a process that involves the construction, cloning and expression of mutant libraries, coupled to high frequency homologous DNA recombination *in vivo*. Here, we present a protocol to create and screen mutant libraries in yeast based on the example of a fungal aryl-alcohol oxidase (AAO) to enhance its total activity. Two protein segments were subjected to focused-directed evolution by random mutagenesis and *in vivo* DNA recombination. Overhangs of ~50 bp flanking each segment allowed the correct reassembly of the AAO-fusion gene in a linearized vector giving rise to a full autonomously replicating plasmid. Mutant libraries enriched with functional AAO variants were screened in *S. cerevisiae* supernatants with a sensitive high-throughput assay based on the Fenton reaction. The general process of library construction in *S. cerevisiae* described here can be readily applied to evolve many other eukaryotic genes, avoiding extra PCR reactions, *in vitro* DNA recombination and ligation steps.

Video Link

The video component of this article can be found at http://www.jove.com/video/53761/

Introduction

Directed molecular evolution is a robust, fast and reliable method to design enzymes[1, 2]. Through iterative rounds of random mutation, recombination and screening, improved versions of enzymes can be generated that act on new substrates, in novel reactions, in non-natural environments, or even to assist the cell to achieve new metabolic goals[3-5]. Among the hosts used in directed evolution, the brewer's yeast *Saccharomyces cerevisiae* offers a repertoire of solutions for the functional expression of complex eukaryotic proteins that are not otherwise available in prokaryotic counterparts[6,7].

Used exhaustively in cell biology studies, this small eukaryotic model has many advantages in terms of post-translational modifications, ease of manipulation and transformation efficiency, all of which are important traits to engineer enzymes by directed evolution[8]. Moreover, the high frequency of homologous DNA recombination in *S. cerevisiae* coupled to its efficient proof-reading apparatus opens a wide array of possibilities for library creation and gene assembly *in vivo*, fostering the evolution of different systems from single enzymes to complex artificial pathways[9-12]. Our laboratory has spent the past decade designing tools and strategies for the molecular evolution of different ligninases in yeast (oxidoreductases involved in the degradation of lignin during natural wood decay)[13-14]. In this communication, we present a detailed protocol to prepare and screen mutant libraries in *S. cerevisiae* for a model flavooxidase, -aryl-alcohol oxidase (AAO[15])-, that can be easily translated to many other enzymes. The protocol involves a focused-directed evolution method (MORPHING: Mutagenic Organized Recombination Process by Homologous *in vivo* Grouping) assisted by the yeast cell apparatus[16], and a very sensitive screening assay based on the Fenton reaction in order to detect AAO activity secreted into the culture broth[17].

Protocol

1. Mutant Library Construction

1. Choose the regions to be subjected to MORPHING with the help of computational algorithms based on the available crystal structure or homology models[18].
    1. Here, target two regions of AAO from *Pleurotus eryngii* for random mutagenesis and recombination (Met[α1]-Val109, Phe392-Gln566), while amplifying the remainder of the gene (844 bp) by high-fidelity PCR (**Figure 1**).
    Note: Several segments can be studied by MORPHING in an independent or combined manner[16].
2. Amplify the targeted areas by mutagenic PCR. Create overlapping areas between segments (~50 bp each) by superimposing PCR reactions of the defined regions.

    1. Prepare mutagenic PCR of targeted segments in a final volume of 50 µl containing DNA template (0.92 ng/µl), 90 nM oligo sense (RMLN for segment M-I and AAO-BP for segment M-II), 90 nM antisense primer (AAO-92C for segment M-I and RMLC for segment M-II) , 0.3 mM dNTPs (0.075 mM each), 3% (v/v) dimethylsulfoxide (DMSO), 1.5 mM $MgCl_2$, 0.05 mM $MnCl_2$ and 0.05 U/µl *Taq* DNA polymerase. Primers sequences are detailed in **Figure 1**.
    2. Use the following PCR program: 95 °C for 2 min (1 cycle); 95 °C for 45 sec, 50 °C for 45 sec, 74 °C for 45 sec (28 cycles); and 74 °C for 10 min (1 cycle).

3. Amplify the non-mutagenic regions with ultra-high fidelity polymerase and include the corresponding areas overlapping the mutagenic segments and/or linearized vector overhangs.
    1. Prepare reaction mixtures in a final volume of 50 µl containing: DNA template (0.2 ng/µl), 250 nM oligo sense HFF, 250 nM oligo antisense HFR, 0.8 mM dNTPs (0.2 mM each), 3% (v/v) dimethylsulfoxide (DMSO) and 0.02 U/µl *iproof* DNA polymerase. Primers sequences are detailed in **Figure 1**.
    2. Use the following PCR program: 98 °C for 30 sec (1 cycle); 98 °C for 10 sec, 55 °C for 25 sec, 72 °C for 45 sec (28 cycles); and 72 °C for 10 min (1 cycle).
    Note: With conditions described in 1.2 and 1.3 overlaps of 43 bp (plasmid-M1 region); 46 bp (M1 region-HF region); 47 bp (HF region-M2 region) and 61 bp (M2 region- plasmid) are designed (**Figure 1**) to favor *in vivo* splicing in yeast.
    3. Purify all the PCR fragments (mutagenic and non-mutagenic) with a commercial gel extraction kit according to manufacturer's protocol.

4. Linearize the vector such that flanking regions of approximately 50 bp are created that are homologous to the 5´- and 3´-ends of the target gene.
    1. Prepare a linearization reaction mixture containing 2 µg DNA, 7.5 U *Bam*HI, 7.5 U *Xho*I, 20 µg BSA and 2 µl of Buffer *Bam*HI 10x in a final volume of 20 µl.
    2. Incubate the reaction mixture at 37 °C for 2 hr and 40 min. Afterwards, proceed with inactivation at 80 °C for 20 min.

5. Purify the linearized vector by agarose gel extraction to avoid contamination with the residual circular plasmid (**Figure 2**).
    1. Load the digestion reaction mix into the mega-well of a semi-preparative low melting point agarose gel (0.75%, w:v) as well as an aliquot (5 µl) of the reaction mix in the adjacent well as a reporter.
    2. Run DNA electrophoresis (5 V/cm between electrodes, 4 °C) and separate the agarose gel corresponding to the mega-well and store it at 4 °C in 1x TAE.
    3. Stain the lane with the molecular weight ladder and the reporter. Visualize the bands under UV light. Nick the position where the linearized vector places.
    Note: As the quality of the purified linearized vector is a critical factor for successful recombination and assembly in yeast, avoid gel staining for semi-preparative DNA electrophoresis. The use of dyes and UV exposure for gel extraction may affect the stability of the DNA vector, compromising the *in vivo* recombination efficiency. As alternative to toxic EtBr dyes, Gel Red and SYBR dyes are commonly used for gel staining.
    4. In the absence of UV light, identify the linearized vector in the mega-well fragment using the guidance of the nicks in the stained reporter lane so that it can be isolated.
    5. Extract the linearized vector from agarose and purify it with a commercial gel extraction kit according to manufacturer's protocol.
    Note: Use high-copy episomal shuttle vectors with antibiotic and auxotrophy markers: In this example we employed the uracil independent and ampicillin resistance pJRoC30 vector, under the control of the yeast GAL1 promoter.

6. Prepare an equimolar mixture of the PCR fragments and mix it with the linearized vector at a 2:1 ratio, with no less than 100 ng of linearized plasmid (test different ratios of equimolar library/open vector to achieve good transformation yields).
    1. Measure the absorbance of the PCR fragments and linearized vector at 260 nm and 280 nm to determine their concentration and purity.

7. Transform yeast competent cells with the DNA mixture using a commercial yeast transformation kit (see **Table** for supplies) according to manufacturer's instructions.
    1. Here, use a protease deficient and $URA3^-$ dependent *S. cerevisiae* strain, BJ5465. Transform the cells with the parental circularized vector as an internal standard during screening (see below). Additionally, check the background by transforming the linearized vector in the absence of PCR fragments.
    Note: In case of detecting initial low secretion levels, use *S. cerevisiae* protease deficient strains like BJ5465 to foster the accumulation of active protein in culture supernatants. If the target enzyme undergoes hyperglycosylation, the use of glycosylation-deficient strains (e.g. Δ*kre2* that is only capable of attaching smaller mannose oligomers) could be a suitable option.

8. Plate the transformed cells on SC drop-out plates and incubate them at 30 °C for three days. Plate (on SC drop-out plates supplemented with uracil) $URA3^-$ *S. cerevisiae* cells lacking the plasmid as a negative control for screening (see below).

2. High-Throughput Screening Assay (Figure 3)

1. Fill an appropriate number of sterile 96-well plates (23 plates to analyze a library of 2,000 clones) with 50 µl minimal medium per well with the help of a pipetting robot.
2. Pick individual colonies from the SC-drop out plates and transfer them to the 96-well plates.
    1. In each plate, inoculate column number 6 with the parental type as an internal standard and well H1 with $URA3^-$ *S. cerevisiae* cells (in SC medium supplemented with uracil) with no plasmid as a negative control.
    Note: Well H1 is filled specifically with drop-out media supplemented with uracil. A blank well containing media without cells can be also prepared as an additional sterility control.

3. Cover the plates with their lids and wrap them in Parafilm. Incubate plates for 48 hr at 30 °C, 225 rpm and 80% relative humidity in a humid shaker.

Copyright © 2016 Journal of Visualized Experiments

4. Remove the Parafilm, add 160 µl of expression medium to each well with the help of the pipetting robot, reseal the plates and incubate them for a further 24 hr.
   Note: Minimal medium and expression medium are prepared as reported elsewhere[19]. Secretion levels may vary depending on the gene under study and accordingly, the incubation times must be optimized in each case to synchronize the cell growth in all the wells.
5. Centrifuge the plates (master plates) at 2,800 x *g* for 10 min at 4 °C.
6. Transfer 20 µl of the supernatant from the wells in the master plate to the replica plate using a liquid handling robotic multistation.
   Note: To favor enzyme secretion it is advisable to replace the native signal peptide of the target protein by signal peptides commonly used for heterologous expression in yeast (*e.g.* the α factor prepro-leader, the leader of the K_1 Killer toxin from *S. cerevisiae*, or even chimeric versions of both peptides[13]). Alternatively, the native signal peptide can be exclusively evolved for secretion in yeast.
7. Add 20 µl of 2 mM *p*-methoxybenzylalcohol in 100 mM sodium phosphate buffer pH 6.0 with the help of the pipetting robot. Stir the plates briefly with a 96-well plate mixer and incubate them for 30 min at room temperature (RT).
8. With the pipetting robot, add 160 µl of the FOX reagent to each replica plate and stir briefly with the mixer (final concentration of FOX mixture in the well: 100 µM xylenol orange, 250 µM $Fe(NH_4)_2(SO_4)_2$ and 25 mM H_2SO_4).
   1. Add several additives to the reagent to enhance sensitivity, such as organic co-solvents (DMSO, ethanol, methanol) or sorbitol[17]. Here, amplify the response by adding sorbitol to a final concentration of 100 mM (**Figure 4**).

9. Read the plates (end-point mode, t_0) at 560 nm on a plate reader.
10. Incubate the plates at RT until the color develops and measure the absorption again (t_1).
    1. Calculate the relative activity from the difference between the Abs value after incubation and that of the initial measurement normalized to the parental type for each plate ($\Delta t_1 - t_0$).

11. Subject the best mutant hits to two consecutive re-screenings to rule out false positives.
    Note: Typically, re-screenings include plasmid isolation from yeast, amplification and purification in *Escherichia coli*, followed by transformation of fresh yeast cells with the plasmid[19]. Each selected clone is re-screened in pentaplicate.

Representative Results

AAO from *P. eryngii* is an extracellular flavooxidase that supplies fungal peroxidases with H_2O_2 to start attacking lignin. Two segments of AAO were subjected to focused-directed evolution by MORPHING in order to enhance its activity and its expression in *S. cerevisiae* [19]. Irrespective of the foreign enzymes harbored by *S. cerevisiae*, the most critical issue when constructing mutant libraries in yeast concerns the engineering of specific overlapping regions to favor the splicing between fragments and their cloning into the linearized vector. In the current example, for each PCR reaction, all the fragments had overhangs of approximately 50 bp to promote *in vivo* splicing in yeast. The number of recombination events is dependent on the number of segments to be assembled and cloned with the linearized vector (*i.e.* two crossover events took place between the three PCR segments -the two mutagenic segments flanking the non-mutagenized segment- plus two additional crossovers with the linearized vector; **Figure 1**). According to our experience, overlapping sequences longer than 50 bp decrease the likelihood of internal recombination while they do not improve transformation efficiency.

Mutational loads were adjusted by sampling mutant libraries with different landscapes, calculating the number of clones with <10% of the parental enzyme activity, and further checking them by sequencing a random sample of active and non-active variants (**Figure 5A**). For the determination of the coefficient of variance *S. cerevisiae* cells were transformed with the parental AAO and plated on SC-drop out plates. Individual colonies were picked and inoculated in a 96 well-plate and the activity of the clones was evaluated from fresh preparations. Mutagenic sample 2 (*Taq*/$MnCl_2$ 0.05 mM) was chosen as the departure point for library construction and screening.

As the biological activity of AAO increases the H_2O_2 concentration in the reaction medium, we searched for a sensitive and accurate assay to quantify minor changes in H_2O_2. FOX is a chemical method based on the Fenton reaction[20], whereby oxidation by H_2O_2 drives the reaction of Fe^{3+} with xylenol orange to form a blue-purple complex (*o*-cresolsulfone-phthalein 3',3''-bis(methylimino)diacetate $\varepsilon_{560} = 1.5 \times 10^4\ M^{-1}cm^{-1}$). The ferrous oxidation step was amplified by adding sorbitol to enhance the sensitivity of the assay, increasing the propagation of radicals with an apparent $\varepsilon_{560} = 2.25 \times 10^5\ M^{-1}cm^{-1}$ (**Figure 4**).

The detection limit of this assay (in the µM range) was calculated by the Blank determination method in a 96-well plate with standards in triplicate (0, 0.5, 1, 1.5, 2, 2.5, 3 and 4 µM H_2O_2) and using several supernatants from *S. cerevisiae* lacking the $URA3^-$ plasmid (**Figure 5B**). The assay was linear in the presence of sorbitol (up to 8 µM of H_2O_2), and although linearity was more persistent in the absence of this sugar (at least up to 30 µM of H_2O_2) the response was weaker (*e.g.,* at 6 µM of H_2O_2, a 4-fold enhancement was obtained in the presence of sorbitol -deep purple- from an absorbance of 0.24 in its absence -dark orange- (**Figure 5B**)). The relationship between Abs and the AAO concentration was evaluated with increasing amounts of enzyme (from yeast supernatants) and a linear response was observed; $R^2 = 0.997$ (**Figure 5C**).

It is notable that the FOX signal was stable for several hours without any apparent interference by the different elements in the culture broth. The estimated sensitivity of FOX was ~0.4 µM of H_2O_2 produced by the AAO in the supernatant in the presence of sorbitol, and ~2 µM in its absence.

A mutant library of 2,000 clones was constructed and screened with this assay. Several AAO mutants were identified with notably improved secretion and activity against *p*-methoxybenzyl alcohol (**Figure 5D**)[19].

Copyright © 2016 Journal of Visualized Experiments

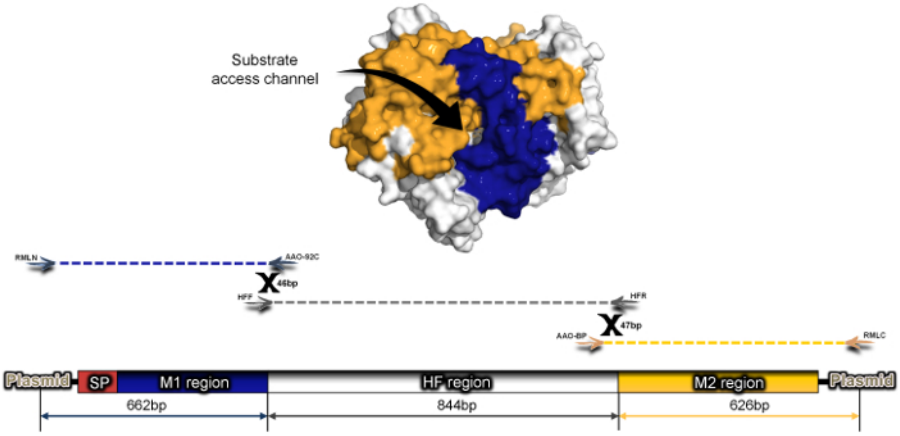
Substrate access channel
RMLN
AAO-92C
X 46bp
HFF
HFR
X 47bp
AAO-BP
RMLC
Plasmid
SP
M1 region
HF region
M2 region
Plasmid
662bp
844bp
626bp

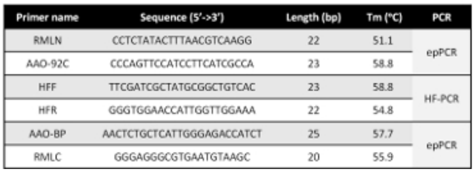

Primer name	Sequence (5'->3')	Length (bp)	Tm (°C)	PCR
RMLN	CCTCTATACTTTAACGTCAAGG	22	51.1	epPCR
AAO-92C	CCCAGTTCCATCCTTCATCGCCA	23	58.8	
HFF	TTCGATCGCTATGCGGCTGTCAC	23	58.8	HF-PCR
HFR	GGGTGGAACCATTGGTTGGAAA	22	54.8	
AAO-BP	AACTCTGCTCATTGGGAGACCATCT	25	57.7	epPCR
RMLC	GGGAGGGCGTGAATGTAAGC	20	55.9	

Figure 1.MORPHING Protocol for AAO Evolution. Two different regions of AAO were targeted for random mutagenesis and recombination: M1 (blue, 590 bp) that includes the signal peptide (SP); M2 (yellow, 528 bp). The HF region (grey, 844 bp) was amplified with high fidelity polymerases. Mutagenic regions were mapped in the crystal structure of AAO (PDB ID: 3FIM). Please click here to view a larger version of this figure.

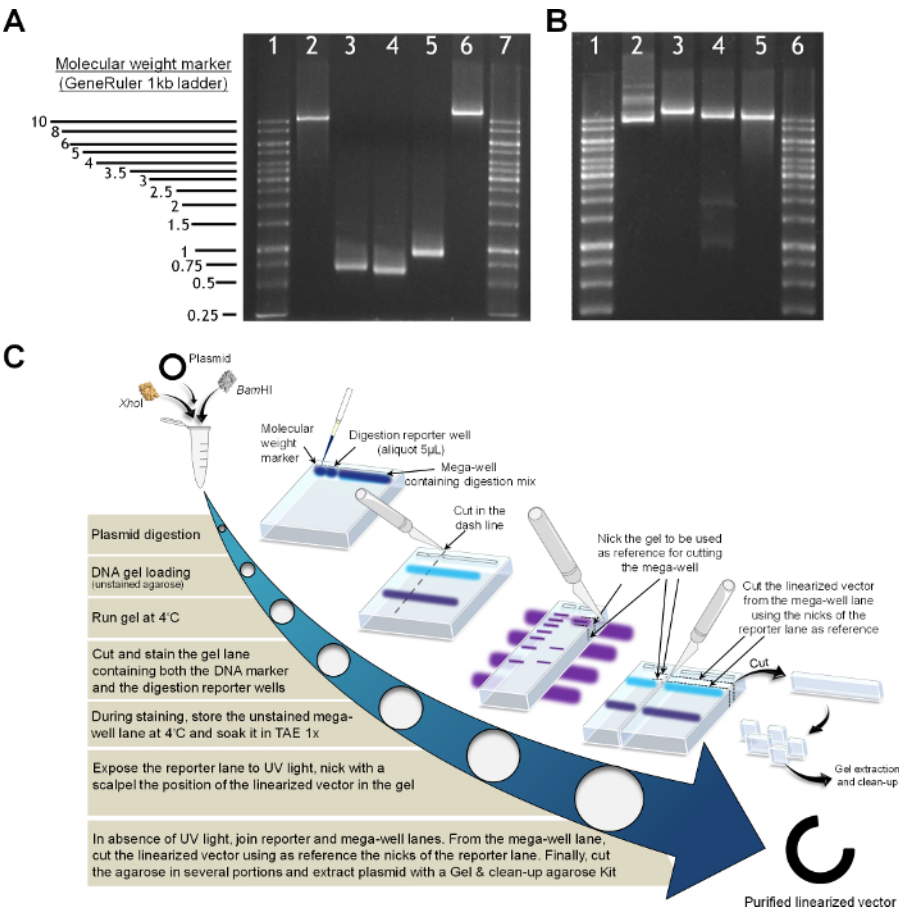
A
Molecular weight marker
(GeneRuler 1kb ladder)
10
8
6
5
4
3.5
3
2.5
2
1.5
1
0.75
0.5
0.25
1 2 3 4 5 6 7
B
1 2 3 4 5 6
C
Plasmid
XhoI
BamHI
Molecular weight marker
Digestion reporter well (aliquot 5μL)
Mega-well containing digestion mix
Cut in the dash line
Nick the gel to be used as reference for cutting the mega-well
Cut the linearized vector from the mega-well lane using the nicks of the reporter lane as reference
Cut
Gel extraction and clean-up
Plasmid digestion
DNA gel loading (unstained agarose)
Run gel at 4°C
Cut and stain the gel lane containing both the DNA marker and the digestion reporter wells
During staining, store the unstained mega-well lane at 4°C and soak it in TAE 1x
Expose the reporter lane to UV light, nick with a scalpel the position of the linearized vector in the gel
In absence of UV light, join reporter and mega-well lanes. From the mega-well lane, cut the linearized vector using as reference the nicks of the reporter lane. Finally, cut the agarose in several portions and extract plasmid with a Gel & clean-up agarose Kit
Purified linearized vector

Figure 2. Preparation of PCR Products and the Linearized Vector. (**A**) Analytical agarose gel (1% w:v) containing a molecular weight marker (1 kb ladder) in lanes 1 and 7; the *Bam*HI and *Xho*I linearized vector, lane 2; PCR segment M1, lane 3; PCR segment M2, lane 4; PCR segment HF, lane 5; the *in vivo* reassembled vector linearized with *Nhe*I (containing the full AAO gene with regions M-I, HF and M-II), lane 6. (**B**) Vector linearization, lanes 1 and 6 molecular standards, 1 Kb ladder; plasmid miniprep, lane 2; plasmid linearized with *Nhe*I, lane 3; plasmid linearized with *Bam*HI and *Xho*I, lane 4; linearized plasmid obtained by gel extraction and clean-up after digestion, lane 5. (**C**) Protocol for plasmid purification. Please click here to view a larger version of this figure.

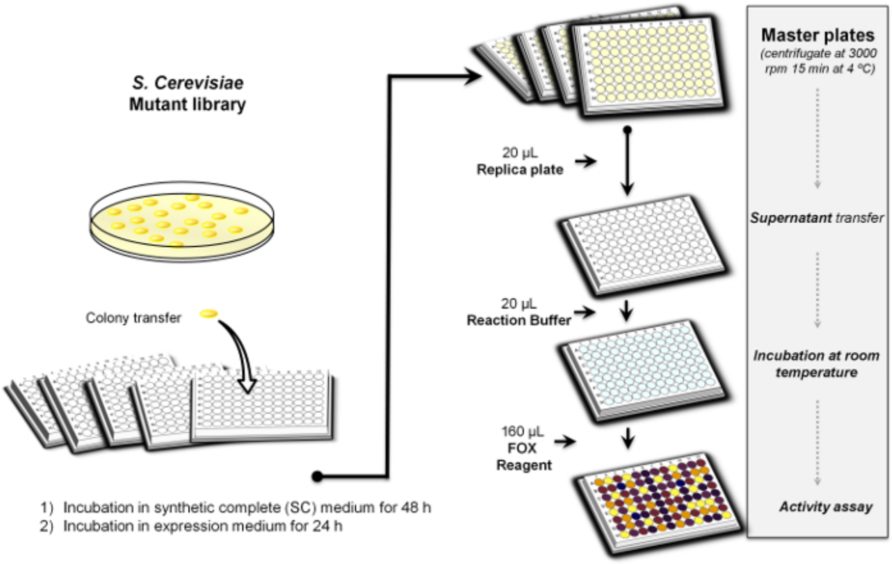
S. Cerevisiae
Mutant library
Colony transfer
1) Incubation in synthetic complete (SC) medium for 48 h
2) Incubation in expression medium for 24 h
20 μL
Replica plate
20 μL
Reaction Buffer
160 μL
FOX
Reagent
Master plates
(centrifugate at 3000 rpm 15 min at 4 °C)
Supernatant transfer
Incubation at room temperature
Activity assay

Figure 3. High-throughput Screening Protocol. Overview of the process. Please click here to view a larger version of this figure.

Fenton reaction

$Fe^{2+} + H_2O_2 \rightarrow Fe^{3+} + OH^{\bullet} + OH^-$

Fe^{3+} + Xylenol Orange → **Blue-purple complex**

$Fe^{2+} + H_2O_2 \rightarrow Fe^{3+} + OH^{\bullet} + OH^-$

$\text{Sorbitol} + OH^{\bullet} \rightarrow \text{Sorb.}^{\bullet} + H_2O$

$\text{Sorb.}^{\bullet} + O_2 \rightarrow \text{Sorb.}O_2^{\bullet} \rightarrow \text{Sorb.(keto)} + HO_2^{\bullet}$

$Fe^{2+} + HO_2^{\bullet} \rightarrow Fe^{3+} + H_2O_2$

Figure 4. The FOX Method. White-rot fungi attack the cell wall of wood through a Fenton reaction that produces hydroxyl radical $OH^{\bullet}$. The FOX method couples this reaction to xylenol orange (XO), and the absorbance of the XO-Fe^{3+} complex is measured at 560 nm. Ferrous oxidation is amplified by the addition of sorbitol to the reagent mixture. Please click here to view a larger version of this figure.

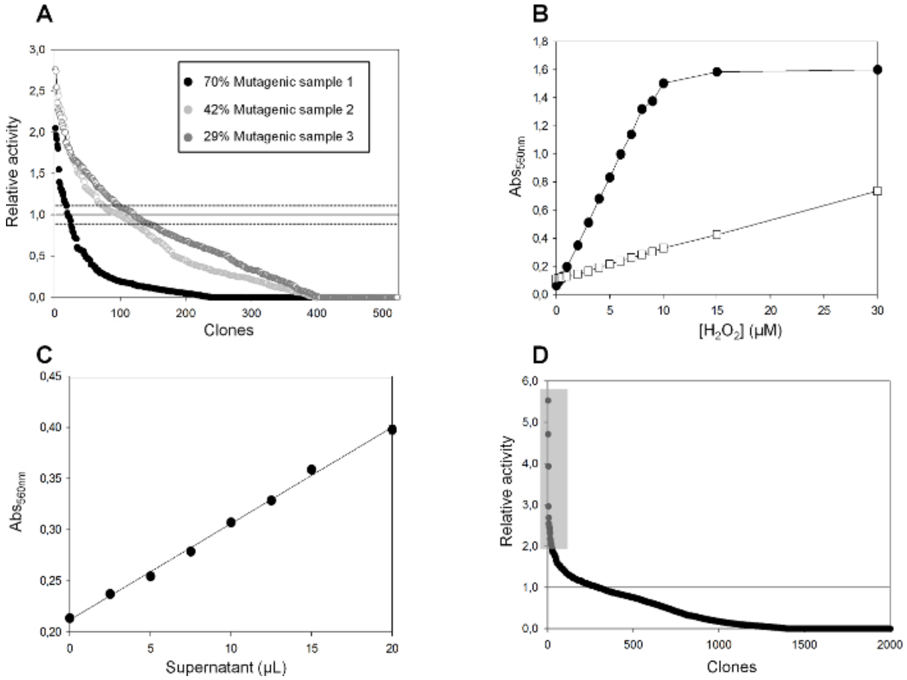

Figure 5. Mutagenic Landscapes for MORPHING Libraries Using Different Error Prone PCR Conditions and Validation of the Screening Assay. (**A**) MORPHING landscapes. Solid horizontal line shows the activity of the parental type in the assay while the dashed lines indicate the coefficient of variance of the assay. The percentages indicate the number of clones with less than 10% of the parental enzyme activity. Activities are plotted in descending order. (**B**) The FOX detection limit was evaluated with increasing concentrations of H_2O_2 in the presence (black circles) and absence (white squares) of sorbitol. (**C**) Linear correlation between AAO concentration (transformant supernatants) and Abs_{560nm}. Each point corresponds to the average of 8 experiments and includes the standard deviation. (**D**) Mutant library landscape. The selected variants (shadowed square) were rescreened as reported elsewhere[19]. Solid line shows the activity of AAO parental type. Please click here to view a larger version of this figure.

Discussion

In this article, we have summarized most of the tips and tricks employed in our laboratory to engineer enzymes by directed evolution in *S. cerevisiae* (using AAO as an example) so that they can be adapted for use with many other eukaryotic enzyme systems by simply following the common approach described here.

In terms of library creation, MORPHING is a fast one-pot method to introduce and recombine random mutations in small protein stretches while leaving the remaining regions of the protein unaltered[16]. Libraries with several mutational loads can be readily prepared and recombined *in vivo*, along with the linearized plasmid, to generate a full autonomously replicating vector. It is critical that overlapping sequences flank each stretch to allow the fragments of the full gene to be reassembled through *in vivo* recombination, avoiding extra PCR reactions and *in vitro* ligation steps. In this protocol, the frequency of crossover events between PCR fragments can be increased by reducing the size of the overlapping regions, although this may compromise the transformation efficiency. Regardless of the DNA polymerases used for mutagenic PCR, the mutational loads can be adjusted by previously constructing and analyzing small mutant library landscapes (**Figure 5A**). If the GeneMorph II Kit is used, it is still advisable to follow this approach since *in vivo* DNA recombination can notably modify the mutational loads estimated by the manufacturer. In general terms, mutant landscapes in which 35 - 50% of the total clones screened have less than 10% of the parental activity are suitable for directed evolution campaigns, although this number varies in function of the target protein and its activity. Typically, the analysis of mutant libraries landscapes are further verified by DNA sequencing of a random sample of mutants. In the current example, the *Taq* DNA polymerase was used due to its high error rate, which is linked to the lack of 3´→5´proof-reading exonuclease activity. The mutational loads in *Taq* libraries were modified by the addition of different concentrations of $MnCl_2$, but the use of unbalanced dNTPs and/or the reduction in gene template concentrations are also suitable options. Inherent limitations of MORPHING come from the number of segments to be recombined. According to our experience, up to four protein blocks (five crossover events counting the recombination areas with the linearized vector) can be spliced with good transformation yields (~10^5 clones per transformation reaction). This method can be easily modified to performed multiple site-saturation mutagenesis (*e.g.* using NDT degenerated primers or creating degeneracy for 22 unique codons) to explore several positions simultaneously while reducing significantly the screening efforts[21,22].

The direct "*blind*" screening protocol for AAO is extremely sensitive and reliable (based on the direct detection of H_2O_2 regardless of the substrate used by the enzyme), representing a complementary assay to other well established indirect protocols to detect peroxides (mostly coupling peroxidases with colorimetric substrates). Indeed, the FOX assay has been routinely employed to measure H_2O_2 in biological fluids, and it can now be easily translated into protocols to evolve AAO and any other H_2O_2 producing enzymes (*e.g.,* glucose oxidases, cellobiose dehydrogenases, glyoxal oxidases, methanol oxidases), particularly for activity on non-natural substrates where responses are otherwise hard to detect.

S. cerevisiae is the most adequate host for directed evolution of eukaryotic genes since it offers high transformation efficiencies (up to 1 x 10^6 transformants/µg DNA), it performs complex post-translational processing and modifications (including N- and C-terminal processing, and glycosylation) and it exports foreign proteins into the culture broth *via* a secretory pathway. In addition, well-established molecular biology tools are available to work with this yeast, including uni- or bi-directional episomal (non-integrative) shuttle vectors under the control of promoters of different strengths. Last but not least, its high frequency of homologous DNA recombination has allowed a range of methods to be developed to obtain DNA diversity that are currently being used to evolve single proteins, as well as more complex enzyme pathways[8, 12, 13, 23]. The *in vivo* gap repair and the proof-reading device of this yeast can be also employed to create chimeras when recombining different genes (with approx. 60% of DNA sequence identity), as well as to shuffle best offspring/mutations from a directed evolution campaign, or to bring together *in vitro* and *in vivo* recombination methods in one round of evolution, thereby enriching mutant libraries in terms of foldability and function.

Disclosures

The authors have nothing to disclose.

Acknowledgements

This work was supported by the European Commission project Indox-FP7-KBBE-2013-7-613549; a Cost-Action CM1303-Systems Biocatalysis; and the National Projects Dewry [BIO201343407-R] and Cambios [RTC-2014-1777-3].

References

1. Jäckel, C., Hilvert, D. Biocatalysts by evolution. *Curr. Opin. Biotechnol.* **21** (6), 753-759 (2010).
2. Bornscheuer, U. T., *et al.* Engineering the third wave of biocatalysis. *Nature.* **485** (7397), 185-194 (2012).
3. Renata, H., Wang, Z. W., Arnold, F. H. Expanding the enzyme universe: accessing non-natural reactions by mechanism-guided directed evolution. *Angew. Chem. Int. Ed.* **54** (11), 3351-3367 (2015).
4. Cobb, R. E., Chao, R., Zhao, H. Directed evolution: past, present and future. *AIChE J.* **59** (5), 1432-1440 (2013).
5. Abatemarco, J., Hill, A., Alper, H. S. Expanding the metabolic engineering toolbox with directed evolution. *Biotechnol. J.* **8** (12), 1397-1410 (2013).
6. Pourmir, A., Johannes, T. W. Directed evolution: selection of the host organism. *Comput Struct Biotechnol J.* **2** (3), e201209012 (2012).
7. Krivoruchko, A., Siewers, V., Nielsen, J. Opportunities for yeast metabolic engineering: lessons from synthetic biology. *Biotechnol J.* **6** (3), 262-276 (2011).
8. Gonzalez-Perez, D., Garcia-Ruiz, E., Alcalde, M. *Saccharomyces cerevisiae* in directed evolution: an efficient tool to improve enzymes. *Bioeng Bugs.* **3** (3), 172-177 (2012).
9. Alcalde, M. Mutagenesis protocols in *Saccharomyces cerevisiae* by *In Vivo* Overlap Extension. *Methods Mol. Biol.* **634**, 3-14 (2010).
10. Bulter, T., Alcalde, M. Preparing libraries in *Saccharomyces cerevisiae. Methods. Mol. Biol.* **231**, 17-22 (2003).
11. Ostrov, N. Wingler, L. M., Cornish, W. Gene assembly and combinatorial libraries in *S. cerevisiae* via reiterative recombination. *Methods. Mol. Biol.* **978**, 187-203 (2013).
12. Shao, Z., Zhao, H., Zhao, H. DNA assembler, an *in vivo* genetic method for rapid construction of biochemical pathways. *Nucleic Acids Res.* **37** (2), e16 (2009).
13. Alcalde, M. Engineering the ligninolytic enzyme consortium. *Trends Biotechnol.* **33** (3), 155-162 (2015).
14. Garcia-Ruiz, E., *et al.* Directed evolution of ligninolytic oxidoreductases: from functional expression to stabilization and beyond. In: *Cascade Biocatalysis: integrating stereoselective and environmentally friendly reactions.* Wiley-VCH. 1-22 (2014).
15. Hernandez-Ortega, A., Ferreira, P., Martinez, A. T. Fungal aryl-alcohol oxidase: a peroxide-producing flavoenzyme involved in lignin degradation. *Appl. Microbiol. Biotechnol.* **93** (4), 1395-1410 (2012).
16. Gonzalez-Perez, D., Molina-Espeja, P., Garcia-Ruiz, E., Alcalde, M. Mutagenic organized recombination process by homologous *in vivo* grouping (MORPHING) for directed enzyme evolution. *PLoS One.* **9**, e90919 (2014).
17. Rhee, S. G., Chang, T., Jeong, W., Kang, D. Methods for Detection and Measurement of Hydrogen Peroxide Inside and Outside of Cells. *Mol. Cells.* **29** (6), 539-549 (2010).
18. Sebestova, E., Bendl, J., Brezovsky, J.,Damborsky, J. Computational tools for designing smart libraries. *Methods. Mol. Biol.* **1179**, 291-314 (2014).
19. Viña-Gonzalez, J., Gonzalez-Perez, D., Ferreira, P., Martinez, A. T., Alcalde, M. Focused directed evolution of aryl-alcohol oxidase in yeast using chimeric signal peptides. *Appl. Environ. Microbiol.* In press (2015).
20. Gay, C., Collins, J., Gebicki, J. M. Hydroperoxide Assay with the Ferric-Xylenol orange Complex. *Anal. Biochem.* **273** (2), 149-155 (1999).
21. Reetz, M. T. Biocatalysis in organic chemistry and biotechnology: Past, present, and future. *J. Am. Chem. Soc.* **135** (34), 12480-12496 (2013).
22. Mate, D. M., Gonzalez-Perez, D., Mateljak, I., Gomez de Santos, P., Vicente, A. I., Alcalde, M. The pocket manual of directed evolution: Tips and tricks. *In:Biotechnology of Microbial Enzymes: Production, Biocatalysis and Industrial Applications.* Brahmachari, Demain and Adrio Eds. Elsevier. In press.
23. Chao, R., Yuan, Y., Zhao, H. Recent advances in DNA assembly technologies. *FEMS Yeast Res.* 15, 1-9 (2015).

Received: 16 January 2018 | Revised: 19 February 2018 | Accepted: 8 March 2018
DOI: 10.1002/bit.26585

ARTICLE

WILEY BIOTECHNOLOGY and BIOENGINEERING

Functional expression of aryl-alcohol oxidase in *Saccharomyces cerevisiae* and *Pichia pastoris* by directed evolution

Javier Viña-Gonzalez[1] | **Katarina Elbl**[1] | **Xavier Ponte**[2] | **Francisco Valero**[2] | **Miguel Alcalde**[1]

[1] Department of Biocatalysis, Institute of Catalysis, CSIC, Cantoblanco, Madrid, Spain

[2] Departamento de Ingeniería Química, Biológica y Medioambiental, Escuela de Ingeniería, Universidad Autónoma de Barcelona, Bellaterra, Barcelona, Spain

Correspondence
Miguel Alcalde, Department of Biocatalysis, Institute of Catalysis, CSIC, Cantoblanco, 28049 Madrid, Spain.
Email: malcalde@icp.csic.es

Funding information
Ministerio de Ciencia y Tecnología, Grant number: BIO2016-79106-R-Lignolution; Seventh Framework Programme, Grant number: FP7-KBBE-2013-7-613549-INDOX

Abstract

Aryl-alcohol oxidase (AAO) plays a fundamental role in the fungal ligninolytic secretome, acting as a supplier of H_2O_2. Despite its highly selective mechanism of action, the presence of this flavooxidase in different biotechnological settings has hitherto been hampered by the lack of appropriate heterologous expression systems. We recently described the functional expression of the AAO from *Pleurotus eryngii* in *Saccharomyces cerevisiae* by fusing a chimeric signal peptide (preαproK) and applying structure-guided evolution. Here, we have obtained an AAO secretion variant that is readily expressed in *S. cerevisiae* and overproduced in *Pichia pastoris*. First, the functional expression of AAO in *S. cerevisiae* was enhanced through the in vivo shuffling of a panel of secretion variants, followed by the focused evolution of the preαproK peptide. The outcome of this evolutionary campaign—an expression variant that accumulated 4 mutations in the chimeric signal peptide, plus two mutations in the mature protein- showed 350-fold improved secretion (4.5 mg/L) and was stable. This secretion mutant was cloned into *P. pastoris* and fermented in a fed-batch bioreactor to enhance production to 25 mg/L. While both recombinant AAO from *S. cerevisiae* and *P. pastoris* were subjected to the same N-terminal processing and had a similar pH activity profile, they differed in their kinetic parameters and thermostability. The strong glycosylation observed in the evolved AAO from *S. cerevisiae* underpinned this effect, since when the mutant was produced in the glycosylation-deficient *S. cerevisiae* strain Δ*kre2*, its kinetic parameters and thermostability were comparable to its poorly glycosylated *P. pastoris* recombinant counterpart.

KEYWORDS
aryl-alcohol oxidase, bioreactor, directed evolution, functional expression, *Pichia pastoris*, *Saccharomyces cerevisiae*

1 | INTRODUCTION

Aryl-alcohol oxidase (AAO, EC.1.1.3.7) is a monomeric extracellular flavoprotein that oxidizes a wide range of aromatic alcohols to their corresponding carbonyl compounds, concomitantly releasing H_2O_2. As a member of the glucose-methanol-choline (GMC) oxidoreductase superfamily, this FAD-dependent enzyme is secreted by different basidiomycetes involved in natural wood decay. The main role of AAO in nature is to supply ligninolytic peroxidases with H_2O_2, as well as to switch on the Fenton reaction in the combustion of lignin (Ferreira

© 2018 Wiley Periodicals, Inc.

et al., 2005; Hernandez-Ortega, Ferreira, & Martinez, 2012). In terms of biotechnological settings, AAO could be used in lignocellulose biorefineries to produce 2nd generation biofuels and added-value chemicals (Alcalde, 2015; Martinez, Ruiz-Dueñas, Martínez, del Río, & Gutierrez, 2009). Moreover, and thanks to a highly enantioselective mechanism, AAO becomes very attractive for the chiral resolution of secondary alcohols aimed at obtaining valuable building blocks for pharmaceutical processes (Hernandez-Ortega, Ferreira, Merino, et al., 2012). Along these lines, recent findings highlight the oxidative potential of this enzyme with renewal chemicals, such as furfural derivatives for the (bio)polymer industry (Carro et al., 2015; Martinez et al., 2017). Despite these promising features, the lack of suitable heterologous functional expression systems in which the properties of AAO can be sculptured by directed evolution has precluded the use of this versatile flavooxidase in different industrial applications. We previously reported the initial functional expression of AAO from the white-rot fungus *Pleurotus eryngii* in *Saccharomyces cerevisiae* (Viña-Gonzalez, Gonzalez-Perez, Ferreira, Martinez, & Alcalde, 2015). This was achieved by designing a chimeric signal peptide (preαproK) that fused the pre- and pro-region of the α-factor and the K_1 killer toxin prepro-leaders from *S. cerevisiae*, and subsequently employing directed evolution to restricted AAO regions. We obtained a panel of AAO secretion variants that was led by the $_{Sac}$FX7 mutant, in which the consensus/ancestral substitution (H91N) was responsible for a ~100-fold improvement in total activity, as well as enhanced stability in terms of temperature and pH.

The current work describes a tandem-yeast expression system for AAO that links the directed evolution for secretion in *S. cerevisiae* to its over-production in *Pichia pastoris* on a bench-bioreactor scale. Harnessing the high frequency of homologous DNA recombination of *S. cerevisiae*, mutant libraries were constructed by shuffling $_{Sac}$FX7 with an ensemble of AAO secretion variants, while the chimeric peptide was further subjected to independent mutational loading. The resulting evolved AAO was transferred to *P. pastoris* for overproduction in a fed-batch bioreactor and characterized biochemically. To shed light on the effects exerted by hyperglycosylation in *S. cerevisiae*, the recombinant variant expressed in *P. pastoris* was further benchmarked with its counterpart secreted by a glycosylation-deficient *S. cerevisiae* strain.

2 | MATERIAL AND METHODS

2.1 | Strains and chemicals

All chemicals were reagent-grade purity. Basal salts, PTM1 salts, *p*-methoxybenzyl alcohol, veratryl alcohol, benzyl alcohol, 2,4-hexadien-1-ol, ABTS (2,2′-azino-bis(3-ethylbenzothiazoline-6-sulphonic acid)), horseradish peroxidase (HRP), Taq polymerase and the Yeast Transformation Kit were purchased from Sigma–Aldrich (SaintLouis, MO). Zymoprep Yeast Plasmid Miniprep, Yeast Plasmid Miniprep Kit I and Zymoclean Gel DNA Recovery Kit were from Zymo Research (Orange, CA). The *P. pastoris* expression vector (pPICZ B), the *P. pastoris* strain X–33 and zeocin were purchased from Invitrogen (Carlsbad, CA). The protease deficient *S. cerevisiae strain* BJ5465 (α ura3-52 trp1 leu2Δ1 his3Δ200 pep4::HIS3 prb1Δ1.6R can1 GAL) was from LGC Promochem (Barcelona, Spain) whereas the glycosylation deficient *S. cerevisiae strain* YDR483W BY4742 (MATalpha his3delta1 leu2delta0 lys2delta0 ura3delta0 deltaKRE2) was from ATCC (Manassas, VA). The *Escherichia coli* strain XL2-Blue competent cells and Phusion DNA Polymerase were obtained from Agilent Technologies (Santa Clara, CA). Restriction endonucleases BsaI, XhoI, XbaI, KpnI, PmeI, the DNA Ligation Kit, the Antarctic phosphatase, EndoH and T4 DNA Ligase were purchased from New England Biolabs (Ipswich, MA). Oligonucleotide primers were acquired from Isogen Life Science (Barcelona, Spain).

2.2 | Culture media

2.2.1 | Culture media for *Saccharomyces cerevisiae*

Minimal medium contained 0.67% (w:v) yeast nitrogen base, 1.92 g/L yeast synthetic drop-out medium supplement without uracil, 2% (w:v) raffinose and 25 μg/ml chloramphenicol. SC drop-out plates contained 0.67% (w:v) yeast nitrogen base, 1.92 g/L yeast synthetic drop-out medium supplement without uracil, 2% (w:v) bacto agar, 2% (w:v) D-glucose and 25 μg/ml chloramphenicol. YP medium contained 10 g yeast extract, 20 g peptone and double-distilled H_2O (ddH_2O) to 650 ml. Expression medium contained 144 mL YP 1.55×, 13.4 ml 1M KH_2PO_4 pH 6.0 buffer, 22.2 ml 20% galactose (w:v), 0.222 ml 25 μg/ml chloramphenicol and ddH_2O to 200 ml.

2.2.2 | Culture media for *Pichia pastoris*

YPD medium contained 10 g/L yeast extract, 20 g/L peptone, 4 g/L D-glucose, and 25 μg/ml zeocin whereas YPD plates also contained 2% (w:v) bacto agar. BMD1 medium contained 100 mM potassium phosphate buffer pH 6.0, 3.5 g/L yeast nitrogen base without amino acids, 400 μg/L biotin and 10 g/L D-glucose. BMM2 medium contained 100 mM potassium phosphate buffer pH 6.0, 3.5 g/L yeast nitrogen base without amino acids, 400 μg/L biotin and 2% methanol (v:v). BMM10 medium contained 100 mM potassium phosphate buffer pH 6.0, 3.5 g/L yeast nitrogen base without amino acids, 400 μg/L biotin and 10% methanol (v:v). BMMY medium contained 100 mM potassium phosphate buffer pH 6.0, 3.5 g/L yeast nitrogen base without amino acids, 400 μg/L biotin and 0.5% methanol (v:v). Basal salts medium contained 26.7 ml/L 85% phosphoric acid, 0.93 g/L $CaSO_4 \cdot 2H_2O$, 14.9 g/L $MgSO_4 \cdot 7H_2O$, 18.2 g/L K_2SO_4, 4.13 g/L KOH and 40 g/L glycerol.

2.2.3 | Culture media for *Escherichia coli*

Luria-Bertani (LB) medium contained 10 g NaCl, 5 g yeast extract, 10 g peptone, 1 ml 100 mg/ml ampicillin and ddH_2O to 1 L whereas LB agar plates also contained 2% (w:v) bacto agar.

2.3 | Laboratory evolution

2.3.1 | In vivo shuffling

PCR reactions were performed separately with mutants $_{Sac}$FX7, $_{Sac}$13H2, $_{Sac}$10G5, $_{Sac}$7A11, $_{Sac}$4C7, and $_{Sac}$12G12. Reaction mixtures were prepared in a final volume of 50 µl containing DNA template (0.92 ng/µl), 90 nM oligo sense RMLN (5′-CCTCTATACTTTAACGTCAAGG-3′), 90 nM Reverse primer RMLC (5′-GGGAGGGCGTGAATGTAAGC-3′), 0.3 mM dNTPs (0.075 mM each), 3% (v:v) dimethylsulfoxide (DMSO), 1.5 mM $MgCl_2$, increasing concentrations of $MnCl_2$ (0.025, 0.05, 0.1 mM) and 0.05 U/µl Taq DNA polymerase. PCRs were performed in a thermocycler (Mycycler, Bio-Rad, Hercules, CA) and parameters were: 95 °C for 2 min (1 cycle); 95 °C for 45 s, 50 °C for 45 s, 74 °C for 45 s (28 cycles); and 74 °C for 10 min (1 cycle). The PCR products were mixed with the linearized episomal shuttle vector pJRoC30 (at a PCR product/linearized plasmid ratio of 6:1) and transformed into competent *S. cerevisiae* cells to promote in vivo DNA shuffling. The whole gene was reassembled in vivo by transformation into *S. cerevisiae*, a process facilitated by the design of ∼50-bp overhangs flanking each recombination area. Transformed cells were plated on SC drop-out plates and incubated for 3 days at 30 °C. Colonies containing the whole autonomously replicating vector were picked and subjected to high-throughput screening.

2.3.2 | MORPHING library at the preαproK

The preαproK signal peptide of $_{Sac}$FX8 variant (261 bp) was used as DNA template for focused random mutagenesis technique MORPHING (Mutagenic Organized Recombination Process by Homologous IN vivo Grouping) (Gonzalez-Perez, Molina-Espeja, Garcia-Ruiz, & Alcalde, 2014). Mutagenic PCR was prepared in a final volume of 50 µL containing: 90 nM RMLN, 90 nM C-ter prokiller (5′-ACGCTTGGCCACTGCTGGAAT-3′), 0.3 mM dNTPs (0.075 mM each), 3% DMSO, 0.1 mM $MnCl_2$, 1.5 mM $MgCl_2$, 0.05 U/µl l Taq polymerase DNA, and 0.92 ng/µl template. The amplification parameters were 95 °C for 2 min (1 cycle); 94 °C for 45 s, 50 °C for 45 s, and 74 °C for 30 s (28 cycles); and 74 °C for 10 min (1 cycle). The whole AAO gene (1701 bp) was amplified by high-fidelity PCR in a final volume of 50 µl containing: 250 nM oligo sense N-ter AAO (5′-GCCGATTTTGACTACGTTGTCG TCG-3′), 250 nM oligo antisense RMLC, 1 mM dNTPs (0.25 mM each), 3% DMSO, 0.05 U/µL Phusion DNA polymerase, and 2 ng/µL template. High-fidelity PCR was performed using the following parameters: 95 °C for 2 min (1 cycle); 94 °C for 30 s, 50 °C for 30 s, 74 °C for 2 min (30 cycles); and 74 °C for 10 min (1 cycle). PCR products were mixed in equimolar amounts, 200 ng mutagenic signal peptide and 200 ng mature non-mutagenized protein, and transformed with linearized pJRoC30 (200 ng) into chemically competent cells, as described above.

2.3.3 | High-throughput screening (HTS) assay

Individual clones were picked and cultured in sterile 96-well plates containing 50 µl of minimal medium. In each plate, column number 6 was inoculated with the parental type (internal standard) and well H1 with URA3- *S. cerevisiae* cells (negative control). Plates were sealed to prevent evaporation and incubated at 30 °C, 225 rpm and 80% relative humidity in a humidity shaker (Minitron-INFORS, INFORS-HT, Switzerland). After 48 hr, 160 µl of expression medium were added to each well and cultured for additional 48 hr. Aliquots of 20 µl of yeast supernatants were transferred to a 96-well plate with liquid handler robotic station Freedom EVO (Tecan, Männedorf, Switzerland) and 180 µl of HRP-ABTS reagent (final concentrations of HRP-ABTS reagent in the well: 1 mM *p*-methoxybenzyl alcohol, 2.5 mM ABTS, 1 µg/ml HRP in 100 mM phosphate buffer pH 6.0) were dispensed with Multidrop™ Combi Reagent Dispenser (Thermo Scientific, Waltham, MA). The plates were incubated at room temperature and measured in kinetic mode at 418 nm ($\varepsilon ABTS^{\bullet +} = 36000\ M^{-1}\ cm^{-1}$). The HTS-assay incorporated two consecutive re-screenings to rule out the selection of false positives as described elsewhere (Viña-Gonzalez et al., 2016).

2.4 | AAO in *S. cerevisiae*

2.4.1 | Shake-flask fermentation

A single colony from the *S. cerevisiae* clone containing the AAO fusion gene was picked from a SC drop-out plate, inoculated in minimal medium (20 ml) and incubated for 48 hr at 30 °C and 220 rpm. An aliquot of cells was removed and used to inoculate minimal medium (100 ml) in a 500 mL flask ($OD_{600} = 0.25$). The cells completed two growth phases (6–8 hr; $OD_{600} = 1$) and then expression medium (900 ml) was inoculated with the pre-culture (100 ml) (OD_{600} of 0.1). After incubating for 72 hr at 25 °C and 220 rpm (maximal AAO activity; $OD_{600} = 25–30$), the cells were recovered by centrifugation at 4500 rpm and 4 °C (Avanti J-E centrifuge, Beckman Coulter Inc., CA) and the supernatant was double-filtered (using both glass membrane filter and a nitrocellulose membrane of 0.45 µm pore size). The incubation for the expression in glycosylation deficient *S. cerevisiae* strain YDR483W BY4742 was stopped after 18 hr to avoid proteolytic degradation of the AAO by extracellular yeast proteases.

2.5 | AAO in *P. pastoris*

2.5.1 | AAO cloning in *P. pastoris*

The coding region of the evolved AAO variant (1962 bp) was cloned into the expression vector pPICZ-B. First, pJRoC30-FX7/FX9 was used to amplify AAO variants with the primers ppKpnAAO-dir (5′-GGGGTACCATGAGATTTCCTTCAATTTTTACTGC-3′) and ppAAO-rev (5′- GCTCTAGACTACTGATCAGCCTTGATAAGATCGGC-3′), the primers included targets for restriction enzymes KpnI and XbaI, respectively (underlined). The PCR reactions were prepared in a final volume of 50 µl containing 250 nM of each primer, 1 mM dNTPs (0.25 mM each), 3% DMSO, 0.05 U/µl Phusion DNA polymerase, and 2 ng/µl template. The parameters for the PCR were: 95 °C for 2 min (1 cycle); 94 °C for 30 s, 50 °C for 30 s, 74 °C for 2 min (30 cycles); and 74 °C for 10 min (1 cycle). The pPICZ-B vector and the PCR product were digested with the restriction enzymes KpnI and XbaI at 37 °C for 1 hr. The 5′ and 3′ends of the linearized pPICZ-B plasmid were dephosphorylated using antarctic phosphatase at 37°C for 1 h adding 1 U of enzyme per every 200 ng of linearized vector. The PCR product and the linearized vector were loaded onto a preparative agarose gel, purified using the Zymoclean Gel DNA Recovery kit and ligated with

T4 DNA ligase at room temperature for 30 min. After transformation of the pPICZ-B-AAO construct into chemically competent *E. coli* XL2-Blue cells, the plasmid was proliferated, linearized with the restriction enzyme PmeI at 37 °C for 1 hr and transformed into electro-competent *P. pastoris* X–33 cells. Electro-competent *P. pastoris* cells were prepared and transformed with the construction as described in the protocol from Lin-Cereghino and Cregg (2000) mixing 200 ng of linearized vector and 50 µl of competent cells. Transformants were grown on YPD plates.

2.5.2 | Deep-well plate fermentation

P. pastoris colonies containing AAO under the control of the AOX1 promoter (pPICZ-B-AAO) were picked and cultivated in 96-deep-well plates containing 300 µl of BMD1 medium per well. The plates were incubated at 25 °C, 300 rpm and 80% humidity for 2 days in a humidity shaker. Afterwards, 300 µl of BMM2 medium were added per well. After 12 hr of incubation, 70 µl of BMM10 medium were added to each well repeating this addition every 24 hr for 3 days. After 142 hr, the activity with *p*-methoxybenzyl alcohol was measured (final concentrations in the reaction mixture: 1 mM *p*-methoxybenzyl alcohol, 2.5 mM ABTS, 1 µg/ml HRP in 100 mM phosphate buffer pH 6.0).

2.5.3 | Shake-flask fermentation

Transformants with the best activity from the deep-well plate fermentations were grown in YPD agar plates and inoculated in 3 ml of liquid YPD at 30 °C and 250 rpm. The culture reached the optical density at 600 nm at 1 after 6–7 hr and was inoculated in 20 ml of BMMY medium in 100 ml shaken flasks. The cultures were incubated at 25 or 30 °C and they were supplemented with 250 µl of methanol every 24 hr. After 3 days of methanol addition, the best clone with the highest activity was selected for the bioreactor fermentation.

2.5.4 | Production in bioreactor

The FX9 mutant ($_{\pi}$FX9) under the control of the AOX1 promoter in the pPICZ-B-FX9 construct was produced in a 5 L vessel fermenter (Minifors, INFORS-HT, Switzerland). The bioreactor was filled with 2 L of basal salts medium (initial volume: 2 L). After sterilization, 4.35 ml/L PTM1 trace salts and 1 ml Antifoam 204 were added to the medium and the pH was adjusted with ammonium hydroxide to 5.0. The fermentation was started with the addition of 0.2 L of preculture grown on YPD medium in several baffled shaken flasks at 150 rpm and 30 °C overnight (OD_{600} between 6 and 10). According to the *Pichia Fermentation Process Guidelines* of Invitrogen the batch fermentation was run at 30 °C, 600 rpm and air aeration 1 vvm. Once all the glycerol from the batch was consumed, the glycerol fed phase was initiated by the addition of 50% (w/v) glycerol feed containing 12 ml/L PTM1 trace salts to achieve higher cell density at a 21.8 ml/hr rate. After 2 hr, the glycerol feed faded out by a linear ramp 14.6–0 ml/hr over 2 hr and the methanol feed containing 12 ml/L PTM1 trace salts started at a 7.2 ml/hr for the culture to transition and adapt to methanol. From this time on the temperature was set to 25 °C and the Dissolved Oxygen (DO) above 20% with the control of the stirring speed between 600 and 1200 rpm and aeration using mixtures of air and O_2 within 0.7 and 1 vvm. At the end of the transition phase the methanol/PTM1 feeding was increased to 14.6 ml/hr until the end of the process. Water evaporation losses were minimized during the process with an exhaust gas condenser and cooling water at 4 °C. The fermentation was controlled by taking samples for biomass analysis and AAO activity: The cell concentration was monitored by measuring the optical density of cultures at 600 nm (OD_{600}). For wet dry weight (CDW) measurement, cells were separated from 1 ml culture broth by centrifugation at 10,000 g for 5 min using pre-weighed 1.5 ml tubes. The wet weight is measured immediately after all the yeast supernatant has been removed. AAO activity was measured with HRP/ABTS method with *p*-methoxybenzyl alcohol as the substrate.

2.6 | AAO purification

The FX9 variants expressed in *S. cerevisiae* (protease deficient strain BJ5465 and glycosylation deficient strain YDR483W BY4742) and *P. pastoris* were purified to homogeneity as described in a former work (Viña-Gonzalez et al., 2015).

2.7 | AAO biochemical characterization

2.7.1 | N-terminal analysis and pI determination

Purified AAO variants were subjected to SDS/PAGE, and the protein band was blotted onto PVDF membranes. The PVDF membrane was stained with Coomassie Brilliant Blue R-250, after which the enzyme band was excised and processed for N-terminal amino acid sequencing on a precise sequencer at the Protein Chemistry Service at the The Biological Research Center (Madrid, Spain). Purified FX9 (8 µg) was subjected to two-dimensional electrophoresis gel in order to determine the pI.

2.7.2 | Determination of kinetic-thermostability (T_{50})

Appropriate dilutions of AAO were prepared for the assay. The gradient scale ranging from 30 to 80 °C was established as follows: 30.0, 31.4, 34.8, 39.3, 45.3, 49.9, 53, 55, 56.8, 59.9, 64.3, 70.3, 75, 78.1, and 80 °C. This gradient profile was achieved using a thermocycler. After 10 min of incubation, AAO samples were removed and chilled out on ice for 10 min and incubated further at room temperature for 5 min. Finally, samples of 20 µl were added to 180 µl volumes of 100 mM sodium phosphate pH 6.0 buffer containing 1 mM *p*-methoxybenzyl alcohol and activity was measured as anisaldehyde production as absorption at 285 nm ($\varepsilon_{285} = 16{,}950\ M^{-1}\ cm^{-1}$). Thermostability values were calculated from the ratio between the residual activities incubated at different temperature points and the initial activity at room temperature. The T_{50} value was determined by the transition midpoint of the inactivation curve of the protein as a function of temperature, which in our case was defined as the temperature at which the enzyme lost 50% of its activity following an incubation of 10 min. All reactions were performed by triplicate.

2.7.3 | pH activity profile

Appropriate dilutions of enzyme samples were prepared in such a way that aliquots of 20 µl gave rise to a linear response in kinetic mode. The optimum pH activity was determined using 100 mM citrate-phosphate-borate buffer at different pH values (2.0, 3.0, 4.0, 5.0, 6.0, 7.0, 8.0 and 9.0) containing 0.3 *p*-methoxybenzyl alcohol.

2.7.4 | Kinetic parameters

Kinetic constants for AAO were estimated in 100 mM sodium phosphate pH 6.0. Reactions were performed by triplicate and substrates oxidations were followed by measuring the absorption at 285 nm for *p*-methoxybenzyl alcohol, $\varepsilon_{285} = 16{,}950\ M^{-1}\ cm^{-1}$; 310 nm for veratryl alcohol, $\varepsilon_{310} = 9{,}300\ M^{-1}\ cm^{-1}$; 250 nm for benzyl alcohol, $\varepsilon_{250} = 13{,}800\ M^{-1}\ cm^{-1}$; 280 nm for 2,4-hexadien-1-ol, $\varepsilon_{280} = 30{,}140\ M^{-1}\ cm^{-1}$. Steady-state kinetics parameters were determined by fitting the initial reactions rates at different substrate concentrations to the Michaelis-Menten equation for one substrate, $v/e = k_{cat}.S/(K_m + S)$ where e represent the enzyme concentration, k_{cat} is the maximal turnover rate, S is the substrate concentration and K_m the Michaelis constant. Data were fit using SigmaPlot 10.0 (Systat. Software Inc. Richmond, CA).

2.7.5 | Protein modeling

A structural model of the AAO from *P. eryngii* crystal structure at a resolution of 2.55 Å (Protein Data Bank Europe [PDB] accession number 3FIM, (Fernandez et al., 2009) was used as scaffold for the wild type AAO model and the FX9 mutant homology model, obtained by PyMol (Schrodinger LLC.; http://www.pymol.org).

2.7.6 | DNA sequencing

All genes were verified by DNA sequencing (BigDye Terminator v3.1 Cycle Sequencing Kit). The primers for the genes cloned in the pJRoC30 plasmid were: primers sense, RMLN and AAOsec1F 5′-GTGGATCAACAGAAGATTTCGATCG-3′ and primers antisense RMLC 5′-GCTTACATTCACGCCCTCCC-3′, AAOsec2R 5′-GTGGTTAGCAATGAGCGCGG-3′ and AAOsec3R 5′-GGAGTCGAGCCTCTGCCCCT-3′. For the AAO genes cloned in the pPICZ-B plasmid primers were: ppKpnAAO-dir and AAOsec1F as primers sense and ppAAO-rev, AAOsec2R and AAOsec3R as primers antisense.

3 | RESULTS AND DISCUSSION

3.1 | Improved secretion in *S. cerevisiae* by in vivo shuffling and MORPHING of the chimeric signal peptide

During the first evolutionary campaign to increase AAO secretion in yeast, six mutants (carrying 7 beneficial mutations) were identified with improvements in total activity that ranged from roughly 2- up to 100-fold (for $_{Sac}$FX7), Figure 1 (Viña-Gonzalez et al., 2015). Given that most of these mutations were >20 residues from one another, they were shuffled in vivo by taking advantage of the homologous recombination machinery of *S. cerevisiae* (Gonzalez-Perez, Garcia-Ruiz, & Alcalde, 2012). The mutant library was screened in the HRP-ABTS assay using *p*-methoxybenzyl alcohol as the substrate as described previously (Viña-Gonzalez et al., 2015, 2016). The best mutant from this round of DNA shuffling was $_{Sac}$FX8, which showed 2.6- and 250-fold improved total activity over $_{Sac}$FX7 and the parental AAO, respectively. As planned, several crossover events took place that allowed mutations from different parental types to be convened: the consensus-ancestral mutation H91N from $_{Sac}$FX7; the L170M mutation from $_{Sac}$10G5; and the T50A mutation at the K_1 killer toxin pro-leader inherited from $_{Sac}$12G12, Figure 1. To further enhance secretion, we evolved the preαproK signal leader by MORPHING, a domain-focused mutagenesis technique that allows mutations and crossover events to be randomly introduced in defined stretches (Gonzalez-Perez et al., 2014). With this strategy 3 new mutations were included in the preαproK (F3S at the preα, and H25N- F52L at the K_1 pro-leader), giving rise to the final $_{Sac}$FX9 secretion variant with a 350-fold improvement in activity relative to the parental AAO type, expression levels of 4.5 mg/L in flask culture and high thermostability.

The evolved leader sequence of $_{Sac}$FX9 derived from the DNA shuffling and the focused evolution experiments carried four substitutions relative to the original preαproK chimeric construction, Figures 1 and 2a. The preα-leader segment carries the F[3_α]S mutation which agrees well with substitutions at the same position (F[3_α]P/L) previously found in α-factor prepro-leaders that improved antibody secretion (Rakestraw, Sazinsky, Piatesi, Antipov, & Wittrup, 2009). An acidic residue was introduced into the proK-peptide with the new substitution N[25_K]D, whereas mutation T[50_K]A, inherited from the parental 12G12, together with F[52_K]L increase the hydrophobic load of the middle sequence. In the mature protein, the mutation L170M from 10G5 is located in an α-helix at the surface and mutation H91N from FX7 is in the catalytic pocket, Figures 2b and 2c. As we described previously, Asn91 is a consensus residue situated at the *si*-face of the FAD that stabilizes the conformation of the cofactor, thereby enhancing secretion and AAO stability (Viña-Gonzalez et al., 2015).

3.2 | Functional expression of recombinant AAO in *pastoris* and scaling-up

The use of compatible tandem-expression systems for protein engineering and overproduction can overcome certain limitations when dealing with complex eukaryotic enzymes like AAO (Alcalde, 2015). In particular, combining *S. cerevisiae* as the host of choice for the directed evolution of eukaryotic ligninases with the methylotrophic yeast *P. pastoris* (currently reclassified as *Komagataella phaffii*) for overproduction offers many attractive advantages, as demonstrated recently (Mate, Gonzalez-Perez, Kittl, Ludwig, & Alcalde, 2013; Molina-Espeja, Ma, Mate, Ludwig, & Alcalde, 2015). Heterologous expression in *S. cerevisiae* and *P. pastoris* falls under the lowest-common-denominator of a well-defined secretory apparatus and the ability to perform complex post-translational modifications, which

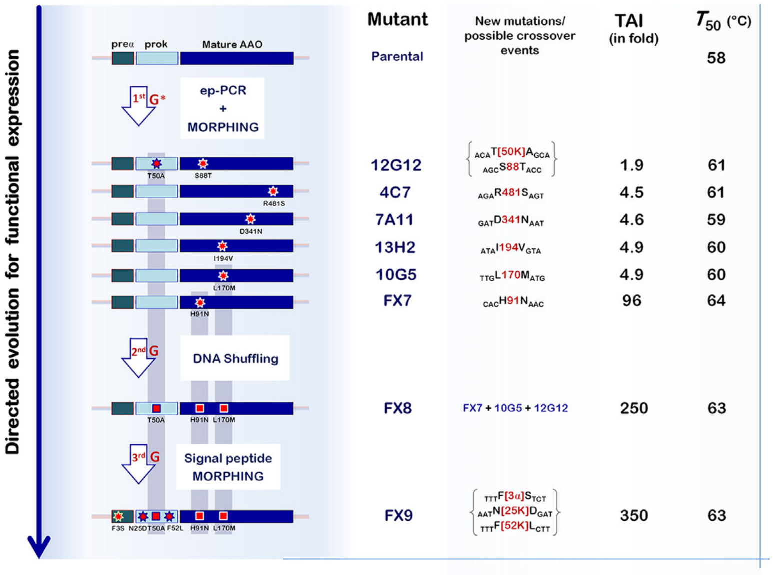
Directed evolution for functional expression
preα
prok
Mature AAO
1st G*
ep-PCR + MORPHING
T50A
S88T
R481S
D341N
I194V
L170M
H91N
2nd G
DNA Shuffling
3rd G
Signal peptide MORPHING
F3S
N25D
F52L
Mutant
New mutations/ possible crossover events
TAI (in fold)
T_{50} (°C)
Parental
58
12G12
$_{ACA}$T[50K]A_{GCA}
$_{AGC}$S88T_{ACC}
1.9
61
4C7
$_{AGA}$R481S_{AGT}
4.5
61
7A11
$_{GAT}$D341N_{AAT}
4.6
59
13H2
$_{ATA}$I194V_{GTA}
4.9
60
10G5
$_{TTG}$L170M_{ATG}
4.9
60
FX7
$_{CAC}$H91N_{AAC}
96
64
FX8
FX7 + 10G5 + 12G12
250
63
FX9
$_{TTT}$F[3α]S_{TCT}
$_{AAT}$N[25K]D_{GAT}
$_{TTT}$F[52K]L_{CTT}
350
63

FIGURE 1 Laboratory evolution of the AAO from *Pleurotus eryngii* towards functional expression in yeast. New mutations are represented as stars and accumulated mutations as squares. The preα-leader segment is depicted in green, the prok-leader segment in light blue and the mature AAO in dark blue. The TAI (total activity improvement) is the value indicating the improvement in AAO activity detected in *S. cerevisiae* supernatants relative to the parental type. Kinetic thermostability expressed by the T_{50} value (the temperature at which the enzyme retains 50% of its activity after a ten minute incubation). *1st G, results from the first generation of variants published in Viña-Gonzalez et al. (2015)

frequently results in reasonable secretion of the active and stable enzyme. However, *S. cerevisiae* has a broad variety of episomal vectors, high-transformation efficiencies and a precise recombination apparatus to aid the creation and screening of mutant libraries for directed evolution. While *P. pastoris* lacks such properties, it outperforms *S. cerevisiae* in terms of protein production under the control of strong and tightly regulated promoters, reaching extremely high cell densities in bioreactor (Ahmad, Hirz, Pichler, & Schwab, 2014). Hence, during the heterologous expression of AAO in yeast, the question that arises is can the improvements in secretion obtained by directed evolution in *S. cerevisiae* be transferred to *P. pastoris*, or in other words, how well are the improvements in secretion preserved in both yeasts.

To assess the compatibility of these two systems, the evolved variants $_{sac}$FX7 and $_{sac}$FX9 were cloned into *P. pastoris* to determine if

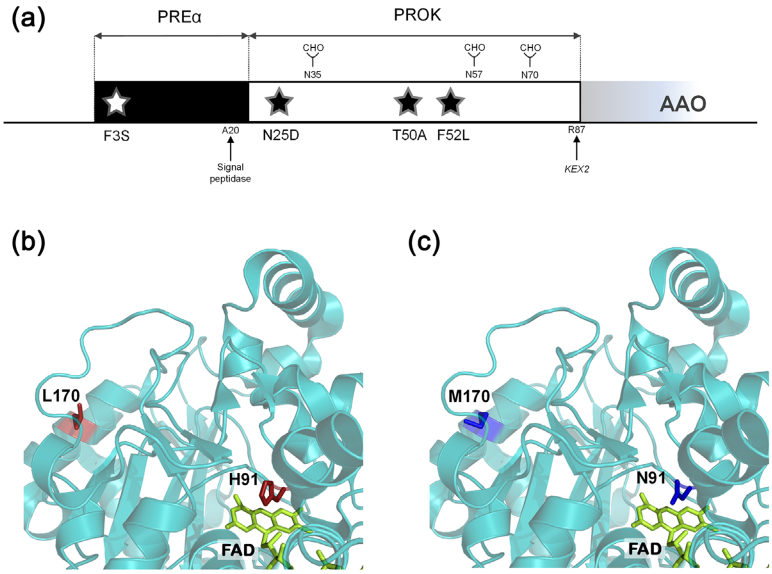
(a)
PREα
PROK
CHO
N35
CHO
N57
CHO
N70
AAO
F3S
A20
Signal peptidase
N25D
T50A
F52L
R87
KEX2
(b)
L170
H91
FAD
(c)
M170
N91
FAD

FIGURE 2 Mutations presented by FX9. (a) Substitutions in the chimeric preαproK signal peptide. (b and c) Molecular model using the *Pleurotus eryngii* AAO crystal structure as a template (PDB code 3FIM). (b) wild type AAO and (c) the FX9 variant. FAD is depicted in yellow and the details of the two mutations in FX9 (blue) are compared with the corresponding residues in the wild type (red)

TABLE 1 Biochemical properties of recombinant FX9 mutant

Biochemical properties	${}_{sac}$FX9	${}_{\Delta}$FX9	${}_{\pi}$FX9
MW (Da)[1]	150,000	63,000	63,000
MW (Da)[2]	60,952	60,952	60,952
Glycosylation degree (%)	60	n.m	n.m
Thermal stability, T_{50} (°C)	63	61.2	61.3
pI	4.8	4.6	4.5
N-terminal end	ADFDYVVVG	ADFDYVVVG	ADFDYVVVG
Secretion levels (mg/L)	4.5	n.d.	4.3

N.m (non-measurable); n.d. (non-determined).

[1] Estimated by SDS–PAGE.

[2] Estimated from amino acid sequence.

the improvements in secretion furbished by the mutations are consistent between hosts. Under the methanol inducible AOX1 promoter, transformants were grown in deep-well plate micro-fermentations and screened for secretion −*P. pastoris* can integrate up to six copies of the foreign gene into its genome-. Selected clones, ${}_{\pi}$FX7 and ${}_{\pi}$FX9, were then produced in 100 mL shaking flask cultures, producing total activity values of 50 and 235 U/L, respectively. Hence, the beneficial mutations for secretion in *S. cerevisiae* retained their effects in *P. pastoris* and they were even associated with an improvement in total activity from 3.6-fold in *S. cerevisiae* to 4.7-fold in *P. pastoris*. To harness the high cell titers of *P. pastoris* in the bioreactor, ${}_{\pi}$FX9 was transferred to a 5L fed-batch fermenter and after six days, maximal volumetric activity was reached (1378 U/L) with the production of AAO (25.5 mg/L) surpassing that obtained in shaking-flask cultures roughly 6-fold. Since AAO is secreted similarly by *S. cerevisiae* and *P. pastoris* (Table 1), this improved production can be solely attributed to the high cell densities achieved by *P. pastoris* in the bioreactor (up to 260 g wet biomass/L; $OD_{600} \sim 430$), Figure 3a.

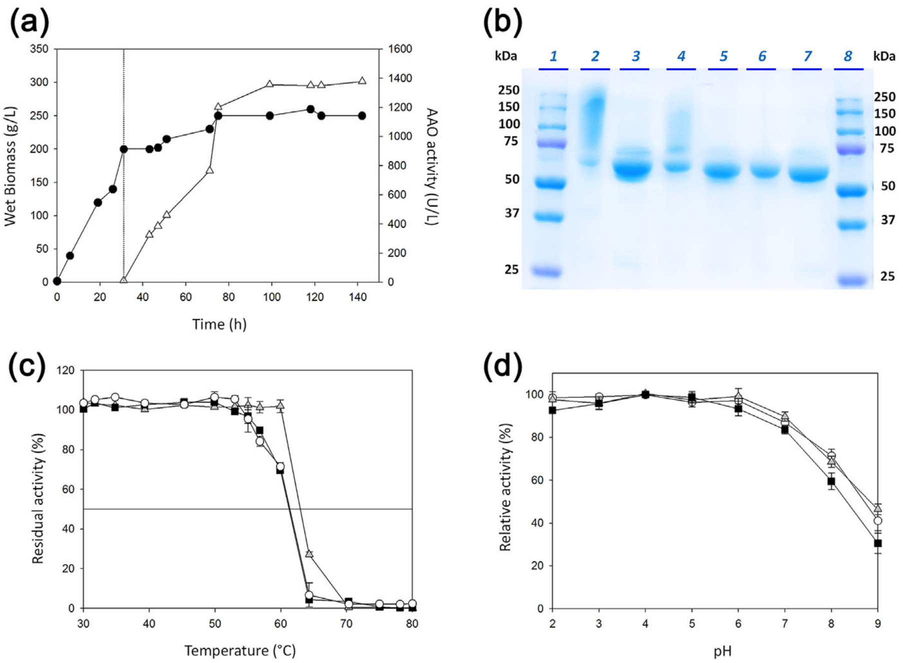

FIGURE 3 (a) Fermentation in a 5 L bioreactor of recombinant ${}_{\pi}$FX9 expressed in *P. pastoris*. Fermentation was performed in four steps: glycerol-batch phase for 26 hr, glycerol-fed phase for 4h, transition phase for 4 hr and methanol induction phase for 112 hr. The black circles represent the wet biomass, the white triangles the volumetric AAO activity and the dotted vertical line the beginning of the induction phase. (b) Molecular mass of recombinant AAO. 10% SDS-polyacrylamide gel: Lanes 1 and 8, protein markers; 2, purified ${}_{sac}$FX9 mutant; 3, deglycosylated ${}_{sac}$FX9; 4, purified ${}_{\Delta}$FX9; 5, deglycosylated ${}_{\Delta}$FX9; 6, purified ${}_{\pi}$FX9; 7 deglycosylated ${}_{\pi}$FX9. (c) Kinetic thermostability (T_{50}) of the recombinant variants: ${}_{sac}$FX9 (gray triangles), ${}_{\Delta}$FX9 (black squares), and ${}_{\pi}$FX9 (white circles). (d) pH activity profiles for ${}_{sac}$FX9 (gray triangles), ${}_{\Delta}$FX9 (black squares) and ${}_{\pi}$FX9 (white circles) with *p*-methoxybenzyl alcohol (1 mM). Each point represents the mean and standard deviation of three independent experiments

TABLE 2 Kinetic parameters for yeast-recombinant AAO variants

Substrate	Kinetic constants	${}_{sac}$FX7*	${}_{sac}$FX9	${}_{\Delta}$FX9	${}_{\pi}$FX9
p-methoxybenzyl alcohol	K_m (mM)	0.034 ± 0.001	0.023 ± 0.002	0.022 ± 0.001	0.037 ± 0.004
	k_{cat} (s^{-1})	54 ± 4	41 ± 0.6	56.9 ± 0.6	70 ± 2
	k_{cat}/K_m ($mM^{-1}\,s^{-1}$)	1562	1782	2586	1909
Veratryl alcohol	K_m (mM)	0.38 ± 0.02	0.34 ± 0.02	0.36 ± 0.01	0.41 ± 0.01
	k_{cat} (s^{-1})	28 ± 1	24.6 ± 0.7	36.8 ± 0.3	56.9 ± 0.6
	k_{cat}/K_m ($mM^{-1}\,s^{-1}$)	71	72	102	139
Benzyl alcohol	K_m (mM)	0.51 ± 0.01	0.37 ± 0.01	0.38 ± 0.03	0.44 ± 0.02
	k_{cat} (s^{-1})	19 ± 1	15.1 ± 0.2	23.4 ± 0.6	34.4 ± 0.5
	k_{cat}/K_m ($mM^{-1}\,s^{-1}$)	36	41	62	78
2,4-hexadien-1-ol	K_m (mM)	0.059 ± 0.004	0.096 ± 0.009	0.095 ± 0.006	0.106 ± 0.001
	k_{cat} (s^{-1})	52 ± 1	47 ± 1	62 ± 1	89 ± 3
	k_{cat}/K_m ($mM^{-1}\,s^{-1}$)	866	456	653	840

AAO kinetic constants were estimated in 100 mM phosphate buffer pH 6.0 at 25 °C. All reactions were performed by triplicate.
*Kinetic values from Viña-Gonzalez et al. (2015).

3.3 | Influence of glycosylation on biochemical parameters

The ${}_{Sac}$FX9 and ${}_{\pi}$FX9 variants were purified to homogeneity and characterized biochemically. N-terminal sequencing confirmed the correct cleavage of the chimeric preαproK by the KEX2 protease in the Golgi compartment in both yeasts, Table 1. It is well known that *S. cerevisiae* produces strong glycosylation during heterologous protein expression. Indeed, as occurred with the parental ${}_{Sac}$FX7 (Viña-Gonzalez et al., 2015), ${}_{Sac}$FX9 underwent hyperglycosylation (~60% glycosylation) and the wide smear produced by the different glycoforms (ranging from ~200,000 to 63,000 Da in SDS–PAGE) collapsed into a single 63,000 Da band after deglycosylation with EndoH, Figure 3b, Table 1. By contrast, in *P. pastoris* the same variant (${}_{\pi}$FX9) produced a single ~63,000 Da band before and after treatment with EndoH, highlighting the weak glycosylation expected in *P. pastoris*, Figure 3b. The T_{50} (the temperature at which the enzyme retains 50% of its activity after a ten minute incubation) of ${}_{Sac}$FX9 was slightly higher (1.7 °C) than that of ${}_{\pi}$FX9, possibly due to this hyperglycosylation, Table 1, Figure 2c. As such, the kinetic thermostability of both the recombinant variants expressed by the yeasts exceeded that reported for wild type AAO expressed in *E. coli* after in vitro refolding by ~15 °C ($T_{50} = 47.5$ °C), emphasizing the beneficial effect of: (i) natural folding and heterologous secretion in yeast and (ii) the introduction of the stabilizing consensus-ancestor mutation H91N, as described previously (Viña-Gonzalez et al., 2015). The pH activity profile of ${}_{Sac}$FX9 and ${}_{\pi}$FX9 with *p*-methoxybenzyl alcohol was similar, maintaining over 90% of their activity from pH 2.0 to 6.0, Figure 3d. When the steady kinetic parameters were measured for the oxidation of aromatic and aliphatic alcohols, Table 2, the catalytic efficiencies of ${}_{Sac}$FX9 were similar to those of the parental type ${}_{Sac}$FX7, as was the order of preference for the different substrates. By contrast, ${}_{\pi}$FX9 retained similar K_m values to that of ${}_{Sac}$FX9 but improved by ~2-fold the k_{cat} irrespective of the alcohol tested.

The discrepancies in the kinetic parameters and thermostability between ${}_{Sac}$FX9 and ${}_{\pi}$FX9 may be related to the different degrees of glycosylation in *S. cerevisiae* and *P. pastoris*. To assess this, FX9 was also cloned into the glycosylation-deficient Δ*kre2 S. cerevisiae* strain. Δ*kre2* is thought to attach smaller mannose oligomers than wild type strains to the 7 predicted N-glycosylation motifs (Asn-X-Ser/Thr) in AAO (*i.e.* N62, N138, N151, N222, N303, N325, and N369). After production and purification, the variant secreted by Δ*kre2* (${}_{\Delta}$FX9) was characterized biochemically. As predicted, noticeable lower glycosylation was evident by SDS–PAGE, resolving to a smooth smear with the largest spot at ~63,000 Da, and it unequivocally tightened into a single band upon deglycosylation, Figure 3b, Table 1. The ${}_{\Delta}$FX9 variant displayed a similar pH activity profile to its AAO counterparts together with a T_{50} value identical to that of ${}_{\pi}$FX9 (i.e., 1.7 °C lower than ${}_{Sac}$FX9), Figures 3c and 3d. To complete the breakdown of the biochemical properties of the recombinant AAOs, the kinetic parameters of ${}_{\Delta}$FX9 were measured. As expected, they came close to those of ${}_{\pi}$FX9 due to the ~1.5-fold enhancement in the k_{cat} while the K_m was maintained, Table 2. Together, the expression of FX9 in Δ*kre2* confirmed that the variation in kinetics and thermostability between ${}_{Sac}$FX9 and ${}_{\pi}$FX9 were produced by the distinct degree of glycosylation.

4 | CONCLUSIONS

This study shows how to harness a tandem-yeast expression system to engineer a fungal AAO by directed evolution and overproduce it in a bioreactor. The properties acquired during the evolution cycles in *S. cerevisiae* are easily decoded by *P. pastoris*, which can produce the recombinant enzyme while retaining its catalytic properties and general stability. As a natural progression, future studies could focus on the production of the recombinant enzyme at the g/L scale in other strong industrial hosts like *Trichoderma* or *Aspergillus sp.* Certainly, the findings presented here invite a further exploration and extension of the biotechnological potential of AAO, for example tailoring its activity to oxidize secondary alcohols and resolve chiral mixtures, or tuning the AAO catalysis to furfural-derivative cascade reactions (Carro et al., 2015; Hernandez-Ortega, Ferreira, Merino, et al., 2012; Martinez et al., 2017).

ACKNOWLEDGMENTS

This research was supported by the EU project FP7-KBBE-2013-7-613549-INDOX and by the Spanish Government project BIO2016-79106-R-Lignolution.

ORCID

Miguel Alcalde http://orcid.org/0000-0001-6780-7616

REFERENCES

Ahmad, M., Hirz, M., Pichler, H., & Schwab, H. (2014). Protein expression in *Pichia pastoris*: Recent achievements and perspectives for heterologous protein production. *Applied Microbiology and Biotechnology*, *98*, 5301–5317. https://doi.org/10.1007/s00253-014-5732-5

Alcalde, M. (2015). Engineering the ligninolytic enzyme consortium. *Trends in Biotechnology*, *33*, 155–162. https://doi.org/10.1016/j.tibtech.2014.12.007

Carro, J., Ferreira, P., Rodriguez, L., Prieto, A., Serrano, A., Balcells, B., … Martinez, A. T. (2015). 5-hydroxymethylfurfural conversion by fungal aryl-alcohol oxidase and unspecific peroxygenase. *FEBS Journal*, *282*, 3218–3229. https://doi.org/10.1111/febs.13177

Fernandez, I. S., Ruiz-Dueñas, F. J., Santillana, E., Ferreira, P., Martinez, M. J., Martinez, A. T., & Romero, A. (2009). Novel structural features in the GMC family of oxidoreductases revealed by the crystal structure of fungal aryl-alcohol oxidase. *Acta Crystallographica Section D*, *65*, 1196–1205. https://doi.org/10.1107/S0907444909035860

Ferreira, P., Medina, M., Guillén, F., Martínez, M. J., Van Berkel, W. J, & Martínez, A. T. (2005). Spectral and catalytic properties of aryl-alcohol oxidase, a fungal flavoenzyme acting on polyunsaturated alcohols. *Biochemical Journal*, *389*, 731–738. https://doi.org/10.1042/BJ20041903

Gonzalez-Perez, D., Garcia-Ruiz, E., & Alcalde, M. (2012). *Saccharomyces cerevisiae* in directed evolution: An efficient tool to improve enzymes. *Bioengineered*, *3*, 1–6. https://doi.org/10.4161/bbug.19544

Gonzalez-Perez, D., Molina-Espeja, P., Garcia-Ruiz, E., & Alcalde, M. (2014). Mutagenic organized recombination process by homologous in vivo grouping (MORPHING) for directed enzyme evolution. *PLoS ONE*, *9*, e90919. https://doi.org/10.1371/journal.pone.0090919

Hernandez-Ortega, A., Ferreira, P., & Martinez, A. T. (2012). Fungal aryl-alcohol oxidase: A peroxide-producing flavoenzyme involved in lignin degradation. *Applied Microbiology and Biotechnology*, *93*, 1395–1410. https://doi.org/10.1007/s00253-011-3836-8

Hernandez-Ortega, A., Ferreira, P., Merino, P., Medina, M., Guallar, V., & Martinez, A. T. (2012). Stereoselective hydride transfer by aryl-alcohol oxidase, a member of the GMC superfamily. *ChemBioChem*, *13*, 427–435. https://doi.org/10.1002/cbic.201100709

Lin-Cereghino, J., & Cregg, J. M. (2000). Heterologous protein expression in the methylotrophic yeast *Pichia pastoris*. *FEMS Microbiology Reviews*, *24*, 45–66. https://doi.org/10.1111/j.1574-6976.2000.tb00532.x

Martinez, A. T., Ruiz-Dueñas, F. J., Camarero, S., Serrano, A., Linde, D., Lund, H., … Alcalde, M. (2017). Oxidoreductases on their way to industrial biotransformations. *Biotechnology Advances*,, *35*, 815–831. https://doi.org/10.1016/j.biotechadv.2017.06.003

Martinez, A. T., Ruiz-Dueñas, F. J., Martínez, M. J., del Río, J. C., & Gutierrez, A. (2009). Enzymatic delignification of plant cell wall: From nature to mill. *Current Opinion in Biotechnology*, *20*, 348–357. https://doi.org/10.1016/j.copbio.2009.05.002

Mate, D., Gonzalez-Perez, D., Kittl, R., Ludwig, R., & Alcalde, M. (2013). Functional expression of a blood tolerant laccase in *Pichia pastoris*. *BMC Biotechnology*, *13*, 38. https://doi.org/10.1186/1472-6750-13-38

Molina-Espeja, P., Ma, S., Mate, D. M., Ludwig, R., & Alcalde, M. (2015). Tandem-yeast expression system for engineering and producing unspecific peroxygenase. *Enzyme and Microbial Technology*, *73–74*, 29–33. https://doi.org/10.1016/j.enzmictec.2015.03.004

Rakestraw, J. A., Sazinsky, S. L., Piatesi, A., Antipov, E., & Wittrup, K. D. (2009). Directed evolution of a secretory leader for the improved expression of heterologous proteins and full-length antibodies in *Saccharomyces cerevisiae*. *Biotechnology and Bioengineering*, *103*, 1192–1201. https://doi.org/10.1002/bit.22338

Viña-Gonzalez, J., Gonzalez-Perez, D., & Alcalde, M. (2016). Directed evolution method in Saccharomyces cerevisiae: Mutant library creation and screening. *Journal of Visualized Experiments*, *110*, e53761. https://doi.org/10.3791/53761

Viña-Gonzalez, J., Gonzalez-Perez, D., Ferreira, P., Martinez, A. T., & Alcalde, M. (2015). Focused directed evolution of aryl-alcohol oxidase in yeast by using chimeric signal peptides. *Applied and Environmental Microbiology*, *81*, 6451–6462. https://doi.org/10.1128/AEM01966-15

How to cite this article: Viña-Gonzalez J, Elbl K, Ponte X, Valero F, Alcalde M. Functional expression of aryl-alcohol oxidase in *Saccharomyces cerevisiae* and *Pichia pastoris* by directed evolution. *Biotechnology and Bioengineering*. 2018;1–9. https://doi.org/10.1002/bit.26585

FULL PAPER DOI: 10.1002/adsc.201900134 Advanced Synthesis & Catalysis

Structure-Guided Evolution of Aryl Alcohol Oxidase from *Pleurotus eryngii* for the Selective Oxidation of Secondary Benzyl Alcohols

Javier Viña-Gonzalez,[a] Diego Jimenez-Lalana,[a] Ferran Sancho,[b] Ana Serrano,[c] Angel T. Martinez,[c] Victor Guallar,[b, d] and Miguel Alcalde[a,*]

[a] Department of Biocatalysis, Institute of Catalysis, CSIC, Cantoblanco, 28049 Madrid, Spain
Fax: (+31)-91 5854760; phone: (+34)-91 5854806
E-mail: malcalde@icp.csic.es
[b] Barcelona Supercomputing Center, Jordi Girona 31, 08034 Barcelona, Spain
[c] Biological Research Center, CSIC, Ramiro de Maeztu 9, 28040 Madrid, Spain
[d] ICREA, Passeig Lluís Companys 23, 08010 Barcelona, Spain

Manuscript received: January 29, 2019; Revised manuscript received: March 7, 2019;
Version of record online: April 4, 2019

Supporting information for this article is available on the WWW under https://doi.org/10.1002/adsc.201900134

Abstract: Aryl alcohol oxidase (AAO) is a fungal flavoenzyme capable of oxidizing aromatic primary alcohols into their correspondent aldehydes through a stereoselective hydride abstraction. Unfortunately, this enzyme does not act on secondary benzyl alcohols in racemic mixtures due to the strict control of substrate diffusion and positioning at the active site restricted to primary benzyl alcohols. Here we describe the engineering of AAO from *Pleurotus eryngii* to oxidize chiral benzyl alcohols with high enantioselectivity. The secondary benzyl alcohol oxidase was remodeled at the active site through four cycles of structure-guided evolution, including a final step of *in vivo* site-directed recombination to address the positive epistatic interactions between mutations. The final variant, with five substitutions and a renovated active site, was characterized at biochemical and computational level. The mutational sculpting helped position the bulkier (S)-1-(*p*-methoxyphenyl)-ethanol, improving the mutant's catalytic efficiency by three orders of magnitude relative to the native enzyme while showing a high enantioselectivity (ee >99%). As a promising candidate for racemic resolution, this evolved secondary benzyl alcohol oxidase maintained its natural stereoselective mechanism while displaying activity on several secondary benzyl alcohols.

Keywords: aryl alcohol oxidase; secondary benzyl alcohols; *Saccharomyces cerevisiae*; directed evolution

Introduction

With global annual sales of $ 1 trillion, an increasingly important challenge in drug development that the pharmaceutical sector must overcome is that posed by chiral chemistry.[1] Indeed, enantiopure building blocks are in strong demand to produce drugs with particular biological activities, while they are also paramount for the production of fine chemicals.[2] Biocatalysis has found an important niche in the field of chiral technology, with enzymatic and whole-cell biotransformations offering stereo-, regio- and chemio-selectivity under mild reaction conditions. Classically, two fundamental approaches are followed in the industrial production of chiral molecules: enantioselective synthesis and racemic mixture separation. While asymmetrical synthesis involves complex and expensive processes,[3] dynamic kinetic resolution (DKR) is currently one of the most efficient sources of chiral molecules, in which separation is coupled to the in situ re-racemization of one of the enantiomers. Another recently described transformative source of enantiomers is cyclic de-racemization. Based on cyclic oxidation-reduction sequences, after the selective oxidation of one of the enantiomers, the achiral intermediate (ketone or imine) is non-selectively reduced to the racemic initial material. After a certain number of cycles, a theoretical 100% yield of the non-reactive enantiomer can be accumulated.[4] The core step in racemic separation, kinetic resolution, has been achieved for secondary alcohols using either whole-cell systems[5] or isolated enzymes, such as alcohol

© 2019 Wiley-VCH Verlag GmbH & Co. KGaA, Weinheim

dehydrogenases,[6] lipases[7] and particularly, oxidases.[8] This latter solution is the simplest means to prepare optically pure secondary benzyl alcohols, given their trivial requirements (only needing O_2 from the air) and high enantioselectivity.[8a, 9]

Among these enzymes, aryl alcohol oxidase (AAO, EC 1.1.3.7) is a promising candidate for the enantioselective oxidation of chiral benzyl alcohols. AAO is a flavoenzyme belonging to the GMC (glucose-methanol-choline) superfamily of oxidoreductases and it is naturally secreted as a part of the fungal enzymatic consortium involved in lignin degradation.[10] Accepting a variety of aromatic alcohols as substrates, the activity of AAO is initially divided into two half-reactions. The first reductive half-reaction involves highly enantioselective hydride transfer from the alcohol's α-C to the FAD co-factor. This process yields the corresponding aldehyde, such that the FAD can then be reoxidized by O_2, releasing H_2O_2 as a by-product of the second oxidative half of the reaction.[11] Unfortunately, the active site of AAO is buried under a hydrophobic constriction formed by residues Tyr92, Phe397 and Phe501. As a result, substrates bulkier than primary aromatic alcohols cannot easily be accommodated, reducing the enzyme's activity on chiral molecules to a residual trace. Until recently the failure to functionally express AAO in an appropriate heterologous host had prevented its directed evolution. However, fusing the enzyme to a chimeric signal prepro-leader has enabled this protein to be successfully evolved for secretion by yeast.[12]

Taking advantage of this expression system, here we have combined different laboratory evolution strategies to unlock the activity of AAO on secondary aromatic alcohols. We first carried out a carefully structure-guided campaign of evolution using chiral 1-(*p*-methoxyphenyl)-ethanol as the substrate, thereby generating a palette of secondary benzyl alcohol oxidase mutants. Employing *in vivo* site-directed recombination approaches, mutations were curated by comparing them with their correspondent parental reversions. The differential oxidation of secondary benzyl alcohols by the final benzyl alcohol oxidase variant was characterized, while the rationale behind these changes was analyzed computationally at the atomic level.

Results and Discussion

Laboratory Evolution

First Generation: Unlocking Activity for Secondary Aromatic Alcohols

The departure point of this study was a secretion mutant of the AAO from *Pleurotus eryngii* named FX9. This mutant is the product of several rounds of directed evolution aimed to promote functional expression in *Saccharomyces cerevisiae*.[12] In this FX9 variant, the AAO is fused to a chimeric prepro-leader (preα-factor-proKiller) that enhanced secretion by introducing the F[3α]S, N[25proK]D, T[50proK]A and F[52proK]L mutations into the pre-α and pro-Killer leaders. In addition, two substitutions were included in the mature AAO: L170M in an α-helix situated at the protein surface, and the consensus, ancestral mutation H91N in the FAD attachment loop. These latter mutations enhanced stability and improved production by *S. cerevisiae* to 4.5 mg/L and by *Pichia pastoris* in bioreactor to 25.5 mg/L, while conserving the general biochemical features of the native AAO.[12]

As a substrate for the screening assay we chose 1-(*p*-methoxyphenyl)-ethanol, a chiral molecule with similar structure to the natural *p*-methoxybenzyl alcohol substrate, the oxidation of which by AAO can be rapidly assessed in a coupled Amplex Red/HRP assay (see Experimental Section for details). As the activity of AAO on secondary alcohols is irrelevant, no response was detected with 1-(*p*-methoxyphenyl)-ethanol when the parental FX9 was screened in microtiter fermentations of the supernatant (i.e. cultures in 96 well plates). As indicated previously, AAO's failure to oxidize secondary aromatic alcohols is due to steric perturbation of the residues forming the catalytic cavity when trying to accommodate bulkier, chiral molecules. Specifically, Phe501 is thought to be a steric liability at the active site, particularly given the very weak but detectable activity on 1-(*p*-methoxyphenyl)-ethanol of a F501A variant expressed in *E. coli* after *in vitro* refolding.[21] A more recent rational attempt to achieve secondary alcohol oxidation based on PELE (Protein Energy Landscape Exploration) suggested Ile500 was another possible obstacle for ligand diffusion. Indeed, the I500A substitution conferred better transit of the substrate to the active site due to channel broadening.[22]

To ensure that the activity on secondary benzyl alcohol could be measured at the start of the laboratory evolution campaign, we first prepared three mutants from the FX9 secretion variant: I500A, F501A and I500A-F501A (Figure S2A, B). When isolated from yeast supernatants these variants did not appear to act on 1-(*p*-methoxyphenyl)-ethanol. Hence, we performed combinatorial saturation mutagenesis of the Ile500-Phe501 residues and we found several clones with activity on 1-(*p*-methoxyphenyl)-ethanol, which were scaled up to a 100 mL flask to estimate the overall improvement in activity. Of these, the I500Q-F501W, I500L-F501I, I500M-F501V and I500M-F501W mutants presented a 5-, 15-, 30- and 160-fold enhancement in activity relative to the parental FX9, respectively. The activity of the I500M-F501W mutant (named 15G12) was further tested against a panel of primary and secondary alcohols (Table 1). Its specific activity on primary alcohols was dramatically reduced

© 2019 Wiley-VCH Verlag GmbH & Co. KGaA, Weinheim

Table 1. Specific activity of AAO variants with primary and secondary alcohols.

	Benzyl alcohol	Cinnamyl alcohol	*p*-Methoxy benzyl alcohol	*p*-Chloro benzyl alcohol	3,4-Dimethoxy benzyl alcohol	2,4-Hexadien -1-ol	1-Phenyl ethanol	*p*-Fluoro-α-methyl benzyl alcohol	1-(*p*-Methoxyphenyl)-ethanol
	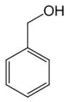	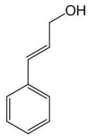	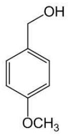	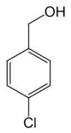	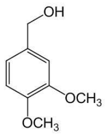	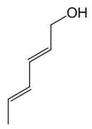	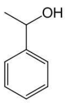	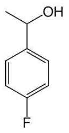	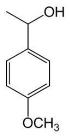
FX9 (U/mg)	15.6	41.1	46.6	26.6	22.2	43.4	n.d.	n.d.	2.2x10^{-3}
15G12 (U/mg)	0.6	18.4	0.3	0.6	0.03	13	6x10^{-3}	6x10^{-3}	0.3

Specific activities were estimated in 100 mM phosphate buffer pH 6.0 containing 5 mM of each alcohol. Each reaction was performed by triplicate and substrate conversion was followed by measuring the absorption at 563 nm ($\varepsilon_{563} = 56000\ \mathrm{M}^{-1}\mathrm{cm}^{-1}$) using the HRP/Amplex red coupled assay as described in the experimental section.

depending on the chemical nature of the molecule, with practically no activity on *p*-methoxybenzyl alcohol (c.a. 0.6% of that of the parental FX9 variant). By contrast, the activity of the 15G12 variant on secondary aromatic alcohols rose from undetectable levels, to weak yet evident activity on 1-phenylethanol and 4-fluoro-α-methylbenzyl alcohol, and up to 0.3 U/mg on 1-(*p*-methoxyphenyl)-ethanol (Table 1). Given that hydride abstraction of *p*-methoxybenzyl alcohol to the flavin of AAO occurs exclusively from the pro-R position, in deracemization reactions of secondary alcohols hydrogen abstraction should produce S enantioselective oxidation of the alcohol to the corresponding ketone.

To confirm this, reactions were performed with the optically pure (R) and (S)-4-fluoro-α-methylbenzyl alcohol enantiomers, and as expected, only activity on the latter was detected.[23]

Paradoxically, while the initial search for a wider space for secondary aromatic alcohol accommodation focused on the I500A-F501A mutations, the bulky alcohol would appear to be much better oxidized in a narrower catalytic pocket following the substitution of Ile500 and Phe501 by the more expansive Met and Trp, respectively (Figure S2C, D). Thus, these two mutations at the active site reposition the secondary alcohol, favouring catalysis, as confirmed by computational analysis (see below).

Second and Third Generations: Searching for new Beneficial Mutations

After unlocking the activity on secondary benzyl alcohols, different protein segments of the 15G12 mutant were targeted for random mutagenesis and DNA recombination by MORPHING, with a view to further optimize its activity on secondary alcohols. This focused structural evolution tool allows the protein to be divided into defined mutagenic areas, each of which can be interrogated in conjunction with the *in vivo* recombination of the different DNA fragments in *S. cerevisiae*.[14] This approach has already been successfully applied during the evolution of AAO towards functional expression in yeast[12] and on this occasion, the design involved the study of three protein blocks in independent libraries (Figure 1A, B). The first of these was the MA block at the N-terminus (Leu48-Thr100), which is associated with the access channel and the FAD-binding domain, and that contains important determinants like Pro79, Asn91, Tyr92 and Val90.

The second MB block (Leu310-Ile417) covers the wall of the catalytic pocket and it contains the aromatic Phe397, a residue implicated in substrate positioning and product release. The third MC block (Glu490-Gln566) is situated in the C-terminal region, and it contains the catalytic His502 and several amino acids related to substrate positioning (Met500, Trp501 and His546). Together, these three blocks encompass the complete active site and the aromatic bottleneck formed by Tyr92, Phe397 and Trp501 (Figure 1C).[16,23,24]

We carried out the three independent libraries of MORPHING; besides, we prepared a conventional error-prone PCR (ep-PCR) mutagenic library that targeted the whole AAO gene (in total over 4,000 clones were screened). From the pool of libraries, seven mutants with stronger activity on the secondary 1-(*p*-methoxyphenyl)-ethanol were selected for further analysis, ranging from a 1.4 to 2.2-fold enhancement

© 2019 Wiley-VCH Verlag GmbH & Co. KGaA, Weinheim

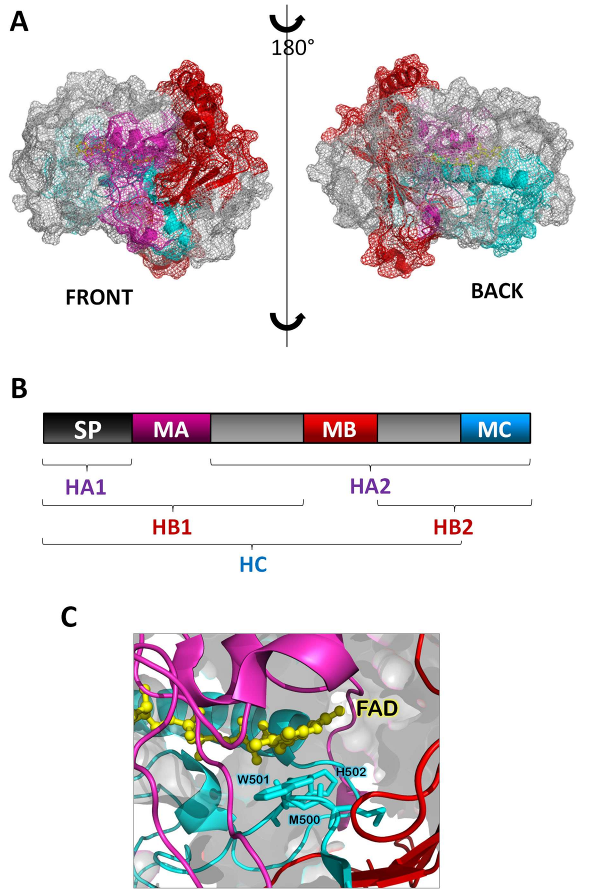

Figure 1. MORPHING fragments for focused evolution. (A) Front and back views of AAO, with the MA, MB and MC MORPHING blocks shown in purple, red and blue, respectively. (B) The dark grey box corresponds to the signal peptide, and the three mutagenic fragments considered for MORPHING are shown as purple, red and blue boxes. For the first MORPHING library, mutagenic block MA was *in vivo* assembled with high-fidelity fragments HA1 and HA2. For the second library, mutagenic fragment MB was recombined from high-fidelity fragments HB1 and HB2. The third library was constructed with the assembly of mutagenic block MC and high-fidelity fragment HC. (C) The catalytic pocket of AAO with the contribution of the MORPHING blocks MA, MB and MC (purple, red and blue, respectively). Model prepared with the crystal structure of the AAO from *P. eryngii* (PDB 3FIM).

over 15G12 (Figure 2). The most successful MORPHING corresponded to the MA block, with five of the seven improved AAO variants from this library. Interestingly, all the mutations identified were located within a 14 amino acid span, from Ile76 to Val90. The mutations carried by the best variant (3F10) were I76V and M83I, which in conjunction with the rest of the substitutions in this stretch (A77V, R80C, I76V and V90A) highlight the importance of the access channel in modulating oxidative activity. Indeed, it should be noted that the R80C substitution was also found in the triple 6G3 mutant from the whole gene ep-PCR library, together with two superficial substitutions: E39G and Q466R (Figure 2). The MORPHING method was also successful in fragment MB, where the 12D12 variant presented two mutations at the surface: F332L and V340A. Applying focused mutagenesis to the area corresponding to the catalytic pocket, the MC block, was ineffective since variants with improvements were not detected.

To further enhance secondary alcohol oxidation, the best variants from each library were submitted to ep-PCR and *in vivo* shuffling in *S. cerevisiae*: 3F10 and 11H2 from the MA library, the 12D2 variant from the MB library, and the 6G3 variant obtained through whole-gene mutagenic amplification. From this third generation, the 3C11 variant was seen to enhance the activity roughly 1.2-fold compared to 3F10 (412-fold relative to the FX9 parental type), retaining the I76V mutation from 3F10 and acquiring the V90A change, also previously detected in the 9F2 variant, as well as incorporating the new Q174R substitution (Figure 2).

Fourth Generation: Mutational Polishing by in vivo site-directed Recombination

After careful evaluation of the mutations obtained in the second and third generations (Table 2), we decided to undertake a final round of evolution to assess whether there were any positive epistatic effects among the mutations. We constructed a combinatorial library by *in vivo* site-directed recombination, such that the 10 mutations and their corresponding reversions could be rapidly combined in an one-pot transformation reaction, evaluating the library in order to obtain the optimal combination of substitutions for the oxidation of chiral alcohols (Figure S1). From this ensemble of mutations, the three best variants identified shared the same backbone of substitutions: A77V-R80C-V340A. The third best variant was the 24H3 mutant that carried the A77V-R80C-Q174R-F332L-V340A-Q466R muta-

Table 2. Selected mutations for site-directed recombination.

Mutation	Variant	Library	Secondary motif
${}_{\mathrm{GAG}}\mathrm{E39G}_{\mathrm{GGG}}$	6G3	ep-PCR	Loop
${}_{\mathrm{ATT}}\mathrm{I76V}_{\mathrm{GTT}}$	3F10, 4D8	MA	Loop
${}_{\mathrm{GCG}}\mathrm{A77V}_{\mathrm{GTG}}$	11H2	MA	Loop
${}_{\mathrm{CGC}}\mathrm{R80C}_{\mathrm{TGC}}$	6G3, 7B4	ep-PCR, MA	Loop
${}_{\mathrm{ATG}}\mathrm{M83I}_{\mathrm{ATA}}$	3F10	MA	Loop
${}_{\mathrm{GTT}}\mathrm{V90A}_{\mathrm{GCT}}$	9F2	MA, mutagenic shuffling	Loop
${}_{\mathrm{CAA}}\mathrm{Q174R}_{\mathrm{CGA}}$	3C11	Mutagenic Shuffling	Alpha helix
${}_{\mathrm{TTC}}\mathrm{F332L}_{\mathrm{CTC}}$	12D2	MB	Alpha helix
${}_{\mathrm{GTT}}\mathrm{V340A}_{\mathrm{GCT}}$	12D2	MB	Alpha helix
${}_{\mathrm{CAA}}\mathrm{Q466R}_{\mathrm{CGA}}$	6G3	ep-PCR	Loop

© 2019 Wiley-VCH Verlag GmbH & Co. KGaA, Weinheim

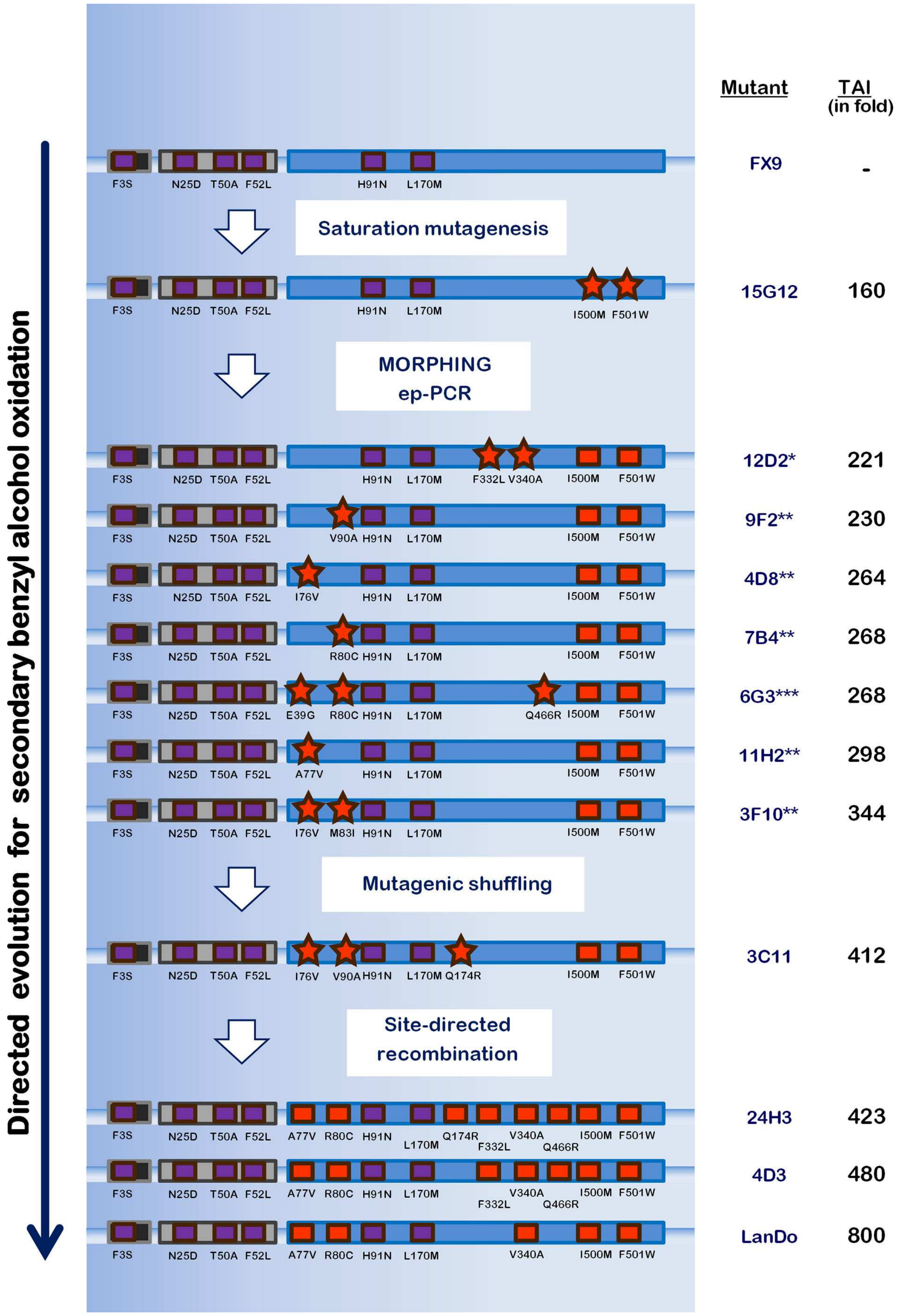
Directed evolution for secondary benzyl alcohol oxidation
Mutant
TAI (in fold)
F3S N25D T50A F52L H91N L170M
FX9 -
Saturation mutagenesis
F3S N25D T50A F52L H91N L170M I500M F501W
15G12 160
MORPHING ep-PCR
F3S N25D T50A F52L H91N L170M F332L V340A I500M F501W
12D2* 221
F3S N25D T50A F52L V90A H91N L170M I500M F501W
9F2** 230
F3S N25D T50A F52L I76V H91N L170M I500M F501W
4D8** 264
F3S N25D T50A F52L R80C H91N L170M I500M F501W
7B4** 268
F3S N25D T50A F52L E39G R80C H91N L170M Q466R I500M F501W
6G3*** 268
F3S N25D T50A F52L A77V H91N L170M I500M F501W
11H2** 298
F3S N25D T50A F52L I76V M83I H91N L170M I500M F501W
3F10** 344
Mutagenic shuffling
F3S N25D T50A F52L I76V V90A H91N L170M Q174R I500M F501W
3C11 412
Site-directed recombination
F3S N25D T50A F52L A77V R80C H91N L170M Q174R F332L V340A Q466R I500M F501W
24H3 423
F3S N25D T50A F52L A77V R80C H91N L170M F332L V340A Q466R I500M F501W
4D3 480
F3S N25D T50A F52L A77V R80C H91N L170M V340A I500M F501W
LanDo 800

Figure 2. Laboratory evolution of AAO for the oxidation of secondary benzyl alcohols. New mutations are represented as stars and accumulated mutations as squares. The chimeric prepro-leader is depicted in grey and the mature AAO in blue. The TAI (total activity improvement) refers to the fold improvement of AAO activity with 1-(*p*-methoxyphenyl)-ethanol as a substrate and it was estimated relative to the FX9 parental type from *S. cerevisiae* supernatants: *Mutants from the MB library; **Mutants from the MA library; ***Mutant from the ep-PCR library.

© 2019 Wiley-VCH Verlag GmbH & Co. KGaA, Weinheim

tions, displaying activity more than 420-fold better than the FX9 parental type. In the case of 4D3, the only difference from the 24H3 variant was the absence of the Q174R mutation, which translated into a 480-fold increase in activity, highlighting a detrimental effect of Q174R within this mutational context. The further purging of Q466R and F332L gave rise to the LanDo variant that carried the A77V-R80C-V340A mutations in conjunction with I500M-F501W and the 6 secretion mutations of FX9, this variant representing the best performer with a total 800-fold enhancement of activity relative to the parental type (Figures 2, 3).

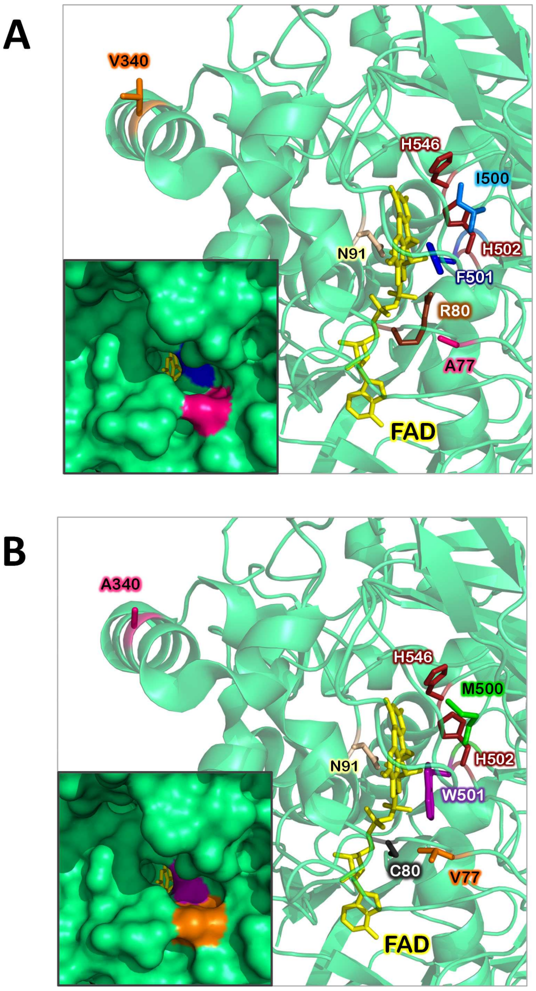

Figure 3. Location of the mutations in the evolved secondary benzyl alcohol oxidase. (A) FX9 parental type and (B) LanDo mutant. The FAD molecule is represented in yellow, the catalytic base His502 and His546 is depicted in red, and the consensus ancestral mutation Asn91 is in light pink. A77V, R80C, V340A, I500M and F501W are represented following a color code (before and after mutation). The mutation L170M at the surface of the enzyme is not present in the fragment represented. The inset shows a detail of the protein surface at the access channel. The model was prepared with a crystal structure of the AAO from *P. eryngii* (PDB 3FIM).

Biochemical Characterization

To characterize the LanDo mutant and the FX9 parental variant, they were produced and purified to homogeneity. To determine the enantioselectivity of the LanDo variant, transformation of the racemic 1-(*p*-methoxyphenyl)-ethanol was followed by chiral-HPLC (Figure 4) and 100% conversion with an enantiomeric excess (ee) >99% was achieved after a two hour reaction. The configuration of the remaining alcohol in the reaction was confirmed by optical rotation (Figure S3, Table S2), the positive rotation corresponding to the R enantiomer meaning the natural oxidation of the S enantiomer by AAO was maintained after evolution.[23] Despite the remarkably specific activity for the secondary 1-(*p*-methoxyphenyl)-ethanol (2.9 U/mg), the five new mutations carried by the LanDo variant did not negatively affect its secretion (4.6 mg/L). The activity of LanDo with secondary alcohols was tested against available commercial secondary (aromatic) alcohols that were representative of the structural scope of the AAO. The initial turnover rates of the LanDo variant relative to the wildtype AAO (wtAAO, heterologous expressed in *E. Coli* after *in vitro* refolding) increased 30, 20 and 100-fold times for 1-(*p*-methoxyphenyl)-ethanol, *p*-fluoro-α-methylbenzyl alcohol and 1-phenylethanol, respectively. Indeed, the LanDo variant even showed activity on 1-

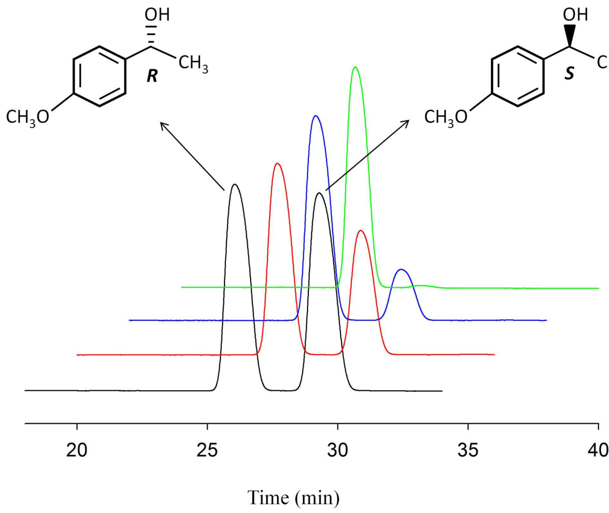

Figure 4. Chiral HPLC analysis. HPLC elution profiles after the reaction of the AAO variant LanDo (1 μM) with racemic 1-(*p*-methoxyphenyl)-ethanol (2.5 mM). Reactions were performed at room temperature in 100 mM phosphate buffer pH 6.0 with continuous shaking and the aliquots were analyzed by chiral HPLC at different times. The separation of the R and S enantiomers in the negative control is represented in black, whereas the 15, 45, and 90 min reactions are represented in red, blue and green, respectively.

© 2019 Wiley-VCH Verlag GmbH & Co. KGaA, Weinheim

phenylpropanol, a substrate not oxidized by wtAAO (Table 3). The kinetic parameters were measured under air-saturated conditions for 1-(*p*-methoxyphenyl)-ethanol, and for the primary alcohols *p*-methoxybenzyl alcohol and 2,4-hexadien-1-ol. LanDo displayed an outstanding increase in the catalytic efficiency for enantioselective oxidation of 1-(*p*-methoxyphenyl)-ethanol, three orders of magnitude. Interestingly, the activity on primary alcohols that was dramatically reduced after inserting the I500M-F501 W pair in the first cycle of evolution in 15G12 variant (Table 1, Figure 2), was recovered to a considerable extent for *p*-methoxybenzyl alcohol and the aliphatic 2,4-hexadien-1-ol. This result indicates the beneficial effect that A77V, R80C and V340A exerted on LanDo's overall activity (Table 4).

Table 3. Initial turnover rates for secondary alcohols.

	p-Fluoro-α-methylbenzyl alcohol	1-Phenylethanol	1-Phenylpropanol
wtAAO	0.35 ± 0.01	0.10 ± 0.03	n.m.
LanDo	7.3 ± 0.1	10 ± 0.5	1 ± 0.1

Turnover rates (min^{-1}) were estimated in 100 mM phosphate buffer pH 6.0 containing 5 mM of each secondary alcohol with the exception of 1-phenylpropranol (2.5 mM). Each reaction was performed by triplicate and substrate conversion was followed by measuring the absorption at 563 nm (ε_{563} = 56000 $M^{-1} cm^{-1}$) using the HRP/Amplex red coupled assay as described in the experimental section.

Computational Analysis

In order to rationalize the effect of the mutations identified, PELE simulations were run for wtAAO and the variants obtained in the different rounds of directed evolution. The oxidation of alcohols by AAO involves a non-synchronous concerted reaction, where both proton transfer from the hydroxyl group to the catalytic base His502 and hydride abstraction from the benzylic position by the flavin are taking place at the same reaction step.[11] PELE results were plotted placing both catalytic distances in the X and Y axis, and the interaction energy between the protein and the ligand was represented by colors (Figure 5).

No significant differences were evident between the wtAAO and the secretion mutant FX9 (H91N-L170M) in these plots, consistent with the experimental evidence that this variant does not improve the activity on secondary alcohols but does increase expression and stability. The 15G12 variant included the I500M and F501W mutations on top of the previous ones, accumulating a total of 4 mutations in the mature protein. In this case, the plot shows how the ligand can reach catalytic positions 2.5 Å away from both the FAD and the histidine at the same time, producing better catalytic constants than those of the wtAAO. In addition, a minimum could be seen where the ligand-histidine distance was ~2.2 Å, although the interaction energies were much higher and they were therefore less accessible.

The largest improvement came after introducing an additional three mutations in the LanDo variant: A77V, R80C, and V340A. These three substitutions allow the ligand to achieve even smaller catalytic distances, up to ~2 Å for the histidine and 2.4 Å for the FAD, with reasonable interaction energies. Considering that closer catalytic distances imply a decrease in energy barriers, this agreed well with the higher kinetic constants. Moreover, the increase in the number of structures with good catalytic distances could reflect the ease with which the ligand can find catalytic positions, explaining the lower K_m values for this variant.

Despite the large number of mutations in LanDo (7 in total, excluding the mutations in the chimeric prepro-leader), there are no major conformational changes in the protein or in the positioning of the ligand. Nevertheless, we did note subtle modifications that were sufficient to improve the catalytic position of

Table 4. Kinetic parameters for AAO variants.

Substrate	Kinetic constants	wtAAO**	LanDo
1-(*p*-methoxyphenyl)-ethanol	K_m (mM)*	24.9 ± 1.1	0.65 ± 0.1
	k_{cat} (s^{-1})	0.18 ± 0.002	4.9 ± 0.1
	k_{cat}/K_m ($mM^{-1} s^{-1}$)	0.007	7.5
p-methoxybenzyl alcohol**	K_m (mM)	0.027 ± 0.004	0.02 ± 0.003
	k_{cat} (s^{-1})	142 ± 5	72 ± 3
	k_{cat}/K_m ($mM^{-1} s^{-1}$)	5233	3600
2,4-hexadien-1-ol**	K_m (mM)	0.094 ± 0.005	0.095 ± 0.006
	k_{cat} (s^{-1})	119 ± 2	40.9 ± 0.7
	k_{cat}/K_m ($mM^{-1} s^{-1}$)	1271	430.5

AAO kinetic constants were measured in 100 mM phosphate buffer pH 6.0 at 25 °C. All reactions were performed by triplicate. *Referred to the S enantiomer, as 50% of the racemic mixture. **Calculated for wtAAO as described previously.[22,26]

© 2019 Wiley-VCH Verlag GmbH & Co. KGaA, Weinheim

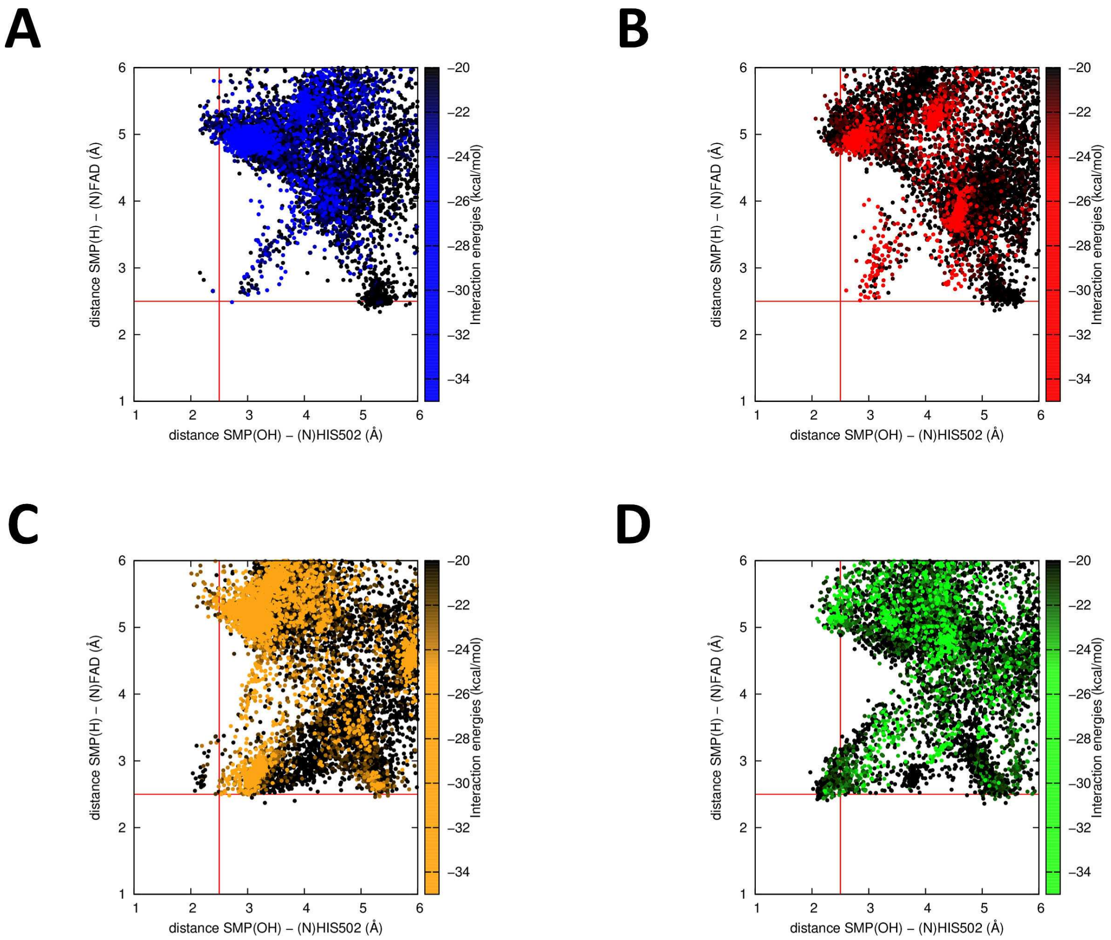

Figure 5. Substrate diffusion computational PELE simulations. Plots represent the PELE simulations relating catalytic distances (X and Y) and interaction energies (color scheme, right Y axis) for different AAO variants: (A) wtAAO; (B) the FX9 secretion mutant; (C) the 15G12 mutant; (D) the final evolved benzyl alcohol oxidase, LanDo mutant.

(S)-1-(*p*-methoxyphenyl)-ethanol. In particular, the R80C mutation was found repeatedly in independent libraries during evolution (Figure 2) and it created an empty space at the top of the FAD cofactor. Consequently, the backbone containing H502 shifts in that direction (Figure 6A). Moreover, Arg80 interacts with the oxygen of the backbone of residue 501, such that this mutation frees Trp501 to form a hydrogen bond with the oxygen backbone of Val77 (Figure 6B). All these subtle adjustments allow the ligand to adopt conformations with better catalytic distances (Figures 5, 6).

Conclusion

Focusing evolution on structural elements made it possible to identify mutations in the catalytic pocket and access channel that allowed an AAO to be designed that acts on different secondary benzyl alcohols. This final secondary benzyl alcohol oxidase variant maintained strong enantioselectivity, providing a potential catalyst for chiral de-racemization. The complex enzyme-substrate relationships of this enzyme were highlighted by an enhancement of three orders of magnitude in the catalytic efficiency, an effect produced by a combination of bulky substitutions in the catalytic cavity and other unpredicted changes. Paradoxically, a steric problem appeared to be resolved by introducing bulkier residues, something difficult to anticipate from a rational point of view. It is worth noting that the resolution of molecules like 1-phenylpropanol could be of use to obtain moiety precursors of serotonin/norepinephrine reuptake inhibitors like Fluoxetine or Atmoxetine.[6]

The results obtained here also highlight the importance and efficacy of *S. cerevisiae* as a platform for both the functional expression of eukaryotic genes and as a molecular tool-box to generate DNA libraries for directed evolution campaigns. The data presented open new opportunities for the evolution of AAO, which include the oxidation of furfural derivatives for the synthesis of biopolymers or the *in situ* production

© 2019 Wiley-VCH Verlag GmbH & Co. KGaA, Weinheim

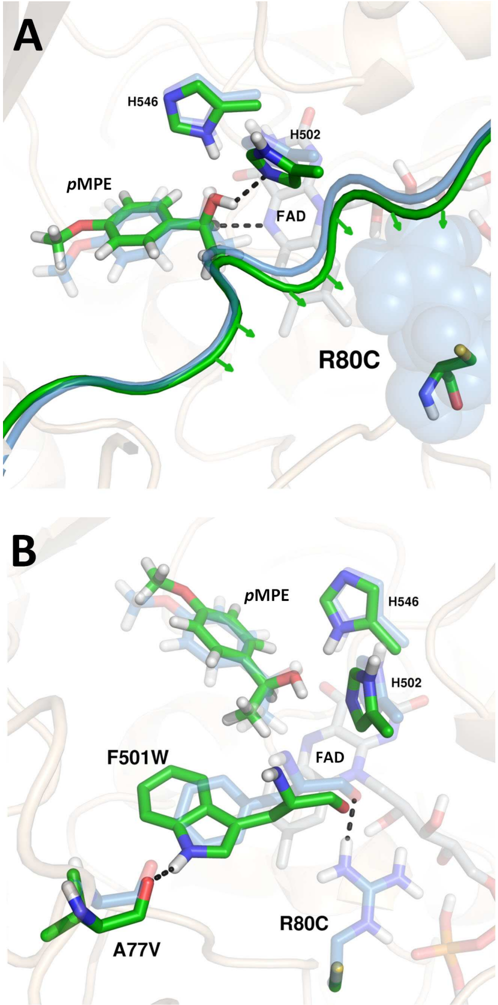

Figure 6. Conformational changes at the catalytic pocket of AAO. (A) Backbone displacement (green) to better position (S)- 1-(p-methoxyphenyl)-ethanol (pMPE). (B) Interruption of the interaction of Arg80 with the backbone of residue 501, and the formation of a hydrogen bond between Val77 and Trp501.

of H_2O_2 in cascade oxyfunctionalization reactions by peroxygenases.[25]

Experimental Section

Materials

All chemicals were reagent-grade purity. Benzyl alcohol, *p*-chlorobenzyl alcohol, 3,4-dimethoxybenzyl alcohol, *p*-Methoxybenzyl alcohol, 1-phenylethanol, 1-phenylpropanol, 1-(*p*-methoxyphenyl)-ethanol, 4-fluoro-α-methylbenzyl alcohol, (R)-4-fluoro-α-methylbenzyl alcohol, (S)-4-fluoro-α-methylbenzyl alcohol, 2,4-hexadien-1-ol, cinnamyl alcohol, Horseradish peroxidase (HRP), Taq polymerase and the Yeast Transformation Kit were purchased from Sigma (Madrid, Spain). Amplex® Red reagent (10-acetyl-3,7-dihydroxyphenoxazine) was obtained from Biogen (Madrid, Spain). Zymoprep Yeast Plasmid Miniprep, Yeast Plasmid Miniprep Kit I and Zymoclean Gel DNA Recovery Kit were from Zymo Research (Orange, CA, USA). Restriction enzymes BamHI and XhoI were from New England Biolabs (Hertfordshire, UK). I-Proof high-fidelity DNA polymerase was from Biorad (Hercules, CA, USA). The episomal shuttle vector pJRoC30 was from the California Institute of Technology (CALTECH, USA). The protease deficient *S. cerevisiae* strain BJ5465 was from LGC Promochem (Barcelona, Spain). E. coli XL2-Blue competent cells were from Stratagene (La Jolla, CA, USA). Primers were acquired from Isogen Life Science (Barcelona, Spain) and are included in Table S1.

Culture Media

Minimal medium SC contained 100 mL 6.7% (w:v) sterile yeast nitrogen base, 100 mL 19.2 g/L sterile yeast synthetic drop-out medium supplement without uracil, 100 mL sterile 20% raffinose (w:v), 700 mL sddH_2O and 1 mL 25 g/L chloramphenicol. YP medium contained 10 g yeast extract, 20 g peptone and ddH_2O to 650 mL whereas YPD medium also contained 20% glucose (w:v). AAO expression medium contained 144 mL YP 1.55×, 13.4 mL 1 M KH_2PO_4 pH 6.0 buffer, 22.2 mL 20% galactose (w:v), 0.222 mL 25 g/L chloramphenicol and ddH_2O to 200 mL. Luria Broth (LB) medium contained 10 g sodium chloride, 5 g yeast extract, 10 g peptone, 1 mL 100 mg/mL ampicillin and ddH_2O to 1 L. AAO selective expression medium (SEM) contained 100 mL 6.7% (w:v) sterile yeast nitrogen base, 100 mL 19.2 g/L sterile yeast synthetic drop-out medium supplement without uracil, 100 mL sterile 20% galactose (w:v), 100 mL 1 M KH_2PO_4 pH 6.0, 600 mL sddH_2O and 1 mL 25 g/L chloramphenicol.

Construction of Variants I500A, F501A and I500A-F501A

All the PCR products were cleaned, concentrated, loaded onto a preparative agarose gel (1%, w:v) and purified using the Zymoclean Gel DNA Recovery kit before being cloned into the shuttle vector pJRoC30 under the control of the GAL1 promoter. BamHI and XhoI were used to linearize the plasmid pJRoC30 and to remove the parent gene. FX9 variant was amplified from pJRoC30-FX9[12b] with two PCR reactions for each mutant containing overhang segments for the whole plasmid to be reassembled in the yeast. PCR reactions were carried out in a final volume of 50 μL containing 3% DMSO, 0.8 mM dNTPs (0.2 mM each), 0.03 U/μL Iproof DNA polymerase, and 0.2 ng/μL template. The oligos used for each PCR reaction were: For I500 A, PCR1 (oligo sense RMLN and oligo antisense I500Ar), PCR2 (oligo sense I500Af and oligo antisense RMLC). For F501 A, PCR1 (RMLN and oligo antisense F501Ar), PCR2 (oligo sense F501Af and RMLC). For double mutant I500A-F501 A, PCR1 (RMLN and oligo antisense DM500-1Ar), PCR2 (oligo sense DM500-1Af and RMLC). Amplification reactions were carried out in a thermal cycler MycyclerTM (BIO-RAD, USA) with the following PCR program: 98 °C for 30 seconds (1 cycle); 98 °C for 10 seconds, 50 °C for 25 seconds and 72 °C for 60 seconds (28 cycles); and 72 °C for ten minutes (1 cycle). After purification, PCR products (400 ng each) were mixed with the linearized pJRoC30 (100 ng; ratio PCR product: vector = 4:1) and transformed in

© 2019 Wiley-VCH Verlag GmbH & Co. KGaA, Weinheim

yeast (Yeast transformation kit) for the recombination and in vivo cloning. 176 colonies were picked, expressed and screened as described below. Each construct was recovered and its sequence confirmed by DNA sequencing.

Directed Evolution

First generation: combinatorial saturation mutagenesis at positions Ile500 and Phe501: Two PCR reactions were carried out in a final volume of 50 μL containing 3% DMSO, 0.8 mM dNTPs (0.2 mM each), 0.03 U/μL iproof DNA polimerase, and 0.2 ng/μL FX9 template and different primers according to the 22-trick protocol.[13] PCR1 contained 0.25 μM RMLN and 0.25 μM mix of reverse primers: 22c1R, 22c2R, 22c3R, 22c4R, 22c5R, 22c6R, 22c7R, 22c8R and 22c9R. PCR2 contained 0.25 μM RMLC and 0.25 μM mix of forward primers: 22c1F, 22c2F, 22c3F, 22c4F, 22c5F, 22c6F, 22c7F, 22c8F and 22c9F. Amplification reactions were carried out in a thermal cycler MycyclerTM (BIO-RAD, USA) with the following PCR program: 98 °C for 30 seconds (1 cycle); 98 °C for 10 seconds, 50 °C for 25 seconds and 72 °C for 60 seconds (28 cycles); and 72 °C for ten minutes (1 cycle). After purification, PCR products (400 ng each) were mixed with the linearized pJRoC30 (100 ng; ratio PCR product: vector = 4:1) and transformed in yeast for in vivo cloning. According to the 22-trick protocol, a library of 3066 individual colonies was screened as described below.

Second generation: MORPHING: The 15G12 variant was used as the parental template for focused random mutagenesis technique MORPHING (Mutagenic Organized Recombination Process by Homologous IN vivo Grouping).[14] Three libraries were constructed independently targeting 3 protein blocks: MA, MB, and MC. Additionally, a mutagenic library subjecting the whole AAO fusion was prepared by error prone PCR (ep-PCR). Primers were designed to create homologous overlapping areas of ~50 bp for the whole gene to be reassembled in vivo upon transformation in S. cerevisiae. i) ep-PCR for MORPHING blocks and whole AAO gene were carried out in a final volume of 50 μL containing: 90 nM oligo sense (FM1 for MA block, FM2 for MB block, FM3 for MC block and RMLN for whole gene amplification), 90 nM oligo antisense (RM1 for fragment MA, RM2 for fragment MB, RM3 for fragment MC and RMLC for whole gene amplification), 0.3 mM dNTPs (0.075 mM each), 3% DMSO, 0.05 or 0.01 mM $MnCl_2$, 1.5 mM $MgCl_2$, 0.05 U/μL Taq polymerase DNA, and 0.92 ng/ μL15G12 template. The amplification parameters were 95 °C for 2 min (1 cycle); 95 °C for 45 s, 50 °C for 45 s, and 74 °C for 2 min (28 cycles); and 74 °C for 10 min (1 cycle). Concentrations of 0.05 and 0.01 mM $MnCl_2$ were used for MORPHING and full gene ep-PCR, respectively, to adjust the mutational rate to 1–3 mutations per gene. ii) High-fidelity PCRs for MORPHING were carried out in a final volume of 50 μL containing 3% DMSO, 0.8 mM dNTPs (0.2 mM each), 0.03 U/μL iproof DNA polimerase, 0.25 μM oligo sense (RMLN for HA1, HB1 and HC fragments, FHF1 for HA2 and FHF2 for HB2), 0.25 μM oligo antisense (RHF1 for HA1, RHF2 for HB1, RHF3 for MC and RMLC for HA2 and HB2 fragments) and 0.2 ng/μL template. High-fidelity PCR was performed using the following parameters: 98 °C for 30 s (1 cycle); 94 °C for 10 s, 48 °C for 30 s, 72 °C for 30 s (30 cycles); and 72 °C for 10 min (1 cycle). The assembly of the fragments for the different libraries is described in Figure 1B. PCR products were cleaned, concentrated, loaded onto a preparative agarose gel, purified, mixed in equimolar amounts, (200 ng mutagenic fragment and 200 ng non-mutagenic fragment) and transformed with linearized pJRoC30 (200 ng) into chemically competent cells, as described above.

Third generation: mutagenic shuffling: ep-PCR reactions were performed separately with mutants 3F10, 11H2, 12D2 and 6G3. Reaction mixtures were prepared in a final volume of 50 μL containing DNA template (0.92 ng/μL), 90 nM oligo sense RMLN (5'-CCTCTATACTTTAACGTCAAGG-3'), 90 nM Reverse primer RMLC (5'-GGGAGGGCGTGAATGTAAGC-3'), 0.3 mM dNTPs (0.075 mM each), 3% (v:v) dimethylsulfoxide (DMSO), 1.5 mM MgCl2, 0.1 mM MnCl2 and 0.05 U/μL Taq DNA polymerase. PCRs were performed in a thermocycler (Mycycler, Bio-Rad, Hercules, CA, USA) and parameters were: 95 °C for 2 min (1 cycle); 95 °C for 45 s, 50 °C for 45 s, 74 °C for 45 s (28 cycles); and 74 °C for 10 min (1 cycle). The PCR products were mixed with linearized pJRoC30 (at a PCR product/linearized plasmid ratio of 4:1) and transformed into competent S. cerevisiae cells to promote in vivo DNA shuffling. Transformed cells were plated on SC (synthetic complete) drop-out plates and incubated for 3 days at 30 °C. Colonies containing the whole autonomously replicating vector were picked and subjected to high-throughput screening as described below.

Fourth generation: site-directed recombination: The 3C11 variant was used as template and primers were designed for the 10 selected mutations (E39G, I76V, A77V, R80C, M83I, V90A, Q174R, F332L, V340A, and Q466R) for the *in vivo* site-directed recombination of mutations vs. corresponding reversions at each position of the combinatorial library. A total of 6 PCR reactions were performed. Reactions were carried out in a final volume of 50 μL containing 3% DMSO, 0.8 mM dNTPs (0.2 mM each), 0.03 U/μL iproof DNA polimerase, and 0.2 ng/μL 3 C11 with 0.25 μM of the following oligos: PCR1 used oligo sense RMLN and oligo antisense R116 (containing position 39). PCR2 was performed with oligo sense F116 (containing position 39) and oligo antisense R5 (containing positions 76, 77, 80, 83 and 90). PCR3 used oligo sense F5 (containing positions 76, 77, 80, 83 and 90) and oligo antisense R521 (containing position 174). PCR4 used oligo sense F521 (containing position 174) and oligo antisense R9419 (containing positions 332 and 340). PCR5 was performed with oligo sense F9419 (containing positions 332 and 340) and oligo antisense R1397 (containing position 466). PCR6 was performed with oligo sense F1397 (containing position 466) and oligo antisense RMLC, (Figure S1, Table S1). For the in vivo assembly of the whole gene, the fragments were designed with overhangs of around 40 bp between them. Amplification reactions were carried out in a thermal cycler and the PCR program was: 98 °C for 30 seconds (1 cycle); 98 °C for 10 seconds, 50 °C for 25 seconds and 72 °C for 30 seconds (28 cycles); and 72 °C for ten minutes (1 cycle). After purification, PCR products (400 ng each) were mixed with the linearized pJRoC30 (100 ng; ratio PCR product: vector = 4:1) and transformed in yeast for in vivo cloning. A library of 3070 individual colonies was screened as described below.

© 2019 Wiley-VCH Verlag GmbH & Co. KGaA, Weinheim

High-throughput Screening (HTS) Assay

Transformed cells were plated in SC drop-out plates and incubated for 3 days at 30 °C, individual clones were fermented in sterile 96-well plates containing 200 µL of SEM medium. Plates were sealed and incubated at 30 °C, 225 rpm and 80% relative humidity in a humidity shaker (Minitron-INFORS, Biogen, Spain) for 72 hours. Aliquots of 20 µL of yeast supernatants were transferred to a 96-well plate using a robotic station for liquid handling Freedom EVO (Tecan, Männedorf, Switzerland) and 180 µL of HRP-Amplex Red reagent for secondary alcohol activity detection. The final concentrations in the well were 5 mM 1-(*p*-methoxyphenyl)-ethanol, 70 µM Amplex Red, 3 µg/mL HRP in 100 mM phosphate buffer pH 6.0. Reagents were dispensed with Multidrop™ Combi Reagent Dispenser (Thermo Scientific, Massachusetts, USA). The plates were incubated at room temperature and activity with the chiral alcohol was determined as H_2O_2 production coupled to the oxidation of Amplex Red reagent by the HRP and measured at 563 nm ($\varepsilon_{\text{resorufin } 563} = 56000\ M^{-1}cm^{-1}$). Reaction mixture with *p*-methoxybenzyl alcohol (1 mM final concentration) was also prepared to determine activity with a primary alcohol. One unit of AAO activity is defined as the amount of enzyme that converts 1 µmol of alcohol to aldehyde or ketone with the stoichiometric formation of H_2O_2 per min under the reaction conditions. The HTS-assay incorporated two consecutive re-screenings to rule out the selection of false positives as described in previous work.[12a]

Protein Production and Purification

The native AAO, heterologously expressed in *E. coli* and in vitro refolded (wtAAO), was produced and purified as described elsewhere.[15] Evolved variants were produced in yeast[12a] and purified by cationic exchange chromatography, anion exchange chromatography and size-exclusion chromatography (ÄKTA purifier, GE Healthcare, WI, US). The crude extract from *S. cerevisiae* cultures was concentrated and dialyzed in 20 mM sodium phosphate/citrate at pH 3.3 (buffer A) by tangential ultrafiltration (Pellicon; Millipore, USA) through a 10-kDa-pore-size membrane (Millipore, USA) by means of a peristaltic pump (Masterflex easy load; Cole-Parmer, USA). The sample was filtered and loaded onto a strong cation-exchange column (HiTrap SP FF; GE Healthcare) pre-equilibrated with buffer A and coupled to the ÄKTA purifier system. The proteins were eluted with a linear gradient of buffer P (20 mM piperazine buffer pH 5.5) + 1 M NaCl in two phases at a flow rate of 1 ml/min: from 0 to 50% during 15 min and from 50 to 100% in 2 min. Fractions with AAO activity were pooled, dialyzed against buffer P, concentrated and loaded onto a high-resolution resin, strong-anion-exchange column (Biosuite MonoQ 10 cm; Waters, USA) pre-equilibrated in buffer P. The proteins were eluted with a linear gradient from 0 to 0.5 M of NaCl in two phases at a flow rate of 1 ml/min: from 0 to 50% during 20 min and from 50 to 100% in 2 min. Fractions with AAO activity were pooled, dialyzed against 20 mM phosphate buffer pH 6.0, concentrated and further purified by a Superose 12 HR 10/30 molecular exclusion column (Amersham Bioscience; Amersham, UK) pre-equilibrated with 150 mM NaCl in 20 mM phosphate buffer pH 6.0 at a flow rate of 0.5 ml/min. The fractions with AAO activity were pooled, dialyzed against buffer 20 mM phosphate buffer pH 6.0, concentrated and stored.

Biochemical Characterization

Steady-state kinetic constants: Alcohol oxidation kinetics for 1-(*p*-methoxyphenyl)-ethanol, *p*-methoxybenzyl alcohol and 2,4-hexadien-1-ol were measured in 100 mM phosphate buffer pH 6.0 at 25 °C in air-saturated conditions (0.256 mM O_2 concentration). Reactions were performed by triplicate and substrates oxidations were followed by measuring the absorption at 285 nm for *p*-methoxybenzyl alcohol, $\varepsilon_{285} = 16{,}950\ M^{-1}cm^{-1}$ and at 280 nm for 2,4-hexadien-1-ol, $\varepsilon_{280} = 30{,}140\ M^{-1}cm^{-1}$. The oxidation of 1-(*p*-methoxyphenyl)-ethanol was measured indirectly coupled with saturated conditions of HRP and Amplex Red substrate (4.5 U/mL HRP and 75 µg/mL Amplex Red final concentrations) following activity at 563 nm ($\varepsilon_{563} = 56000\ M^{-1}\ cm^{-1}$).

HPLC analysis and optical rotation: The enantioselectivity of LanDo variant was analyzed by chiral HPLC with equipment consisting of a tertiary pump (Varian/AgilentTechnologies) coupled to an autosampler (Merck Millipore) and a Lux 5 µm Cellulose-1 column (Phenomenex). For the mobile phase hexane and isopropanol in a ratio 9:1 was used. The separation of the enantiomers was performed at a flow rate of 1.0 mL/min. The rotary polarization was measured with a JASCO P-2000 polarimeter. After full conversion, a reaction mixture with the remaining alcohol (1 mg/mL of 1-(p-methoxyphenyl)-ethanol) was extracted with ethyl acetate and dissolved in methanol. The measurement was made at 25 °C with a sodium lamp at 589 nm.

Protein modeling: A structural model of the AAO from *P. eryngii* crystal structure at a resolution of 2.55 Å (Protein Data Bank Europe [PDB] accession number 3FIM,[16] was used as scaffold for the wild type AAO model and the homology models for different mutants were made from 3FIM by PyMol (Schrodinger LLC.; http://www.pymol.org).

DNA sequencing: All genes were verified by DNA sequencing (BigDye Terminator v3.1 Cycle Sequencing Kit) using the following primers: primers sense, RMLN and AAOsec1F and primers antisense RMLC, AAOsec2R, and AAOsec3R.

Computational Methods

The diffusion and binding of the secondary alcohol (S)-1-(*p*-methoxyphenyl)-ethanol were studied using the new adaptive-PELE (Protein Energy Landscape Exploration) software.[17] This adaptive protocol offers improved sampling by running multiple and consecutive short PELE simulations (epochs), setting the initial conditions of each epoch following a reward function that favours sampling of unexplored areas. Even though the ligands were parameterized based on the OPLS2005 force field, the electrostatic charges were derived from the electrostatic potential obtained through quantum calculations at the M06/6-31G* level with Jaguar,[18] and its rotamer library was built with Macromodel.[19] Similarly, the FAD cofactor was optimized with a mixed QM/MM calculation at the same level of theory using Qsite.

© 2019 Wiley-VCH Verlag GmbH & Co. KGaA, Weinheim

A single adaptive-PELE simulation was enough to explore the diffusion and binding of (S)-1-(*p*-methoxyphenyl)-ethanol for the native protein and the different variants. The ligand was initially placed between residues Gly52 and Asn56 in all cases. Each simulation used 192 processors, producing 60 epochs of 20 PELE steps each. During the simulation, ligand perturbations (rotations and translations) are coupled with the backbone perturbation to allow protein flexibility. This is achieved by using an anisotropic network model[20] applied to every Cα atom, while all sidechain conformations within 6 Å of the ligand were predicted each step. An epsilon value of 0.2 was used in the adaptive protocol, meaning that 20% of the processors started each epoch from the structure with the best ligand-FAD distance.

Acknowledgements

This research was supported by the EU project FP7-KBBE-2013-7-613549-INDOX, by the Spanish Government projects BIO2016-79106-R-Lignolution, CTQ2016-74959-R (MINECO/FEDER, EU) and by the Comunidad de Madrid project Y2018/BIO4738-EVOCHIMERA.

References

[1] https://www.statista.com/statistics/263102/pharmaceutical-market-worldwide-revenue-since-2001

[2] a) J. Caldwell, *Hum. Psychopharmacol.* **2001**, *16*, S67-S71; b) B. S. Sekhon, *J. Mod. Med. Chem.* **2013**, *1*, 10–36; c) N. Chhabra, M. L. Aseri, D. Padmanabhan, *Int J App Basic Med Res.* **2013**, *3*, 16–18.

[3] N. M. Maier, P. Franco, W. Lindner, *J. Chromatogr. A* **2001**, *12*, 906(1-2):3-33.

[4] a) K. Faber, *Chemistry.* **2001**, *3*, 7(23):5004-10; b) O. Pàmies, J. E. Bäckvall, *Trends Biotechnol.* **2004**, *22*, 130–5; c) N. J. Turner, *Curr. Opin. Chem. Biol.* **2004**, *8*, 114–9.

[5] a) G. Fantin, M. Fogagnolo, A. Medici, P. Pedrini, S. Poli, M. Sinigaglia, *Tetrahedron Lett.* **1993**, *34*, 883–884; b) Y. L. Li, J. H. Xu, Y. Xu, *J. Mol. Catal. B* **2010**, *64*, 48–52; c) C. Voss, C. Gruber W. Kroutil, *Angew. Chem. Int. Ed.* **2008**, *47*, 741–745.

[6] T. Matsuda, R. Yamanaka, K. Nakamura, *Tetrahedron: Asymmetry.* **2009**, *20*, 513–557.

[7] a) A. Ghanem, H. Y. Aboul-Enein, *Chirality.* **2005**, *17*, 1–15; b) S. Qin, Y. Zhao, B. Wu, B. He, *Appl. Biochem. Biotechnol.* **2016**, *180*, 1456–1466.

[8] a) F. Escalettes, N. J. Turner, *ChemBioChem* **2008**, *14*, 9, 857–60; b) M. M. Musa, K. I. Ziegelmann-Fjeld, C. Vieile, J. G. Zeikus, R. S. Phillips, *J. Org. Chem.* **2007**, *72*, 30–34.

[9] a) W. Kroutil, H. Mang, K. Edegger K. Faber, *Adv. Synth. Catal.* **2004**, *346*, 125–142; b) E. W. van Hellemond, L. Vermote, W. Koolen, T. Sonke, E. Zandvoort, D. P. Heuts, D. B. Janssen, M. W. Fraaije, *Adv. Synth. Catal.* **2009**, *351*, 1523–1530; c) W. P. Dijkman, C. Binda, M. W. Fraaije, A. Mattevi, *ACS Catal.* **2015**, *5*, 1833–1839.

[10] F. J. Ruiz-Dueñas, A. T. Martinez, *Microb. Biotechnol.* **2009**, *2*, 164–77.

[11] P. Ferreira, A. Hernandez-Ortega, B. Herguendas, A. T. Martinez, M. Medina, *J. Biol. Chem.* **2009**, *284*, 24840–24847.

[12] a) J. Viña-Gonzalez, D. Gonzalez-Perez, P. Ferreira, A. T. Martinez, M. Alcalde, *Appl. Environ. Microbiol.* **2015**, *81*, 6451–62; b) J. Viña-Gonzalez, K. Elbl, X. Ponte, F. Valero, M. Alcalde, *Biotechnol. Bioeng.* **2018**, *115*, 1666–1674.

[13] S. Kille, C. G. Acevedo-Rocha, L. P. Parra, Z. G. Zhang, D. J. Opperman, M. T. Reetz, J. P. Acevedo, *ACS Synth. Biol.* **2013**, *2*, 83–92.

[14] D. Gonzalez-Perez, P. Molina-Espeja, E. Garcia-Ruiz, M. Alcalde, *PLoS One.* **2014**, *9*, e90919.

[15] F. J. Ruiz Dueñas, P. Ferreira, M. J. Martínez, A. T. Martínez, *Prot. Exp. Purif.* **2006**, *45*, 191–199.

[16] I. S. Fernandez, F. J. Ruiz-Dueñas, E. Santillana, P. Ferreira, M. J. Martinez, A. T. Martinez, A. Romero, *Acta Crystallogr. Sect. C* **2009**, *65*, 1196–1205.

[17] D. Lecina, J. F. Gilabert, V. Guallar, *Sci. Rep.* **2017**, *7*, 8466.

[18] A. D. Bochevarov, E. Harder, T. F. Hughes, J. R. Greenwood, D. A. Braden, D. M. Philipp, D. Rinaldo, M. D. Halls, J. Zhang, R. A. Friesner, *Int. J. Quantum Chem.* **2013**, *113*, 2110–2142.

[19] a) R. B. Murphy, D. M. Philipp, R. A. Friesner, *J. Comput. Chem.* **2000**, *21*, 1442–1457; b) G. M. Sastry, M. Adzhigirey, T. Day, R. Annabhimoju, W. Sherman, *J. Comput.-Aided Mol. Des.* **2013**, *27*, 221–234.

[20] A. R. Atilgan, S. R. Durell, R. L. Jernigan, M. C. Demirel, O. Keskin, I. Bahar, *Biophys. J.* **2001**, *80*, 505–515.

[21] A. Hernandez-Ortega, P. Ferreira, A. T. Martinez, *Appl. Microbiol. Biotechnol.* **2012**, *93*, 1395–1410.

[22] A. Serrano, F. Sancho, a J. Viña-González, J. Carro, M. Alcalde, V. Guallar, A. T. Martínez, *Catal. Sci. Technol.* **2019**, *9*, 833–841.

[23] A. Hernandez-Ortega, P. Ferreira, P. Merino, M. Medina, V. Guallar, A. T. Acta Crystallogr. Sect. DMartinez, *ChemBioChem.* **2012**, *13*, 427–435.

[24] a) P. Ferreira, F. J. Ruiz-Dueñas, M. J. Martinez, W. J. H. van Berkel, A. T. Martínez, *FEBS J.* **2006**, *273*, 4878–4888; b) A. Hernandez-Ortega, F. Lucas, P. Ferreira, M. Medina, V. Guallar, A. T. Martinez, *Biochemistry.* **2012**, *51*, 6595–6608; c) J. Carro, P. Amengual-Rigo, F. Sancho, M. Medina, V. Guallar, P. Ferreira, A. T. Martínez, *Sci. Rep.* **2018**, *8*, 8121.

[25] J. Carro, E. Fernandez-Fueyo, C. Fernandez-Alonso, J. Cañada, R. Ullrich, M. Hofrichter, M. Alcalde, P. Ferreira, A. T. Martinez, *Biotechnol. Biofuels* **2018**, *11*, 86.

[26] P. Ferreira, M. Medina, F. Guillén, M.J. Martínez, W. J. Van Berkel, A. T. Martínez, *Biochem. J.* **2005**, *1*, 731–8.

© 2019 Wiley-VCH Verlag GmbH & Co. KGaA, Weinheim

FULL PAPER

Structure-Guided Evolution of Aryl Alcohol Oxidase from *Pleurotus eryngii* for the Selective Oxidation of Secondary Benzyl Alcohols

Adv. Synth. Catal. **2019**, *361*, 1 – 13

J. Viña-Gonzalez, D. Jimenez-Lalana, F. Sancho, A. Serrano, A. T. Martinez, V. Guallar, M. Alcalde*

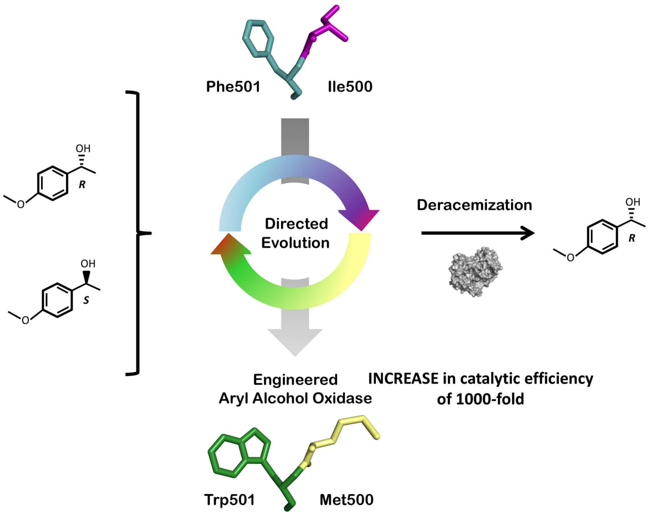
Phe501
Ile500
OH
R
OH
S
Directed Evolution
Deracemization
OH
R
Engineered Aryl Alcohol Oxidase
INCREASE in catalytic efficiency of 1000-fold
Trp501
Met500

Supporting Information

© Copyright Wiley-VCH Verlag GmbH & Co. KGaA, 69451 Weinheim, 2019

Structure-Guided Evolution of Aryl Alcohol Oxidase from *Pleurotus eryngii* for the Selective Oxidation of Secondary Benzyl Alcohols

Javier Viña-Gonzalez, Diego Jimenez-Lalana, Ferran Sancho, Ana Serrano, Angel T. Martinez, Victor Guallar, and Miguel Alcalde*

Supporting information for:

Structure-Guided Evolution of Aryl Alcohol Oxidase from *Pleurotus eryngii* for the Selective Oxidation of Secondary Benzyl Alcohols

Javier Viña-Gonzalez[1], Diego Jimenez-Lalana[1], Ferran Sancho[2], Ana Serrano[3], Angel T. Martinez[3], Victor Guallar[2,4] and Miguel Alcalde[1*]

[1]Department of Biocatalysis, Institute of Catalysis, CSIC, Cantoblanco, 28049 Madrid, Spain.

[2]Barcelona Supercomputing Center, Jordi Girona 31, 08034 Barcelona, Spain.

[3]Biological Research Center, CSIC, Ramiro de Maeztu 9, 28040 Madrid, Spain.

[4]ICREA, Passeig Lluís Companys 23, 08010 Barcelona, Spain.

*Corresponding author: malcalde@icp.csic.es

Table of contents

Supporting Table S1

Supporting Figure 1

Supporting Figure 2

Supporting Figure 3

Supporting Table S2

Supporting Table 1. List of primers

Oligo	**Sequence**
RMLN	5’-CCTCTATACTTTAACGTCAAGG-3’
RMLC	5’-GGGAGGGCGTGAATGTAAGC-3’
I500Af	5’- GAGACAACGCCAACACG*GCT*TTCCACCCAGTTGGAACGGC -3’
I500Ar	5’- GCCGTTCCAACTGGGTG*GAA*AGCCGTGTTGGCGTTGTCTC -3’
F501Af	5’-GAGACAACGCCAACACGATT*GCT*CACCCAGTTGGAACGGC -3’
F501Ar	5’- GCCGTTCCAACTGGGTGAGC*AAT*CGTGTTGGCGTTGTCTC -3’
DM5001Af	5’- GAGACAACGCCAACACG*GCTGCT*CACCCAGTTGGAACGGC -3’
DM5001Ar	5’- GCCGTTCCAACTGGGTG*AGCAGC*CGTGTTGGCGTTGTCTC -3’
22c1F	5’-GAGACAACGCCAACACG*NDTNDT*CACCCAGTTGGAAC-3’
22c1R	5’-GTTCCAACTGGGTG*AHNAHN*CGTGTTGGCGTTGTCTC-3’
22c2F	5’-GAGACAACGCCAACACG*NDTVHG*CACCCAGTTGGAAC-3’
22c2R	5’-GTTCCAACTGGGTG*CDBAHN*CGTGTTGGCGTTGTCTC-3’
22c3F	5’-GAGACAACGCCAACACG*NDTTGG*CACCCAGTTGGAAC-3’
22c3R	5’-GTTCCAACTGGGTG*CCAAHN*CGTGTTGGCGTTGTCTC-3’
22c4F	5’-GAGACAACGCCAACACG*VHGNDT*CACCCAGTTGGAAC-3’
22c4R	5’-GTTCCAACTGGGTG*AHNCDB*CGTGTTGGCGTTGTCTC-3’
22c5F	5’-GAGACAACGCCAACACG*VHGVHG*CACCCAGTTGGAAC-3’
22c5R	5’-GTTCCAACTGGGTG*CDBCDBC*GTGTTGGCGTTGTCTC-3’
22c6F	5’-GAGACAACGCCAACACG*VHGTGG*CACCCAGTTGGAAC-3’
22c6R	5’-GTTCCAACTGGGTG*CCACDB*CGTGTTGGCGTTGTCTC-3’
22c7F	5’-GAGACAACGCCAACACG*TGGNDT*CACCCAGTTGGAAC-3’
22c7R	5’-GTTCCAACTGGGTG*AHNCCA*CGTGTTGGCGTTGTCTC-3’
22c8F	5’-GAGACAACGCCAACACG*TGGVHG*CACCCAGTTGGAAC-3’
22c8R	5’-GTTCCAACTGGGTG*CDBCCA*CGTGTTGGCGTTGTCTC-3’

22c9F	5’-GAGACAACGCCAACACG*TGGTGG*CACCCAGTTGGAAC-3’
22c9R	5’-GTTCCAACTGGGTG*CCACCA*CGTGTTGGCGTTGTCTC-3’
RHF1	5’-GGAACAAGGCCGGGCGCAAG-3’
FM1	5’-TAGGGGCAGAGGCTCCACTC-3’
RM1	5’-GCATAGCGATCGAAATCTTC-3’
FHF-1	5’-TCATGATGCGTGGATCAACA-3’
RHF-2	5’-AGGAGCAAATGGTCGGATAG-3’
FM2	5’-ATCCTAGCGTAGGCCGAAAC-3’
RM2	5’-TCTCCGCGAGCTACAGGAGA-3’
FHF-2	5’-TTATGAGTGTTACAAACGCGTTGATT-3’
RHF-3	5’-GTTGGCGTTGTCTCTAATGTACGACTC-3’
FM3	5’-CGACGGACGATGCTGCTATC-3’
F116	5’-ACGTGTCCGTCTTGGTCCTAGAGGCGGGTGTATCAGAT*GRG*AA-‘3
R116	5’-TCTGCCCCTAATACATT*CYC*A-‘3
F5	5’-CA*RTTGYG*TATCCT*YGC*GGCCGT*ATR*CTAGGGGGGTCTAGCTCT*GYT*AA-‘3
R5	5’-TT*ARC*AGAGCTAGACCCCCCTAG*YAT*ACGGCC*GCR*AGGATA*CRCAAY*TG-‘3
F521	5’- GCGTCATGGCCACGACG*CRA*GAGCAAA-‘3
R521	5`- GTCGGGATTGAAGAAGAACTCTTCGCTTTGCTC*TYG*CGTCGTGG -‘3
F9419	5’-ATAACATC*YTC*AGAGACTCGTCCGAGTTCAAC*GYT*GATTTA-‘3
R9419	5’-TAAATC*ARC*GTTGAACTCGGACGAGTCTCT*GAR*GATGTTAT-‘3
F1397	5’-TTCGTTTCCTCTCTGGT*CRA*GC-‘3
R1397	5’-GTATAACGAAGTCCGCCCACGC*TYG*ACC-’3
AAOsec1F	5’-GTGGATCAACAGAAGATTTCGATCG-3’
AAOsec2R	5’-GTGGTTAGCAATGAGCGCGG-3’
AAOsec3R	5’-GGAGTCGAGCCTCTGCCCCT-3’

Codon substitutions are shown in italics (where N = A/T/C/G; D = no C; V =no T, H = no G; B = no A; R = A/G; Y = C,T).

Supporting Table 2. Polarimeter measurements for the LanDo variant reaction with 1-(*p*-methoxyphenyl)-ethanol (correspondent to the remaining R-enantiomer). Number of cycles: 8 with 1 sec cycle iterval. Path length 100mm.

PMT Voltage[V]	Temperature[ºC]	Optical Rotation Monitor
353	24.96	0.0592
353	24.95	0.0601
353	24.96	0.0593
354	24.96	0.0602
353	24.98	0.0586
353	24.99	0.0603
354	25.01	0.0600
354	25.03	0.0589

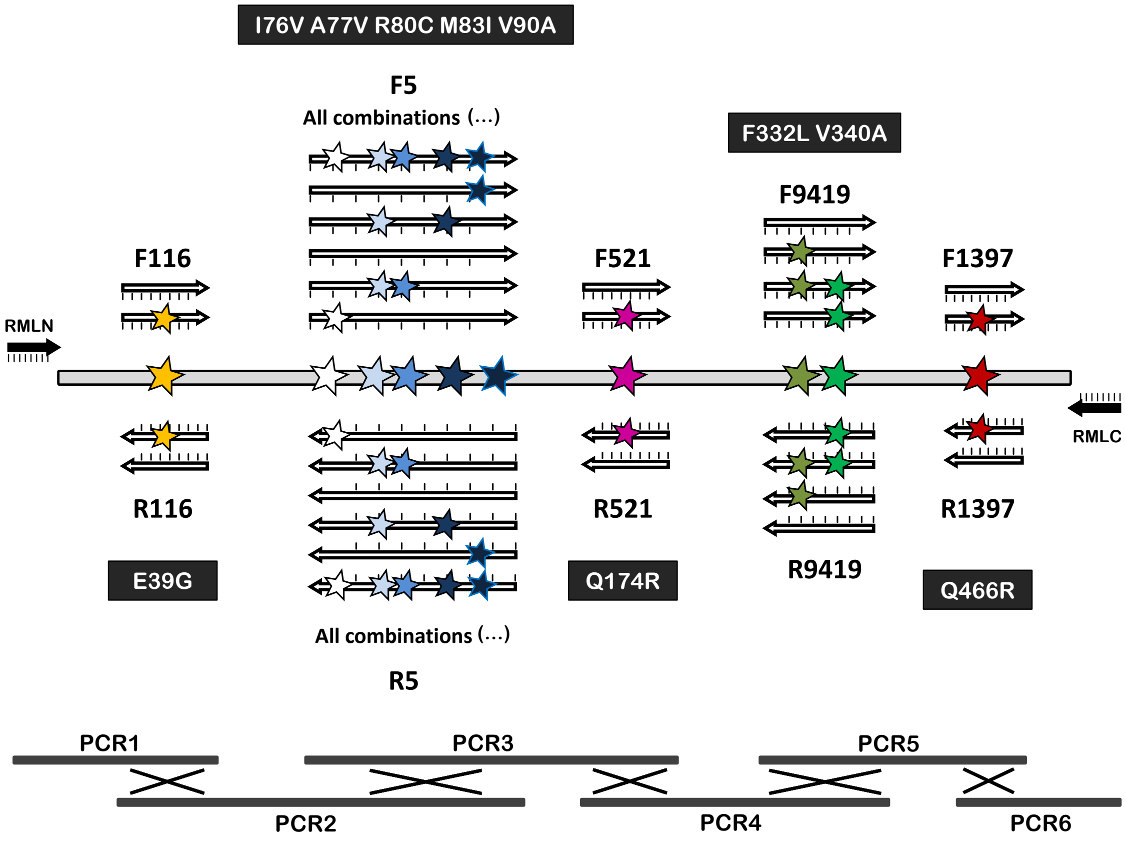
I76V A77V R80C M83I V90A
F5
All combinations (...)
F332L V340A
F9419
F116
F521
F1397
RMLN
RMLC
R116
R521
R1397
R9419
E39G
Q174R
Q466R
All combinations (...)
R5
PCR1
PCR3
PCR5
PCR2
PCR4
PCR6

Figure S1. Method for *in vivo* site-directed recombination. Primers designed to be used in the site-directed recombination experiment for the PCR amplification of the selected mutated positions (in black). For each mutation, adjacent sense and antisense primers were synthesized that were 50% mutated at the sites of interest. Six PCR reactions were performed with ~40 bp homologous sequences at each end to foster *in vivo* recombination (7 crossover events). The PCR fragments were assembled by transformation into yeast with the linearized vector to yield a library of all combinations of the mutations/reversions in one-pot .

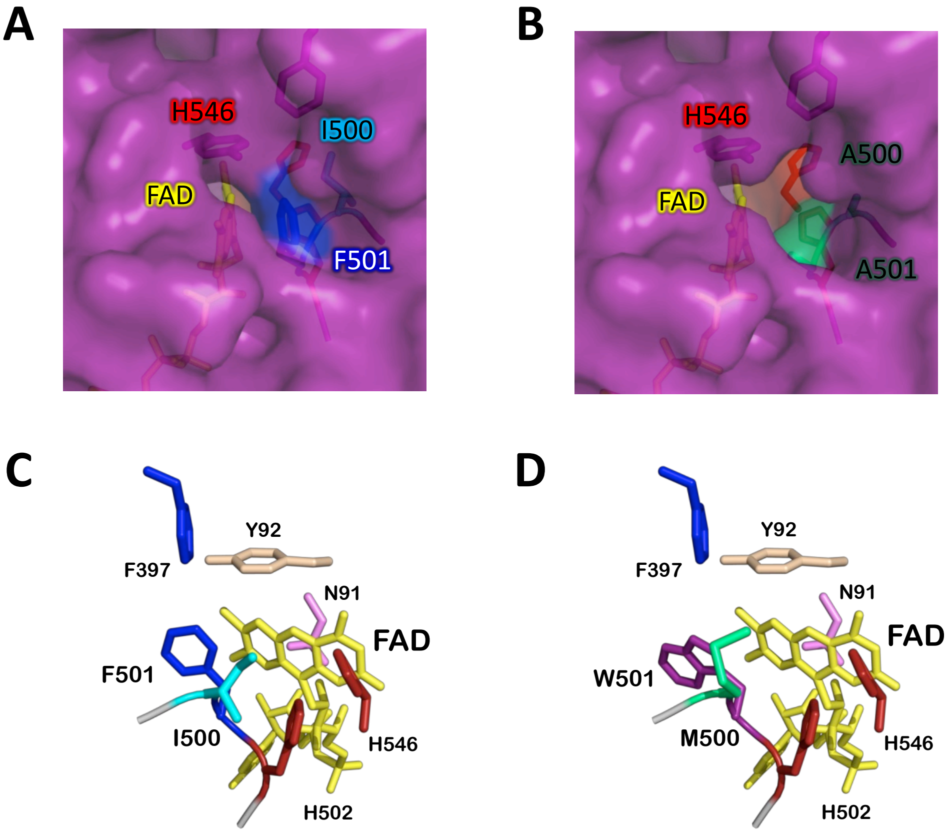
A
H546
I500
FAD
F501
B
H546
A500
FAD
A501
C
Y92
F397
N91
FAD
F501
I500
H546
H502
D
Y92
F397
N91
FAD
W501
M500
H546
H502

Figure S2. The access channel and catalytic pocket before and after mutation. The channel giving access to the active site in the FX9 (**A**) and I500A-F501A (**B**) mutants: the FAD molecule is depicted in yellow, the Phe501 and Ile500 residues in the parental type are in blue and light blue, the Ala500 and Ala501 mutations are in green, and histidine 546 at the catalytic pocket is in red. Catalytic pocket in the FX9 (**C**) and 15G12 (**D**) variants: His502 and His546 at the active site are depicted in red, FAD is depicted in yellow, ancestral/consensus mutation Asn91 is in pink, Phe397 and Phe501 are in blue, Ile500 in light blue, Tyr92 is depicted in white, whereas the new Trp501 and Met500 substitutions are depicted in purple and light green, respectively. The models were prepared from the crystal structure of *P. eryngii* AAO (PDB 3FIM).

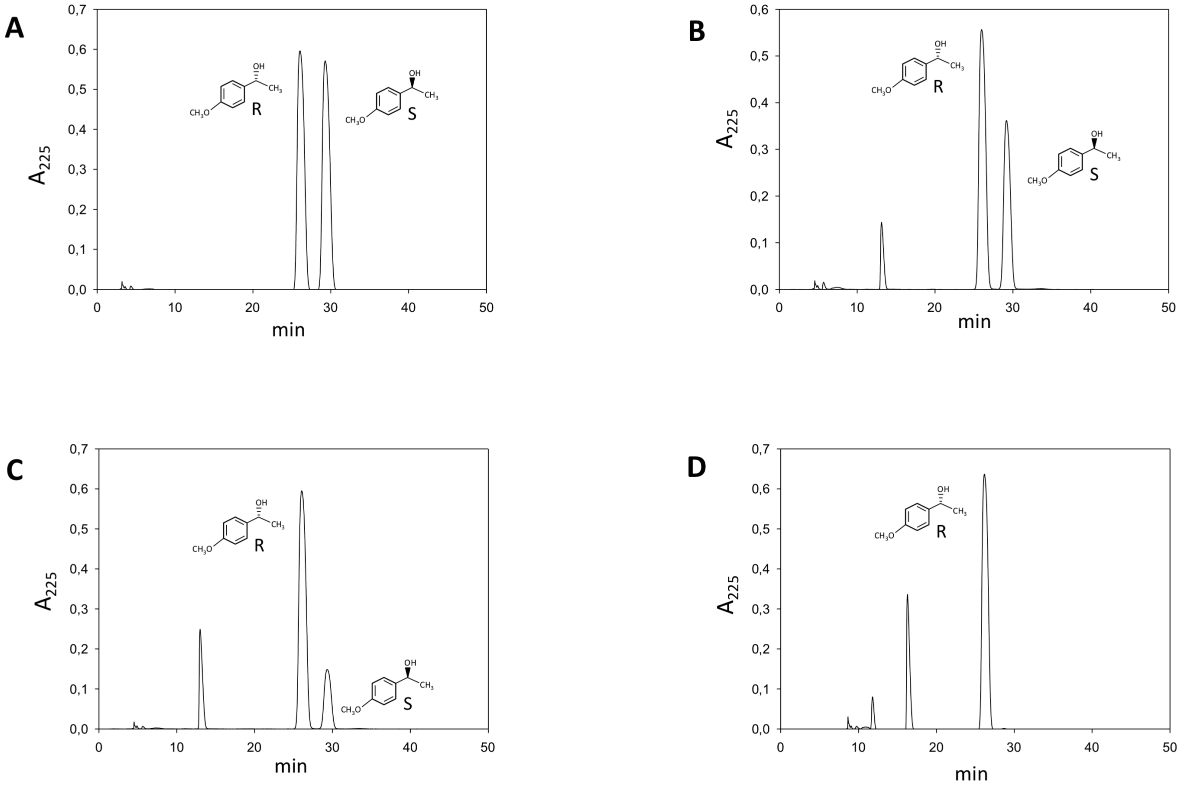

Figure S3. **Chiral HPLC chromatograms**. Elution profiles of the reaction of LanDo variant (1 µM) with racemic 1-(*p*-methoxyphenyl)-ethanol (2.5 mM). Negative control (A), after 15 minutes reaction (B), after 45 min reaction (C) and after 90 min reaction (D).